Development of Inhibitors of Amyloid Fibril Propagation

Maya Bendifallah

université PARIS-SACLAY

NNT : 2019SACLS578

UNIVERSITÉ PARIS SUD
Comprendre le monde, construire l'avenir

Development of inhibitors of amyloid fibril propagation

Thèse de doctorat de l'Université Paris-Saclay
préparée à Université Paris Sud

École doctorale n°568 signalisations et réseaux intégratifs en biologie (biosigne)
Spécialité de doctorat: aspects moléculaires et cellulaires de la biologie

Thèse présentée et soutenue à Fontenay-aux-Roses, le 16 décembre 2019, par

Maya Bendifallah

Composition du Jury :

Dr. Sandrine Sagan Directeur de recherche, Sorbonne Université (CNRS)	Rapporteur
Dr. Yann Verdier Maître de Conférences, ESPCI (CNRS)	Rapporteur
Dr. Olga Corti Directeur de recherche, Sorbonne Université (INSERM, ICM)	Examinateur
Pr. Pierre Le Maréchal Professeur Émérite, Université Paris-Saclay (CNRS, NeuroPsi)	Président
Dr. Ronald Melki Directeur de recherche, Université Paris-Saclay (CNRS, CEA, MIRCen)	Directeur de thèse
Dr. Elodie Monsellier Chargée de recherche, Université Paris-Saclay (CNRS, CEA, MIRCen)	Invitée Co-encadrante
Dr. Virginie Redeker Chargée de recherche, Université Paris-Saclay (INSERM, CEA, MIRCen)	Invitée Co-encadrante

Thèse de doctorat

"Things work out best for those who make the best of how things work out."

John Wooden

ACKNOWLEDGMENTS

First, I would like to thank DIM Cerveau et Pensée for funding my doctoral project, my various training courses and my two conferences.

Next, I would like to thank my two referees Dr. Sandrine Sagan and Dr. Yann Verdier for having accepted to read and review my manuscript. I would also like to thank Dr. Olga Corti and Pr. Pierre Le Maréchal for agreeing to be a part of my PhD defense jury.

Thank you to Ronald, my PhD director, for the opportunity to work on this project and for your guidance all throughout.

Thank you to Elodie, my co-PhD supervisor, for setting me up in the lab, our many discussions, your constructive feedback and your availability.

Thank you to Virginie for your help with the cross-linking experiments and most importantly for conducting the mass spectrometry experiments and analyses!

Thank you to the numerous other previous and present members of the lab, in alphabetical order: Alexis, Amu, Audrey, Emilie, Jimmy, Karine, Laura, Laurent, Luc, Margaux[2], Marion, Maud, Mehdi, Nolwen, Pauline, Stéphane and Tracy for the many tea time discussions (thank you particularly to Jimmy and Tracy for preparing the tea most of the time), thinking of me when you bring desserts (Emilie, Jimmy, Nolwen), and/or help in the lab, whether by giving advice or preparing the foundation for all of our experiments (thank you Tracy!!). Importantly, thank you to Emilie, Maud, Nolwen, Laurent and Stéphane for your continuous moral support at (and outside of) work. Thank you to everyone who gave feedback on parts or all of my dissertation.

I'd also like to thank many members of MIRCen for having received us so warmly (no one would have expected otherwise), for your help getting us set up after the move, and for making MIRCen run, in alphabetical order: Alexis, Alix, Anastasie, Audrey[2], Brahim, Camille, Cécile, Charlène, Charlotte, Clémence, Emmanuel, Fanny, Francesco, Géraldine, Giles, Gwenaëlle, JB, Karine, Kristell, Laurene, Laurent, Maria, Mélissa, Noëlle, Océane, PA, Pascale, Pauline, Philippe, and Suzanne, notably.

In particular, thank you to Angélique, Cécile, Karine, Kristell, Gwenaëlle, Jeanne, Laurent, Luc, and Odile for your help with orders and administrative paperwork and to Géraldine for help with the L2 lab.

Thank you to Dr. Olga Corti and Dr. Anselme Perrier for your feedback during my PhD committees.

Finally, I would like to thank Chelsea, Claire, Hannah, G, Geoff, Jared, N and my parents for their unconditional support (in general) but especially these last few years. I owe you a great deal of gratitude.

TABLE OF CONTENTS

Page

ABBREVIATIONS

αAc	αA-crystallin
AAV	adeno-associated virus
αBc	αB-crystallin
Aβ	amyloid-β
AD	Alzheimer's disease
ALS	Amyotrophic lateral sclerosis
AMPA	α-amino-3-hydroxy-5-methylisoxazole-4-propionic acid
APP	amyloid precursor protein
BBB	blood-brain barrier
BPA	benzophenone
BSE	bovine spongiform encephalopathy
CD	circular dichroism
Cdk5	cell division protein kinase 5
CHIP	carboxyl terminus of Hsc70-interacting protein
CJD	Creutzfeldt-Jakob disease
CNS	central nervous system
Cryo-EM	cryo-electron microscopy
CSF	cerebrospinal fluid
Csg	curli-specific genes
CTE	C-terminal extension
C-ter	C-terminus
DLB	dementia with Lewy bodies
ECM	extracellular matrix
FFI	fatal familial insomnia
FPOP	fast photochemical oxidation of proteins
GAG	glycosaminoglycan
HBS	hydrogen-bond surrogate
HD	Huntington's disease
HDX	hydrogen–deuterium exchange
Hsc70	heat shock cognate 71kDa
Hsp	heat shock protein
HSPG	heparan sulfate proteoglycan
IB	inclusion body, intranuclear inclusion
IDP	intrinsically disordered protein
LAG3	lymphocyte-activation gene 3
LB	Lewy body
LC	liquid chromatography
LID	levadopa-induced dyskenesia
LN	Lewy neurite
MS	mass spectrometry

MSA	multiple system atrophy
NAC	non-amyloid component
NBD	nucleotide binding domain
NCAA	non-canonical amino acid
ND	neurodegenerative disease
NEF	nucleotide exchange factors
NFT	neurofibrillary tangle
NKA	Na^+/K^+-ATPase
NKApep	Na^+/K^+-ATPase-derived peptide
NMDA	N-methyl-D-aspartate
NMR	nuclear magnetic resonance
NTE	N-terminal extension
N-ter	N-terminus
PD	Parkinson's disease
PEG	polyethylene glycol
PHF	paired helical fragment
PPIs	protein-protein interfaces
PQC	protein quality control
Prion	proteinaceous infectious particle
PrP	prion protein
PrP^{sc}	pathogenic, scrapie-like, prion protein
PSD-95	post-synaptic density scaffolding protein 95
Q-TOF	quadripole-time of flight
RBD	REM sleep behavior disorder
REM	rapid eye movement
SBD	substrate binding domain
sHSP	small heat shock protein
SOD1	superoxide dismutase 1
SNpc	substantia nigra pars compacta
ss-NMR	solid state NMR
TDP-43	transactive response (TAR) DNA-binding protein 43
TH	tyrosine hydroxylase
TSEs	transmissible spongiform encephalopathies
UPS	ubiquitin proteasome system

LIST OF TABLES, FIGURES AND ANNEXES

Table **Page**

Figure **Page**

Appendix **Page**

PART 1:

INTRODUCTION

Chapter 1: Proteinopathies

1.1 Neurodegenerative proteinopathies

Proteinopathies are diseases linked to misfolded proteins, whose aggregation and subsequent loss of the protein's normal activity lead to cellular toxicity and eventually cell death. Protein aggregation in cells of the central nervous system leads to neurodegeneration. The risk of developing neurodegenerative proteinopathies greatly increases with age, making their treatment a looming serious public health issue. Each disease differs in its genetic and environmental risk factors, the proteins that aggregate, the cells containing aggregated protein deposits, and the brain regions where affected cells are located, all of which lead to distinct clinical symptoms **(Figure 1**, **Table 2**). Some well-known neurodegenerative proteinopathies or diseases (NDs) are Creutzfeldt-Jakob disease (CJD), Alzheimer's disease (AD), Parkinson's disease (PD), Huntington's disease (HD) and Amyotrophic lateral sclerosis (ALS), which are characterized, respectively, by aggregation of prion protein (PrP), amyloid-β (Aβ) and Tau, α-Synuclein (αSyn), mutated Huntingtin (mHTT), and superoxide dismutase 1 (SOD1).

These diseases lead to progressive, selective neurodegeneration and eventually death. The diseases can be categorized in two major groups: movement disorders or dementias. Movement disorders are characterized by impaired motor control, with tremors, bradykinesia (slow movement), akinesia (loss of voluntary movements), and rigidity or ataxia (inability to coordinate muscles), among other motor symptoms. PD and HD are movement disorders, although patients also harbor cognitive defects and psychiatric problems (Aldaz et al., 2019; Zucchi et al., 2019). Dementias are defined by a severe decline in cognitive function, as seen in patients with AD and prion diseases, for example. While less common, dementias also can have concombinant motor symptoms

(Tsolaki et al., 2001). The definitive diagnosis for most NDs is only possible with autopsy, as the clinical and biochemical overlap between diseases is high.

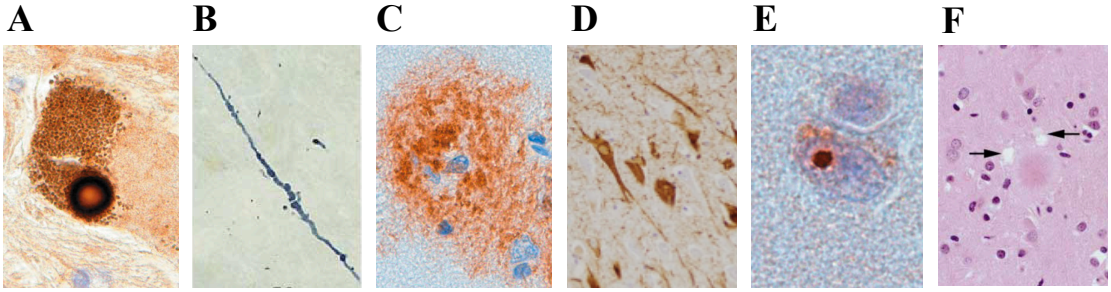

Figure 1: Aggregate depositions in PD, AD, HD, and CJD.
A) αSyn in a Lewy Body (LB) in the substantia nigra of a PD patient (Forman et al., 2004). **B)** αSyn in a Lewy Neurite (LN) in the substantia nigra of a PD patient (Braak et al., 2003a). **C)** Extracellular Aβ plaque in the neocortex of an AD patient (Forman et al., 2004). **D)** Phosphorylated Tau in neurofibrillary tangles (NFT) in the hippocampus of an AD patient (Gibbons et al., 2019). **E)** Intranuclear inclusion bodies (IB) containing mHTT deposits in the neocortex of an HD patient (Forman et al., 2004). **F)** Spongiform changes (arrows) and prion protein (PrP)-positive extracellular amyloid plaques. (Johnson and Gibbs, 1998).

Table 1: A sample of neurodegenerative proteinopathies.
Only the top four genetic risk factors are listed here. Synucleinopathies: adapted from (Bonifati, 2014; Hershey and Coleman-Jackson, 2019; Katzeff et al., 2019; McCann et al., 2014; Outeiro et al., 2019; Rana et al., 2019; Vann Jones and O'Brien, 2014; Wong and Krainc, 2017). Tauopathies: adapted from (Armstrong et al., 2013; Barragán Martínez et al., 2019; Bateman et al., 2011; Dugger and Dickson, 2017; Gaugler et al., 2016; Kovacs, 2015; Mahapatra et al., 2004). PolyQ diseases: adapted from (Bates et al., 2015; Ross et al., 2014; Walker, 2007). Prion diseases: adapted from (Chen and Dong, 2016; Johnson and Gibbs, 1998; Mackenzie and Will, 2017). *APOEε4* apolipoprotein E; *APP* amyloid precursor protein; *DMV* dorsal nucleus of vagus nerve; *EO* early onset; *GBA* beta-glucocerebrosidase; *GCI* glial cytoplasmic inclusions; *LC* locus coeruleus; *LO* late onset; *LRRK2* leucine-rich repeat kinase 2; *PINK1* PTEN induced putative kinase; *polyQ;* polyglutamine; *PRKN* parkin; *RBD* rapid-eye movement (REM) sleep behavior disorder; *SCARB2* scavenger receptor class B, member 2; *sCJD* sporadic CJD; *SNCA* synuclein alpha; *SNpc* substantia nigra pars compacta; *PRNP* prion protein ; *PSEN* presenilin.

	Proteinopathy	Prevalence / Incidence (World)	Sporadic/Familial Risk genes	Onset + Disease duration; years	Aggregating proteins	Neuropathology	Clinical symptoms
Synucleinopathies	**Parkinson's disease (PD)**	Prevalence: 1 to 2 per 100 over 60 years; 4 per 100 over 75 years Incidence: 1 to 2 per 10,000 person-years; 12 per 10,000 person-years for people over 70 years	95% sporadic; 5% familial EOPD: *SNCA*; *PINK1* LOPD: *LRRK2*, *GBA*	Onset: 60 (EOPD); 70 (LOPD) Duration: 15 (EOPD); 5-10 (LOPD)	αSyn	SNpc dopaminergic degeneration; αSyn LB//LN neuronal pathology; neuronal loss in the DMV olfactory bulb and LC	Parkinsonism (resting tremors, postural instability, muscular rigidity, bradykinesia) Nonmotor symptoms (constipation, RBD, anosmia)
	Dementia with Lewy Bodies (DLB)	Prevalence: 0.87 per 1,000 over 65 years Incidence: 3.5 per 100,000 person-years	100% sporadic No high penetrance risk genes *APOEε4, SNCA, GBA, SCARB2*	Onset: 76 Duration: 6	αSyn Tau 3R, 4R	SNpc/Cholinergic dopaminergic degeneration αSyn LB/LN pathology Aβ plaques and tau tangles	Parkinsonism, dementia, psychosis
	Multiple system atrophy (MSA)	Prevalence: 1.9 to 4.4 per 100,000 Incidence: 3 per 100,000 person-years over 50 years	100% sporadic No consensus on risk genes	Onset: 60 Duration: 6-9	αSyn	αSyn oligodendrocytic pathology (GCIs); SNpc / olivopontocereballer degeneration; absence of LBs	Parkinsonism, cerebellar ataxia, autonomic failure Nonmotor symptoms (RBD, urinary incontinence, sexual dysfunction)
Tauopathies	**Alzheimer's disease (AD)**	Prevalence: 3 per 100 people under 64; 36 per 100 people over 85 Incidence: 2 per 1000 person-years aged 65 – 74; 13 per 1000 aged 75-84; 37 per 1000 over 85	99% sporadic, 1% familial EOAD: *APP, PSEN1, PSEN2* LAOD: *APOEε4*	Onset: 30-50 (EOAD); >65 (LOAD) Duration: 8.5	Tau 3R, 4R Aβ	Extracellular Aβ plaques; intracellular Tau neurofibrillar tangles; hippocampal atrophy	Dementia, psychiatric problems
	Corticobasal Degeneration (CBD)	Unknown	No clear familial links; H1/H1c subhaplotype of *MAPT*	Onset: 64 Duration: 7	Tau 4R	Asymmetric atrophy; cortical and striatal filamentous tau inclusions; glial lesions	Asymmetric movement disorder (parkinsonism)
	Pick's disease	Very rare	No clear risk genes	Onset: 63 Duration: 7.2	Tau 3R	Frontal and temporal lobe degeneration; neuronal cytoplasmic Pick bodies	Progressive aphasia, dementia
PolyQ	**Huntington's disease (HD)**	In western populations: Prevalence: 10.6 to 13.7 per 100,000 Incidence: 4.7–6.9 per million person-years	100% familial (autosomal dominant) mHTT	Mean onset: 45; polyQ length dependent Duration: 15-30	mHTT	Medium spiny neuron cell loss/atrophy; intranuclear deposits of mHTT	Dementia, motor, psychiatric and cognitive problems
Prion	**Creutzfeldt-Jakob Disease (CJD)**	Prevalence: 1-9 per million Incidence: 1 to 2 per million person-years	85% sporadic; 10-15% familial (*PRNP*); 1% iatrogenic	sCJD onset: 50 – 70 Duration: 5 months	PrP (prion)	PrP positive plaques; spongiform degeneration	Dementia, ataxia, psychiatric problems, insomnia

1.1.1 Parkinson's disease & synucleinopathies

PD is the most common movement disorder and the second most common ND after AD. Epidemiological studies have identified over 10 million people above the age of 60 living with PD (Tysnes and Storstein, 2017), such that PD affects nearly 2% of the world population above 60 years of age and 4-5% above 80. The disease was first described by James Parkinson in 1817 when he outlined its main motor symptoms: slowness of movement (bradykinesia), tremors and, in some cases, an absence of voluntary movements (akinesia). Fifty years later, Jean-Martin Charcot helped to refine the disease symptoms. In the late 19th and early 20th century, work by Blocq, Marinesco, and Trétiakoff led to the implication of the substantia nigra pars compacta (SNpc) in Parkinsonism. In 1912, Friedrich Lewy identified what came to be called Lewy bodies (LBs) (**Figure 1A**), the hallmark marker of PD and other related diseases, subsequently called Lewy Body diseases. Other variants of Lewy pathology such as Lewy Neurites (LNs) are found in PD patient brains (**Figure 1B**). Lewy's contribution fueled the debate concerning the affected regions of PD, in light of the fact that LBs were first reported in the striatum and not in the SNpc. This debate was resolved when the dopaminergic nigrostriatal pathway was discovered and dopamine was identified as a neurotransmitter (Przedborski, 2017). Subsequently, discovery of familial PD patients with mutations in or multiplications of the SNCA gene coding for the protein αSyn (Ibáñez et al., 2004; Polymeropoulos et al., 1997; Singleton, 2003), plus the identification of αSyn in LBs, implicated this protein in PD and led to the classification of PD, Dementia with Lewy Bodies (DLB), Multiple System Atrophy (MSA), and five other diseases as synucleinopathies (Goedert and Spillantini, 2012, 1998; M. G. Spillantini et al., 1998; Maria Grazia Spillantini et al., 1998; Spillantini et al., 1997). Since then, other genes have been associated with early onset PD or late onset PD risk that are implicated in the

following pathways: protein aggregation, vesicle sorting and transport, mitochondrial quality control and lysosomal function (**Appendix 1**, Brás et al., 2015).

Parkinsonism is used to label clinical conditions with bradykinesia or akinesia and at least one of the following symptoms: resting tremor, postural instability, and muscle rigidity. However, PD only accounts for 80% of parkinsonism cases (Przedborski, 2017); the remaining 20% is due to the other synucleinopathies. Non-motor symptoms also have been associated with parkinsonism, including sleep disorders, olfactory dysfunction, constipation or other forms of autonomic dysfunction, pain, fatigue, cognitive impairment, and psychiatric symptoms (Kalia and Lang, 2015, **Appendix 2**). Many of these non-motor symptoms appear before the onset of motor symptoms, since motor symptoms only appear after a 50-70% loss of neurons in the SNpc (Cheng et al., 2010). Neither mood disorders nor constipation, two prodromal PD symptoms that have both been shown to lead to almost twice the risk of subsequently developing PD (Noyce et al., 2012), are specific to NDs and thus cannot be used solely to aid in an early PD diagnosis. Rapid eye movement (REM) sleep behavior disorder (RBD), on the other hand, has more potential, as 28-45% and 40-65% of RBD patients developed neurodegenerative syndromes at 5- and 10-year follow-ups, respectively. In other studies, 50% of RBD patients developed parkinsonism and the other half developed dementia (Postuma et al., 2012). RBD patients who converted into PD had more severe gait, faster appearance of motor symptoms and reduced responses to levodopa, a precursor to dopamine (Chan et al., 2018). While RBD has high specificity for diagnosing prodromal PD, its sensitivity is low, given that only 15-33% of PD patients have RBD. In contrast, 40% of patients with DLB and 70% of patients with MSA have RBD (Chan et al., 2018). If patients with severe forms of RBD presented themselves to doctors, they could benefit from a window before the appearance of motor symptoms for regular follow-ups. Loss of sense of smell is another prodromal

symptom, appearing two to five years before motor symptoms (Goldman and Postuma, 2014). While olfactory loss had high sensitivity for PD, affecting 70% of PD patients, its specificity for developing the disease is still quite low, as one third of the elderly population reports olfactory loss (Postuma et al., 2012). Patients usually die from secondary conditions such as pneumonia.

αSyn is a 140 amino acid protein that is primarily expressed in the CNS in presynaptic nerve terminals (Jakes et al., 1994). αSyn, β-synuclein and γ-synuclein are part of the synuclein family only described in vertebrates (George, 2002). αSyn has three functionally-defined domains: first, its N-terminal 60 amino acids are known for binding to lipids and are the site of the six missense mutations associated with familial PD; second, its hydrophobic core that contains the non-amyloid component (NAC) peptide (61-95); and third, its acidic C-terminal (**Figure 2**). There are seven imperfect 11-mer repeats of KTKEGV in the first 95 residues of the protein, which are implicated in lipid and interprotein binding. αSyn can be phosphorylated at multiple sites, including notably S129, found in LBs (Fujiwara et al., 2002). Furthermore, αSyn undergoes other post-translational modification such as nitration, sumoylation, acetylation and ubiquitination (Pajarillo et al., 2018). Truncated forms of αSyn, notably at the C-ter, are formed in cells (Pieri et al., 2016) and found in LBs, although in smaller quantities than the whole protein (Baba et al., 1998). Furthermore, the expression of C-terminal tructated αSyn in mice can lead to greater toxicity than the full-length protein (Rochet et al., 2012). Regarding its structure, monomeric αSyn is primarily unfolded. Its N-ter forms α-helices upon membrane binding and its C-ter is dynamic with no defined structure. αSyn may exist as a monomer (Burré et al., 2013; Fauvet et al., 2012; Theillet et al., 2016) or aggregation-resistant tetramers (Bartels et al., 2011; Dettmer et al., 2015; Gurry et al., 2013; Selkoe et al., 2014). αSyn is thought to be involved in synaptic vesicle trafficking (Abeliovich et

al., 2000; Nemani et al., 2010) and in maintaining presynaptic sensitive factor attachment protein receptor (SNARE) complex assembly (Burré et al., 2010), among other functions (Burré et al., 2018).

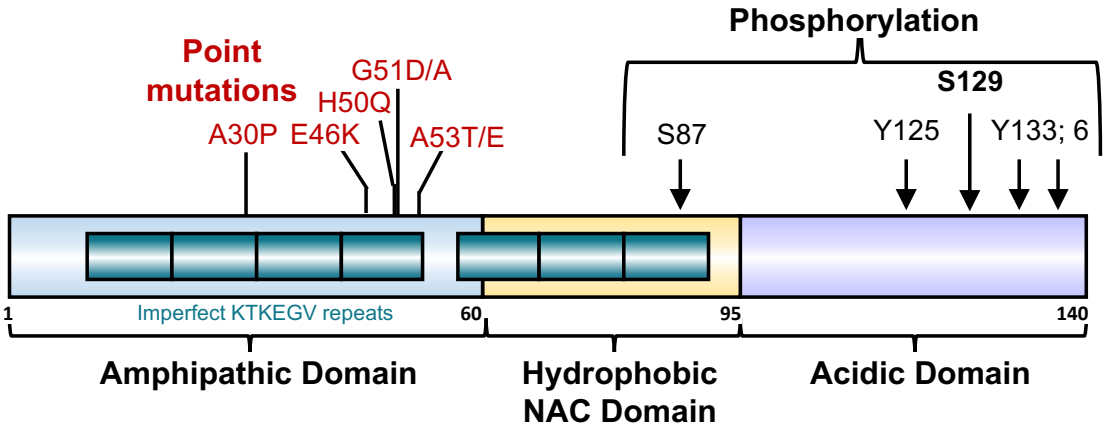

Figure 2: Primary structure of αSyn.
αSyn 1-140 with domains, mutations and phosphorylation sites annotated. αSyn is phosphorylated at S129 in brain tissue from patients with synucleinopathies. Adapted from Barrett and Timothy Greenamyre, 2015; Rosborough et al., 2017.

1.1.2 Alzheimer's disease & tauopathies

AD is the most common form of dementia, accounting for 50-75% of cases (Barragán Martínez et al., 2019). It is estimated that around 50 million people worldwide live with AD (Karlawish et al., 2017). The percentage of people with AD is age related, with 16% of people between the ages of 65 and 74 years being afflicted and up to 36% for those over 85 years old (Alzheimer Association, 2019). AD was first identified by Alois Alzheimer in 1907 (Stelzmann et al., 1995) and was combined with presenile dementia by Emil Kraepelin three years later to become known as Alzheimer's Disease. AD was further expanded 60 years later to include senile dementia. Alois Alzheimer connected dementia in one female patient with the presence in her cerebral cortex of abundant neuritic plaques (**Figure 1D**) and neurofibrils (**Figure 1E**), today known as neurofibrillary tangles (NFTs), the two pathological features defining the disease (Spillantini and Goedert, 2013). Indeed, post-mortem identification of these hallmarks

still constitutes the definite diagnosis of the disease. These extracellular plaques were revealed to contain mostly the peptide amyloid-β (Aβ) (Masters et al., 1985), a cleavage product from the amyloid precursor protein (APP), while the NFTs are composed of paired helical filaments made of hyperphosphorylated Tau, a microtubule stabilizing protein (Goedert et al., 1988; Wischik et al., 1988). The identification of genes connected to early-onset AD that are involved in Aβ processing helped to elucidate some of the mechanisms behind the creation of the neuritic plaques. In addition, genes associated with risk of AD are involved in Tau or cholesterol metabolism, immune response, endocytosis, cytoskeleton development, and epigenetics, or in some cases are not yet characterized (**Appendix 1**, Barragán Martínez et al., 2019). In parallel, mutations in the MAPT gene coding for Tau were associated with Frontotemporal dementia and parkinsonism linked to chromosome 17 (FTDP-17, Wilhelmsen et al., 1994), a disease with clinical overlap with AD. Nowadays, there are over 20 NDs associated with aggregated Tau, called Tauopathies (Lee et al., 2001, **Appendix 4**). The exact interplay and timing between Aβ and Tau aggregation in AD are unclear: neurodegeneration usually begins 20-30 years before clinical onset, with memory problems appearing as plaque and NFT load increase. This preclinical phase is referred to as Mild Cognitive Impairment (MCI) and 10-15% of MCI patients develop AD every year (Blennow et al., 2006). Ultimately, as diagnostics improve, patients diagnosed with MCI could be treated at very early stages, therefore intervening before the passage to major neurodegeneration.

As I mentioned earlier, two main proteins aggregate in AD: Aβ and Tau. Aβ is a 40–42 residue peptide derived from APP (**Figure 3**). APP is a type-1 transmembrane glycoprotein. Its cleavage by multiple proteases, notably, α-secretase, β-secretase (or β-site APP-cleaving enzyme, BACE), and γ-secretase, act on APP in pairs to lead to either non-amyloidogenic cleavage (α- and γ-secretase) or amyloidogenic cleavage (β- and γ-

secretase) (Sambamurti et al., 2002). The amyloidogenic processing, producing Aβ peptides 1-40 and 1-42 ($A\beta_{1-40}$ & $A\beta_{1-42}$), also occurs in healthy people, as Aβ peptides are found in their cerebrospinal fluid (CSF) and plasma, albeit in different ratios than AD patients (Shaw et al., 2009). While most mutations affecting Aβ are located in the final cleaved product, two are at the extremity of the cleavage sites. $A\beta_{1-42}$ has a higher tendency to aggregate and increased toxicity, likely due to the addition of two hydrophobic residues compared to $A\beta_{1-40}$.

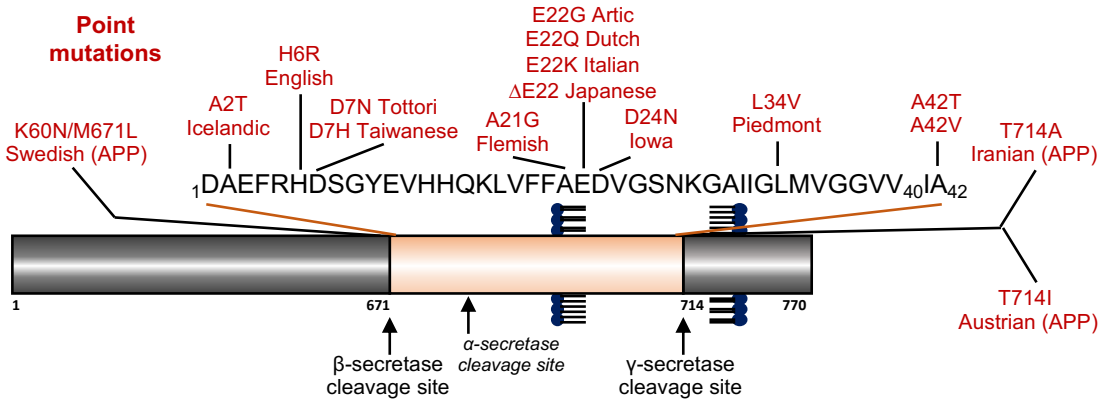

Figure 3: Primary structure of APP & Aβ.
APP 1-714 and the secretase cleavage sites (β- and γ-secretase) leading to $A\beta_{1-40}$ or $A\beta_{1-42}$. The transmembrane portion of APP is visualized between the phospholipids. Mutations in APP or Aβ are annotated. Adapted from Thal et al., 2015.

Tau is a 352-441 residue protein whose mRNA undergoes alternative splicing, leading to six isoforms expressed in the adult human brain (**Figure 4**). These isoforms vary in the number of N-terminal repeats (0N, 1N or 2N) and/or the presence or absence of an additional 31 amino acid repeat sequence from exon 10 (3R or 4R). The domain containing these repeated sequences is the microtubule binding domain. Two hexapeptide sequences in the R2 and R3, ^{275}VQIINK^{280} and ^{306}VQIVYK^{311}, particularly promote aggregation (Falcon et al., 2015; Seidler et al., 2018; von Bergen et al., 2001, 2000). There are eighty potential phosphorylation sites for Tau, with forty shown to be phosphorylated at serine/threonine residues and two at tyrosine residues in PHFs (Iqbal

et al., 2016). Most phosphorylation sites are outside the microtubule binding domain. When phosphorylated, Tau undergoes conformational changes and loses its ability to bind microtubules (Buée et al., 2000; Uversky et al., 1998), and a hallmark pathology of AD is hyperphosphorylated, β-sheet-rich Tau. Tau is truncated *in vivo*, and products such as $Tau_{151-391}$ have been found in AD brain extracts and its overexpression in transgenic rats led to Tau pathology and cognitive defects (Zilka et al., 2006). In addition, Tau undergoes many other post-translational modifications such as sumolation, nitration, lipoperoxidation, O-GlcNacylation, N-glycosylation, and glycation (Iqbal et al., 2016).

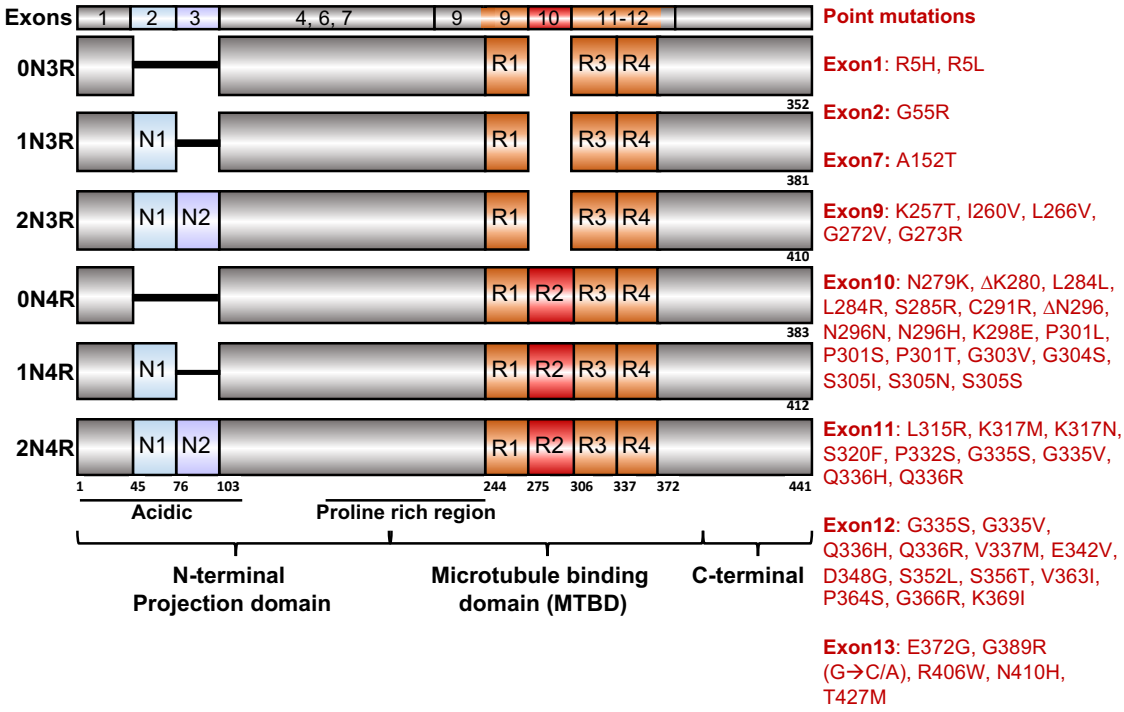

Figure 4: Primary structures of the six isoforms of Tau.
The six isoforms of Tau, with domains and mutations associated with tauopathies, are listed. Adapted from Goedert and Spillantini, 2017; Strang et al., 2019; Vasili et al., 2019.

1.1.3 Huntington's disease

HD is an autosomal dominant polyglutamine disorder and the most common monogenic neurological disorder. Its prevalence and incidence are much smaller in East Asia or Africa, and to date, no worldwide estimate of prevalence or incidence is known

(Bates et al., 2015). It was first thoroughly described by George Huntington in 1872 (Huntington, 1872). It was not until 1993 that the gene *HTT*, coding for the protein huntingtin, was discovered by The Huntington's Disease Collaborative Research Group (Huntington's Disease Collaborative Research Group et al., 1993). This gene has a [CAG] repeat in the first exon that leads to a polyglutamine stretch (polyQ) when transcribed and translated. These researchers showed that 98% of sequenced genes in healthy people had between 11 and 24 repeats, with 34 repeats as the maximum number in their healthy cohort. At the same time, they found 40% of HD patients to have between 42 and 47 repeats and 60% to have over 48 repeats in mutated huntingtin (mHTT). Later on, it was shown that over 41 repeats leads to full penetrance of HD, with partial penetrance for 36-40 repeats and no association for 35 or fewer repeats (McNeil et al., 1997; Rubinsztein et al., 1996). The HTT gene was shown to be unstable, leading to variations in [CAG] length over generations, meaning a parent with intermediate penetrance could have a child with full penetrance, especially if the carrier was male. Most patients have 37 to 48 repeats, while juvenile patients have over 55, as the age of onset of the disease is inversely proportional to the repeat length (Langbehn et al., 2010; Rosenblatt et al., 2006, **Appendix 5**). HD patients exhibit loss of striatal neurons, especially medium spiny neurons (Bates et al., 2015; Ross and Tabrizi, 2011; Walker, 2007). They usually die from problems linked to progressive difficulties with swallowing (Parsons and Raymond, 2015).

The huntingtin protein is a 3144 amino acid (348 kDa) protein mostly expressed in the CNS and testes. It is important for development, as knock-outs are not viable. The CAG repeat site on Exon1 is flanked by a 17-residue N-terminal region (N17) and a proline-rich (PR) region at its C-terminal **(Figure 5**), capable of enhancing or inhibiting polyQ aggregation *in vitro*, respectively (Lakhani et al., 2010; Monsellier et al., 2015).

Following the C-terminal region of Exon1 are 66 exons and clusters of HEAT repeats (huntingtin, elongation factor 3, the PR65/A subunit of protein phosphatase 2A and the lipid kinase Tor; α-helix-loop-α-helix motifs which are involved in protein-protein interactions, Nguyen and Weydt, 2018). Interestingly, the HTT gene can be translated into a RNA transcript that either leads to the full length protein or, in the case of an expanded CAG repeat, only Exon1 (Bates et al., 2015; Neueder et al., 2017). While the full-length protein is predominantly found in the cytosol, pathogenic, N-terminal fragments of mHTT, including those containing the caspase 6 or endopeptidase cleavage sites or corresponding to Exon1 (hereinafter referred to as HTTExon1Qn), accumulate in intranuclear inclusions or inclusion bodies (DiFiglia et al., 1997; Hoffner et al., 2005, IBs, **Figure 1E**). HTTExon1$Q_{>36}$ is sufficient on its own to aggregate and be toxic. With the development of the first transgenic mouse model for HD, where ubiquitous expression of HTTExon1$Q_{>100}$ led to chorea and reduced brain weight, the whole protein was demonstrated to be unnecessary to induce partial symptoms of the disease (Mangiarini et al., 1996). Additionally, conditional models showed that elimination of HTTExon1Q94 expression was sufficient to reduce IBs and behavioral changes (Yamamoto et al., 2000), thereby further connecting protein expression with pathology and associated clinical phenotypes.

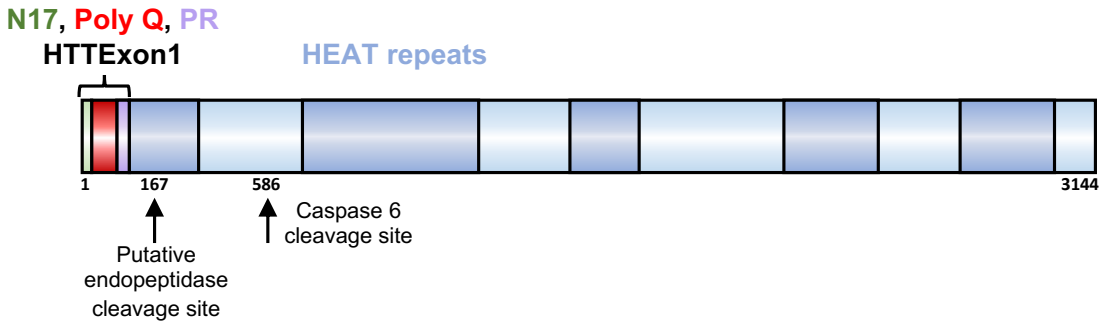

Figure 5: Primary structure of huntingtin (HTT).
Sequence numbers assume a 23 polyQ repeat. Adapted from Ratovitski et al., 2009.

1.1.4 Prion diseases

Prion diseases in mammals, otherwise known as transmissible spongiform encephalopathies (TSEs), are caused by the conversion of soluble prion protein (PrP^{C}) into fibrillar, pathogenic PrP^{sc}, the suffix "sc" alluding to the disease "scrapie" first described in sheep in the 1700s (Prusiner, 1998). This conformational change entails a significant increase in β-sheet content, from 3% to 45% (Colby and Prusiner, 2011). TSEs in humans encompass multiple diseases including kuru, iatrogenic or variant Creutzfeldt-Jakob Disease (i/vCJD), fatal familial insomnia (FFI), and Gerstmann-Sträussler-Scheinker syndrome (GSS). These conditions lead to progressive neurodegeneration, dementia, loss of motor control, and, in all cases, death (Prusiner, 1998). A common pathological hallmark is the accumulation of the prion protein and the presence of "sponge"-like tissue (**Figure 1F**). The origins of these diseases vary from entirely environmental for kuru, spurring from the cannibalistic consumption human tissue, including the brain, by tribes in Papau New Guinea (Liberski et al., 2019), to mostly sporadic for CJD (Gambetti et al., 2003), to entirely genetically linked for FFI (Lugaresi et al., 2006). As mentioned earlier, PrP^{sc} causes scrapie in sheep and goats, as well as chronic wasting disease (CWD) in deer and bovine spongiform encephalopathy (BSE) in cows (Johnson and Gibbs, 1998). Consumption of cows with "mad cow disease" (BSE) in the United Kingdom in the early 1990s is believed to have led to the variant CJD (vCJD), with an earlier age of onset and slower disease progression (Will et al., 1996), demonstrating that PrP^{sc} is capable of crossing the species barrier, with this latter phenomenon being dictated by the different sequences of the prion proteins between species.

Prions, or "PRoteinaceous Infection ONly particles", are pathogenic and infectious proteins capable of causing disease without genetic material. This disruption

of the typical dogma that infectivity requires nucleic acids led to Stanley Prusiner receiving the Nobel Prize in Physiology or Medicine in 1997. At a biochemical level, prions can self-replicate their alternative conformation by initiating endogenous proteins to take on their structural features (Prusiner, 1991), discussed more in the next section. In particular, prions are capable of forming multiple aggregate conformations, leading to structural heterogeneity among proteins of the same sequence, hereinafter referred to as "strains". As a protein's structure governs its function, the strain, or specific conformation of PrP^{sc}, similarly determines the disease. Importantly, pathogenic prion proteins are capable of transmission between cells, organs and organisms, as evidenced by the cases of kuru disease onset following ingestion of pathogenic PrP^{sc} (Liberski et al., 2019). The ability of the protein alone to be infectious through a natural mode of disease transmission is one of the key factors in prion propagation. The concept of pathogenic protein spreading linked to NDs has recently been applied to the protein aggregates involved in PD, AD and HD, among other NDs, although for now they are referred to as "prion-like" diseases for reasons discussed below in section 1.3.4.

1.2 Protein folding and misfolding

1.2.1 Mechanisms of protein aggregation

All of the above NDs are characterized by misfolding proteins. Under normal conditions, proteins could, in theory, fold into an astronomical number of conformations. However, the reality of the energy associated with various conformations dictates the folding of proteins, leading to fewer possible conformations (**Figure 6A**). In particular, folding is driven by the formation of intramolecular contacts among hydrophobic residues to protect them from the polar solvents. During this process, various intermediate conformations will arise, followed by the interaction of key residues in order to form the

native state of the protein, if it has one (Dobson, 2003). For globular proteins, once this native state is reached, the susceptibility of the protein to aggregate is lessened due to its buried hydrophobic regions and the subsequent stabilization of its structure. The drive to protect hydrophobic residues from the solvent, under certain circumstances, leads to aggregation through the establishment of intermolecular contacts. These interactions spawn amorphous or structured amyloid aggregation due to the low energy states of these aggregates (Dobson, 2003).

The energy dynamics of protein folding are dependent on protein sequence. In particular, hydrophobicity, low net charge, and low proline or glycine residue count tip the scale towards aggregation. Furthermore, proteins with frequent repetitive patterns of alternating hydrophobic and hydrophilic residues favor β-sheet formation and thus favor aggregation (Broome and Hecht, 2000). As mentioned earlier, exposed hydrophobic residues favor the intermolecular contacts involved in protein aggregation (Schwartz et al., 2001). In contrast, high net charge can inhibit intermolecular contacts (Chiti and Dobson, 2006). Glycine but more so proline residues, due to their structural constraints that are incorporated with difficulty into β-sheet structure, discriminate against protein aggregation (Lise and Jones, 2005; Parrini et al., 2005). Intrinsically disordered proteins (IDPs), or proteins or fragments lacking a native folded state, have sequences adapted to low aggregation propensity, although this does not prevent aggregation (Campioni et al., 2010).

There are many other possible triggers for aggregation. Spontaneous aggregation during folding, as indicated above, can arise from proteins with aggregation-prone sequences. In addition, IDPs, have fewer intramolecular contacts and are thus free to make intermolecular contacts, thereby leading to aggregation. It is not surprising that many proteins involved in proteinopathies are IDPs: for example, αSyn, Tau, Aβ, and

islet amyloid polypeptide (IAPP), a protein that forms pancreatic aggregates in type 2 diabetes. Another potential trigger is the occurrence of point mutations predisposing the protein towards aggregation (Ono et al., 2011). Certain post-translational modifications, such as phosphorylation for Tau at a few key sites, can increase the propensity of the protein to aggregate (Alonso et al., 2001; Despres et al., 2017). Furthermore, protein expression levels contribute to aggregation propensity, such as occurs with a copy number variation leading to steady state protein levels past a critical threshold. To illustrate, in PD, duplications and triplications of the SNCA gene can lead to early disease onset. Additionally, AD onset is affected by APP gene copy numbers, as is seen with people with Down syndrome who carry an extra copy of the APP locus on chromosome 21 and can develop AD in their forties, as well as sporadic AD cases displaying genetic mosaicism that included multiplications of the APP gene in single neurons compared to healthy controls (Bushman et al., 2015). Furthermore, changes in intracellular environment such as temperature, pH or oxidative stress can induce aggregation (Herczenik and Gebbink, 2008). Lastly, trauma (McKee et al., 2014), toxin exposure (Dauer and Przedborski, 2003), metal ions, or other mechanisms are involved in aggregation onset (Campioni et al., 2010; Sanders et al., 2016).

Naturally, cells have developed multiple defense mechanisms against protein aggregation, notably through the protein quality control (PQC) machinery. The PQC is composed of several pathways designed to stop further aggregation, ensure proper protein trafficking and eliminate existing aggregates. The PQC is composed of molecular chaperones (discussed in chapter 2), the ubiquitin-proteosome system (UPS), and autophagy (chaperone mediated autophagy, microautophagy and macroautophagy). Nonetheless, these mechanisms are not eternally efficient, as their capabilities decline with age (see section 2.1.2).

Amyloid formation is a multi-step process (Eichner and Radford, 2011; Knowles et al., 2014; Morris et al., 2009) (**Figure 6B**). *In vitro*, monomers first find themselves in an aggregation-prone state, allowing for the formation of "on-pathway" (β-structured) oligomers and protofibrils. This period of nucleation is the lag phase, which can be bypassed by adding preformed fibrils as seeds. Next, monomers bind to the exposed ends of the protofibrils in the elongation phase, leading to short and eventually long fibrils with cross-β-structure (Riek and Eisenberg, 2016). Fibrils can be fragmented (Cliffe et al., 2019; Tanaka et al., 2006; Xue et al., 2009), leading to more seeds, thus perpetuating the process.

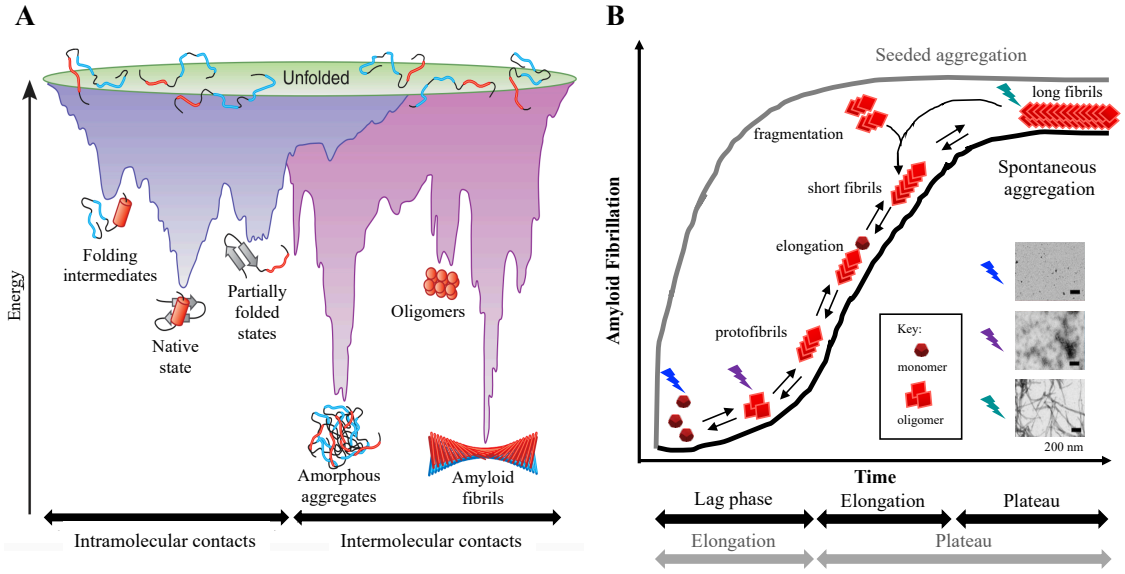

Figure 6: Schematics of protein folding and misfolding.
A) Schematic of the energy landscape of protein folding (Hartl and Hayer-Hartl, 2009). B) Schematic of spontaneous and seeded amyloid aggregation, inspired by Hanspal et al., 2017.

Typically, amyloid fibril formation is followed through measures of β-sheet content (see section 1.2.3), transmission electron (TEM) or atomic force microscopy (AFM), or supernatant-pellet partition experiments, given that fibrils pellet upon centrifugation.

This aggregation process has been identified *in vitro*. Naturally, aggregation within a cellular environment is expected to be much more complicated, as 30% of the space is taken up by macromolecules. Indeed, *in vitro* experiments that demonstrate the impact of crowding on aggregation show that the kinetics are significantly altered compared to the proteins alone (Despa et al., 2005; Munishkina et al., 2004). Furthermore, specific actors in the cell such as reactive oxygen species, metal ions or various macromolecules, can lead to elevated aggregation kinetics (Campioni et al., 2010). This highlights the importance of evaluating the efficiency of inhibitory molecules in cellular environments.

1.2.2 Toxicity: gain or loss of function?

Protein aggregates lead to toxicity through loss-of-function, gain-of-function, or a combination of the two mechanisms. While much less common, loss-of-function mechanisms act as primary causes for toxicity in diseases such as Gaucher's disease and cystic fibrosis due to the loss of the essential functions of β-glucocerebrosidase (Sidransky, 2012) and cystic fibrosis transmembrane conductance regulator (CFTR) (Moran, 2017), respectively. On the other hand, most proteinopathies manifest primary toxicity linked to the cellular dysfunction caused by misfolded proteins (**Figure 7**). This gain-of-function toxicity can be accompanied by a lesser loss-of-function toxicity, as has been described, for example, for phosphorylated Tau which loses its ability to bind microtubules (Johnson and Stoothoff, 2004), or for mHTT, which has impaired regulation of vesicular transport of neurotrophic factors like BDNF (brain-derived neurotrophic factor, Gauthier et al., 2004; Pineda et al., 2009; Saudou and Humbert, 2016). In addition, aggregated proteins can lead to loss-of-function toxicity for other proteins, such as what occurs with the clustering of membrane proteins upon fibril binding (Shrivastava et al., 2017).

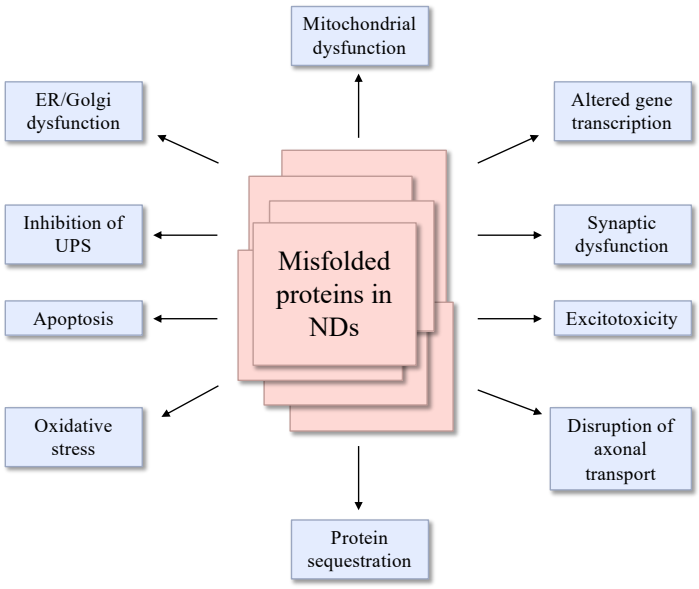

Figure 7: Mechanisms for gain-of-function toxicity in proteinopathies. Adapted from (Forman et al., 2004; Villar-Piqué et al., 2016; Wong and Krainc, 2017; Zuccato et al., 2010). *ER* endoplasmic reticulum;

1.2.3 Amyloid fibrils

Structure

Amyloid fibrils are composed of β-strands running perpendicular to the fibril axis (cross-β structure, **Figure 8A**). This cross-β structure is stabilized thanks to the intermolecular hydrogen bonds formed between the backbone amide and carbonyl groups of the stacking monomers. Amyloid fibrils are often microns in length and 5-15 nm in diameter (Toyama and Weissman, 2011). They are composed of 2-8 protofilaments of 2-7 nm in diameter that either twist around each other or stack laterally upon each other.

The cross-β structure, a hallmark of amyloids, was first identified thanks to the X-ray fiber diffraction pattern of amyloids (**Figure 8B**). Spectrometry techniques like circular dichroism (CD) or fourier-transform infrared spectroscopy (FTIR, **Figure 8C**) show specific β-sheet and amyloid β-sheet signatures (Byler and Susi, 1986). The cross-β structure, in most cases, allows for the use of dyes like Thioflavin-T (ThT), Thioflavin-S (ThS), Congo Red, or Primuline, which upon binding to amyloid fibrils display altered spectral properties (Biancalana and Koide, 2010), as readouts for amyloid fibrillation

(**Figure 8D**). This can however lead to false negatives if the binding site to these molecules is perturbed, such as through a mutated residue or through competitive binding with partners or contaminants present in some dye solutions (Schütz et al., 2011).

Due to their large size, obtaining atomic resolution structures of amyloid fibrils through traditionally pursued methods such as X-ray crystallography or solution-state NMR cannot be applied. Nonetheless, some structures of amyloid fibrils of short peptides formed *in vitro*, for example derived from Aβ or TDP-43, have been elucidated. The majority of structures of amyloid fibrils formed *in vitro* are from cryostatic electron microscopy (cryo-EM) for amyloid cores (Fitzpatrick and Saibil, 2019; Gremer et al., 2017; Guerrero-Ferreira et al., 2019, 2018; Li et al., 2018b; Murzin et al., 2019) and solid state nuclear magnetic resonance (ss-NMR) for amyloid cores or full-length fibrils (Bousset et al., 2013; Gath et al., 2014; Hoop et al., 2016; Tuttle et al., 2016). Recently, improvements in aggregate extraction from patient brains of Tau filaments has led to the *ex-vivo* cryo-EM structures associated with AD (Fitzpatrick et al., 2017), Pick's disease (Falcon et al., 2018) and chronic traumatic encephalopathy (Falcon et al., 2019).

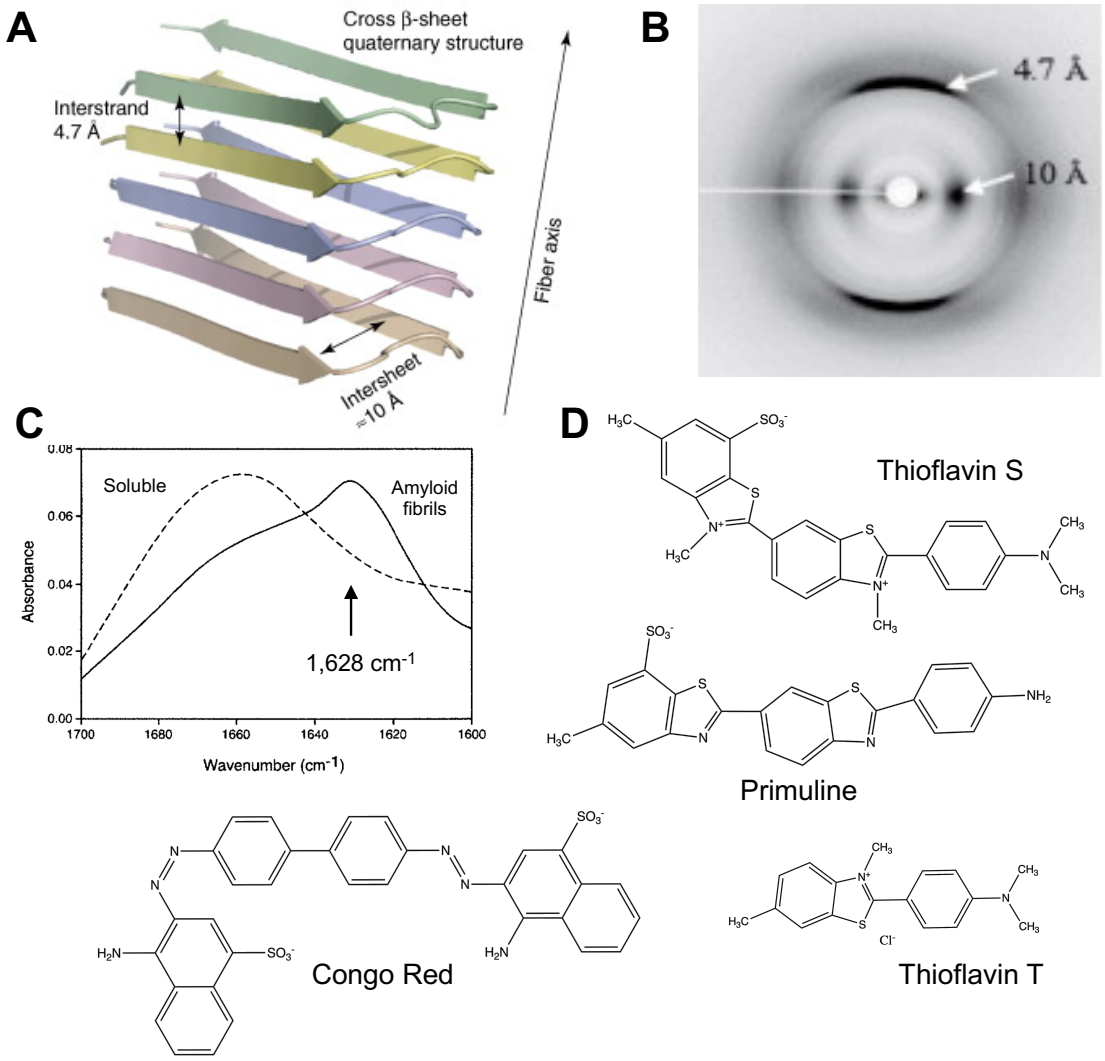

Figure 8: Structural elements for amyloid fibril recognition.
A) Cross β-sheet quaternary structure with the 4.7 Å interstrand and 10 Å intersheet distances, as exemplified by $A\beta_{1\text{-}42}$ fibrils (PDB ID: 2BEG). **B)** X-ray fiber-diffraction pattern displaying the characteristic reflections at 4.7 Å and 10 Å, from the interstrand repeats and the intersheet packing, respectively. A-B are from (Fowler et al., 2007). **C**) FTIR spectra of soluble P301S-1N4R and fibrillar P301S-1N4R Tau. The signature amyloid fibril β-sheet peak at 1,628cm^{-1} is indicated (Berriman et al., 2003). **D)** Structures of four molecules that exhibit fluorescence changes upon binding to amyloid fibrils. They are thought to intercalate between β-sheets, or as was shown for Congo Red, to bind parallel to the fibril axis (Schütz et al., 2011).

Strains

While all amyloids share the cross-β quaternary structure, secondary structure variations due to environmental conditions such as pH or salt content in which the fibrils

were formed can lead to conformational heterogeneity (Riek and Eisenberg, 2016), notably affecting the segmentation and packing of the core, how the protofibrils intertwine, or both (Lutter et al., 2019). One method to identify the different strains is through limited proteolysis, as exposed regions will be cleaved first, leading to "molecular barcodes" for different fibrils with unique regions exposed to solvents (**Figure 9A**). In addition, high-resolution structures, primarily through ss-NMR and cryo-EM, have elucidated differences between the strains, notably in the core (Gath et al., 2014; Lutter et al., 2019). *In vitro*, αSyn and Aβ were shown to produce differently structured fibrils depending on the conditions in which they were formed (Bousset et al., 2013; Petkova et al., 2004) (**Figure 9B**). *Ex vivo* studies of Tau straight or paired helical filaments (SHF, PHF) or narrow or wide Pick's filaments from AD or Pick's disease patient brains, respectively (Falcon et al., 2018; Fitzpatrick et al., 2017) (**Figure 9C**), as well as Aβ fibrils formed from seeds from AD patient brains with different clinical symptoms (Qiang et al., 2017; Tycko, 2015), were shown to have different structures, suggesting that strains in other NDs may resemble those of prion proteins, where each strain leads to a different disease (Brundin and Melki, 2017). The large clinical spectrum of Tauopathies, for example, could be in part explained because of the heterogeneity of Tau aggregates in patient brains (Dujardin et al., 2018). This concept has been further supported in cellular and animal model studies, with the appearance of different pathologies, regional vulnerability, seeding capacity, and behaviors depending on the strain used or the disease associated with the brain-derived material (Bousset et al., 2013; Clavaguera et al., 2013; Dujardin et al., 2018; Gribaudo et al., 2019; Kaufman et al., 2017, 2016; Peelaerts et al., 2015; Sanders et al., 2014; Woerman et al., 2016).

Relevance of *in vitro* fibrils

Since the discovery of the main proteins encompassing neuronal deposits in NDs, studies have been conducted using aggregated proteins purified *in vitro*. There remains some controversy as to the relevance of using these model fibrils. Fibrils formed *in vivo* are formed in much more complex cellular milieus than preformed fibrils, leading to the probability of high rates of heterogeneity not taken into account in *in vitro* studies. Additionally, fibrils formed from proteins expressed in *E.coli* bacteria, as is commonly done, do not have any post-translational modifications, which are known to influence the formation and behavior of amyloid fibrils (Alonso et al., 2001; Despres et al., 2017; Johnson and Stoothoff, 2004; Samuel et al., 2016). In addition, Tau fibrils, routinely formed *in vitro* in presence of polyanions like heparin, had different structures than brain-derived Tau aggregates (Murzin et al., 2019). Furthermore, Tau fibrils formed *in vitro* with heparin were more resistant to proteinase K digestion and guanidine hydrochloride disaggregation than Tau fibrils present in P301S transgenic mice brain homogenates or Tau fibrils formed *in vitro* through seeding with the above-mentioned homogenates. Detailed, high resolution structures of brain-derived fibrils besides Tau have yet to be elucidated, so it is unclear how their structures may differ from fibrils formed in controlled conditions. Nevertheless, evidence presented in the next section demonstrates that fibrils formed *in vitro* are able to propagate between neuronal cells and lead to pathology reminiscent of their associated NDs, suggesting clinical relevance.

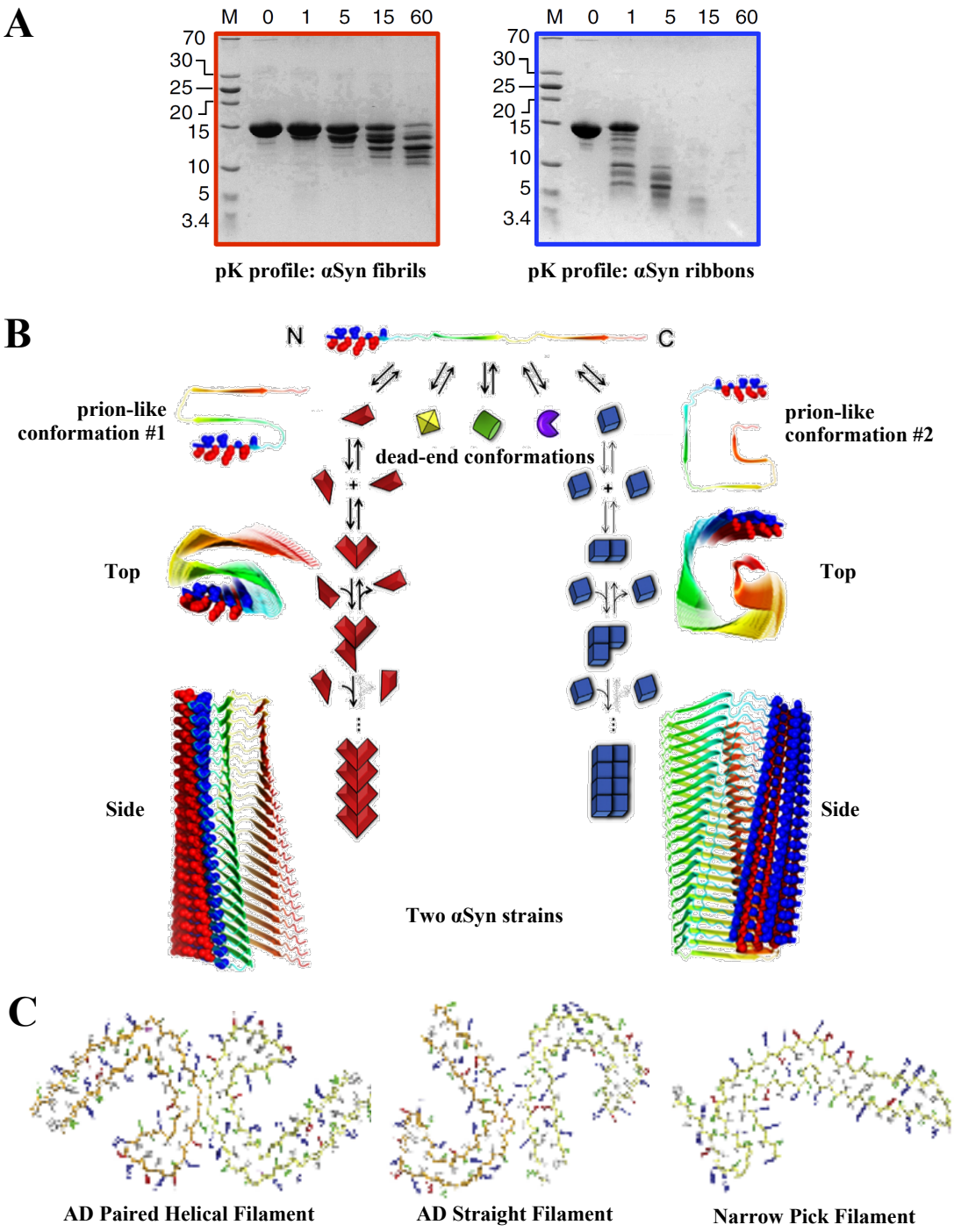

Figure 9: Structural polymorphism of amyloid fibrils.
A) Proteinase-K (pK) profiles of αSyn fibril and ribbon strains via sodium dodecyl sulfate polyacrylamide gel electrophoresis (SDS-PAGE). *M* minutes proteolysis (Bousset et al., 2013). **B**) Schema of strain formation from an unfolded monomer to two amyloid strains. (Peelaerts et al., 2018). **C**) Cryo-EM structures of *ex-vivo* Tau aggregates from AD and Pick's disease patient brains (Lutter et al., 2019).

1.3 Fibril Propagation

1.3.1 Principle and evidence of propagation in prion-like diseases

First evidence in humans

The idea that αSyn aggregates could propagate, transfer, transmit or spread between neuronal cells in the brain of PD patients (hereinafter referred to as "propagate") initially came after the discovery by Braak and colleagues that PD patients at early stages had αSyn-positive LB and LN pathology in olfactory structures and the dorsal motor nucleus, whereas patients at late stages had pathology in interconnected brain regions (Braak et al., 2004, 2003a) **(Figure 10A)**. Specifically, stage one begins with lesions in the olfactory bulb, dorsal motor nucleus of the vagus, and anterior olfactory nucleus (Ordonez et al., 2018). In the second stage, pathology is found in the lower raphe nuclei, the locus coeruleus, and the magnocellular portions of the reticular formation (Prots et al., 2018). The third stage is defined by pathology in the midbrain, notably in the substantia nigra pars compacta (Braak et al., 2003a). While cognitive decline increases from stage three onward, most clinical symptoms arise during stage four, when pathology moves to the mesocortex but not the neocortex (Braak et al., 2006c, 2003b, 2003a). Finally, in stages five and six, the pathology reaches the prefrontal neocortex followed by the premotor areas, the primary sensory areas and the primary motor field. In summary, the pathology follows anatomical connections throughout the brainstem, limbic and autonomic system and finally the neocortex. The aforementioned stages are still used today for diagnostics and are referred to as "Braak staging" I-VI. While not pictured in **Figure 10A**, another theory is that αSyn pathology could begin in the gastrointestinal tract, propagating up the vagal nerve into the brain (Braak et al., 2006b). However, patients do not always follow Braak staging, with reports of 17–49% of some degree of divergence (Rietdijk et al., 2017). It may be that more aggressive PD patients better fit

Braak staging than late onset PD patients (Halliday et al., 2008). Further studies are thus required to better stratify the heterogenous pool of PD patients.

In AD, patients also manifest progressive Tau pathology (**Figure 10B**) that correlates with clinical symptoms (Braak et al., 2006a, 1993; Braak and Del Tredici, 2016). First, Tau neurofibrillary changes, or neurofibrillary tangles, neuropil threads, and/or neuritic plaques, appear in the transentorhinal region during stage one before reaching the entorhinal regions during stage two. Clinical dementia is not present yet. Next, the Tau neurofibrillary changes progress to the hippocampus in stage three, followed in stage four by other limbic areas such as the medial temporal gyrus as well as the insular cortex. Finally, in stages five and six, the neurofibrillary changes reach the neocortex and primary sensory areas. As is the case for αSyn pathology, Tau pathology progresses through connected brain regions, as exemplified by the case of an AD patient who had a disconnected area of the frontal cortex, due to a surgical lesion, leaving the frontal cortex free of Tau pathology (Duyckaerts et al., 1997). Nonetheless, the exact reasons behind the selective vulnerability of certain connected regions over others are not clear. Indeed, while the dentate gyrus is connected through the performant path to the entorhinal cortex, which is the region affected in stage one of AD, the dentate gyrus is only affected in stage six. Lastly, in contrast to Tau neurofibrillary changes, Aβ pathology progression is not dictated by the same anatomical connections and is poorly correlated with cognitive decline (Nelson et al., 2012).

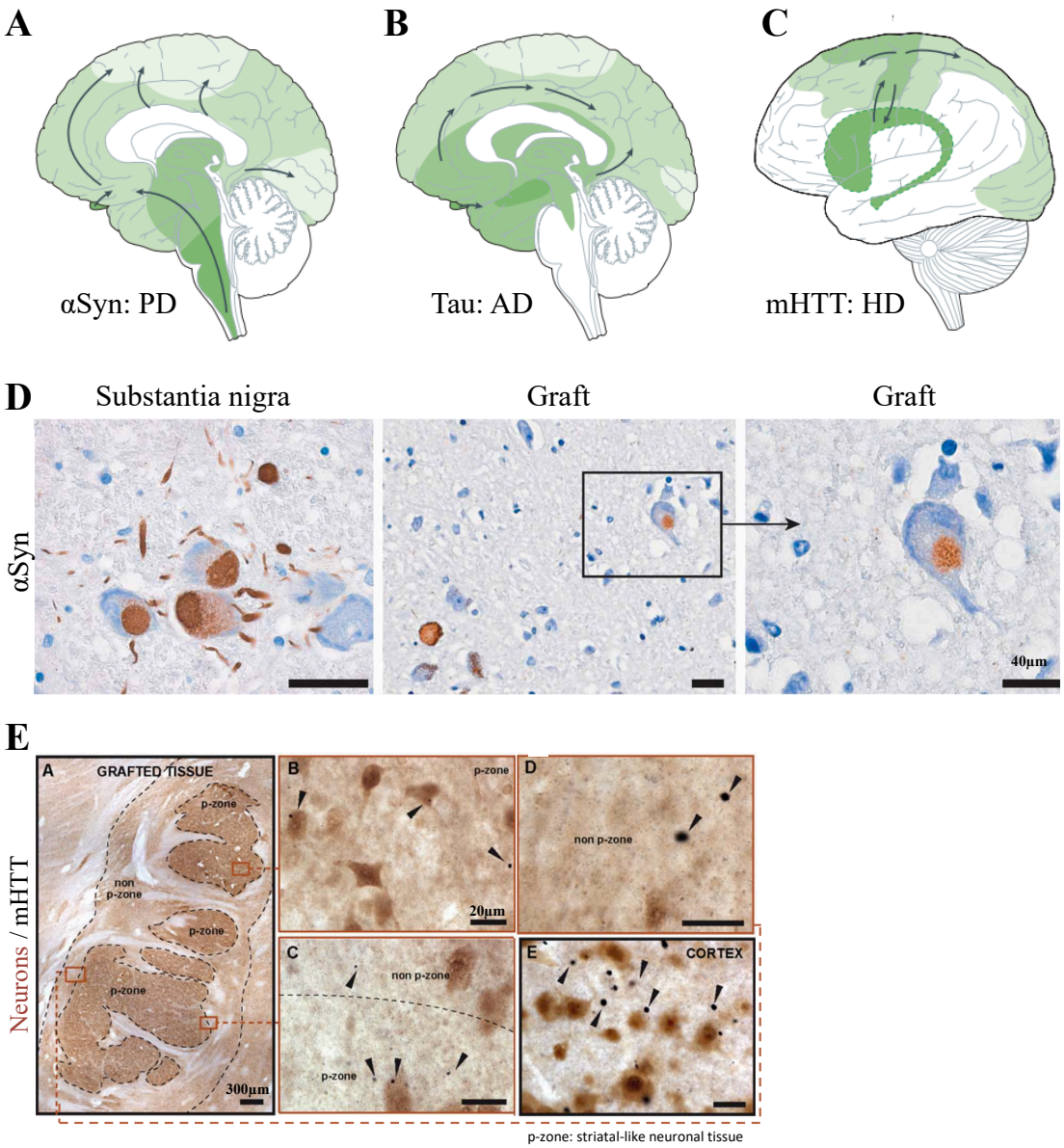

Figure 10: First evidence in humans for prion-like propagation in PD, AD and HD. **A-C**) Stereotypical progression of αSyn Lewy bodies and neurites, Tau neurofibrillary tangles and mHTT pathology in brains of patients with PD, AD and HD, respectively (Brundin et al., 2010). Regions with pathology appearing earlier in time are darker green. Mid-sagittal view for PD and AD; lateral view for HD. **D)** αSyn-positive Lewy bodies in a dopaminergic neuron graft in a PD patient 16 years after transplantation (Li et al., 2008). **E)** mHTT-positive inclusions in striatal grafted tissue in a HD patient 9 years after transplantation (Cicchetti et al., 2014).

In HD, stereotypical pathology progression can equally be observed. Through brain imaging studies of pre-symptomatic carriers (Rosas et al., 2008), cortical degeneration was implicated in the earliest stages of the disease. Later stages are characterized by degeneration of the putamen and caudate nucleus of the striatum (**Figure**

10C) (Aylward et al., 2004; Vonsattel et al., 1985). While cognition and motor symptoms are correlated with the stereotypical progression mentioned above, psychiatric and behavioral symptoms do not fit a stepwise progression in accordance with disease severity (Walker, 2007).

The original speculation that aggregated proteins propagate throughout the brain was supported by post-mortem analyses on PD patients who had received striatal grafts of embryonic neural tissue in order to replace damaged dopaminergic neurons. Over ten years after the procedure, αSyn-positive LB and LN pathology was found in the cells of the grafted tissue (**Figure 10D**, Kordower et al., 2008; Kurowska et al., 2011; Li et al., 2008). Notably, this pathology was detected in 2-5% of grafted cells, similar to the percentage of neurons with Lewy pathology in the SNpc in PD. However, for patients surviving 24 years, this number increased to 11-12% of grafted dopaminergic neurons, demonstrating that the appearance of Lewy pathology was ongoing (Li et al., 2016). Similarly, six years later, mHTT aggregates were found in HD patient brain grafts a decade after the procedure (**Figure 10E**, Cicchetti et al., 2014). However, it is worth noting that the deposits were only found in the extracellular matrix (ECM) whereas in ungrafted patient brains, deposits are found in neurons, neuropil, the ECM, and blood vessels (Cicchetti et al., 2014). Recently, transplants of cell suspension allografts in HD patients demonstrated that mHTT pathology was found within cell bodies of the innervated grafted tissue twelve years after the surgery, unlike what was seen for solid tissue transplants (Maxan et al., 2018). While the appearance of αSyn or mHTT aggregates in the grafted tissue could have arisen from propagation of aggregates present in neighboring cells in these patients' brains, we cannot exclude the possibility that it also could be due to aggregation induced by the trauma of placing the grafts, inflammation, excitotoxicity, oxidative stress, and/or loss of neurotrophic support (Braak and Del

Tredici, 2008; Brundin et al., 2008; Cicchetti et al., 2011, 2009; Newell et al., 1999). To investigate the first hypothesis, researchers established *in vivo* and cellular models to determine whether aggregate propagation is possible and how it functions.

Propagation to transplanted grafts in animal models

Initially, experiments replicating aspects of the graft studies in humans found that in αSyn over-expressing mice or rats, αSyn pathology was identified in the graft site in either the hippocampus (Desplats et al., 2009) or the striatum (Angot et al., 2012; Hansen et al., 2011; Kordower et al., 2011). Both grafting stem cells or mature neurons led to this phenomenon. The appearance of αSyn pathology in the grafted cells was not observed in WT mice (Desplats et al., 2009). While most HD animal models with stem cell transplants did not display mHTT pathology (Holley et al., 2018), one study did observe mHTT pathology in IPSC striatal grafted tissue a later time point of 33 weeks (Jeon et al., 2012). These results encouraged the development of various cellular and animal models to further explore the hypothesis of amyloid fibril propagation and elucidate its mechanisms.

Cellular models for propagation studies

Cellular models are particularly useful for the identification of specific aspects of mechanisms of intercellular propagation of aggregated proteins, are discussed in more detail below in section 1.3.2. *In vitro* experiments utilize a wide range of cell types, including non-neuronal cell lines such as cervical cancer Henrietta Lacks (HeLa) cells or human embryonic kidney (HEK293) cells, neuronal cell lines like the mouse Neuro-2a or human SH-SY5Y or PC-12, primary rodent cultures (neuronal and non-neuronal), and (patient-derived) induced (neuronal and non-neuronal) pluripotent stem cells (iPSCs).

Most experiments rely on three basic models with either expression of or exposure to the amyloidogenic proteins of interest. First are the common experiments using single cultures with either exposition to or (over)expression of amyloidogenic proteins (**Figure 11A-B**). In the second type of experimental cellular models, inoculation of conditioned medium from one separate culture into another, or contact-independent co-culture, allows for the study of the lifecycle of exported proteins and the capacity of serial propagation of amyloid aggregates (**Figure 11C-E**). In particular, certain exported material like exosomes or aggregates can be concentrated before secondary application. Contact-independent culture can be established using a filter to only allow exported material to enter the acceptor culture or through microfluidic devices. Experiments with inoculation of conditioned medium allowed for the demonstration of an "inter-organism" level of spreading by amyloid fibrils. For example, Tau and SOD1 were shown to propagate over serial passages in cultures (Grad et al., 2014; Kaufman et al., 2016). Furthermore, microfluidic experiments allow for the precise control over the microenvironments in which presynaptic and postsynaptic neurons interact. Experiments with microfluidic devices have been particularly helpful in demonstrating the anterograde and retrograde transport of αSyn (Brahic et al., 2016; Freundt et al., 2012; Volpicelli-Daley et al., 2011), Tau (Wu et al., 2013), Aβ (Brahic et al., 2016; Freundt et al., 2012) and mHTT (Brahic et al., 2016) fibrils.

In the third type of experimental model are those utilizing contact-dependent co-culture models, for example using *ex-vivo* (organotypic slice) cultures (Loria et al., 2017; Pecho-Vrieseling et al., 2014), 3D cultures (Cantley et al., 2018; Choi et al., 2014), larger 3D organoids called "mini-brains" (Koh et al., 2018), or simple co-cultures (**Figure 11F-G)**. Co-culture models or models exposing conditioned medium to acceptor cells need to

pay particular attention to the cell density, proliferation and death of the donor and acceptor cells, as they can impact the level of protein transfer (Reyes et al., 2015).

Acceptor cells, which are used in three types of models, merit further discussion. They often express amyloidogenic proteins fused to tags such as GFP and mCherry to distinguish proteins from the exogenous donor or donor cell and those from the acceptor cell, therefore permitting colocalization studies that can equally distinguish endogenous protein aggregation (**Figure 11H**). Alternatively, the donor and acceptor cell can each express one half of a tag that requires both halves to be in close proximity in order to fluoresce, thereby visualizing internalization-dependent interaction with the endogenous protein (**Figure 11I**). Instead, each cell type could express proteins containing different epitopes for FRET (Fluorescence Resonance Energy Transfer) antibodies. These techniques have been heavily exploited in the studies of seeding mechanisms.

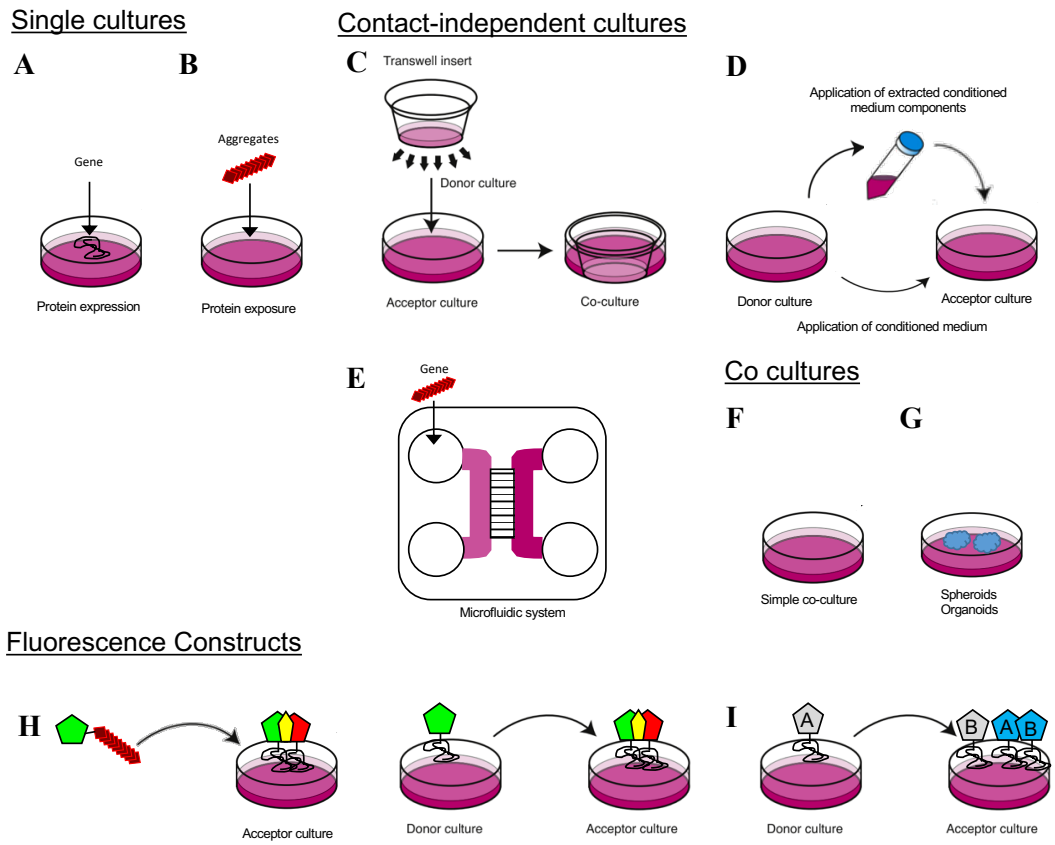

Figure 11: Various cellular models for examining fibril propagation.
Adapted from (Hanspal et al., 2017).

Propagation induced by exogenous aggregate exposure

It is important to address the specific role fibrillar aggregates play in neuronal propagation. Many experiments have subsequently been done to examine the propagation of Tau, αSyn, mHTT, Aβ, and SOD1 fibrils, such as in ND models through exposure of either preformed fibrils or brain-derived aggregates in cells or animals, as summarized non-exhaustively for αSyn, Tau and mHTT aggregates in **Table 2.** For this table, propagation is defined as (i) the induction of seeding, i.e. the induction of aggregation of endogenous monomers (see section 1.3.2), or (ii) positive staining for various antibodies or stains that recognize aggregated proteins or phosphorylated sites found in human brain aggregates (**Appendix 6**). These studies cover a wide range of experimental conditions, with notable usages of WT or transgenic non-human primate, rodent or cellular models, *in vitro* preformed or human or animal brain-derived aggregates, and WT or mutated fibrils.

Due to the varied cellular and animal models available, it is important to evaluate these studies by examining the conditions in which the experiments were done. For example, if an overexpression model is being used, what are the relative expression levels and location compared to those in sporadic or familial disease? It is for this reason that witnessing fibril propagation in WT cellular and animal models was an essential step in validating the infectivity of aggregated proteins in associated ND model expose to preformed fibrils, as well as animal or human brain derived aggregates, has been observed in WT mice, rats and marmosets (**Table 2**). Nonetheless, WT animals are less sensitive to preformed aggregate-induced pathology than transgenic or adeno-associated virus (AAV)-injected animals. This difference is well demonstrated by the absence of glial inclusions in the rat brain after injection with αSyn ribbons in WT rats compared to A53T-rAAV2/7 rats (Peelaerts et al., 2015). As for Tau, data using Tau preformed fibrils

injected into WT mice examines internalization, but does not examine seeding or intercellular propagation of pathology (Holmes et al., 2013). Innoculation with preformed Tau K18PL fibrils in WT mice did not induce propagation (Peeraer et al., 2015). Expose to brain homogenates in WT animals has led to variable results. Un-sonicated PHF from AD brains, when injected into WT mice, did not lead to propagation, while Tau oligomers from the same brains did in an endogenous-Tau dependent manner (Lasagna-Reeves et al., 2012). Whether the PHF seeds would be capable of seeding in a more potent transgenic model, or whether PHFs prepared in this particular manner do not seed Tau pathology, was not explored further. Nonetheless, induction of Tau pathology in WT mice was observed after injection of sarkosyl-insoluble PHFs from AD brains which were briefly sonicated before injection (Guo et al., 2016). To further support the notion that aggregates are indeed the infectious species that induce pathology, brain-derived aggregates immunodepleted of Tau or αSyn were unable to induce seeding (Guo et al., 2016; Recasens et al., 2014).

Seeding requires the presence of endogenous protein, as exemplified by the lack of pathology in KO animals or cells after exposure of preformed or brain-derived fibrils (Kim et al., 2019; Luk et al., 2012; Peelaerts et al., 2015; Recasens et al., 2014; Volpicelli-Daley et al., 2011). Furthermore, the efficiency of seeded aggregation is proportional to the sequence similarity between the soluble protein and the aggregated seed (Colby and Prusiner, 2011). This explains the slightly or significantly reduced levels of propagation in rodent models with induction of human fibrillated material (Rey et al., 2016). Despite sequence differences, human fibrils, or fibrils containing a mutation, are able to seed or be seeded in various animal and cellular models. For example, addition of mHTT to WT cells and animals is able to induce aggregation of WT HTT (Masnata et al., 2019).

Nonetheless, among proteins of the same sequence, not all species seed at the same rates. Multiple studies have found MSA aggregates to be the most aggressive, followed by those from DLB and then those from PD, with sometimes a total absence of pathology induction using PD samples (**Table 2**). The aggressiveness of MSA seeds is not unexpected given the fast time course of disease onset. Perhaps propagation of PD-derived material requires particular cellular conditions, found in patients but not fully replicated in animal models. As for Tauopathies, seeds from brains of patients with different diseases led to Tau pathology reminiscent of what is seen in the disease from where they originated (Clavaguera et al., 2013).

A non-negligible aspect of the prion hypothesis in NDs is the spatiotemporal propagation of pathology. It is thus important that the animal models used to identify and characterize therapeutic molecules equally experience this phenomenon. Many studies have shown that αSyn propagates trans-synaptically. Nonetheless, some propagation did not appear to follow neuroanatomic connectivity, thus indicating other mechanisms for αSyn propagation (Sorrentino et al., 2017). Interestingly, PD brain extracts injected into the gastric walls of an A53T mouse model induced propagation in the brain (Lee et al., 2011). Furthermore, propagation of αSyn preformed fibrils was abolished when the injection followed the severing of the vagus nerve (Kim et al., 2019; Uemura et al., 2018). These and other (Holmqvist et al., 2014; Ulusoy et al., 2017; Van Den Berge et al., 2019) studies support propagation via the vagus nerve and the involvement of the gastric system and as a potential site of early aggregation in PD .

Most studies have exposed animals to fibrils through intracerebral, intraperitoneal, or intravenous injection. One recent study, however, challenged one of the primary hallmarks of prion diseases and demonstrated that αSyn pathology can be induced through oral administration of fibrils, albeit with significantly reduced efficiency and

penetration as compared to multiple modes of injection (Lohmann et al., 2019). This suggests that if αSyn fibrils were able to enter the environment and be ingested by a healthy person, that they may risk the development of pathology in the healthy individual. However, the doses required (50µg or 500µg) for pathology induction in only two or four out of eight mice, respectively, suggest that this risk is likely very low. As of now, this accidental transfer of αSyn has never been witnessed in humans, and with the awareness of a potential health risk associated with αSyn-contaminated materials, along with studies demonstrating the proper decontamination methods for various αSyn aggregated species (Fenyi et al., 2018), accidents are unlikely to occur as they did in the past for Aβ or PrP^{sc} (see section 1.3.4).

Protein	Type of Seed	Non-neuronal cells propagation	Neuronal cells propagation	Animal model	Aggregates employed ***In vivo* propagation**: yes = ●, no = ○ **Motor defects**: yes = ■, no = ⌂, not tested = nt **Cognitive defects**: yes = ◆, no = ◇, not tested = nt
αSyn	Preformed synthetic fibrils	Yes[1]	Yes[2–12]	WT mice[5,7,12–16]	hPFFs (● nt nt)[13,16] (● ⌂ nt)[14]; (● ⌂ nt)[5]; mPFFs (● nt nt)[14,16]; (● ■ nt)[15]; (● ■ nt)[12];(○ nt nt)[23]; C136T-mPFFs(● nt nt)[7]
				WT rats[17,18]	hPFFs (● ■ nt)[17]; hPFRs (● ⌂ nt)[17]; hPFFs (● ⌂ nt)[18]
				WT marmosets[19]	mPFFs (● nt nt)[19]
				M20 mice	hPFFs (● nt nt)[23]
				Gfap-luc$^{+/-}$ mice[20]	mPFFs (○ nt nt)[20]
				M83$^{+/-}$ Gfap-luc$^{+/-}$ mice[20]	hPFFs (● nt nt)[20]
				M83$^{+/-}$ mice[21]	hPFFs (● nt nt)[21]
				M83$^{+/+}$ mice[22]	hPFFs (● nt nt)[22], hαSyn$_{1-120}$-Myc PFFs (● nt nt)[22]
				A53T-rAAV2/7 rats[17]	hPFFs (● ■ nt)[17]; hPFRs (● ■ nt)[17]
				WTαSyn-AAV6 rats[18]	hPFFs (● ■ nt)[18]
	Animal brain samples			M83$^{+/+}$ mice[22,24]	Old M83$^{+/+}$ mice bh (● nt nt) [22,24]
				αSyn$^{-/-}$ mice[22]	Old M83$^{+/+}$ mice bh (○ nt nt)[22]
				WT rats[17]	Old Thy1-hA30P mice bh (● ⌂ nt)[17]
				A53TrAAV2/7 rats[17]	Old Thy1-hA30P mice bh (● ■ nt)[17]
	Human brain samples	Yes (MSA bh)[25]	Yes (DLB exosomes)[26]	WT mice[27,28]	PD nigral LB (● nt nt)[27]; PD nigral LB id for αSyn (○ ntnt)[27]
					PD stellate ganglia purified aggregates (○ nt/nt)[28]
					DLB si bh fraction (● nt nt)[14]; (● nt nt)[7]
			Yes (MSA >> DLB si fractions)[7]		DLB bd exosomes (● nt nt)[26]; MSA si bh fraction (● nt nt)[7]
				WT/MPTP macaques[27]	PD nigral LB (● ⌂ nt)[27]
				M83$^{+/-}$ mice[25,29]	MSA bh (● nt nt) [25,29]; PD bh (○ nt nt)[25]
				mαSyn$^{-/-}$-hαSyn$^{+/+}$ mice[30]	iLBD si cortical be (● ⌂ nt)[30]
					MSA si cortical be (● ⌂ nt)[30]
				αSyn$^{-/-}$ mice[27]	PD nigral LB (○ nt nt)[27]
PolyQ	Preformed synthetic fibrils	Yes[31–33]	Yes[31,32]	WT mice[31]	HTTExon1Q25 fibrils (○ ⌂ ◇)[31]; HTTExon1Q48 fibrils (● ■ ◇)[31]
				R6/2 mice[31]	HTTExon1Q25 fibrils (○ ⌂ ◇)[31]; HTTExon1Q48 fibrils (● ■ ◆)[31]
					HTTExon1Q72 fibrils (● nt nt)[34]
	Human samples		Yes (HD143F exosomes)[35]		

Tau	Preformed synthetic fibrils	Yes[36,37]	Yes[3,36,38–40]	WT mice[41] 2N4R mice[41] 2N4R P301L mice[36,41] PS19 mice[38]	K18PL fibrils (○ nt nt)[41] K18PL fibrils (○ nt nt)[41] Short fibrils (● nt nt)[36]; K18PL fibrils (● nt nt)[41] 2N4R-P301S-K18PL tau fibrils (● nt nt)[38]
	Animal brain samples	Yes[36]		ALZ17 mice[42] P301S mice$^{+/+}$[42–44]	hP301S tau mice bh (● nt nt)[42] hP301S Tau mice bh (● nt nt)[42] WT mice bh injected 18m prior with AGD bh (● nt nt)[42] Old P301S mice bh with HMW, AT8+ AT100+ nitrated tau (● nt/nt)[43] Old P301S mice bh (● nt/nt)[44]
	Human brain samples		Yes (AD si Tau filaments); No (id Tau)[45] Yes (CTE, PSP, AGD, CBD bh)[46]	Young WT mice[47 48] Old WT mice[45] ALZ17 mice[48]	AD PHF (○ nt ◇)[47] ; AD si PHF (● nt nt)[45]; AD, TD, AGD, and PSP bh (● nt nt)[48] AD si PHF (● nt nt)[45] AD, TD, PiD, AGD, PSP, CBD bh(● nt nt)[48]

Table 2: Cellular and *in vivo* evidence of αSyn, mHTT and Tau fibril propagation after aggregate inoculation.

Non exhaustive compilation of experiments demonstrating aggregate-induced propagation. *AGD* Argyrophilic grain disease; *ALZ17* 2N4R$^{+/+}$ under the human neural Thy1 promoter; *Bd* brain derived; *bh* brain homogenate, includes both soluble and insoluble material; *CBD* Corticobasal degeneration; *CTE* Chronic traumatic encephalopathy; *h* human; *HD143F* fibroblasts from a juvenile HD patient; *id* immunodepleted; *iLBD* incidental Lewy Body disease; *K18PL* truncated (Q244-E372)-P301L; *m* murin; *M20* WT αSyn under the mouse prion promoter; *M83* αSyn A53T under the mouse prion promoter; *pff* preformed fibrils; *pfr* preformed ribbons; Tau 2N4R; *PHF* paired helical filament; *PiD* Pick's disease; *PS19* 1N4R-P301S under the mouse prion promoter; *PSP* Progressive Supranuclear Palsy; *R6/2* HTTExon1Q144$^{+/+}$; *si* sarkosyl-insoluble; *TD* Tangle only dementia.

1. Luk, K.C. et al. *Proc. Natl. Acad. Sci.* 2009
2. Volpicelli-Daley, L.A. et al. *Neuron* 2011
3. Nonaka, T. et al. *J. Biol. Chem.* 2010
4. Mao, X. et al. *Science* 2016
5. Tarutani, A. et al. *J. Biol. Chem.* 2016
6. Lee, H.J. et al. *Biochem. Biophys. Res. Commun.* 2008
7. Tarutani, A. et al. *Acta Neuropathol. Commun.* 2018
8. Gribaudo, S. et al. *Stem Cell Reports* 2019
9. Sacino, A.N. et al. *J. Neurochem.* 2017
10. Brahic, M. et al. *Acta Neuropathol.* 2016
11. Freundt, E.C. et al. *Ann. Neurol.* 2012
12. Ren, X. et al. *Mol. Ther. - Nucleic Acids* 2019
13. Masuda-Suzukake, M. et al. *Acta Neuropathol. Commun.* 2014
14. Masuda-Suzukake, M. et al. *Brain* 2013
15. Luk, K.C. et al. *Science* 2012
16. Rey, N.L. et al. *J. Exp. Med.* 2016
17. Peelaerts, W. et al. *Nature* 2015
18. Thakur, P. et al. *Proc. Natl. Acad. Sci.* 2017
19. Shimozawa, A. et al. *Acta Neuropathol. Commun.* 2017
20. Breid, S. et al. *J. Virol.* 2016
21. Lohmann, S. et al. *Acta Neuropathol.* 2019
22. Luk, K.C. et al. *J. Exp. Med.* 2012
23. Sorrentino, Z.A. et al. *Mol. Neurodegener.* 2017
24. Mougenot, A.L. et al. *Neurobiol. Aging* 2012
25. Prusiner, S.B. et al. *Proc. Natl. Acad. Sci.* 2015
26. Ngolab, J. et al. *Acta Neuropathol. Commun.* 2017
27. Recasens, A. et al. *Ann. Neurol.* 2014
28. Recasens, A. et al. *Acta Neuropathol. Commun.* 2018
29. Watts, J.C. et al. *Proc. Natl. Acad. Sci.* 2013
30. Bernis, M.E. et al. *Acta Neuropathol. Commun.* 2015
31. Masnata, M. et al. *Acta Neuropathol.* 2019
32. Ren, P.-H. et al. *Nat. Cell Biol.* 2009
33. Ko, J. et al. *Hum. Mol. Genet.* 2018
34. Pecho-Vrieseling, E. et al. *Nat. Neurosci.* 2014
35. Jeon, I. et al. *Acta Neuropathol.* 2016
36. Wu, J.W. et al. *J. Biol. Chem.* 2013
37. Guo, J.L. & Lee, V.M.Y. *J. Biol. Chem.* 2011
38. Iba, M. et al. *J. Neurosci.* 2013
39. Holmes, B.B. et al. *Proc. Natl. Acad. Sci.* 2013
40. Evans, L.D. et al. *Cell Rep.* 2018
41. Peeraer, E. et al. *Neurobiol. Dis.* 2015
42. Clavaguera, F. et al. *Nat. Cell Biol.* 2009
43. Jackson, S.J. et al. *J. Neurosci.* 2016
44. Ahmed, Z. et al. *Acta Neuropathol.* 2014
45. Guo, J.L. et al. *J. Exp. Med.* 2016
46. Woerman, A.L. et al. *Proc. Natl. Acad. Sci.* 2016
47. Lasagna-Reeves, C.A. et al. *Sci. Rep.* 2012
48. Clavaguera, F. et al. *Proc. Natl. Acad. Sci.* 2013

1.3.2 Factors and steps of fibril propagation

Studies described in the above paragraphs have established that propagation occurs by the following steps. In brief, for aggregates added to the extracellular medium, exogenous aggregates will bind to the cell membrane, be internalized and escape into the cytoplasm, after which they will come into contact with endogenous, soluble proteins and induce their aggregation. These new aggregates will then be exported, perpetuating the cycle.

Membrane binding: partners of preformed fibrils

The plasma membrane is the first barrier encountered by extracellular fibrillar aggregates before cellular internalization. Indeed, it has been shown that amyloid fibrils do not freely diffuse past the membrane (Grey et al., 2011; Lee et al., 2008b; Mao et al., 2016), unlike monomers. Extracellular fibrils thus enter the cell through protein, lipid, or ECM component-assisted internalization or lipid permeabilization (**Figure 12B**). Their lateral binding to the cell membrane, demonstrated for αSyn and HTTExon1Q48 fibrils (Monsellier et al., 2016), theoretically allows for more simultaneous binding partners than if they bound the cell membrane through their ends.

Fibrils interact with cell surface proteins and lipids through both nonspecific and specific interactions. PolyQ aggregates were shown to bind membrane proteins through nonspecific interactions. Indeed, pre-treatment of cells by trypsin, a protease that cleaves non-integral membrane proteins, before fibril exposure reduced membrane binding for PolyQ aggregates. Blocking of low affinity, nonspecific binding sites with BSA led to a similar reduction of membrane binding, indicating that the exposed membrane proteins removed through trypsin are likely to bind PolyQ aggregates with low affinity (Trevino et al., 2012).

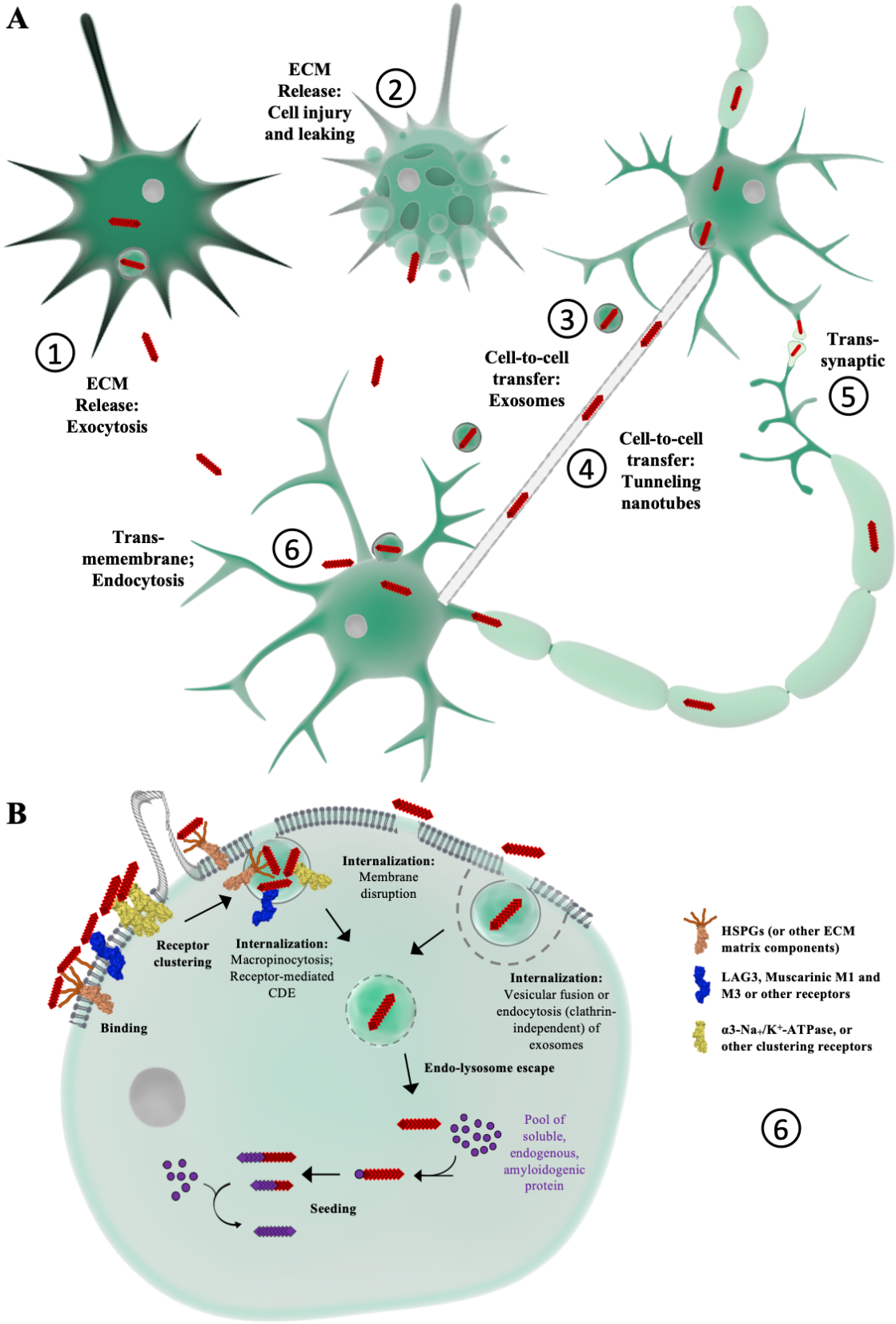

Figure 12: Cellular and molecular mechanisms of fibril propagation.
A: Different pathways for intercellular fibril propagation. **B:** Transmembrane fibril interactions, internalization, and seeding of endogenous proteins into new fibrils, able to

be exported to perpetuate the cycle. *MAP* macropinocytosis; *CDE* clathrin-dependent endocytosis; *ECM* extracellular matrix; *HSPG* heparan sulfate proteoglycans; *LAG3* lymphocyte-activation gene 3. Adapted from Bieri et al., 2018; Grozdanov and Danzer, 2018; Guo and Lee, 2014; S. J. Lee et al., 2010; Shrivastava et al., 2017; Vargas et al., 2019.

Specific interactions have also been demonstrated for amyloidogenic proteins and lipids. First, fibrils (Bousset et al., 2013; Grey et al., 2011; Pieri et al., 2012), oligomers (van Rooijen et al., 2008) or monomers (Burke et al., 2013; Kegel et al., 2009, 2005; Volles and Lansbury, 2002) better associate with anionic lipids than zwitterionic lipids. In addition, amyloidogenic proteins have been shown to interact with the gangliosides GM1 and GM3 (Chi et al., 2007; Di Pasquale et al., 2010; Fantini and Yahi, 2013; Martinez et al., 2007; Shrivastava et al., 2017), two types of amphiphilic glycolipids on the outer membrane with attached sugar residues that are highly enriched at synapses. Lastly, amyloidogenic proteins bind to cholesterol (Fantini et al., 2011). With respect to huntingtin fibrils, although mHTT from a transgenic mouse model was found with lipid raft-enriched, detergent-resistant membranes, its fibrillar nature was not verified (Kegel et al., 2009). Furthermore, fibrillation of both αSyn and Aβ has been shown to increase in presence of certain lipids (Alza et al., 2019; Hellstrand et al., 2013; Rangachari et al., 2018; Ugalde et al., 2019).

αSyn, Tau and Aβ fibrils have been shown to interact with different identified protein partners (Shrivastava et al., 2017). For specific partner identification, transmembrane protein knockout screenings or pull-downs with affinity-tagged or labeled fibrils followed by mass spectrometry have been implemented. For example, identified through the latter proteomics approach, is a protein partner for αSyn, Tau 1N3R and 1N4R fibrils and Aβ oligomers: the α3-subunit of Na^+/K^+-ATPase (NKA), with additional α1 and β1 subunits identified for Tau fibrils (Ohnishi et al., 2015; Shrivastava et al., 2019, 2015). Interestingly, mutations in α3-NKA are linked to rapid-onset dystonia

Parkinsonism (Shrivastava et al., 2018). αSyn fibrils, more so than oligomers or monomers, bind the essential α3-NKA membrane protein. αSyn fibril clustering at the membrane led to α3-NKA redistribution and alteration of its ion pumping capabilities (Shrivastava et al., 2015), while Tau clustering led to a reduced amount of α3-NKA at the synapse (Shrivastava et al., 2019). In addition, Tau fibrils disrupted NKA complexes. Because the α1 subunit was not shown to interact with αSyn fibrils, replacing α1-residues in the α3 sequence led to three chimeras for key residue identification. In particular, mutating $Leu(L)_{878}$ and $Asn(N)_{879}$ led to a significant loss of fibrillar-αSyn induced changes in NKA diffusion (**Appendix 7**) (Shrivastava et al., 2015).

The proteomics-based approach, validated with immunoprecipitation, also led to the identification of AMPA (α-amino-3-hydroxy-5-methylisoxazole-4-propionic acid) receptor GluA1 and GluA2 subunits and NMDA (N-methyl-D-aspartate) receptor GluN2 and Glu2NB subunits as protein binding partners for Tau fibrils (Shrivastava et al., 2019). Tau clustering led to an increase of the GluA2-AMPA receptor at synapses, which could lead to variations in calcium influx. Finally, αSyn fibrils were shown to enhance fibrillar Tau clustering, demonstrating that cross-talk of the two fibrillar proteins, found together in brains of patients with late stage AD and PD, could exacerbate fibril-induced toxicity. Tau also may engage in another form of cross-talk, although this time with APP. An indirect experiment showed, through analysis of downstream seeding, that the N-ter extracellular domain of APP facilitates the internalization of Tau fibrils (Takahashi et al., 2015). However, the experiment did not address whether this comes from direct binding to APP in the cell membrane or from alterations in membrane fluidity due to APP's interaction with cholesterol.

Another protein partner for αSyn fibrils is the neuronally expressed LAG3 (lymphocyte-activation gene 3, part of the immunoglobin family), identified through

transmembrane receptor screening in SH-SY5Y cells (X. Mao et al., 2016). It binds extracellular, preformed αSyn fibrils with nanomolar affinity (K_D of 71 nM) and negligibly binds monomers. Tau 2N4R and Aβ fibril binding was unaffected by LAG3 knockouts, implying that LAG3 is a specific receptor for αSyn fibrils. Fibril binding to LAG3 was followed by endocytosis, phosphorylation at S129, propagation, and toxicity. In addition, all the steps of the propagation cycle were drastically reduced in LAG3 knockout neuronal cultures and in presence of a LAG3 antibody. For example, $LAG3^{-/-}$ mice were spared from reduced tyrosine hydroxylase (TH)- and dopamine transporter (DAT)- positive neurons as well as behavioral defects following αSyn fibril injections. It should also be noted that Mao et al also identified two other protein partners for αSyn fibrils, albeit with weaker selectivity: neurexin 1β and Aβ Precursor Like Protein 1 (APLP1), although functional tests were not performed (X. Mao et al., 2016). Neurexin 1α/2α were also identified in the proteomic screen for αSyn fibrils referenced above, similarly without further pursuit (Shrivastava et al., 2015).

Next, αSyn, Tau, and Aβ, PrP^{sc}, but not mHTT fibrils have been shown to bind to members of the cell adhesion system, specifically heparan sulfate proteoglycans (HSPGs), which are transmembrane or glycolipid-anchored proteins linked to glycosaminoglycan (GAG) heparan sulfate sugars (Holmes et al., 2013; Horonchik et al., 2005; Stopschinski et al., 2018). In particular, the length and sulfation pattern of GAG sugars greatly affect binding and subsequent internalization in a fibril-specific manner (Stopschinski et al., 2018). Inhibition of HSPGs, through genetically blocking the enzyme required for their synthesis or their competitive binding with heparin sugars, blocks fibril entry in cells (Holmes et al., 2013; Horonchik et al., 2005; Stopschinski et al., 2018) and in mice (Holmes et al., 2013).

Furthermore, Tau fibril binding and subsequent dysfunction of calcium homeostasis has been linked to M1 and M3 muscarinic receptors, as identified by using specific agonists and following calcium levels (Gómez-Ramos et al., 2008). These receptors are found in high abundance in adult mice hippocampi and entorhinal cortices, which are regions affected by AD (Braak et al., 2006a). Lastly, Aβ fibrils have been shown to bind a large myriad of cell membrane proteins (Jarosz-Griffiths et al., 2016; Shrivastava et al., 2017; Verdier et al., 2005).

Internalization

Internalization is commonly studied by some or a combination of techniques such as co-localization with proteins implicated in the endocytotic pathway, two-stage immunofluorescence with impermeable and permeable antibodies, fluorescence-activated cell sorting (FACS), the removal of membrane bound fibrils with exposure to trypsin or pronase, western blots, and the addition of trypan blue, a non-permeable compound that quenches extracellular fluorescence, thereby only revealing fibrils at the interior of the cell for microscopy or fluorescence readouts. Fibril internalization has repeatedly been shown to be time dependent and blocked by a temperature drop to 4˚C (Falcon et al., 2015; Lee et al., 2008b; Ruiz-Arlandis et al., 2016), thus implicating endocytosis. Endocytosis pathways are dependent on the size of aggregates, with those from 200 nm to 5 μm going through macropinocytosis ("bulk endocytosis") and those below 100 nm going through micropinocytosis (Lim and Gleeson, 2011). Micropinocytosis comprises multiple mechanisms, mainly separated into clathrin-dependent and independent endocytosis, which subset in turn includes caveolin-dependent and flottilin-dependent endocytosis, among others.

Dynamin, a GTPase involved in the fission of endocytic vesicles from the plasma membrane, is necessary for clathrin- and caveolin-dependent endocytosis. The use of dominant-negative mutants or dynasore have shown that fibrils of αSyn (Abounit et al., 2016; Gribaudo et al., 2019; Lee et al., 2008b; Reyes et al., 2014; Sacino et al., 2017) and mHTT (Ruiz-Arlandis et al., 2016) pass through dynamin-dependent endocytosis. On the other hand, Tau fibril internalization has both been shown to be unaffected (Holmes et al., 2013) and reduced by dynamin inhibitors (Calafate et al., 2016; Evans et al., 2018), and thus more data is needed to better understand the impact of dynamin-mediated mechanisms on its internalization. Interestingly, in a microfluidic model with proximal and distal cortical neurons, uptake of αSyn fibrils was more affected by dynasore in distal neurons than in proximal ones, suggesting different mechanisms for local and distal inter-neuronal uptake (Gribaudo et al., 2019).

Inhibition of receptor/clathrin-dependent endocytosis through genetic or pharmacological manipulations reduced fibrillar αSyn (Gribaudo et al., 2019; Mao et al., 2016; Oh et al., 2016) and mHTT (Ruiz-Arlandis et al., 2016) uptake. αSyn and Tau fibril internalization was increased with addition of an inducer of non-specific, adsorptive-mediated endocytosis, thus implicating yet another pathway of entry (Guo and Lee, 2011; Volpicelli-Daley et al., 2011). Additionally, non-dynamin inhibitors of clathrin-dependent endocytosis reduced uptake of mHTT and αSyn fibrils (Oh et al., 2016; Ruiz-Arlandis et al., 2016), while Tau fibrils co-localize with Dextran10 (Calafate et al., 2016), known to go through clathrin-/dynamin-dependent endocytosis as well as macropinocytosis (Li et al., 2015). Notably, expression of BIN1, a protein involved in clathrin-dependent endocytosis, was inversely correlated with Tau propagation (Calafate et al., 2016). The implication of BIN1 in Tau propagation is of particular interest as its gene is the second most common locus for increased late-onset AD risk (Karch and Goate,

2015). It was surprising, however, to see Tau propagation affected by clathrin-dependent endocytosis in light of the fact that previous experiments showed no change in uptake after knock down of clathrin heavy chain (Holmes et al., 2013). Furthermore, clathrin-independent endocytosis, such as through caveolin- or flotillin-dependent endocytosis, has been implicated for αSyn (Kobayashi et al., 2019; Lee et al., 2008b) but not mHTT (Ruiz-Arlandis et al., 2016) fibrils.

Lastly, macropinocytosis was examined as a mechanism of entry for fibrils. αSyn (Holmes et al., 2013; Stopschinski et al., 2018), Tau (Calafate et al., 2016; Falcon et al., 2015; Holmes et al., 2013; Santa-Maria et al., 2012) and mHTT (Zeineddine et al., 2015) fibril uptake co-localized with Dextran10 or was decreased by blocking macropinocytosis, although in one experiment αSyn fibrils were not sensitive to the Na^+/H^+ exchanger inhibitor, ethylisopropyl amiloride (EIPA), typically used to block macropinocytosis (Zeineddine et al., 2015). Notably, HSPG-dependent macropinocytosis of αSyn fibrils was more common in neurons and oligodendrocytes than in astrocytes and microglia, where other methods of internalization are likely more important (Ihse et al., 2017). Importantly, it must be noted that many inhibitors of endocytotic pathways are not as specific as claimed and can affect cell viability (Dutta and Donaldson, 2012; Vercauteren et al., 2010). Thus, multiple modes of inhibition should be tested in order to confidently implicate one pathway over another in fibril internalization mechanisms.

Internalization rates have also been measured by cell type, with varying rates per cell and per fibril. For example, αSyn fibrils were more internalized by microglia (Lee et al., 2008a) and astrocytes than cortical neurons (Cavaliere et al., 2017; Loria et al., 2017). Additionally, other experiments observed uptake in oligodendrocytes (Reyes et al., 2014), astrocytes (Lee et al., 2010b), and microglia (Liu et al., 2007; Pearce et al., 2015), with notable implication of phagocytosis as a mechanism of glial entry for HTTExon1Q96

aggregates (Pearce et al., 2015). In summary, amyloid fibrils are internalized by multiple different endocytotic pathways in various cell types.

Another mechanism of fibril entry is through disruption of the cellular membrane. Ca^{2+} release after exposure to fibrils, indicating membrane permeabilization, has been demonstrated many times in cells (Bousset et al., 2013; Monsellier et al., 2016; Pieri et al., 2012). $K_2Q_{44}K_2$ fibrils were found in the cytoplasm and did not colocalize with endocytosis markers (Ren et al., 2009), suggesting either direct membrane penetration or an escape from the endo-lysosomal compartments at an earlier time than the experiment readout. Furthermore, calcein or Cal-520 (a Ca^{2+}-sensitive dye) release assays with synthetic vesicles have equally demonstrated lipid permeabilization by fibrils (Bousset et al., 2013; Flavin et al., 2017; Kundel et al., 2018; Pieri et al., 2012).

Seeding

Since fibrils have been shown to primarily enter cells through endocytosis, they will need to escape into the cytoplasm, for example through compromising endo-lysosomal integrity, as was demonstrated for fibrillar αSyn (Flavin et al., 2017; Freeman et al., 2013) and Tau (Calafate et al., 2016). Lysosomal integrity is studied through the ability of a fluorescently-tagged Galectin3 to bind target β-galactosides, which are sugars exclusively found on the exterior leaflet of the plasma membrane or the inner leaflet of internalized vesicles (Di Lella et al., 2011). The loss of a diffuse fluorescently-tagged Galectin3 cellular localization and the appearance of distinct puncta can thus be used to identify endo-lysosomal rupture.

Seeding experiments are often based on the use of reporter WT or mutant proteins, as mentioned above in section 1.3.1. Once in the cytoplasm in presence of their endogenous, monomeric protein, the fibrils can act as seeds and induce nucleation and

aggregation, leading to the formation of new fibrils (Angot et al., 2012; Bousset et al., 2013; Desplats et al., 2009; Falcon et al., 2015; Frost et al., 2009; Gerez et al., 2019; Hansen et al., 2011; Jucker and Walker, 2013; Kfoury et al., 2012; Luk et al., 2009; Peelaerts et al., 2018; Ren et al., 2009; Volpicelli-Daley et al., 2011) (**Figure 12B**). In addition, fragmentation of fibrils, such as by the proteosome holoenzyme for αSyn and Tau fibrils (Cliffe et al., 2019), participates in the creation of new seeds. However, not all seeds are created equal. For example, differences in seeding ability *in vitro* and *in vivo*, not always in a correlated fashion, were observed for Tau strains formed in cells (Kaufman et al., 2017, 2016; Sanders et al., 2014). Interestingly, seeds for mHTT in the cerebrospinal fluid (CSF) of HD patients were able to induce aggregation of mHTT in cultured cells and cell-free lysates (Tan et al., 2015). In addition, fibrils can lead to altered protein expression, disrupted chaperone function, and thus an imbalance of proteostasis, thereby augmenting endogenous protein aggregation indirectly (Cavaliere et al., 2017; Chafekar and Duennwald, 2012; Gidalevitz et al., 2006; Yu et al., 2019).

Export

Amyloidogenic proteins involved in NDs lack a signal peptide that would enable them to be secreted by cells through the typical pathway. Nonetheless, multiple mechanisms have been proposed for fibrillar export into the extracellular milieu (**Figure 12A**). Trans-synaptic secretion following transport along axons, independent of axonal lysis, was reported for αSyn, $A\beta_{1-42}$ and mHTT fibrils (Brahic et al., 2016). Notably, exocytosis has been identified as a primary mechanism of export. Specifically, αSyn fibrils were found to go through endoplasmic / golgi-independent exocytosis (Lee et al., 2005) (**Figure 12A**).

Alternatively, membrane permeabilization by fibrils can lead to cell injury, which coupled with other cellular dysfunction, leads to cell death, resulting in the release of fibrils (Mahul-Mellier et al., 2015; Milanesi et al., 2012; Xue et al., 2010) (**Figure 12A**).

Importantly, fibrils have been found in the extracellular medium. For example, αSyn fibrils were observed in cell culture milieu (Brahic et al., 2016; Lee et al., 2005), with over half of the observed fibrils undergoing export (Brahic et al., 2016). In humans, various species, including αSyn oligomers, were found in the CSF (Borghi et al., 2000; El-Agnaf et al., 2006, 2003; Mollenhauer et al., 2008) and plasma (El-Agnaf et al., 2006, 2003). The presence of fibrils in these fluids was not determined. Interestingly, more αSyn was found in the CSF of PD and DLB patients compared to controls, so its secretion, regardless of the exact species, may be clinically pertinent (El-Agnaf et al., 2006). In addition, the αSyn present in the CSF was found to be primarily from CNS cells (Mollenhauer et al., 2012).

Similarly, Tau species were found in cell culture milieus (Pernègre et al., 2019) and CSF of mouse models (Yamada et al., 2011). Indeed, phosphorylated-Tau to Tau ratios are a CSF biomarker for AD (Schöll et al., 2019). The aggregated nature of these Tau species was not always elucidated. If it is in fact a majority of soluble Tau found extracellularly, seeding could potentially be induced due to the presence of "seed-competent" Tau monomers (Mirbaha et al., 2018). This concept will need to be replicated by independent laboratories and explored further to demonstrate its therapeutic relevance.

The presence of mHTT in the extracellular milieu also has been demonstrated. As mentioned earlier, seed-competent mHTT was found in CSF from HD patients at higher rates than in healthy patients (Tan et al., 2015). In addition, other amyloidogenic proteins like SOD1 (Winer et al., 2013) and TDP-43 (Junttila et al., 2016) or Aβ (Shaw et al., 2009) are all found in the CSF of patients with ALS or AD, respectively, more so than in

healthy controls. Lastly, mHTT aggregates were found in the ECM of grafts years after transplants (Cicchetti et al., 2014). This supports the idea that their export, whether passive or active, is linked to the pathogenesis of disease.

Cell-to-cell transfer pathways

Fibrils found in the ECM through the methods of export stated above can then bind the cell before internalization, seeding, fragmentation, and export again. Alternatively, some fibrils may never enter the extracellular space (**Figure 12A**). These fibrils are capable of transferring between cells through multiple mechanisms. First, exosomes, or small membrane vesicles of 40-150 nm (Yong and Kim, 2017) originating from the endocytic pathway, have been shown to contain fibrils of Tau (Saman et al., 2012; Wang et al., 2017), αSyn (Emmanouilidou et al., 2010; Ngolab et al., 2017) and mHTT (Jeon et al., 2016). Second, tunneling nanotubes, or membranous, actin-rich passages connecting the cytoplasm of two distant cells (Rustom et al., 2004), provide a way for fibrils to propagate without reaching the extracellular milieu. This mechanism has been implicated for Tau (Tardivel et al., 2016), αSyn (Abounit et al., 2016; Rostami et al., 2017) and mHTT (Costanzo et al., 2013) fibrils, among others.

Aggregate nature and propagation capacity

The efficiency of fibril propagation is linked to two factors: variations in the types of aggregates and in the partners they encounter during the process. First, propagation depends on the sequence of the aggregates, as is the case with HTT (Burke et al., 2013; Kegel et al., 2009, 2005) or exemplified by the reduced rates of propagation when using mixed sequence models such as rodents with human amyloidogenic proteins (Rey et al., 2016). Nonetheless, proteins with the same sequence but with different conformations (strains) do not lead to propagation in the same manner (Bousset et al., 2013; Clavaguera

et al., 2009; Gribaudo et al., 2019; Guo and Lee, 2011; Kaufman et al., 2016; Sanders et al., 2014).

Furthermore, the higher β-sheet content of fibrillar aggregates compared to amorphous aggregates was also shown to increase internalization (Trevino et al., 2012). In addition, the charge of aggregates impacts their initial binding with the cell membrane, with positively charged residues preferentially binding to the negatively charged and complex lipid mixtures (Pieri et al., 2012; Trevino et al., 2012). Finally, aggregate size has been appreciably explored. Propagation has been found to favor smaller fibrils in cellular models and in vivo (Jackson et al., 2016; Rey et al., 2016; Tarutani et al., 2016; Tesei et al., 2018; Wu et al., 2013). In addition, shorter αSyn fibrils have been found to be more toxic than long fibrils (Xue et al., 2010). The increased propagation of smaller fibrils could be due to the size limitations of endocytotic vesicles contributing to fibrillar internalization. The impact of aggregate size is interwoven with that of pH and ionic strength. For example, at low ionic strengths, Aβ peptide fibrils of short lengths have greater affinity to lipid bilayers than longer fibrils. However, this size-dependent difference is less prominent at high ionic strengths due to more dominant repulsion forces (Tesei et al., 2018). Finally, the size of the aggregates also affects their membrane binding abilities. For example, mHTT fibrils suffered a drastic reduction of their ability to bind Neuro-2a cell membranes after sonication, implicating the need for multiple, proximal binding sites (Monsellier et al., 2016). In contrast, αSyn long and short fibrils were shown to have equal membrane binding to Neuro-2a cells, implying that less proximal binding sites are required (Monsellier et al., 2016). Therefore, different stages in the propagation process, such as membrane binding and internalization, are impacted in different ways by aggregate size.

In summary, propagation of prion-like proteins is a complex process with multiple partners and steps involved.

1.3.4 Prion or prion-like?

In order for the amyloidogenic, propagating proteins mentioned above to be considered prions, or proteinaceous infectious particles, they need to fulfill a certain number of requirements (Kraus et al., 2013). First, the misfolded aggregates must be able to recruit endogenous proteins into aggregated forms. This property has been demonstrated for αSyn, Tau, mHTT and many other fibrils, as described above. Second, the prion aggregates are conformation-specific, with different strains leading to different diseases. While there is some evidence to support the notion of strains among αSyn and Tau fibrils (Bousset et al., 2013; Dujardin et al., 2018), the implication of these strains in the determination of a specific synucleinopathy or tauopathy is unclear. Nonetheless, some research suggests that for αSyn, strains could be linked to PD or MSA onset (Peelaerts et al., 2015). Furthermore, mice injected with homogenates from patient brains with different Tauopathies developed pathologies similar to what is seen in humans (Clavaguera et al., 2013). Third, prion aggregates are resistant to proteases and many disinfecting agents, a phenomenon equally witnessed with other amyloid fibrils, albeit to lesser degrees (Fenyi et al., 2018).

Fourth, prions are capable of intercellular transmission. Multiple types of amyloid fibrils are internalized by cells and can travel along axons and across the synapse. This concept can be pushed further, with the fifth prion property of tissue migration. Indeed, αSyn, Tau and Aβ, mHTT and TDP-43 have spatiotemporal progression in the brains of PD, AD, HD and ALS patients, respectively (Jucker and Walker, 2013). Sixth, spreading of the pathology happens between organs. This has been observed with αSyn, with fibrils

delivered to the gastric system leading to neuronal pathology (Lee et al., 2011; Lohmann et al., 2019) as well as the identification of gastric αSyn aggregates in PD patients, notably before the appearance of motor symptoms (Fenyi et al., 2019; Shannon et al., 2012). Nonetheless, the enteric nervous system to CNS fibril transfer phenomenon was rare (Manfredsson et al., 2018) and its implication in the triggering of synucleinopathies is still unclear. As for Tau and mHTT fibrils, no evidence of organ spread exists.

Seventh and last, the protein alone must be sufficient for infection. In particular, the protein must go through what are considered natural routes of disease transmission. This would therefore require exogenous seeds to enter the CNS peripherally and lead to disease. As of now, there is no definitive evidence in humans for this infectivity in proteinopathies other than TSEs. The closest proof was for patients who received prion-contaminated cadaveric pituitary-derived growth hormone (CGH), later shown to also contain Aβ and Tau (Duyckaerts et al., 2018; Purro et al., 2018). It was revealed that some relatively young iCJD patients had grey matter, vascular and pituitary gland Aβ pathology that did not co-localize with prion protein deposits (Jaunmuktane et al., 2015; Ritchie et al., 2017). In addition, Aβ pathology was found in patients that died of CJD-independent causes, indicating that Aβ can seed in the absence of prion pathology (Ritchie et al., 2017). Interestingly, none of these patients nor others who equally developed Aβ pathology after receiving CGH treatment or dura mater grafts (Frontzek et al., 2016; Kovacs et al., 2016; Preusser et al., 2006) developed NFT pathology, indicating that while Aβ could potentially be infectious, it did not lead to full AD pathology, at least not in these cases. However, 90% did have signs of cerebral Aβ−amyloid angiopathy (CAA), a disease linked to Aβ deposition in blood vessels that is detected at autopsy in many AD cases (Cali et al., 2018). In contrast, brains from a French cohort had only one Aβ-positive case and three cases with atypical Tau (Duyckaerts et al., 2018). While it is

possible that this Tau pathology was induced by Tau seeding, we cannot eliminate the possibility that it is a byproduct of prion pathology, as Tau pathology occurs in sCJD (Kovacs et al., 2017). In addition, when Tau pathology in iCJD cases was compared to sCJD or non-ND cases, no difference was observed, suggesting age is the primary factor rather than Tau exposure in these cases (Cali et al., 2018). Perhaps if the patients exposed to Aβ and Tau seeds had lived longer (the oldest patients studied were 63 years old), their autopsies would have revealed a more typical AD pathology.

The classification of prion-like instead of prion proteins may not be the most ideal solution. Indeed, choosing to downplay a potential risk of interhuman transfer of amyloidogenic proteins like αSyn, Tau, Aβ or mHTT could have serious health consequences for those working with brain samples and for organ or blood receivers from patients harboring these NDs, if this risk is proven significant. Clearly, these proteins are not as infectious as PrP^{sc}: micrograms of αSyn are needed to induce pathology in animal models, while only picograms of PrP^{sc} are effective (Watts, 2019). The definition of a prion could be expanded to include these other proteins and to use a scale of infectivity, as is acknowledged for viruses and bacteria. For example, different strains among synucleinopathies, such as those derived from MSA brains, seem to be more infectious than those from PD (Prusiner et al., 2015; Woerman et al., 2019, 2018). No matter which term is used, it is widely accepted that these amyloidogenic proteins are capable of prion-like propagation between cells and that the spatiotemporal appearance of pathology is associated with disease progression. This makes fibril propagation a therapeutic target of interest.

1.3.5 Fibril propagation as a new therapeutic target

One of the particular advantages of targeting fibril propagation is the presence of extracellular fibrils, as exemplified above in section 1.3.2. Their accessibility means that targeted treatments would not need to penetrate cells, thereby eliminating one barrier in therapeutic development. Nonetheless, in order to target extracellular fibrils in the CNS, treatments would still need to cross the BBB. Given the variety of protein and lipid partners discussed above, as well as their essential cellular roles as is the case for the α3-NKA, it would be more logical to target the fibrils themselves rather than their individual partners. Finding agents that bind the fibril surfaces would alter their surface and physico-chemical properties, thereby disrupting their interaction with lipid and protein partners at the cell membrane and reducing the number of internalized fibrils. In conclusion, targeting the fibril surfaces could reduce propagation between neuronal cells and slow down the progression of the associated disease **(Figure 13)**. In the second part of this introduction, I will describe one possible strategy to bind to amyloid fibrils and protect them from interacting with cell membranes, based on molecular chaperones. Before that, however, I will describe in the next paragraphs which treatments are currently available for NDs.

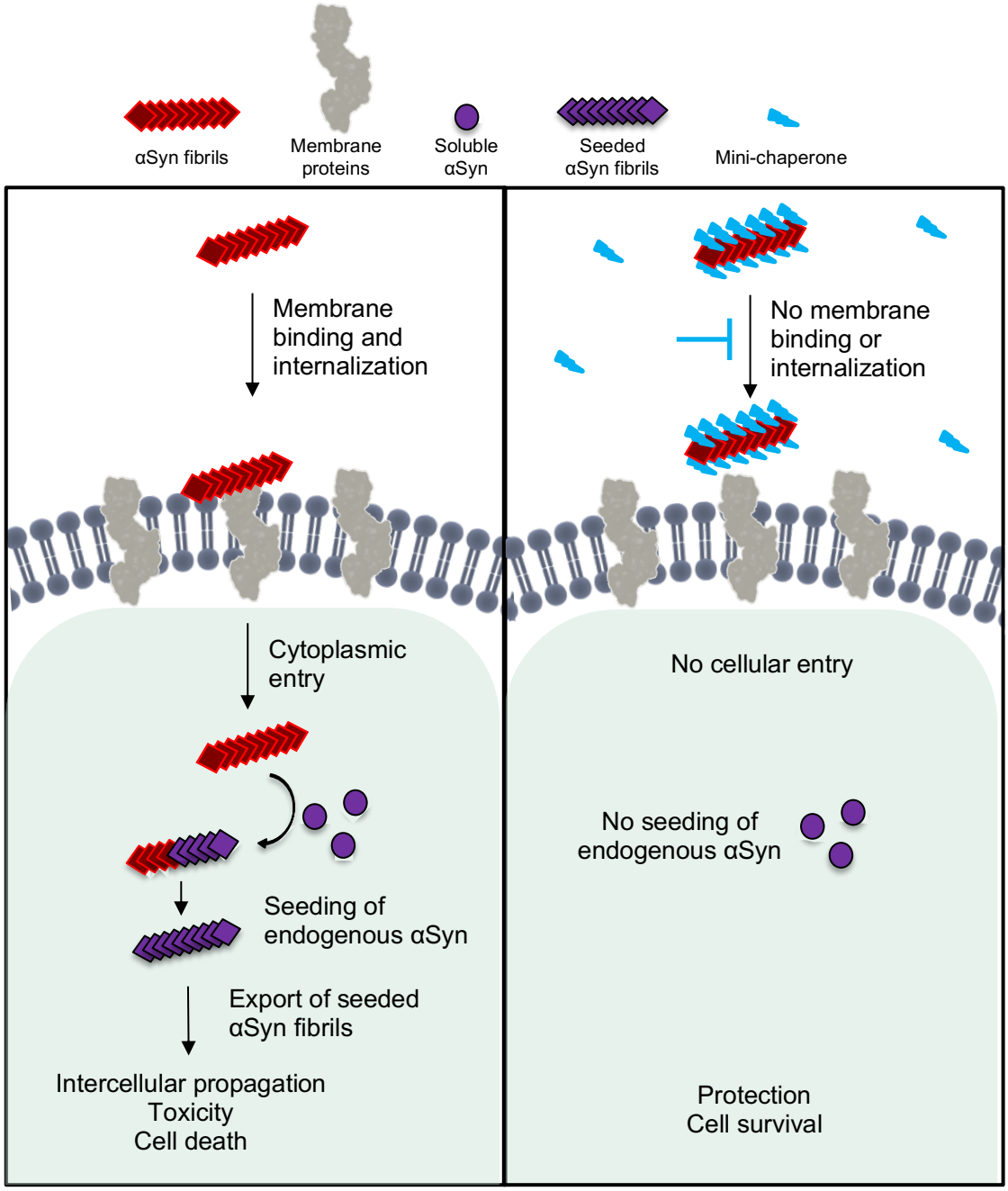

Figure 13: Targeting amyloid fibril propagation.
Adapted from (Ren et al., 2019)

1.4 Available treatments

1.4.1 Existing therapies

No treatments are on the market to treat the causes of NDs. Nonetheless, multiple approaches for symptomatic relief exist. First, grafts of healthy cells into degenerated brain regions, as mentioned above in section 1.3.1, proved helpful to PD patients for over

ten years (Li et al., 2016; Lindvall, 2015; Piccini et al., 1999). However, grafting of dopaminergic neurons can only treat dopamine-related symptoms, thus classifying this approach as partially effective. In addition, treatment was less effective for more disabled patients or patients with significant denervation (Lindvall, 2015). As for HD, only mild clinical relief was observed in patients receiving grafts for one year, despite long-term graft survival (Cicchetti et al., 2014; Maxan et al., 2018). Alternatively, deep-brain stimulation has been shown to have positive long term effects in PD patients (Hitti et al., 2019). However, this treatment is only available for 5–10% of PD patients (Pereira and Aziz, 2006) and also does not help with most non-motor symptoms of the disease (Kalia et al., 2013).

For PD, all approved pharmacological therapies lead to increased striatal dopamine levels in order to relieve associated motor deficits (Ellis and Fell, 2017). The gold standard is levodopa, or L-dopa, which is converted to dopamine in the brain. Levodopa treatment, however, leads to involuntary movements or levadopa-induced dyskenesia (LID). LID risk after 5 years is 50% for people with young-onset PD (40-59 years of age) as compared to 16% in people over 70 years old with PD (Kumar et al., 2005), and it may necessitate nigral damage (Di Monte et al., 2000). Similarly, involuntary movements can be addressed pharmacologically for HD patients. Tetrabenazine (TBZ), which leads to decreased dopaminergic neurotransmission (Hayden et al., 2009), was proven useful in HD patients in clinical trials (Huntington Study Group, 2006). Currently prescribed drugs for AD target cholinesterase inhibitors and/or antagonize NMDA and generally lead to a delay in cognitive decline in early- or mid-stages of the disease (Yiannopoulou and Papageorgiou, 2013).

1.4.2 Research perspectives

Translational difficulties

As much as animal models allow for *in vivo* evaluation of drug prospects, they have not proven accurate in predicting efficacy in humans. In order to address the translational problems faced by researchers, better animal models need to be developed, such as models with humanization, with the incorporation of human DNA or cells into the mouse genome or tissue (Nair et al., 2019) or with particular attention paid to promoters and expression. Rodent models, for example, may not be well adapted to study specific mechanisms in HD, where the rodent caudate nucleus and putamen, two affected regions in larger animals with (induced) HD, are indistinguishable. Similarly, in stage four PD, amygdala LBs precede cortical lesions in the transetorhinal region, which is non-existent in non-primates, thus explaining why propagation of pathology in non-primate models after the amygdala does not reflect what we observe in humans (Braak and Del Tredici, 2017). Accordingly, non-human primate PD models may be more therapeutically relevant for certain propagation studies (Yan et al., 2018). In conjunction with models with similar brain structures for better mechanism understanding and therapeutic evaluation of drug candidates, improvement of diagnostics would allow for better selection of patients for clinical trials as well as earlier identification of disease onset. For example, a clinical trial is underway to examine immunotherapy against soluble Aβ (Solanezumab) or fibrillar Aβ (Gantenerumab) in non-symptomatic familial AD people (ClinicalTrials.gov Identifier: NCT01760005). Given that phase 3 clinical trials with Solanezumab in mild AD patients failed to show reproducible significant improvement, providing this treatment before disease onset will help to elucidate if its failure was due to the wrong target or timing. Current work on diagnostics for NDs focuses on fluid biomarkers (Blennow et al., 2016; Nair et al., 2018; Schöll et al., 2019),

neuroimaging (Coughlin and Irwin, 2017; Leuzy et al., 2019; Mathis et al., 2017; Schöll et al., 2019; Wang and Edison, 2019), and amplification of aggregated material (Fenyi et al., 2019; Shahnawaz et al., 2017). The latter allows for the identification and characterization of aggregates from samples with concentrations below the threshold of detection.

Molecular targets

Improving diagnosis of NDs is influenced by our understanding of the molecular mechanisms and targets involved in disease progression. To this end, a wide range of molecular targeting strategies are being explored (Chanpimol et al., 2016). While there are many strategies targeting neuroinflammation (Gelders et al., 2018), gene expression (Recasens et al., 2016), amyloidogenic protein synthesis (Adams et al., 2018), or the microbiome (Sampson et al., 2016), among others, I will discuss below three alternate targeting strategies directly related to amyloid fibrils before broaching my approach involving molecular chaperones.

One such strategy aims at reducing the aggregation of amyloidogenic proteins. This can be addressed through stabilizers of normal protein folding or binders of the hydrophobic core, thereby disrupting the interactions required for β-sheet formation (β-blocking), or outcompeting monomers or oligomers. Even though this strategy has been highly explored (Cheng et al., 2013; Das et al., 2018; Eisele et al., 2015; Giorgetti et al., 2018; Kumar et al., 2016; Paleologou et al., 2005; Perni et al., 2018; Seidler et al., 2018; Tatenhorst et al., 2016; Wolfgang et al., 2005; Zaman et al., 2019), it requires therapeutics that can access the intercellular space. A second strategy involves the clearance of preformed aggregates (Arotcarena et al., 2019; Bae et al., 2012; Chan et al., 2017; Hebron et al., 2013; Li et al., 2018a; Silva et al., 2019). This approach is particularly exciting, as

it could potentially reverse protein-deposit-induced damage. Additionally, some protein deposits are extracellular and thus more accessible. However, targeting clearance has not always shown promise. Indeed, removing the amyloid load in the brain is only advantageous if it is the cause of the motor and/or cognitive symptoms dealt with by patients instead of merely another symptom of cellular dysfunction. As of now, all antibodies that successfully cleared extracellular Aβ plaques in AD patients did not lead to an improvement in cognitive symptoms and the clinical trials were stopped. It remains possible that targeting clearance must be done in patients at earlier stages of disease such that, if targeted early enough, cognition would remain stable compared to aged controls or possibly even improve. Alternatively, neurodegeneration, at least in AD, may not be due to the presence of plaques (Hashimura et al., 1991; Nelson et al., 2012; Terry et al., 1981). Instead, plaques could reflect a strategy for cells to isolate and store toxic protein aggregates in one location. In addition, derailing of APP metabolism may play a more important role than Aβ aggregation in AD, thus rendering Aβ therapies poorly targeted (Kametani and Hasegawa, 2018). Nonetheless, clearance of amyloid deposits made of other proteins like Tau, αSyn or mHTT could be a more fruitful strategy.

With the discovery of the prion-like properties of fibrils and smaller molecular weight aggregates, a third strategy emerged to target the propagation of aggregated proteins (Chan et al., 2017; Zella et al., 2019). As of now, antibodies are the preferred weapon of choice. While studies looking at the effect of antibody administration on the propagation of fibrillar αSyn (Bae et al., 2012; Spencer et al., 2018, 2016, 2014; Tran et al., 2014) and Tau (Kfoury et al., 2012; Yanamandra et al., 2013) do show an effect, the mechanisms by which this occurred are not always clear. Indeed, they could be stimulating aggregate clearance (Bae et al., 2012), like the Aβ antibodies mentioned in the above section, blocking the seeding of monomers by sterically hindering their

recruitment, and/or preventing fibrils from binding with the cell membrane. These results have led to the pursuit of immunotherapies against Tau and αSyn, among other amyloidogenic proteins, in clinical trials. I will detail below two of the current five antibodies against αSyn entering Phase 2 clinical trials. All five antibodies display higher affinity for aggregates and either recognize the C-ter (4/5) or the N-ter (1/5) of the protein.

First, 80 patients with early PD are currently in a Phase II clinical trial with an anti-αSyn humanized monoclonal antibody in order to reduce extracellular αSyn propagation via neutralization or clearance (RO7046015 [PRX002], ClinicalTrials.gov Identifier: NCT03100149). Phase 1b results showed repeated treatment was generally well-tolerated and safe, leading to a reduced amount of αSyn in serum levels and dose-dependent increases of antibody levels in cerebrospinal fluid in the double-blind, placebo-controlled study (Jankovic et al., 2018). Second, BIIB054, originally isolated from B cell lines from a healthy elderly cohort, is a monoclonal antibody directed against the N-terminus of αSyn that has been found in PD and DLB brain sections (Weihofen et al., 2019). Currently, the antibody is being tested in a multinational Phase 2 clinical trial with newly diagnosed PD patients (SPARK Study, ClinicalTrials identifier NCT03318523).

Antibody therapeutics, as will be covered more in section 2.4 below, can be burdensome due to the regular intravenous administration requirements. Thus, researchers have turned to other classes of molecules to target fibril propagation. One recent paper demonstrated that aptamers (nucleic acids evolved to have high affinity for their selected targets) that bound to αSyn preformed fibrils led to reduced propagation in primary neurons and WT mice and to improved motor symptoms (Ren et al., 2019). However, their experiments used a pre-treatment with exosome-delivered aptamers, suggesting that this treatment may only be applicable in cases benefiting from a very early diagnosis. For this study and others using inhibitors of fibril propagation, it is essential

to examine a late-application timeline in order to validate more therapeutically realistic treatments.

My research concerns the last strategy, namely, targeting fibril propagation. Specifically, the goal is to develop polypeptides able to bind amyloid fibrils and thus alter their surface chemistry. In doing so, the fibrils would have a lessened ability to bind to the cell membrane and thus initiate interneuronal propagation. The design of these peptidic inhibitors will be based on molecular chaperones, implicated in multiple stages of the amyloid aggregation process. This approach is better detailed in the next chapter.

Chapter 2: Chaperone and mini-chaperone approach to target amyloid fibril propagation

2.1 Molecular chaperones

2.1.1 Classification and cellular roles

Molecular chaperones, part of the PQC system, maintain homeostasis of protein folding in the cell. Their roles include folding assistance, targeting, sequestration, disaggregation, and degradation of proteins in multiple states of protein folding and aggregation, as well as in endocytosis through the uncoating of clathrin vesicles. They notably recognize typically buried, hydrophobic regions of client proteins that become accessible during folding or misfolding (Wentink et al., 2019). Chaperones are specific to the extracellular or intracellular space, and within the latter often to a particular cell type and/or intracellular compartment, although deviations from chaperone primary location do occur. In the extracellular space, while there is less crowding (with only 2% and 6% proteins in interstitial fluids and plasma, respectively), the increased oxidation and sheer stress can promote protein unfolding (Dabbs et al., 2011). There are seven extracellular chaperones, including clusterin and α2-Macroglobulin. Intracellular chaperones are first categorized by their size and ATP-independence (small heat shock proteins, sHSPs or HSPBs; tetratricopeptide repeat [TPR] containing chaperones) or ATP-dependence (multiple chaperone families). The remaining ATP-dependent cytosolic molecular chaperones fall into the following four families: (i) Hsp60/CCTs, (ii) Hsp70 and cochaperones, with particular importance given to the J-domain proteins (JDP or DNAJ proteins or Hsp40s) and nucleotide exchange factors (NEFs) like Hsp110, (iii) Hsp90s and (iv) Hsp100s (Wentink et al., 2019). Major differences among all chaperone families include how they bind substrates, what substrates they bind and what they impose

upon their substrates. Finally, how stress affects chaperone expression, through the induction of heat shock factor 1 (HSF1), is considered (Anckar and Sistonen, 2007). Chaperones are then defined as constitutively expressed, constitutively expressed and induced or only inducible (Alo et al., 2011).

2.1.2 Implications for neurodegenerative diseases

Since molecular chaperones are implicated in protein misfolding and NDs are characterized by the aggregation of certain proteins, it comes as no surprise that molecular chaperone dysfunction has been associated with the appearance of these diseases. The combination of reduced activity of the PQC components with aging (Fawcett et al., 1994; Labbadia and Morimoto, 2014), notably ATP-dependent chaperones (Brehme et al., 2014), and the long lifetime of neurons makes these cells especially susceptible to degeneration (Alo et al., 2011). In NDs, the decrease in ATP-dependent (and simultaneous increase in ATP-independent) chaperones is even more pronounced than during regular aging (Brehme et al., 2014). Chaperone expression being cell dependent suggests that the vulnerability of certain types of neurons to protein accumulation may be linked in part to the chaperones present (Chen and Brown, 2007). For example, some DNAJ proteins are upregulated in the substantia nigra of patients with PD (Moran et al., 2006), with more specific upregulation in astrocytes and eventual co-deposition in LBs (Durrenberger et al., 2009).

Cellular and animal ND models have demonstrated the deregulation of molecular chaperone expression and the implication of molecular chaperones in the progression of disease (Maiti et al., 2014; Yerbury et al., 2016; Yu et al., 2019). For example, HD knock-in mice had reduced expression of HSF1 and Hsp70 in the striata, further exacerbating the chaperone imbalance (Chafekar and Duennwald, 2012). On the other end of the scale,

genetic or chemical activation or local administration of HSF1, which led to increased molecular chaperone expression, reduced aggregation and neuronal toxicity in PD, AD and HD models (Fujikake et al., 2008; Fujimoto et al., 2005; Jiang et al., 2013; Liangliang et al., 2010; Miller et al., 2005; Paris et al., 2010; Pierce et al., 2013; Yu et al., 2019). Alternatively, direct exposure to, expression of, or activation of molecular chaperones resulted in similar results (Jones et al., 2014; Labbadia et al., 2012; Pratt et al., 2015; Wang et al., 2013), albeit without some controversy (Shimshek et al., 2010). However, clinical overexpression or exposure to whole molecular chaperones could lead to significant side effects due immune responses from AAVs (Vandamme et al., 2017) or off-target interactions from the wide array of chaperone partners.

In summary, chaperones interact with and their expression is linked to aggregating proteins involved in NDs. *In vitro*, amyloidogenic proteins such as αSyn, mHTT or Aβ, when in presence of chaperones, often aggregate at slower rates if at all (Bruinsma et al., 2011; Chorell et al., 2015; Evans et al., 2015; Liu et al., 2018; Mok et al., 2018; Pemberton et al., 2011), due to binding of chaperones to monomers (Bruinsma et al., 2011; Liu et al., 2018; Pemberton et al., 2011) with micromolar affinity (Bruinsma et al., 2011; Pemberton et al., 2011). If fibrils are formed, they can be shorter or of different morphology (Bruinsma et al., 2011; Monsellier et al., 2015).

In addition, certain molecular chaperones have been shown to bind various amyloid fibrils, although the characterization of this binding is weak. Immunogold labelling coupled with transmission electron microscopy has demonstrated binding of Hsp70 family members and J proteins to HTTExon1Q48 (Scior et al., 2018), αSyn (Gao et al., 2015) and Tau (Patterson et al., 2011) fibrils, as well as the sHSP αB-crystallin (αBc) to Aβ (Shammas et al., 2011) and αSyn fibrils (Waudby et al., 2010). GroEL, the *E. coli* homologue of Hsp60, and CCT were found in the pellet after centrifugation with

fibrillar αSyn A53T fibrils (Sot et al., 2017). Finally, sHSP Hsp27 and/or αBc equally co-sedimented with fibrillar αSyn (Cox et al., 2018; Rekas et al., 2004; Waudby et al., 2010) or Aβ (Shammas et al., 2011), further supporting the idea that chaperones are good targets for the identification of proteins able to bind amyloid fibrils. Chaperone binding to fibril ends can lead to inhibition of fibril elongation (Shammas et al., 2011; Waudby et al., 2010). Chaperones able to laterally bind amyloid fibrils would be able to alter their surface chemistry, therefore disrupting their membrane binding capacities and subsequent intercellular propagation.

2.2 Chaperones of interest used in this study

In order to narrow down the chaperones capable of interacting with amyloid fibrils, my doctoral research focused on multiple molecular chaperones shown to affect αSyn fibrillation or αSyn-induced toxicity in cellular models, as αSyn has been particularly studied with respect to chaperones (**Table 3**). Notably, these chaperones were small, as the goal of the project was to miniaturize them into mini-chaperones (see below). Hsc70 was the focus of a first study in which I participated. The five chaperones examined in

	Hsc70	**CHIP**	**αBc**	**αBc-core**	**proSAAS$_{62-180}$**	**CsgC**
Size of the monomer	669 AA; 71.4 kDa	303 AA; 34.8 kDa	175 AA; 20.2 kDa	87 AA; 9.9 kDa	122 AA; 12.6 kDa	104 AA; 11.3 kDa
Oligomeric status	monomer	dimer	10-40 mer (avg: 24)	dimer	monomer	monomer
Origin	human	human	human	human	human	bacterial
Affects αSyn fibrillation	yes	not tested	yes	yes	yes	yes
Cellular rescue effect	yes	yes	yes	not tested	yes	not tested
Binds αSyn fibrils	yes	not tested	yes	not tested	not tested	not tested

Table 3: Chaperones of interest for this study.
The associated references are mentioned in the text.

my own research project were CHIP, αBc and its core domain, αBc-core, proSAAS$_{62\text{-}180}$, and CsgC.

2.2.1 Hsc70

The Hsp70 family has 13 members in humans, two of which are Hsp70 (HSPA1) and its constituent chaperone, heat shock cognate 71kDa (Hsc70 or HSPA8). The Hsp70 homologue from *E.coli*, DnaK, has also been extensively studied (Hartl and Hayer-Hartl, 2002; Mack and Shorter, 2016; Mattoo and Goloubinoff, 2014). They are implicated in maintaining proteostasis through interactions with proteins in all stages of existence, from nascent polypeptides, through intermediate conformers or stress-denatured proteins, to aggregates for solubilization, disaggregation or degradation (**Figure 14)**. Furthermore, they are implicated in the stability or assembly of regulatory proteins such as transcription factors and protein complexes involved in DNA replication initiation or clathrin-mediated endocytosis (Mayer and Gierasch, 2019). These proteins exert their chaperone activity with the help of co-chaperones from the Hsp40/DNAJ family (of which there are ~50 members), NEFs and ATP. They also interact with other proteins of the UPS like carboxyl terminus of Hsc70-interacting protein (CHIP), discussed in the next section (Petrucelli et al., 2004; Smith et al., 2013).

Hsp70 family members have two primary functional domains: an ATPase or nucleotide binding domain (NBD) of around 40kDa at the N-terminus, and a substrate binding domain (SBD) of around 25 kDa at the C-terminus. The SBD is composed of an α-helical lid and a β-sandwich subdomain of 15 kDa which interacts with client proteins (Mayer and Gierasch, 2019). The NBD is the site of ATP and ADP binding and is thus responsible for the conformational changes in the SBD (**Figure 14**). Nucleotide exchange determines if the lid will be in an open, low affinity state when bound to ATP, or closed,

high-affinity state when bound to ADP (**Figure 14**). Hsp70s have been shown to have holdase activity that, unlike their foldase activity, is ATP-independent. For example, Hsc70 was better able to prevent αSyn or HTTExon1Q48 fibrillation in absence of NEFs and ATP (Monsellier et al., 2015; Pemberton et al., 2011). In contrast, Hsc70's disaggregation activity is not only ATP-dependent but also co-chaperone dependent, as the presence of all three proteins (Hsc70, the class B J-protein DNAJB1, and an Hsp110 family NEF Apg2) was needed to reduce αSyn fibrils to monomers *in vitro* (Gao et al., 2015).

In vitro, Hsc70 has been shown to inhibit amyloid fibrillation of αSyn (Pemberton et al., 2011), Tau (Baughman et al., 2018; Mok et al., 2018), mHTT (Monsellier et al., 2015), for example. Hsc70 also demonstrated disaggregase activity, however in an ATP- and co-chaperone dependent manner (Gao et al., 2015). In cells, Hsc70 led to reduced fibrillar αSyn- (Pemberton et al., 2011) and mHTT-induced (Monsellier et al., 2015) toxicity.

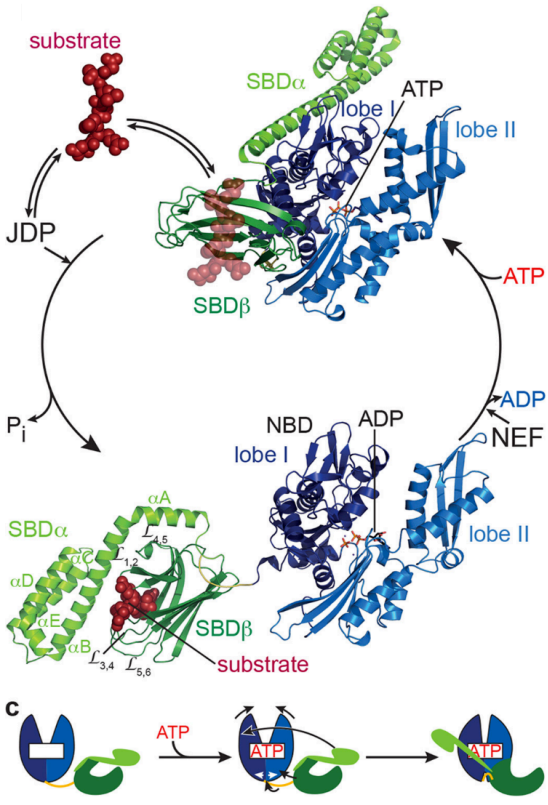

Figure 14: Hsp70 structure and ATPase reaction cycle.
Structures are structures of *E. coli* DnaK (ATP-bound open conformation, PDB code 4B9Q; ADP-bound closed conformation, PDB code 2KHO) (Mayer and Gierasch, 2019). The substrate is a peptide identified to have high affinity for DnaK and that conforms with peptide profiles that bind with high affinities to other chaperones (Zhu et al., 1996).

2.2.2 CHIP

As is no surprise by its name, Hsc70 binds to carboxyl terminus of Hsc70-interacting protein (CHIP), a human dimeric chaperone of 34.8 kDa that is part of the tetratricopeptide repeat (TPR)-domain-containing chaperone family (Ballinger et al., 1999). It is also part of the ubiquitin-proteosome system (UPS), which consists of E1 ubiquitin activating enzymes, E2 ubiquitin conjugating enzymes and E3 ubiquitin ligases. CHIP is composed of a TPR, helical hairpin and U-box domain, the latter enabling E3 ubiquitin ligase activity (Jiang et al., 2001) (**Figure 15**). The helical hairpin domain is responsible for its asymmetrical dimerization, necessary for ubiquitination (Nikolay et al., 2004). Its TPR domain interacts with Hsc70, Hsp70 and Hsp90 at the Hsp EEVD motif (VanPelt and Page, 2017; Zhang et al., 2005). Through binding to Hsp chaperones and E2 ubiquitin-conjugating enzymes, CHIP targets client proteins (Quintana-Gallardo et al., 2019) such as αSyn (Dimant et al., 2014; Kalia et al., 2011), Tau (Dickey et al., 2007; Petrucelli et al., 2004; Sahara et al., 2005) and mHTT (Jana et al., 2005; Miller et al., 2005) aggregates for ubiquitination and leads to their degradation.

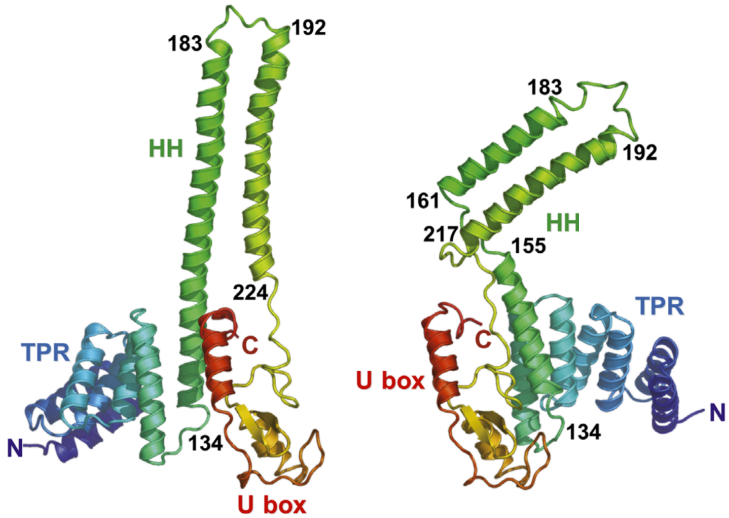

Figure 15: CHIP structure. Each monomer is drawn separately to distinguish their unique structures. PDB accession number 2C2L from murine CHIP (Zhang et al., 2005).

In addition to participating in the ubiquitination of misfolding proteins, CHIP has been shown to improve the chaperone functions of Hsp70 or to act as a chaperone alone. One example was done by observing the amount of soluble HTTExon1Q53 able to enter native sodium dodecyl sulfate polyacrylamide gel electrophoresis (SDS-PAGE) gels, as mHTT aggregates remain in the stacking gel (Monsellier et al., 2015). The addition of CHIP to low amounts of Hsp70, insufficient on its own to prevent mHTT aggregation, led to an increase in soluble mHTT (Rosser et al., 2007). However, CHIP alone did not display chaperone activity towards mHTT as it did for chemically denatured luciferase. In addition, the TPR domain was proven essential in reducing mHTT aggregation in COS7 and PC-12 cell lines, primary mouse cortical neurons and zebrafish embryos, unsurprisingly implicating its Hsp70-interacting TPR domain in its ability to reduce mHTT aggregation (Miller et al., 2005). Furthermore, aggregation prevention was increased when Hsc70 was co-expressed (Jana et al., 2005). In contrast, CHIP mutants missing their U-box domain were unable to prevent aggregation of mHTT in differentiated Neuro-2a cells (Jana et al., 2005). This interaction is specific to mHTT compared to WT HTT, as CHIP immunoprecipitated with and was translocated to N-truncated HTTExon1Q150 aggregates but not HTTExon1Q16 (Jana et al., 2005). In a different paper, CHIP was shown to reduce the aggregation of Tau 0N4R *in vitro*, demonstrating that CHIP in the absence of Hsp70 has chaperone activity against amyloidogenic proteins (Mok et al., 2018).

Cellular experiments demonstrated that CHIP prevented αSyn-induced-toxicity in different models (Shin et al., 2005; Tetzlaff et al., 2008), potentially due to the ubiquitination of toxic αSyn species or to morphological changes in αSyn inclusions formed under CHIP overexpression (Shin et al., 2005). Despite many CHIP-client interactions involving co-chaperones, there is still the potential for a direct relationship

between αSyn and CHIP. CHIPΔTPR, which was unable to bind the Hsp chaperones, was able to immunoprecipitate with αSyn (Tetzlaff et al., 2008).

Last, but not least, CHIP was found to colocalize with αSyn in Lewy bodies or Tau in DLB or Tauopathy patient brains, respectively (Petrucelli et al., 2004; Shin et al., 2005). However, whole CHIP may not be a viable therapeutic strategy for PD, given that CHIP expressed in the SNpc of mice led to TH degradation (Dimant et al., 2014). A mini-chaperone derived from CHIP could potentially avoid this problem (discussed further in section 2.3 below).

2.2.3 αB-crystallin (αBc)

The human genome encodes for ten sHSPs (named HSPB1-10) with monomers of 15 to 25 kDa. sHSPs are considered the first line of defense in the case of cellular stress (Haslbeck et al., 2018), in part due to their ATP independence. These proteins all contain a conserved α-crystallin domain (ACD) of around 100 residues that form a β-sandwich structure composed of seven to eight antiparallel β-sheets. Disordered N- and C-terminal extensions (NTEs and CTEs) of 24-247 (average 56) and less than 20 (average 10) residues, respectively, flank the ACD (Mogk et al., 2019). The conserved IXI/V motif, involved in oligomerization, is located in the CTE. Indeed, most sHSPs form heterogeneous mixtures of large oligomers (12-32 subunits) in equilibrium. Their oligomeric state is involved in chaperone activity regulation, with increased activity associated with smaller multimers (Haslbeck et al., 2018; Wentink et al., 2019). The exact effect of oligomerization on chaperone activity is not clear. Originally, it was thought that the large oligomers act as reservoirs for smaller, active dimers (Van Montfort et al., 2001), supported by the fact that Hsp27 retains chaperone functions even when mutated to only form dimers (Cox et al., 2018). Interestingly, cross-linked HSPB5 (αB-

crystallin, or αBc) equally retained chaperone functions against β-crystallin, suggesting its activity is linked to accessible regions on the surface, whether that be in large oligomers or dimers (Augusteyn, 2004).

αBc is a human sHSP with a monomeric size of 20 kDa that is primarily expressed in the lens. It is one of the two subunits of αcrystallin, responsible for preventing cataracts. It is composed of flexible, unstructured NTE and CTE and a structured central core-domain (αBc-core, 9.9 kDa). αBc forms hexameric units of dimers through interactions between its IXI/V motif, in this case IPI, in the CTE and the β4/β8 strands in the core, units which assemble into large multimers of around 24 monomers (**Figure 16**). The dimer interface is due to β6 + 7 strands interacting in an antiparallel fashion (Braun et al., 2011; Delbecq et al., 2012; Liu et al., 2018). The details of the oligomerization dynamics and their role on αBc chaperone activity are not entirely clear, although phosphorylation of three lysines in the NTE has been implicated in smaller oligomers and increased chaperone activity (Peschek et al., 2013).

αBc has been shown to reduce or prevent the fibrillation of a multitude of amorphous and amyloid aggregates (as referenced in section 2.3.2 below when discussing αBc mini-chaperone activity), notably affecting αSyn (Aquilina et al., 2013; Bruinsma et al., 2011; Cox et al., 2016; Cox and Ecroyd, 2017; Liu et al., 2018; Rekas et al., 2007, 2004; Wang et al., 2008; Waudby et al., 2010), $A\beta_{1\text{-}40}$ (Mainz et al., 2015), and Tau (Liu et al., 2018; Mok et al., 2018). In contrast, it has no effect on mHTT fibrillation (Carra et al., 2005; Muchowski et al., 2000; Vos et al., 2010).

It interacts with amorphous and amyloid aggregating proteins through its N-ter and central β-sandwich, respectively, as demonstrated through NMR spectroscopy (Liu et al., 2018; Mainz et al., 2015). Specifically, the β4 (residues 88-94) and β8 (residues

133-6) strands of αBc-core, were implicated in the binding of $A\beta_{1-40}$ (Mainz et al., 2015), Tau K19 (244-372; 3R) and αSyn (Liu et al., 2018).

Of particular interest is the fact that αBc has been shown to bind to preformed fibrils of αSyn (Cox et al., 2016; Waudby et al., 2010), $A\beta_{1-40}$ (Raman et al., 2005), $A\beta_{1-42}$ (Shammas et al., 2011), and apolipoprotein C-II (apo-CII) (Binger et al., 2013), the latter two with calculated K_Ds of 2 and 5 μM, respectively. In particular, αBc was observed binding the lateral faces of fibrils, a mechanism of notable relevance for mini-chaperones capable of coating the fibril surface.

αBc-core, a homodimer, retains (Hochberg et al., 2014) and improves upon the chaperone activity of its parent protein against αSyn (Cox et al., 2016; Liu et al., 2018). It remains to be shown whether the dimeric core is able to bind fibrils.

In cellular or animal models, αBc has led to reduced aggregate-induced toxicity by $A\beta_{1-40}$ & $A\beta_{1-42}$ (Mannini et al., 2012; Wilhelmus et al., 2006), αSyn (Outeiro et al., 2006; Tue et al., 2012), PolyQ92 (Tue et al., 2012), and mHTT (Muchowski et al., 2008). Its reduction of mHTT-induced toxicity, despite its inability to interfere with mHTT aggregation, could stem from interactions with mHTT fibrils or, for example, its anti-apoptotic activity. Like its parent protein, αBc-core reduced Aβ-induced toxicity (Hochberg et al., 2014).

αBc expression, like that of many other sHSPs in NDs, is increased, for example, in AD (Renkawek et al., 1994; Yoo et al., 2001) and other Tauopathies (Dabir et al., 2004; López-González et al., 2014), PD (Renkawek et al., 1999), and Creutzfeldt-Jakob disease (Renkawek et al., 1992). αBc also colocalizes with LBs in PD neurons (Braak et al., 2001; Iwaki et al., 1992), MSA oligodendrocytes (Valdinocci et al., 2018), and with LBs and LNs in DLB neurons (Outeiro et al., 2006). In addition, αBc colocalizes with neuritic

plaques from AD brains (Shinohara et al., 1993; Yoo et al., 2001) and neuropil threads of the neocortex and globus pallidus of Tauopathy brains (Dabir et al., 2004).

In summary, αBc has been shown to interact with multiple amyloidogenic proteins involved in NDs. In particular, its binding to αSyn and Aβ fibrils, along with its successful miniaturization into its core domain or peptide mini-chaperones derived from the whole protein (see section 2.3.2) that retain chaperone activity against amyloidogenic proteins, makes αBc a good candidate for miniaturization aimed at binding fibrillar aggregates for propagation inhibition.

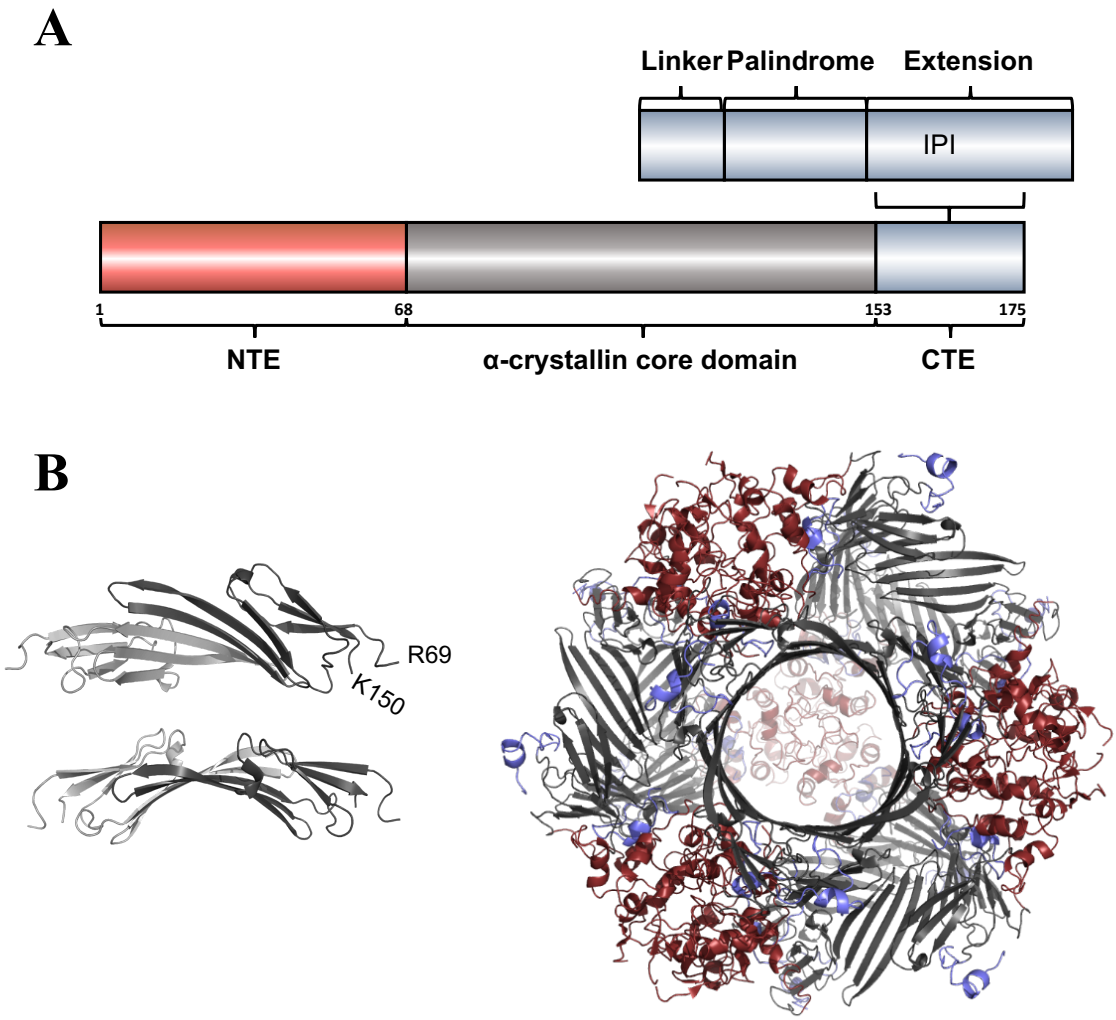

Figure 16: αBc structure.
A) αBc primary sequence. **B)** The dimeric αBc-core solid-state NMR structure at two angles (PDB: 2klr) alongside a 24-mer cryo-EM model at 9.4 Å with the same coloring by domain as in A). (Jehle et al., 2011, 2010).

2.2.4 proSAAS

Proprotein convertase 1 inhibitor, or proSAAS, is a 19 kDa human granin-like, secretory neuroendocrine peptide precursor. While it is a potent inhibitor of prohormone convertase (PC1/3) (Fricker et al., 2000), it is also expressed in tissues without PC1, suggesting other cellular roles (Hoshino et al., 2014). It is found solely in vertebrates, with conserved residues in its central core domain (Kudo et al., 2009), which remain after cleavage (Kikuchi et al., 2003). It has no homology with other proteins and no known structure (Lindberg et al., 2015).

Since its discovery in a peptidomics screen of abundant brain neuropeptides, it has been identified five times as a potential CSF biomarker for various neurodegenerative diseases (Lindberg et al., 2015). It is highly expressed in neurons throughout the brain (Fricker et al., 2000) and has been found to colocalize with Tau inclusions in Pick's disease patient brains (Kikuchi et al., 2003), with NFTs and neuritic plaques in AD and Guamanian Parkinsonism–dementia complex patient brains (Hoshino et al., 2014; Wada et al., 2004), and with Lewy bodies in nigral slices of a PD patient brain (Jarvela et al., 2016).

In vitro studies showed that proSAAS has chaperone activity against $A\beta_{1–42}$ (Hoshino et al., 2014) and αSyn (Jarvela et al., 2016) at sub-stochiometric ratios. In cellular models, proSAAS reduced $A\beta_{1–42}$-oligomer-induced toxicity in Neuro-2a cells (Hoshino et al., 2014) and αSyn-induced toxicity in both SH-SY5Y cells and rat primary nigral dopaminergic neurons (Jarvela et al., 2016). Nonetheless, it had no effect on αSyn oligomerization with the split-venus system (Jarvela et al., 2016). The truncated variant $proSAAS_{97-180}$ was sufficient to block $A\beta_{1–42}$ fibrillation (Hoshino et al., 2014). Likewise, a shorter variant $proSAAS_{62-180}$ had a stronger chaperone ability on αSyn fibrillation than

the whole protein (Jarvela et al., 2016). Accordingly, this proSAAS$_{62-180}$ variant is thus the chaperone chosen for my doctoral research work.

2.2.5 CsgC

CsgC (Curli-specific genes C) is a bacterial protein involved in the curli system in gram-negative bacteria. It is a 110-residue monomeric protein that contains an immunoglobulin-like β-sandwich fold (Taylor et al., 2011, **Figure 17**). It inhibits the amyloid formation of the protein CsgA at sub-stoichiometric concentrations in the periplasm (Evans et al., 2015), to prevent fiber formation before CsgA is extracellular, as these fibers are used for surface adhesion and biofilm (Olsén et al., 1989). While one study suggested CsgC reduced CsgA fibrillation at the nucleation and the elongation steps (Taylor et al., 2016), a more recent study suggests CscC slows down CsgA fibril elongation, possibly by binding the fibrils (Sleutel et al., 2017). CsgA fibrils formed in presence of CsgC were also shorter than those formed alone (Sleutel et al., 2017).

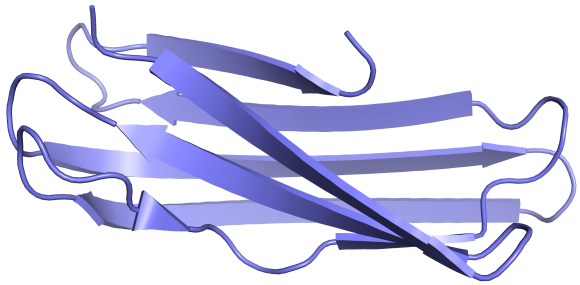

Figure 17: CsgC structure.
CsgC has an immunoglobulin-like β-sandwich fold. PDB code 2Y2Y. From (Taylor et al., 2011).

Given CsgC's propensity to target amyloid fibrillation and the common β-sheet structure of amyloids, it was only logical to test its ability to inhibit αSyn fibrillation *in vitro*. CsgC reduced αSyn fibrillation at sub-stochiometric ratios, as seen by ThT fluorescence (Chorell et al., 2015). Atomic force microscopy experiments identified oligomers at the lowest ratios tested, suggesting CsgC promotes off-pathway oligomer

formation of αSyn. NMR experiments of αSyn and CsgC did not identify any changes in shift intensities of residues, indicating that their interaction is transient. However, after incubating CsgC and αSyn at 37˚C for two days, multiple residues presented strong shift intensity changes. In fact, 38 of the 78 affected residues disappeared or were reduced by 90%, with 32 of these 38 residues in the 30-104 region of αSyn (Chorell et al., 2015). It was estimated that this detectable species was not a monomer, therefore suggesting that CsgC promotes and interacts with αSyn oligomers. CD data showed CsgC-incubated αSyn retained its random-coil secondary structure, compared to αSyn alone which formed β-sheets after two days of incubation. No shift changes in CsgC incubated with αSyn versus CsgC alone were observed, indicating that CsgC is not incorporated into these oligomers.

Another study also found that CsgC inhibited αSyn fibrillation. The sequences targeted by CsgC were further investigated, and comparisons of CsgA and αSyn sequences helped identify a shared D-Q-Φ-X0,1-G-K-N-ζ-E motif (Φ=W/L, ζ=S/E), mapping to residues 98-104 of αSyn and of the repeating unit 3 of CsgA (Evans et al., 2015). Interestingly, this region of αSyn is one of the two regions shown through chemical crosslinking coupled with mass spectrometry (MS; see paragraph 2.3.3) to interact with Hsc70 (Redeker et al., 2012). These residues are consistent with the previous report's NMR data (Chorell et al., 2015). Mutating these residues to alanines decreased the lag time of αSyn fibrillation and severely decreased CsgC's chaperone effect on fibrillation compared to WT αSyn. Therefore, these residues are involved but not necessary for CsgC chaperone activity on αSyn. A second similar motif is found multiple times in CsgA but is not found in αSyn, potentially explaining why CsgC is much more effective at inhibiting CsgA fibrillar formation than it is at inhibiting αSyn fibrillar formation. Lastly, the lack of the motif in $A\beta_{1-42}$ could explain why CsgC had

no effect on its fibrillation, even at an equimolar ratio. In conclusion, CsgC was shown to stoichiometrically inhibit αSyn, but not $A\beta_{1-42}$ fibrillation, in a motif-dependent manner. This motif is potentially accessible in αSyn fibrils as it was shown to be unstructured through solid-state NMR experiments (Gath et al., 2014), despite being predicted as part of the hydrophobic core based on sequence (Pawar et al., 2005). CsgC is thus a potential binding candidate for αSyn fibrils, as well as other amyloid fibrils containing this motif.

2.3 Mini-chaperone rationale

2.3.1 Principle

Data detailed above demonstrates the implication of certain chaperones in amyloidogenic fibrillation inhibition and/or fibril binding. These chaperones are thus good candidates for fibril propagation inhibition testing. However, whole molecular chaperones, due to their pleiotropic cellular roles, are not suitable drug candidates. On the other hand, mini-chaperones, such as domains, sub-domains or peptides derived from molecular chaperones, are of therapeutic interest. We set up a four-step process for the rational design of mini-chaperones targeting fibril propagation. First, candidate molecular chaperones capable of binding fibrils are identified, as presented in section 2.2. Second, the chaperone must be shown to bind amyloid fibrils. Third, a top-down or bottom-up approach can be used to identify regions or residues that are involved in fibril binding. Specifically, this entails testing whether domains, sub domains or peptides retain certain properties of their parent protein and can thus still bind fibrils. However, this functional retention is particularly nuanced, as mini-chaperones capable of fulfilling many of the parent protein's pleiotropic cellular roles is to be avoided. In a top-down approach, the fibril binding chaperone is separated into its constituent domains or sub-domains, or even in a range of peptides spanning its entire sequence, without previous

knowledge of the regions actually involved in fibril binding. The fibril binding abilities of the different fragments are tested, and positive ones can be further miniaturized by applying the same approach. The bottom-up approach lays on the previous knowledge of the regions of the chaperone involved in fibril binding. Peptides including these regions are designed and binding ability can be further improved by protein engineering. Various methods that allow for the identification of residues involved in protein-protein interactions will be discussed in section 2.3.3.

2.3.2 Examples of functional mini-chaperones

Mini-chaperone domains

The concept of mini-chaperones has been explored for many years, with the first use of the term designating the apical domain of GroEL (Zahn et al., 1996). GroEL, a 14-mer of 57 kDa monomers, was successfully reduced, through a top-down approach, to a monomeric mini-chaperone of 185 residues that retained ATP-independent chaperone activity towards rhodanese and cyclophilin A (Zahn et al., 1996), αSyn, $A\beta_{1-42}$, and GroES (Ojha et al., 2016), β2-microglobulin (Chen et al., 2012), and interferon gamma (Guan et al., 2005) *in vitro*, as well as complementation in *E. coli* KO for the whole protein (Chatellier et al., 1998).

Furthermore, a domain-based mini-chaperone was demonstrated effective for the CCT/TRiC (chaperonin containing TCP-1/TCP-1 ring) chaperonin complex, normally composed of eight subunits of three domains each. The apical domain of the subunit CCT1 inhibited aggregation of HTTExon1Q104 *in vitro* through capping the ends of fibrils (Shahmoradian et al., 2013; Sontag et al., 2013; Tam et al., 2006). In neuronal cells expressing HTTExon1Q104, endogenous CCT/TriC mini-chaperone, localized to

the nucleus and cytosol, reduced the number of insoluble mHTT aggregates and mHTT-induced toxicity (Sontag et al., 2013).

Lastly, Hsp70 and Hsc70 SBDs have been tested for chaperone activity. The SBDs of both proteins were shown to delay Tau 0N4R aggregation at similar rates as the parent proteins (Mok et al., 2018). The Hsp70 SBD, but not SBD without the lid or the NBD, was also shown to inhibit αSyn fibrillation, bind to prefibrillar αSyn and prevent lipid vesicle permeabilization by prefibrillar αSyn at similar rates as the whole protein (Huang et al., 2006).

Peptidic mini-chaperones

A particular emphasis has been placed on peptidic mini-chaperones based on either αB-crystallin or αA-crystallin (αAc) (Raju et al., 2016). After identification of hydrophobic residues implicated in chaperone activity through cross-linking, a mini-chaperone peptide derived from the sHSP αAc core domain ($_{70}$KFVIFLDVKHFSPEDLTVK$_{88}$, or αAc$_{70-88}$) was shown to retain the chaperone activity of its parent protein against γ-crystallin (substrate of α-crystallin in the lens) and alcohol dehydrogenase (Banerjee et al., 2015; Sharma et al., 2000). In addition, αAc$_{70-88}$ was shown to have similar β-sheet content as the corresponding region in the parent protein. αAc$_{70-88}$ or variants, along with peptides from the core domain of αBc ($_{73}$DRFSVNLDVKHFSPEELKVK$_{92}$, αBc$_{73-85}$, and $_{101}$HGKHEERQDE$_{110}$) were proven effective in reducing amorphous and amyloid aggregation of a wide range of proteins, including ADH, insulin B chain, heat-denatured citrate synthase, γ- and γD-crystallin, α-lactalbumin, transthyretin, β2-microgobulin, Aβ$_{1–40}$ and Aβ$_{22–35}$, and αSyn (Banerjee et al., 2015; Bhattacharyya et al., 2006; Ghosh et al., 2008; Kumar and Sharma, 2000; Nahomi et al., 2013; Raju et al., 2018; Santhoshkumar and Sharma, 2005; Sharma et al.,

2000; Sreelakshmi and Sharma, 2001; Tanaka et al., 2008). αAc_{70-88} also restored chaperone function *in vitro* to the αAcG98R mutant implicated in autosomal dominant cataract formation (Raju et al., 2012).

Some of these aforementioned peptidic mini-chaperones were tested in cellular and animal models and even in humans. αAc_{70-88} led to reduced Aβ-induced toxicity with rat PC12 cells (Santhoshkumar and Sharma, 2005). In addition, both αAc_{69-88} and αBc_{73-93} prevented oxidative stress-induced apoptosis in retinal pigment epithelium (RPE), human lens epithelial (HLE), and Chinese hamster ovary (CHO) cells (Nahomi et al., 2013; Sreekumar et al., 2013) through prevention of cytochrome-3 release, caspase-3 and -9 activation. These two mini-chaperones were shown to be actively transported into cells through sodium-coupled oligopeptide transporters (Sreekumar et al., 2013). αBc_{73-92} was shown to rescue Golgi localization and the trafficking response of Cu transporter ATP7B-H1069Q, implicated in Gaucher's disease, in fibroblast-like COS7 cells (Allocca et al., 2018). $\alpha Ac_{70-88,}$ with GRD at the C-ter for solubility and a cell penetrating peptide VPTLK at the N-ter, was shown to prevent H_2O_2-induced apoptosis in COS7 and retinal pigmented epithelium (ARPE-19) cells (Raju et al., 2018). Furthermore, both mini-chaperones stopped sodium-selenite-induced cataract formation and reduced protein insolubilization, oxidative stress and caspase activity in rats (Nahomi et al., 2013). αBc_{73-93}K92C reduced retinal ganglion cell (RGC) death due to ischemia/reperfusion injury and ocular hypertension (Stankowska et al., 2019). Injections of αBc_{71-85} into mice with hind-limb paralysis as a model for experimental autoimmune encephalomyelitis, simulating multiple sclerosis, resulted in symptom reduction (Kurnellas et al., 2012), albeit only when injections were recurrent. Symptoms were only reduced when αBc contained three key hydrophobic residues in the β3 strand that were responsible for its chaperone activity, tested here against the β chain of bovine insulin. Lastly, αBc_{73-92} was able to suppress

pro-inflammatory cytokine secretion by CD4+ T cells only in patients with multiple sclerosis as compared to healthy patients (Quach et al., 2013).

Besides peptides derived from αBc and αAc, two peptides from the core domains of sHSPs Hsp20 (G-$_{71}$HFSVLLDVKHFSPEEIAVK$_{91}$) and Hsp27 (D-$_{93}$RWRVSLDVNHFAPDELTVK$_{113}$) were shown to inhibit heat- and/or chemically-induced aggregation of citrate synthase, insulin, lysozyme, and malate dehydrogenase through interactions that involved the formation of a peptide-client complex, at least for citrate synthase (Nahomi et al., 2015). The differences between the two mini-chaperone's activity, while likely sequence specific as scrambled peptides had no effect, was not due to their surface hydrophobicity as it was not significantly different. These mini-chaperones were also functional in cellular models. Indeed, they retained anti-apoptotic properties of their parent proteins and were able to prevent apoptosis in HeLa cells by inhibiting mitochondrial cytochrome c release and caspase-3 activation. In addition, the last four amino acids were shown to be essential for cell entry. Lastly, these two peptides were equally effective in preventing sodium-selenite-induced cataract formation in rats and appeared to cross the blood retinal barrier. Indeed, they prevented a decrease of total soluble lens proteins and the formation of GSH, a readout for oxidative stress, compared to untreated, sodium-selenite exposed rats (Nahomi et al., 2015).

All together, these data show that mini-chaperones, notably from sHSPs, are capable of retaining certain functions of their parent protein such as inhibiting aggregation, client binding or prevention of apoptosis. As of now, however, none of these mini-chaperones has been tested for fibril binding or propagation inhibition. It remains to be shown whether peptides from the core domains of αBc, αAc, Hsp20, and Hsp27 shown to interact with aggregation-prone and amyloidogenic proteins will bind fully formed, amyloid fibrils. There is however significant doubt this would be the case for Hsp27

peptides from the core domain, as this domain was shown to no longer bind to αSyn fibrils, therefore demonstrating that the regions in this protein that are responsible for binding aggregating amyloidogenic proteins and fully formed amyloid fibrils are separate (Cox et al., 2018). This provides even stronger reasoning to pursue the identification of chaperone-fibril interaction sites, rather than only relying on data with soluble amyloidogenic proteins, for mini-chaperone development aimed at reducing intercellular fibril propagation.

2.3.3 Identification of protein-protein interfaces (PPIs) with amyloid fibrils

Different methods for PPI identification

This rational approach to developing mini-chaperones via a bottom-up strategy requires the use of techniques capable of identifying residues involved in protein-protein interactions (PPIs) (**Table 4**), although some are better suited than others when amyloid fibrils are involved. Mutagenesis in order to disrupt binding could lead to unforeseen structural and functional consequences and should thus be applied for confirmation of residues, rather than their identification. While X-ray crystallography and solution state NMR would work for PPI epitope mapping between chaperones and soluble amyloidogenic proteins, the megadalton size and insolubility of and crystallization difficulties inherent to amyloid fibrils are not adapted for these techniques. ss-NMR, on the other hand, has been applied successfully to elucidate fibril secondary structures (Bousset et al., 2013; Gath et al., 2014; Hoop et al., 2016; Lin et al., 2017) and 3D structure (Tuttle et al., 2016), for example. However, this is a very low throughput approach, making it a less ideal choice.

Furthermore, multiple methods take advantage of the change in solvent accessibility of residues involved in protein-protein binding. First, the nonspecific,

reversible chemical labeling in hydrogen–deuterium exchange (HDX) provides insight into residues involved in binding through solvent accessibility of backbone hydrogens. However, the reversible nature of the deuterium label and the technical challenges of the approach make it a less ideal candidate for this study. Alternatively, covalent labelling methods can be applied. Non-specific labelling is primarily accomplished through hydroxyl radical footprinting coupled with MS, for example by fast photochemical oxidation of proteins (FPOP), which identifies primarily hydrophobic, solvent-exposed amino acid side chains (Cornwell et al., 2018). Specific labelling, on the other hand, is achieved through the addition of chemical groups able to react with particular amino acid side chains exposed to the solvent (Zhang et al., 2012).

Finally, specific bi-moiety labelling methods, like photo-chemical or chemical cross-linking coupled with MS, lead to covalently bound complexes that can be further enriched for easier identification, a particular advantage over the previous methods. These techniques can also be applied to proteins in a cellular environment (Suchanek et al., 2005). Photo-chemical cross-linking, however, requires the incorporation of non-natural photoactivatable amino acids and associated extraneous protein purification (Pham et al., 2013). Chemical cross-linking coupled with MS was previously used in our laboratory to identify proximally located residues between monomeric αSyn and the chaperones Hsc70 or Ssa1p (Nury et al., 2015; Redeker et al., 2012) as well as between monomeric HTTExon1Q25 and Hsc70 (Monsellier et al., 2015). Therefore, this method was employed in my research to identify residues implicated in αSyn fibril-chaperone interactions in order to rationally develop mini-chaperones targeting fibril propagation. However, the protocols optimized for chemical cross-linking with monomers needed to be adapted to working with fibrillar aggregates.

Method	Native *vs* modified proteins	Primary output of interest	Disadvantages
Mutagenesis and binding tests	Mutated proteins	Absence or presence of binding with a mutated residue	No guarantee that the mutated protein will act like its native self
Solution state NMR	Isotopic labeling	Residue shift change from mobile residues in labeled protein upon binding	<70kDa proteins; requires high concentrations of pure samples; no guarantee of 100% sequence coverage
Solid state NMR	Isotopic labeling	Residue shift change from mobile residues in labeled protein upon binding	Requires high concentrations of pure samples; low throughput; no guarantee of 100% sequence coverage
X-ray crystallography	Native	Atomic level residue mapping	Not applicable for large amyloid fibril complexes; only applicable if crystal can be formed; static structure; requires high concentrations of pure samples
HDX (chemical labelling) with MS	Native	Kinetics of residue/region deuterated solvent accessibility	No distance information; reversible deuterium label sensitive to extensive treatments; must use acidic proteases
Oxidative footprinting with MS	Native	Oxidized, solvent exposed (primarily hydrophobic) residues	No distance information; oxidation can affect protein structure
Chemical labelling coupled with MS	Native	Solvent-exposed residues	No distance information; requires chemically reactive sites to be located at the PPI
Photo-chemical cross-linking coupled with MS	Use of photoactivatable amino acids	Specific residues within a pre-defined distance	Requires chemically reactive sites to be located at the PPI; resolution is cross-linking agent dependent; large adducts can affect protein structure
Chemical cross-linking coupled with MS	Native	Specific residues within a pre-defined distance	Requires chemically reactive sites to be located at the PPI; resolution is cross-linking agent dependent; large adducts can affect protein structure

Table 4: Methods to identify residues involved in PPIs between amyloid fibrils and protein partners.

All methods with MS include enzymatic digestion. *HDX* hydrogen-deuterium exchange; *MS* mass spectrometry; *NMR* nuclear magnetic resonance; *PPI* protein-protein interface. Adapted from Calabrese and Radford, 2018; Cornwell et al., 2018; Li et al., 2017; O'Reilly and Rappsilber, 2018; Toyama and Weissman, 2011.

Chemical cross-linking coupled with mass spectrometry

Chemical cross-linking exploits the reactivity of certain amino acid side chains and N- and C-termini. Notably, primary amines on Lysines and N-termini, as well as carboxylic acids on Aspartates, Glutamates and C-termini, are the most abundantly targeted residues. However, secondary reactions with amino acids such as Serine, Threonine, and Tyrosine have also been reported (Migneault et al., 2004; Rappsilber, 2011; Sinz, 2018). When exposed to a cross-linker, two spatially proximal residues will form a covalent bond through the cross-linker chemistry. One of the attractions of this technique is the variation of spacer arm lengths of the chemical cross-linkers, which provides specific distance information on cross-linked residues. Chemical cross-linking agents are also defined by their reactivity, their reversibility, and their water solubility. Some agents are made with two isotope variants in order to facilitate mass spectrometry analysis.

At the moment, no studies using chemical cross-linking coupled with MS have been done to identify the interfaces between amyloid fibrils and exogenous ligands. Most cross-linking coupled with mass spectrometry studies on amyloid fibrils have used photo-chemical cross-linkers with modified, photoactivable protein sequences, incorporating diazirines, aryl azides, or benzophenone (Bpa), and were used to extract structural information on the fibril interfaces in absence of ligands (Egnaczyk et al., 2001; Preston et al., 2012; Wong and King, 2015). For example, the addition of p-benzoylphenylalanine (Bpa) groups to specific amino acids allows for a UV-irradiation-induced reaction between the activated benzophenone group and a proximally located hydrogen from a side-chain methylene group or backbone carbon. Then, the ketone carbonyl carbon and attacked methylene carbon will form a covalent bond. These experiments thus rely on targeting the interactions of the specific residues chosen for labelling. Photo-chemical

cross-linking strategies with modified sequence were used with $A\beta_{1-40}$ or Sup35 fibrils (Egnaczyk et al., 2001; Wong and King, 2015) for intramolecular structural studies. In particular, these approaches were used to avoid inherent problems linked to exogenous cross-linker penetration of tightly formed fibril complexes.

The use of amyloid fibrils obliges certain protocol modifications compared to cross-linking with soluble proteins. First, cross-linking agent quantities must be significantly reduced, compared to experiments previously optimized in our laboratory with only soluble proteins, as the nature of the amyloid fibrils leads to high rates of intramolecular cross-linking at relatively low concentrations. Indeed, it is important to find appropriate concentrations of the cross-linking agent that do not favor intermolecular and/or multiple cross-links among the proximally-located fibril monomers. Furthermore, many chaperones are oligomeric, so the conditions must be equally optimized to minimize intermolecular cross-linking among chaperone proteins. Second, in order to observe complex bands on SDS-PAGE gels, fibril-chaperone mixtures must be solubilized beforehand, as the cross-linking reaction leads to larger fibrillar aggregates that get stuck in the stacking gel.

Our workflow for chemical cross-linking of amyloid fibrils to molecular chaperones is the following (**Figure 18A**): after proteins have been cross-linked, they are solubilized before being loaded onto SDS-PAGE gels for complex isolation. The complex and controls are subsequently digested by trypsin and the peptides are extracted from the gel. The peptides are separated by liquid chromatography (LC) on a reverse-phase C18 column before ionization and quadripole-time of flight (Q-TOF) mass spectrometry analysis (**Figure 18B**). In particular, we obtain spectrum and information about the precursor ions (MS) and associated fragmentation spectrum (MS^2). The detected m/z of the precursor ions and their fragmentation ions (preferentially y and b

ions from amide cleavages, **Figure 18C**) deliver peptide sequence information and reveal the particular localization of the cross-linked residues. Indeed, the adduct, or the cross-linking agent, is associated with one or several specific mass increments, depending on its nature. In addition, cross-linked peptides differ from linear peptides in their charge (Rinner et al., 2008) and size (Leitner et al., 2012), facilitating their identification. Specifically, data analysis is first done by determining the sequence coverage of the proteins through database searching with a protein database and decoy database search, as well as a cutoff score from the search engine related to a false discovery rate. Identification of cross-linked peptides, using the mass increments mentioned previously, can be done through various software (O'Reilly and Rappsilber, 2018). To summarize, this technique, along with appropriate software for data analysis, allows for the design of rational peptides found in spatial proximity to amyloid fibrils, which could bind the fibrils, thus altering their surface chemistry, and disrupt the propagation cycle.

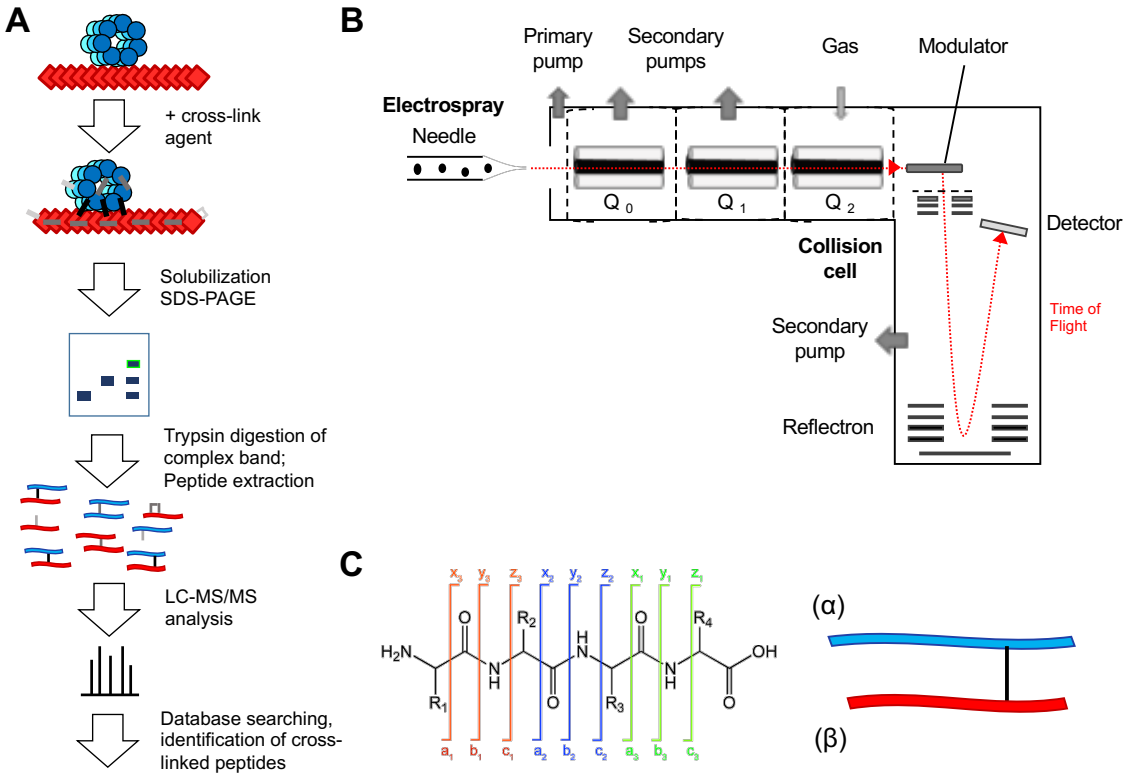

Figure 18: Chemical cross-linking coupled with LC-MS/MS.

A) Experimental workthrough. Black, gray and light gray bands represent intermolecular, intramolecular and dead-end cross-links. **B**) LC-MS/MS tandem mass spectrometry schema of an ESI-Q-TOF mass spectrometer. Following separation, the peptides undergo electrospray ionization and are thus converted into ions in the gas phase. In the Q-TOF, the first quadrupole mass analyzers transfer ions to the second quadrupole Q1 which filters and separates ions according to their mass to charge (m/z) ratio. In the collision cell (corresponding to the Q2 quadrupole), ions are fragmented after collision with neutral gas molecules, otherwise known as collision induced dissociation (CID). The last analyzer, an orthogonal time of flight filters the m/z of the fragment ions generated upon CID fragmentation. **C)** Peptide fragmentation (Biemann, 1992, 1988; Roepstorff and Fohlman, 1984) and intermolecular cross-link nomenclature, with the longer α and shorter β peptides shown (Schilling et al., 2003). For clarity, only a type 2 inter-peptide cross-link is shown, however α and β nomenclature also applies when intramolecular (type 1) or dead-end (type 0) cross-links are present on one or both peptides.

2.4 Peptide Therapy

2.4.1 Advantages & Drawbacks

The development of peptidic mini-chaperones is justified by the increased pursuit and potential of peptide therapy. However, currently peptides only make up a small minority of the current drug market at 2%, while small molecules lead at 80% and biologics make up the remaining 18% (Di, 2015). Small molecules have dominated the market due to their low cost, permeability, stability, good oral bioavailability, and easier synthesis. Nonetheless, they are prone to off-target binding and can produce toxic metabolites. While antibodies, for example, have exquisite selectivity, their invasive administration routes, poor permeability, and distribution leave much to be desired. Peptides, sized between these two classes, share some of the advantages of both groups and, while they have their own share of drawbacks, are amenable to modification and thus are full of potential (**Table 5**). One of the most significant attractions for peptide therapeutics is their targeting of shallow or flat hydrophobic protein-protein interfaces (PPIs, Pérot et al., 2010; Yan et al., 2008). Indeed, peptides bind PPIs with stronger, multiple point binding as compared to smaller molecules (J. Wilson, 2009), as they likely benefit from the linear correlation witnessed of small molecule size and potency in PPI binding (Wells and McClendon, 2007). Aptamers, another smaller, emerging class of therapeutics composed of single-stranded nucleic acids, are able to bind some PPIs despite their 10-30 kDa size (Bunka and Stockley, 2006; Reverdatto et al., 2015). However, they have rapid renal clearance and may lead to hepatotoxicity (Morita et al., 2018). In addition, the identification of selective candidates proves arduous.

Advantages	Drawbacks
• Adept for flat PPI interaction • High specificity & potency • Minimal side effects • Low tissue accumulation • Chemically modifiable to address some drawbacks • High throughput standard production • Low immunogenicity • Ease of synthesis • Minimal cross-reactivity • Potential for diagnostic imaging due to strong, reversible binding • Predictable metabolism – potentially lower toxicity than small molecules	• Chemically and physically unstable • Rapid renal clearance • Sensitive to enzyme degradation • Poor BBB permeability • Poor oral availability → predominantly given intravenously • Synthesis cost (small molecules > peptides > large biologics) • Can be aggregation prone • Can be poorly water-soluble • Natural conformational flexibility

Table 5: Advantages and drawbacks of peptides for therapeutics.
PPI protein-protein interface; *BBB* blood-brain barrier. Adapted from (Craik et al., 2013; Di, 2015; Erak et al., 2018; Fosgerau and Hoffmann, 2015; McGonigle, 2012).

2.4.2 Peptide optimization strategies

As mentioned above, unmodified peptides have considerable drawbacks for therapeutic applications due to their naturally unfavorable pharmacokinetic properties. To this end, many optimization strategies have been developed accordingly (**Figure 19**).

One prominent category of strategies involves modifying the peptide backbone. First, the amide bond can be replaced with a bioisosteric or bioisoelectronic proxy that mimics the natural peptide bond, leading to endoprotease resistance (Góngora-Benítez et al., 2014). Next, cyclization, via head-to-tail, head-to-side chain, side chain-to-tail, or side-chain-to-side-chain interactions, provides structural rigidity and exo or endoprotease resistance. Cyclization is also possible through the amide nitrogen (Góngora-Benítez et al., 2014). Exoprotease resistance can be conferred through N-ter or C-ter modifications, notably through N-acetylation or C-amidation (Corbi-Verge et al., 2017; Erak et al., 2018).

Other peptide alterations that involve the side chains commonly rely on the use of non-canonical amino acids (NCAAs). NCAAs can contain shorter or longer side chains

that better fit PPIs, decrease peptide fragility, improve cell penetration, and which can be used for subsequent chemical reactions for structural modifications (Corbi-Verge et al., 2017; Erak et al., 2018). One type of NCAAs employed is D-amino acids for improved protease resistance. However, substitutions with D-amino acids are likely to lose affinity, as the D-peptide would no longer recognize the L-target. In applicable instances, a D-target can be produced for affinity screening with L-peptides, which, when synthesized with D-amino acids should bind the original L-target of interest (Weinstock et al., 2012).

Structural modifications fight against one major problem in peptide therapeutics, namely, the lack of an adopted structure in the absence of the rest of the protein. If a peptide is supposed to have a specific tertiary structure, stabilizing it may restore or even improve substrate affinity and/or its protease resistance (Verdine and Hilinski, 2012). One NCAA strategy also addresses this issue through a hydrogen-bond surrogate (HBS) strategy, creating a permanent hydrogen bond involved in α-helices for structure stabilization (Góngora-Benítez et al., 2014; Tsomaia, 2015). Additionally, α-helix, turn and β-sheet mimetics have been invoked, albeit with varying results (Cunningham et al., 2017). β-sheet mimetics are less common due to their tendency for aggregation (Modell et al., 2016). However, turn inducers and especially α-helix stabilization are prominently evoked. Peptide stapling is a common strategy for structural reinforcement (Ali et al., 2019). NCAAs with hydrocarbons or cysteine residues already present in the sequence or added purposefully can be exploited for peptide stapling to stabilize α-helical structure (Góngora-Benítez et al., 2014; Verdine and Hilinski, 2012). Another method involves N-terminal capping, where a covalent bond replaces the hydrogen bond between the carobxyl group of the N-ter and the amide group of the i + 3 amino acid, ensuring α-helix formation (Cunningham et al., 2017). The choice of a stapling method depends on the amount of α-helix faces necessary for substrate recognition. For example, staples with

hydrocarbons, triazole linkages, and lactams require one face for stabilization and thus leave two for recognition. On the other hand, stapling with HBS through the peptide backbone and the use of strategically placed α- and β-amino acids leave all three faces of the α-helix available for substrate binding (Modell et al., 2016).

Many of the above modifications are primarily used for protease resistance, structure stability, and improved affinity. Other modifications such as lipidation, i.e., the addition of fatty acids, or the addition of hydrophilic polymers like polyethylene glycol (PEG), drastically improve serum-half life (Weinstock et al., 2012; Witt et al., 2001). Lipids, through binding to serum albumin, bypass the size cut-off for renal clearance. Their capacity to oligomerize also allows for subcutaneous administration (Erak et al., 2018). PEGylation, along with improved renal clearance, also improves solubility due to its binding to water molecules. Both lipidation and PEGylation are some of the most commonly used modifiers for peptide therapeutics, with the former notably used for insulin medications and the latter used in 15 FDA approved protein or peptide drugs (Erak et al., 2018).

Lastly, most peptides are administered intravenously, presenting a challenge for peptide therapeutic acceptance as compared to small molecules that are easily orally available. Nonetheless, some approved, modified peptides have avoided this fate and can be administered subcutaneously, by inhalation or even orally (Erak et al., 2018).

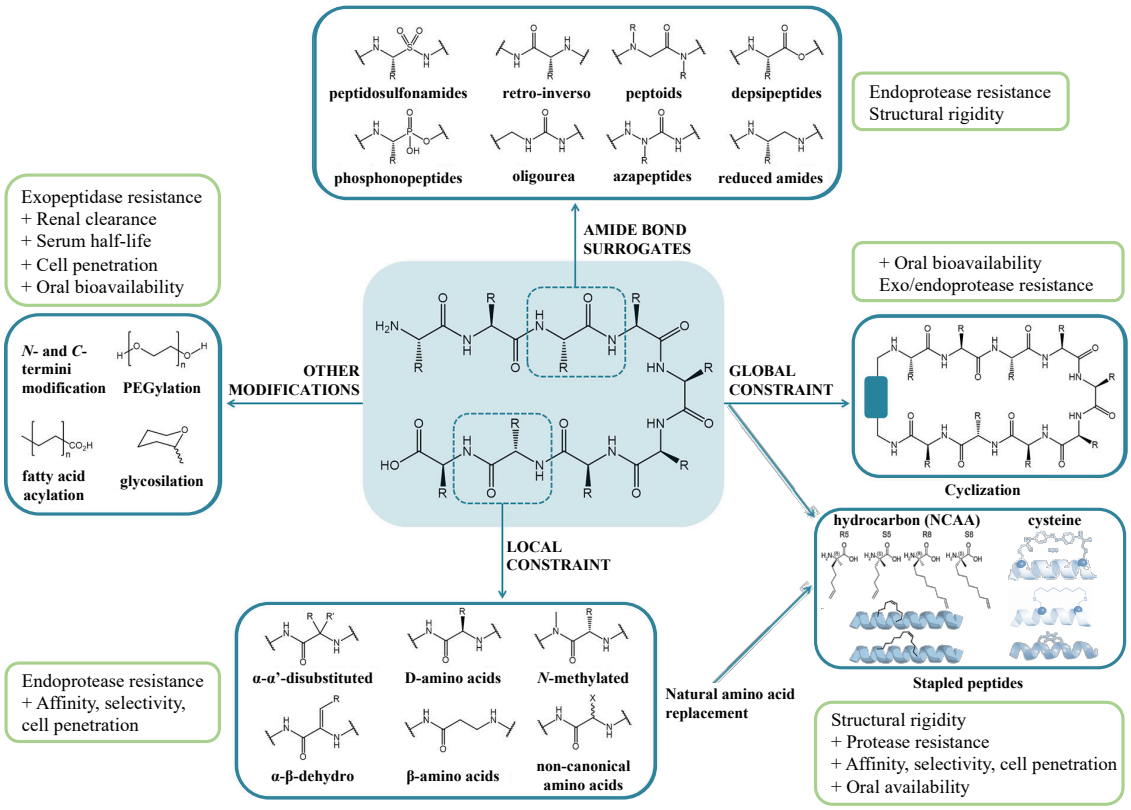

Figure 19: Peptide optimization strategies.
Modified from Fairlie and Dantas de Araujo, 2016; Góngora-Benítez et al., 2014. In green boxes are the benefits from the associated optimization strategies; "+" meaning increased.

2.4.3 Current peptide marketplace

The advantages mentioned above of the use of peptides as therapeutic agents, as well as the wide range of modifiers available for pharmacokinetic enhancement, have led to the recent development and market approval of different peptides for a variety of diseases. As of March 2017, there were 155 peptides in clinical trials and 60 approved peptides in the United States, Europe and Japan (Lau and Dunn, 2018). The average peptide length from approved peptides since 2010 is 20 amino acids, doubled from the 1980s (Lau and Dunn, 2018). Today, there are peptides of all lengths in clinical development. 30% of peptides in clinical development in the last ten years are conjugated.

Despite the ability of certain conjugates to aid in cell penetration, 91% of peptides entering clinical studies in the 2000s had extracellular targets (Tsomaia, 2015).

Peptides in CNS diseases

Potential CNS disease treatments are often rejected due to drug-drug interactions and safety, but peptides are less affected by these problems; accordingly, peptides thus have potential in this field to make it to market (Morimoto, 2018). Nonetheless, very few peptides have been approved for CNS diseases up to this point: three, to be exact, according to data from March 2017 (Lau and Dunn, 2018). In particular, CNS peptides need to be cell permeable in order to cross the BBB. BBB crossing can be achieved passively or actively, although most peptides cannot cross passively due to their hydrophilic nature (Vlieghe et al., 2010). BBB permeability can be engineered through cyclization, as mentioned above, or the addition of cell penetrating peptides like PepNeg, HIV-Tat, or AngioPep-2, among others (Dutot et al., 2010; Heitz et al., 2009; McGonigle, 2012; Morimoto, 2018; Neves-Coelho et al., 2017) or moities that hijack exposed receptors such as the LDL receptor binding domain of apolipoprotein B (Spencer and Verma, 2007).

I will next detail the three approved peptide drugs with CNS targets. First is glatiramer, a random polymer of 5 – 9 kDa composed of the four amino acids EKAP at a precise molar ratio. It was originally created from myelin basic protein to create an experimental autoimmune encephalomyelitis model to study multiple sclerosis. Surprisingly, it led to reduced inflammation and was later suggested to do so through binding to histocompatibility complex class II molecules, thereby competing with myelin antigens and myelin basic protein (Rommer et al., 2019). It was approved for multiple sclerosis via subcutaneous administration in 1996. Second is taltirelin, an analog to the

smallest hormonal peptide, thyrotropin-releasing hormone (TRH, pEHP-NH_2). It targets the TRH receptor and was approved for spinocerebellar degeneration via oral administration in 2000. Recently, it was shown to be neuroprotective in a SH-SY5Y cell model using 1-methyl-4-phenyl-1,2,3,6-tetrahydropyridine (MPTP, Zheng et al., 2018), a neurotoxin capable of inducing Parkinsonism in humans (Langston et al., 1983). Last, is ziconotide, a 25 amino acid peptide that is the synthetic equivalent of a peptide originating from the venom of a cone snail (CKGKGAKCSRLMTNCCTGSCRSGKC). It is a selective antagonist of the N-type voltage-sensitive calcium channel, providing pain relief when administered intrathecally, due to its weak ability to cross the BBB (Mcgivern, 2007). It was approved in 2004.

While multiple CNS peptides are in biochemical, cellular or pre-clinical stages, only 5% of all peptides in clinical development from a 2012 data set were for CNS diseases (Tsomaia, 2015). I will next detail some peptides for CNS therapeutics shown to cross the BBB in animal models. The most advanced peptide drug in CNS diseases is in two Phase 3 clinical trials and has shown to be neuroprotective for stroke. The NMDA receptor, involved with excitotoxicity-induced neuronal damage, binds to post-synaptic density scaffolding protein 95 (PSD-95) intracellularly, leading to downstream signaling. The peptide NA-1, a nine amino acid peptide fused to the eleven amino acid HIV-Tat peptide for cell permeability and brain distribution (Morimoto, 2018), interferes with the NMDA-PSD95 interface. After successful studies in rats and macaques, patients undergoing aneurysm repair surgery in the NA-1 group had a statistically significant decline in the number of lesions than the control group (Hill et al., 2012).

Next is the peptide named TFP5 or CT-526, a 24-amino acid peptide fused to the eleven amino acid HIV-Tat cell penetrating sequence. TFP5 blocks the interaction between its origin protein, p25 (itself a truncated version of p35), and cdk5, therefore

preventing cdk5-overstimulation-induced neurodegeneration (Morimoto, 2018). Notably, TFP5 does not inhibit regular p35/cdk5 function, suggesting that side effects would be minimal. TFP5 has been shown promising in animal models for stroke (Ji et al., 2017), MPTP-induced Parkinsonism (Binukumar et al., 2015), AD (Shukla et al., 2013) and ALS (Binukumar et al., 2019).

Additionally, the peptide known as P8 is eight amino acids long, rich in glutamates and aspartates, and originates from the N-ter of Presenilin-1, part of the γ-secretase complex. P8 disrupts the interaction of γ-secretase and APP, leading to reduced $A\beta_{1-40}$, and $A\beta_{1-42}$ production in APP transgenic mice and WT rats (Dewji et al., 2018, 2015). This highly specific interaction did not affect the catalytic activities of β nor γ secretase nor the level of APP (Dewji et al., 2015). P8, despite a lack of modifications, was shown to be stable in plasma and radiolabeled P8 was found in all areas of the rat brain. Finally, it was found that the peptide had better pharmacokinetic properties when administered intracutaneously (Dewji et al., 2018). P8 is still in pre-clinical trials.

Last of the BBB-crossing peptides highlighted here is the unmodified peptide Ilantide of ten amino acids, derived from the N-ter domain of human interleukin-1 receptor antagonist. It had anti-inflammatory properties in HeLa cells, crossed the BBB, and improved social memory in an Aβ-induced rat model (Klementiev et al., 2014).

In summary, multiple short peptides, some unmodified, are able to cross the BBB, specifically bind to their targets and block their interactions with other proteins in animal models or humans, leading to therapeutic effects of interest. These peptides demonstrate that it is possible to retain binding properties of the parent protein *in vivo*, suggesting the development of mini-chaperones from parent proteins capable of binding amyloid fibrils could be therapeutic candidates for propagation inhibition.

Objectives

Amyloid fibrils composed of the proteins αSyn, Tau and mHTT, implicated in synucleinopathies, tauopathies and HD, respectively, are able to propagate between neuronal cells, contributing to the progression of these fatal diseases. These fibrils have a multitude of protein and lipid partners at the cell membrane, where they initiate the cycle of propagation. Propagation inhibition could thus be targeted through the binding of moieties that alter the fibril surface properties, therefore disrupting interactions with a wide array of potential partners. Molecular chaperones, part of the cellular PQC system designed to prevent or eliminate protein aggregates, are good starting points to identify fibril binding partners. Therapeutically speaking, whole chaperones, due to their pleiotropic cellular roles, are not good candidates and should be reduced to bioactive domains or peptides to avoid off-target interactions. To this end, polypeptidic mini-chaperones containing the residues responsible for amyloidogenic protein binding could be pursued. Thus, the objective of my thesis was to identify molecular chaperones capable of binding fibrillar aggregates and, through a bottom-up approach, develop polypeptides capable of inhibiting fibril propagation.

Previous work in our lab using chemical cross-linking and MS identified binding sites of the molecular chaperone Hsc70 to monomeric αSyn. Furthermore, Hsc70 was shown to bind αSyn fibrils. In parallel, a pull down and MS approach using primary neuronal cells elucidated a binding site for the NKA α3 subunit and αSyn fibrils. These studies led to the development of three sub domains and nine peptide candidates, tested, in chapter 3, for a combination of fibrillation inhibition, fibril binding and/or propagation inhibition, the latter of which I contributed to.

While some molecular chaperones have been shown to bind various amyloid fibrils, this binding has not always been well characterized and its effects on propagation

have been largely untested in cellular models. In chapter 4, which covers my primary research project, I focused on identifying molecular chaperones of diverse origins, oligomeric status and of small size that are capable of binding αSyn amyloid fibrils. I then estimated the dissociation constants for αSyn fibrils and the molecular chaperones αBc and CHIP. With these chaperones, I evaluated the impact of chaperone-fibril binding on αSyn fibril internalization by a neuronal cell line. Finally, I worked to elucidate residues involved in αSyn fibril-αBc and αSyn fibril-CHIP interfaces through chemical cross-linking and MS for the development of mini-chaperones. I performed the cross-linking experiments and Dr. Virginie Redeker performed the MS experiments and analysis.

Lastly, in chapter 5, I further examined the structure of αSyn aggregates formed in presence of αBc or CHIP. In addition, I pursued the binding of my original set of molecular chaperones with Tau or HTTExon1Q48 fibrils and found that, in addition to αSyn fibrils, αBc finds to Tau and HTTExon1Q48 as well. I thus estimated the dissociation constants for the chaperone-fibril pairs.

All together, these studies aim to develop rationally designed, polypeptidic inhibitors of amyloid fibril propagation.

PART 2:

EXPERIMENTAL STUDIES

Chapter 3: Polypeptide binders of α-Synuclein fibrils

3.1 Article 1

Submitted to PLOS One.

Polypeptides derived from α-Synuclein binding partners to prevent α-Synuclein fibrils interaction with and take-up by cells

Elodie Monsellier, Maya Bendifallah, Virginie Redeker and Ronald Melki

CEA, Institut François Jacob (MIRcen) and CNRS, Laboratory of Neurodegenerative Diseases (UMR9199), 18 Route du Panorama, 92265, Fontenay-aux-Roses, France

Corresponding Author:

Ronald Melki, Institut de Biologie François Jacob, Molecular Imaging Research Center (MIRCen), Commissariat à l'Energie Atomique et aux Energies Alternatives (CEA), Laboratoire des Maladies Neurodégénératives, Centre National de la Recherche Scientifique (CNRS), Fontenay-aux-Roses, 92265, France. **ronald.melki@cnrs.fr**

Tel+***33-146549378***

Running title: Polypeptide binders of α-Synuclein fibrils

Abbreviations: αSyn, α-Synuclein; NKA, Na^+/K^+-ATPase; NBD, Nucleotide Binding Domain; SBD, Substrate Binding Domain; TEV, tobacco etch virus; ThT, Thioflavin T.

Keywords: Hsc70; molecular chaperones, Parkinson's disease; α-Synuclein; polypeptide binders

Abstract

α-Synuclein (αSyn) fibrils spread from one neuronal cell to another. This prion-like phenomenon is believed to contribute to the progression of the pathology in Parkinson's disease and other synucleinopathies. The binding of αSyn fibrils originating from affected cells to the plasma membrane of naïve cells is key in their prion-like propagation propensity. To interfere with this process, we designed polypeptides derived from proteins we previously showed to interact with αSyn fibrils, namely the molecular chaperone Hsc70 and the sodium/potassium pump NaK-ATPase and assessed their capacity to bind αSyn fibrils and/or interfere with their take-up by cells of neuronal origin. We demonstrate here that polypeptides that coat αSyn fibrils surfaces in such a way that they are changed affect αSyn fibrils binding to the plasma membrane components and/or their take-up by cells. Altogether our observations suggest that the rationale design of αSyn fibrils polypeptide binders that interfere with their propagation between neuronal cells holds therapeutic potential.

Introduction

The aggregation of proteins into fibrillar high molecular-weight species is involved in human degenerative diseases, including Alzheimer's, Parkinson's, or Huntington's [1]. During the last decade, it has become evident that those protein aggregates traffic between neuronal cells and amplify by seeding the aggregation of their constituting proteins [2–5]. This prion-like phenomenon is thought to be responsible for the stereotypic progression of the pathology in the brain [2,5]. Impeding this phenomenon would be valuable to slow down the progression of disease [6,7].

The spread of amyloid fibrils is a vicious circle involving different steps. First, protein aggregates form with time within neuronal cells [8]. They next escape actively, through export, or passively, upon cell death, the cells where they form [9–12]. The extracellular aggregates dock next to the membrane of naïve neuronal cells [13,14]. This membrane binding steps is followed by the internalization of the fibrils, mainly through endocytosis [15,16]. Once in the cells the aggregates reach the cytoplasm, where they recruit the otherwise soluble endogenous protein they are made of [17], after compromising endo-lysosomal integrity [18]. Alternatively, they imbalance neuronal proteostasis and trigger the de-novo aggregation of other aggregation prone proteins involved in neurodegenerative diseases [19]. The circle completes when amplified aggregates escape into the extracellular media, targeting new cells.

Every single step of the prion-like propagation process is a potential target for the development of new drugs that would delay the progression of disease. The binding of the extracellular aggregates to the membrane is especially attractive for different reasons [7]. As it takes place in the extracellular environment, it is more easily targetable than intracellular mechanisms [20]. Its underlying molecular mechanisms have been particularly well studied over the past few years [21]. The fibrils bind laterally to the

plasma membrane [13]. The binding is mediated by interaction with the plasma membrane lipids [22], with different proteins partners [23–26] and with the extra cellular matrix components [27,28]. The efficiency of the binding depends both on the aggregates characteristics, such as their primary sequence [29,30], their net charge [22], their size [13] or their conformation [17], and on the properties of the membrane, with an emphasis on the role of the membrane curvature [31] and a specific lipid [32] and protein [24,25] composition.

As different membrane components are involved in the interaction with extracellular aggregates in their prion-like propagation process, it seems unlikely that targeting one of them would exert an effect. We therefore decided to target the fibrils themselves, coating them with peptide ligands so that their surface properties are changed and their interaction with membrane partners is compromised. We decided to develop polypeptide binders of fibrils as from a clinical point of view such binders are specific and safe, and their poor pharmacokinetics properties are amenable to optimization [33,34]. Incidentally over 60 peptide drugs have now reached the market [35]. Using a cross-linking and mass spectrometry strategy, we previously mapped the surface interfaces between αSyn monomers or fibrils and two protein partners, namely, the molecular chaperone Hsc70 [36–38] and the sodium/potassium pump Na+/K+-ATPase (NKA) [25]. Here, we designed a set of polypeptides based on the Hsc70 and NKA surface areas we identified to interact with αSyn. We assessed the interaction of the polypeptides derived from Hsc70 and NKA with fibrillar αSyn in vitro. We identify Hsc70-derived polypeptides that bind best αSyn fibrils. We also show that an NKA-derived peptide affect fibrils binding to Neuro-2a cells. Overall, our results lay the basis for developing further such polypeptides and improving their affinity for αSyn fibrils, so that their interactions with and uptake by Neuro-2a neuronal cells are affected.

Results

Hsc70 binds to αSyn fibrils with a high affinity, preventing their interaction with the plasma membrane and their take-up by cultured cells

We previously brought evidence for Hsc70 interaction with fibrillar αSyn using a sedimentation assay [36]. The dissociation constant we measured was 0.1 µM. Here we confirmed the interaction between Hsc70 and fibrillar αSyn using the same sedimentation assay followed by quantitative analysis of the proteins in the pellet and the supernatant fractions by SDS-PAGE (**Figure 1A**). Hsc70 alone remains in the supernatant, whereas it is pulled into the pellet when incubated for 1h at room temperature with pre-formed αSyn fibrils. To determine the affinity of Hsc70 for fibrillar αSyn we incubated preformed αSyn fibrils (1 µM) with increasing amount of ATTO488-labeled Hsc70 (0-2 µM) for 1h at room temperature. The samples were then filtered through cellulose acetate membranes that retains fibrillar αSyn along with their binders, and the amount of ATTO488-Hsc70 was quantified by fluorescence measurements (**Figure 1B**). We measured a dissociation constant (K_D) between Hsc70-ATTO488 and αSyn fibrils of 0.49 ± 0.02 µM, consistent with previously published values [36,39]. We demonstrated that the binding between the two partners was not affected by Hsc70 labelling. Indeed, unlabeled Hsc70 competed in a dose-dependent way with the binding of labeled Hsc70 to αSyn fibrils (**Figure 1C**), and the K_D between Hsc70 and αSyn fibrils was identical to the K_D between Hsc70-ATTO488 and αSyn fibrils (0.45 ± 0.08 µM).

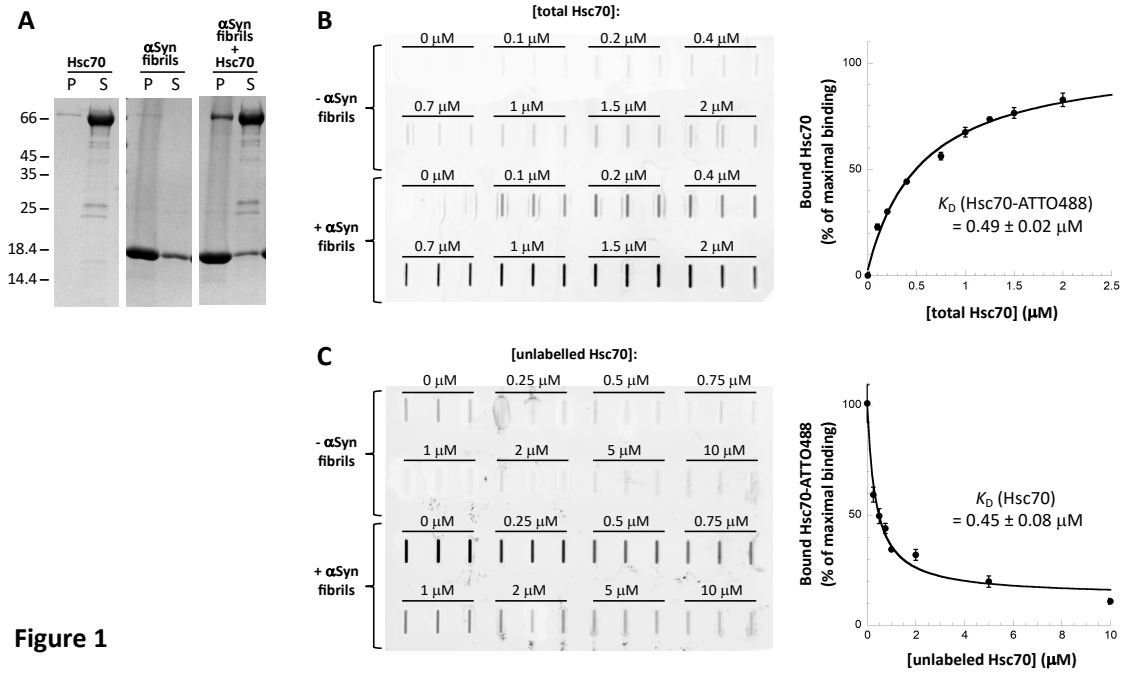

Figure 1

Figure 1. Hsc70 binds to αSyn fibrils with high affinity. A, Hsc70 binds to αSyn fibrils *in vitro*. SDS-PAGE analysis of the pellet (P) and supernatant (S) fractions of Hsc70 (10 μM), fibrillar αSyn (100 μM), and fibrillar αSyn (100 μM) incubated with Hsc70 (10 μM) for 1 h at RT. **B,** Quantification of Hsc70-ATTO488 binding to αSyn fibrils using the cellulose acetate filter trap assay. Hsc70-ATTO488 was diluted with unlabeled Hsc70 (labeled:unlabeled molar ratio of 1:50) to different final concentrations (0-2 μM) and incubated with or without αSyn fibrils (1 μM) for 1h at RT. Each sample was filtered in triplicate through a cellulose acetate membrane and the amount of Hsc70-ATTO488 trapped onto the membrane was quantified. The mean amount of Hsc70-ATTO488 bound to the αSyn fibrils and the associated standard error values were calculated from 3 independent experiments. **C,** Unlabeled Hsc70 compete with Hsc70-ATTO488 for binding to αSyn fibrils. A fixed concentration of Hsc70-ATTO488 (0.2 μM) was incubated with increasing concentrations of unlabeled Hsc70 (0-10 μM) and with or without αSyn fibrils (1 μM). Each sample was then filtered in triplicate through a cellulose acetate membrane. The mean amount of Hsc70-ATTO488 bound to the αSyn

fibrils and the associated standard error values were calculated from 2 independent experiments.

We next assessed the consequences of Hsc70 interaction with αSyn fibrils on fibrils binding to the cell membrane and subsequent internalization. We set-up two different assays to assess separately αSyn fibrils binding and internalization (**Figure 2**). Preformed Alexa488-labeled αSyn fibrils bound to cultured Neuro-2a cells within 30 min incubation in a dose-dependent manner as assessed by quantification of fluorescent foci at cell membranes (**Figures 2A** and **S1A**). The addition of Trypan blue quenched all the fluorescence, indicating that the fibrils are located at the plasma membranes. This robust cellular binding assay was next used to monitor the effect Hsc70-fibrillar αSyn interaction on fibrils binding to Neuro-2a cells. αSyn fibrils (1 μM) were pre-incubated with increasing amounts of Hsc70 (0-10 μM). Neuro-2a cultured cells were then incubated for 30 min with this mix. The data presented in **Figures 2B** and **S1B** clearly demonstrate that Hsc70 affects αSyn fibrils binding to Neuro-2a cells in a dose-dependent manner.

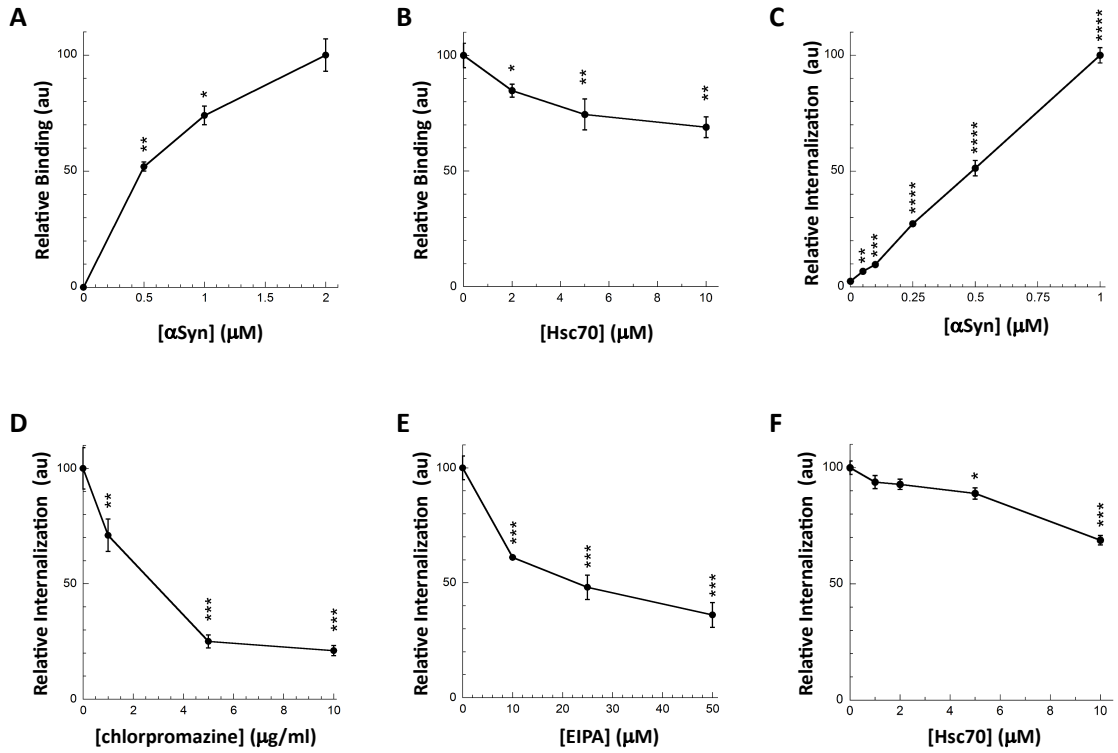

Figure 2

Figure 2. Hsc70 binding to αSyn fibrils interferes with their interaction with the plasma membrane and their subsequent internalization. A, Dose-dependent binding of αSyn fibrils to the plasma membrane of Neuro-2a cells. Neuro-2a cells were exposed for 30 min to αSyn-Alexa488 fibrils (0-2 μM). The cells were extensively washed and the fluorescence quantified. Representative images are shown in Figure S1A. For each concentration the mean percentage of Neuro-2a cells bound with at least 1 αSyn-Alexa488 fibrils foci and its associated standard error value was calculated from 3 independent experiments. The results and the associated significances are expressed relative to maximum binding. **B,** Hsc70 prevents αSyn fibrils binding to the plasma membrane. αSyn-Alexa488 fibrils (1 μM) were incubated with increasing concentrations of Hsc70 (0-10 μM) in DMEM for 30 min at 37°C. Neuro-2a cells were next exposed to the mixture for 30 min. Fluorescence was quantified after extensive washing. Representative images are shown in Figure S1B. For each Hsc70 concentration, the mean percentage of Neuro-2a cells with at least one αSyn-Alexa488 fibrils foci and its

associated standard error value was calculated from 3 to 5 independent experiments. The results and the associated significances are expressed relative to fibrils binding in the absence of Hsc70. **C,** αSyn fibrils take-up by Neuro-2a cells. Neuro-2a cells in 96-wells plates were exposed for 4 hours to increasing concentrations of αSyn-Alexa488 fibrils. Trypan blue was added after extensive washing to quench the fluorescence of plasma membrane-bound αSyn fibrils. The amount of internalized αSyn-Alexa488 was measured on a fluorescence plate reader. Means and their associated standard error values were calculated from 5 independent wells. The results are expressed relative to maximum internalization (1 µM αSyn fibrils). Significances are calculated in comparison to the absence of internalization (no αSyn). **D,E,** Chlorpromazine (D) and l'5-N-ethyl-isopropyl-amiloride (EIPA; E) prevent αSyn fibrils internalization by Neuro-2a cells□□Neuro-2a cells in 96-wells plates were exposed for 1 hour to increasing concentrations of chlorpromazine (0-10 µg/ml) or EIPA (0-50 µM) before addition of αSyn-Alexa488 fibrils (0.5 µM). After 4 hours of incubation and extensive washing, Trypan blue was added to quench the fluorescence of plasma membrane-bound αSyn fibrils. The amount of internalized αSyn-Alexa488 was measured on a fluorescence plate reader. Means and their associated standard error values were calculated from 5 independent wells. The results and the associated significances are expressed relative to the absence of inhibitors. **F,** Hsc70 prevents αSyn fibrils internalization by Neuro-2a cells. αSyn-Alexa488 fibrils (0.5 µM) were incubated with increasing concentrations of Hsc70 (0-10 µM) in DMEM for 30 min at 37°C. Neuro-2a cells in 96-wells plates were exposed for 4 hours to the mixture. Trypan blue was added after extensive washing to quench the fluorescence of plasma membrane-bound αSyn fibrils. The amount of internalized αSyn-Alexa488 was measured on a fluorescence plate reader. Means and their associated standard error values were calculated from 3 independent experiments.

The results and the associated significances are expressed relative to internalization in the absence of Hsc70.

Fibrillar αSyn uptake by cells can be assessed quantitatively by fluorescence microscopy after quenching of the fluorescence at cells plasma membrane by Trypan blue (**Figure S2**). To increase statistical power we set-up a robust 96-wells plate assay. Neuro-2a cells, in 96-wells plate, were exposed for 4h to Alexa488-labeled αSyn fibrils pre-incubated with Hsc70 or not, prior to Trypan blue addition and quantification of Alexa488 fluorescence in a plate-reader. The amount of internalized fibrils was determined in a dose- (**Figure 2C**) and time-dependent manner. Fibrillar αSyn take-up was inhibited in a dose-dependent manner by chlorpromazine and l'5-N-ethyl-isopropyl-amiloride (EIPA), suggesting that the fibrils are taken up by clathrin-mediated endocytosis and macropinocytosis (**Figures 2D,E**). Preincubation of Alexa488-labeled αSyn fibrils with Hsc70 significantly affected their take-up (**Figure 2F**). We used Hoechst staining to ascertain that the number of cells remained constant (see Material & Methods).

We conclude from these observations that Hsc70 binding to αSyn fibrils affects their binding and take-up by neuronal Neuro-2a cells in a dose-dependent manner. The use of full-length Hsc70 for therapeutic purposes has drawbacks because of its pleiotropic effects within cells. We thus aimed at generating fragments of Hsc70 that retain αSyn fibrils binding capacity.

Hsc70 Substrate Binding Domain and sub-domains retain αSyn fibrils binding capacity

In a first step toward the design of Hsc70-derived peptides that would potentially retain their ability to bind αSyn fibrils, we assessed the affinity of different Hsc70 sub-domains

for αSyn fibrils (**Figures 3, 4**). Hsc70 is composed of two domains, a Nucleotide Binding Domain (NBD), responsible for the chaperone ATPase activity, and a Substrate Binding Domain (SBD), that binds Hsc70 clients. We previously used lysine-reactive chemical cross-linkers and mass-spectrometry to map the surface areas within Hsc70 that interact with monomeric αSyn; all the identified areas were within the SBD (**Figures 3A**) [37,38]. To determine whether Hsc70 SBD retains the ability to bind αSyn fibrils we expressed and purified it. Hsc70 SBD (**Figure 3B, left**) can be subdivided in 2 sub-domains, a β-strands/sheet rich (SBDβ; **Figure 3B, middle**) and an α-helical domain, named "SBD-lid" (**Figure 3B, right**). Lysine residues from both of these sub-domains are located within the Hsc70-αSyn interaction interface suggesting that they both contribute to αSyn binding. We therefore expressed and purified SBDβ and SBD-lid.

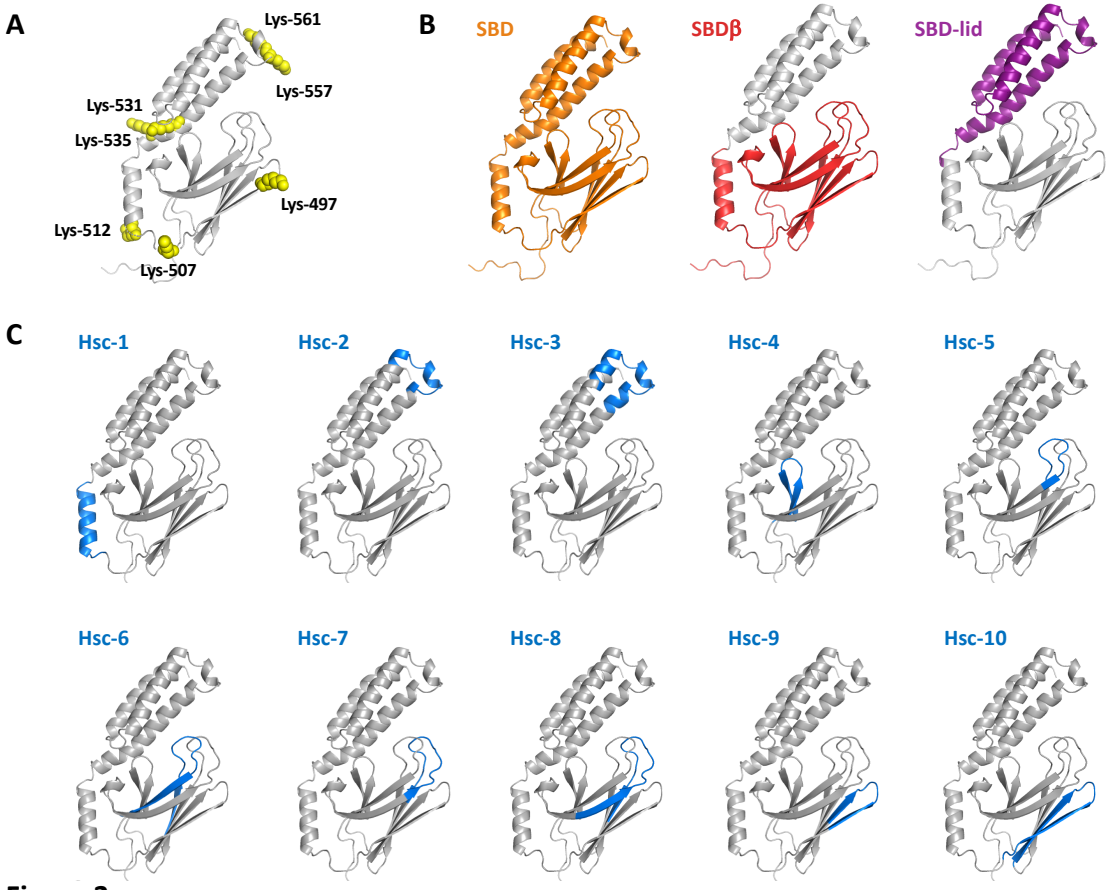

Figure 3

Figure 3. Hsc70 domains and peptides used throughout this study. A, αSyn-binding sites on Hsc70. The binding sites were determined by cross-linking Hsc70 to monomeric αSyn with chemical cross-linkers and identifying the surface interfaces by mass-spectrometry [37,38]. Only the substrate-binding domain (SBD) of Hsc70 is shown. Cross-linked lysines are depicted in yellow (space fill). Hsc70 model was built as described in [37]. **B,** Hsc70 SBD sub-domains. SBD β-sandwich (SBDβ) and lid (SBD-Lid) sub-domain are coloured. **C,** Hsc70-derived peptides. 10 peptides, which primary structure is given in Table 1, reproducing Hsc70 amino acid stretches involved in αSyn binding and the canonical Hsc70 client proteins binding sites [40], were synthesized.

A

Hsc70 domains	Hsc70 sequence	Length (aa)	Measured secondary structure composition (predicted values in brackets) α-helix	β-strand	Other
SBD	382 - 646	265	28 (30) %	26 (31) %	46 (39) %
SBDβ	382 - 526	144	5 (9) %	41 (39) %	54 (52) %
SBD-lid	524 - 646	123	51 (52) %	11 (0) %	38 (48) %

B

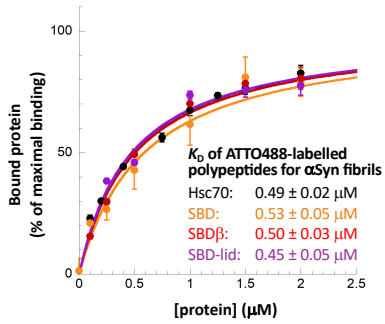

Figure 4

Figure 4. Hsc70 domains and their binding to αSyn fibrils. A, Secondary structure of Hsc70 SBD and sub-domains. The CD spectra used for deconvolution are shown in Figure S3A. **B,** Determination of Hsc70 domains – αSyn interactions K_D. The experiments were performed as in Figure 1B. In each case the mean amount of labeled Hsc70 domain bound to the fibrils and the associated standard error values were calculated from 3 independent experiments. Representative raw data are shown in Figure S4.

The secondary structure content of Hsc70 SBD, SBDβ and SBD-lid was assessed by circular dichroism measurements. The data suggest that the polypeptide conformation is retained (**Figures 3B**, **4A** and **S3A**). We next assessed SBD, SBDβ and SBD-lid binding

to αSyn fibrils as described for full-length Hsc70 and derived dissociation constants from those measurements (**Figures 4B** and **S4**). All three domains bind αSyn fibrils. Moreover, the K_D were similar to that we determined for full-length Hsc70 (**Figure 4B)**. Thus, both Hsc70 SBDβ and SBD-lid contribute to fibrillar αSyn binding as for monomeric αSyn [37,38].

αSyn fibrils Hsc70-derived peptides binders

To identify peptides derived from Hsc70 that have all that is necessary and sufficient to bind αSyn fibrils, we synthesized ten 11 to 24 residues Hsc70-derived polypeptides (**Table 1; Figure 3C**) based on the regions that contribute to αSyn binding (**Figure 3A**). Some peptides were overlapping to maximise binding. Hsc-1, 2, 3, 9 and 10 encompass Hsc70-αSyn interaction surface interfaces [37,38]. Hsc-4, 5 and 6 reproduce Hsc70 canonical client binding cavity [40]. Hsc-7 and 8 decal the rest of Hsc70 SBDβ loops. Hsc-4 and 9 were found insoluble in PBS. Their interaction with αSyn was not further studied. The secondary structure content of the 8 remaining peptides was assessed by circular dichroism measurements (**Table 1** and **Figure S3B**). The peptides were predominantly unstructured, with the exception of Hsc-1 and 10 (52 and 46 % α-helical, respectively). The presence of an α-helical conformation in the Hsc-1 peptide is coherent with the structure of this peptide within Hsc70 while Hsc-10 was expected to adopt a hairpin structure (**Figure 3C**).

Table 1. Hsc70-derived peptides primary and secondary structures. The CD spectra used for deconvolution are shown in Figure S3B.

Peptide	Hsc70 sequence	Sequence	Secondary structure composition		
			α-helix	ß-strand	Other
Hsc-1	510 - 525	LSKEDIERMVQEAEKY	52 %	0 %	48 %
Hsc-2	553 - 566	VEDEKLQGKINDED	6 %	13 %	81 %
Hsc-3	548 - 571	NMKATVEDEKLQGKINDEDKQKIL	9 %	7 %	84 %
Hsc-4	400 - 415	SLGIETAGGVMTVLIK			
Hsc-5	428 - 439	FTTYSDNQPGV	0 %	15 %	85 %
Hsc-6	422 - 444	TKQTQTFTTYSDNQPGVLIQVYE	0 %	20 %	80 %
Hsc-7	461 - 475	LTGIPPAPRGVPQIE	10 %	17 %	73 %
Hsc-8	457 - 477	GKFELTGIPPAPRGVPQIEVT	7 %	24 %	69 %
Hsc-9	489 - 500	SAVDKSTGKENK			
Hsc-10	484 - 505	GILNVSAVDKSTGKENKITITN	46 %	13 %	41 %

Hsc70 binding to monomeric αSyn affects assembly into fibrils [36]. We therefore first assessed Hsc70-derived peptide capacity to interact with monomeric αSyn through their ability to affect assembly into fibrils (**Figure 5**). Monomeric αSyn assembly into fibrils was monitored using Thioflavin T (ThT) binding at 37°C in the absence or the presence of equimolar amounts of each peptide. Hsc-6 significantly slowed down αSyn assembly into fibrils while Hsc-10 accelerated aggregation (**Figure 5 A, B**). The fibrillar nature of the assemblies obtained at the end of the reactions were assessed by transmission electron microscopy (**Figure 5C**). We conclude from these observations that 2 out of the 8 Hsc70-derived peptides we tested (Hsc-6 and 10) interact with monomeric αSyn in such a way that the time course of assembly into fibrils is significantly affected.

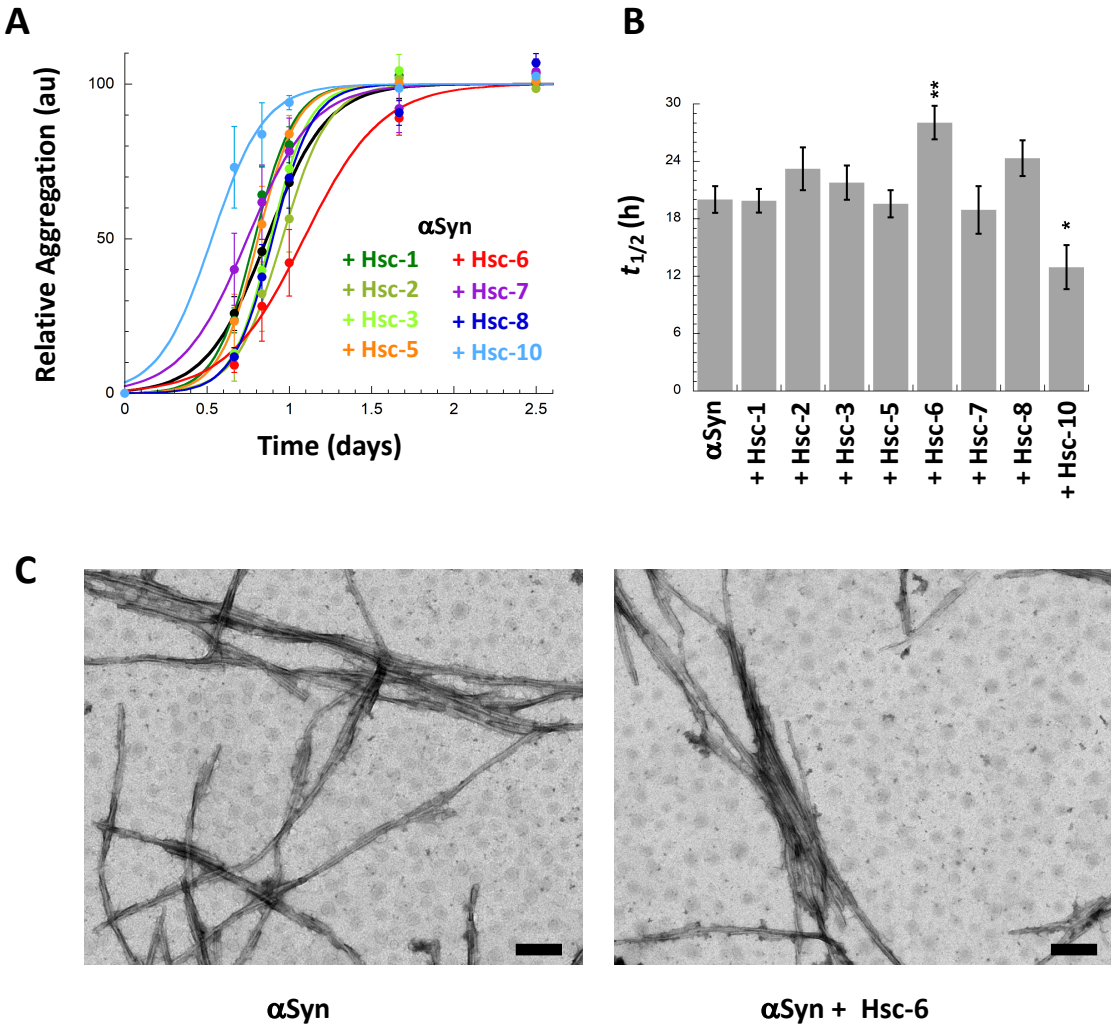

Figure 5

Figure 5. Effect of Hsc70 SBD-derived peptides on αSyn aggregation. **A,** Time-course of αSyn aggregation in the absence or presence of Hsc70 SBD-derived peptides. Soluble αSyn (50 µM) was incubated with or without Hsc70-derived peptides (50 µM) at 37°C and 600 rpm in PBS. The assembly reactions were monitored by Thioflavin T binding. Means and their associated standard errors values were calculated from 4 independent experiments. The lines through the data points represent the best fits to a sigmoid function. **B,** Effect of Hsc70-derived peptides on the half-time ($t_{1/2}$) of αSyn aggregation. For each independent experiment, the $t_{1/2}$ parameter was extracted from the best fit to a sigmoid function. The means and their associated standard error values were calculated

from 4 independent experiments. **C,** Negative stained electron micrographs of αSyn assembled alone (left) or in the presence of equimolar concentration of Hsc-6 (right). Scale bar, 200 nm.

We next assessed Hsc70-derived peptides binding to fibrillar αSyn. Fibrillar αSyn (100 μM) was incubated with each peptide (200 μM). The fibrils were sedimented and resuspended and the bound Hsc70-derived peptides were quantified by reversed phase chromatography. The results are presented in **Table 2** and **Figure S5A-C**. Hsc-1, 2, 3, 5, 7 and 8, did not bind to αSyn fibrils. Hsc-6 and 10 did bind to the fibrils. As a positive control we used the aromatic molecule Surfen, which is known to bind to the SEVI amyloid fibrils and to prevent their interaction with cells [41]. Surfen was found to bind to αSyn fibrils (**Table 2**).

Table 2. Binding of the Hsc70-derived peptides to αSyn fibrils assessed by phase reverse chromatography analysis

Sample	Bound peptides μM	(%)
Hsc-1	1.2	0.6 %
Hsc-2	1.0	0.5 %
Hsc-3	1.2	0.6 %
Hsc-5	2.8	1.4 %
Hsc-6	68	34 %
Hsc-7	1.2	0.6 %
Hsc-8	1.6	0.8 %
Hsc-10	72	36 %
Surfen	176	88 %

The affinities of Hsc-6 and 10 for αSyn fibrils were determined and the K_D was over 100 μM (**Figure S5E,F**). Nonetheless, to determine whether Hsc70-derived peptides affect fibrillar αSyn uptake by cells, Alexa488-labeled αSyn fibrils were pre-incubated with up to 10 molar excess of the different Hsc70-derived peptides and fibrils uptake by Neuro-

2a cells was quantified. None of the Hsc70-derived peptides had an effect on αSyn fibrils take-up (**Figure 6**). This is consistent with the poor affinity of the best fibrillar αSyn peptide binders. In contrast, preincubation of αSyn fibrils with Surfen affected, in a dose-dependent way, their take-up by Neuro-2a cells (**Figure 6**).

Figure 6

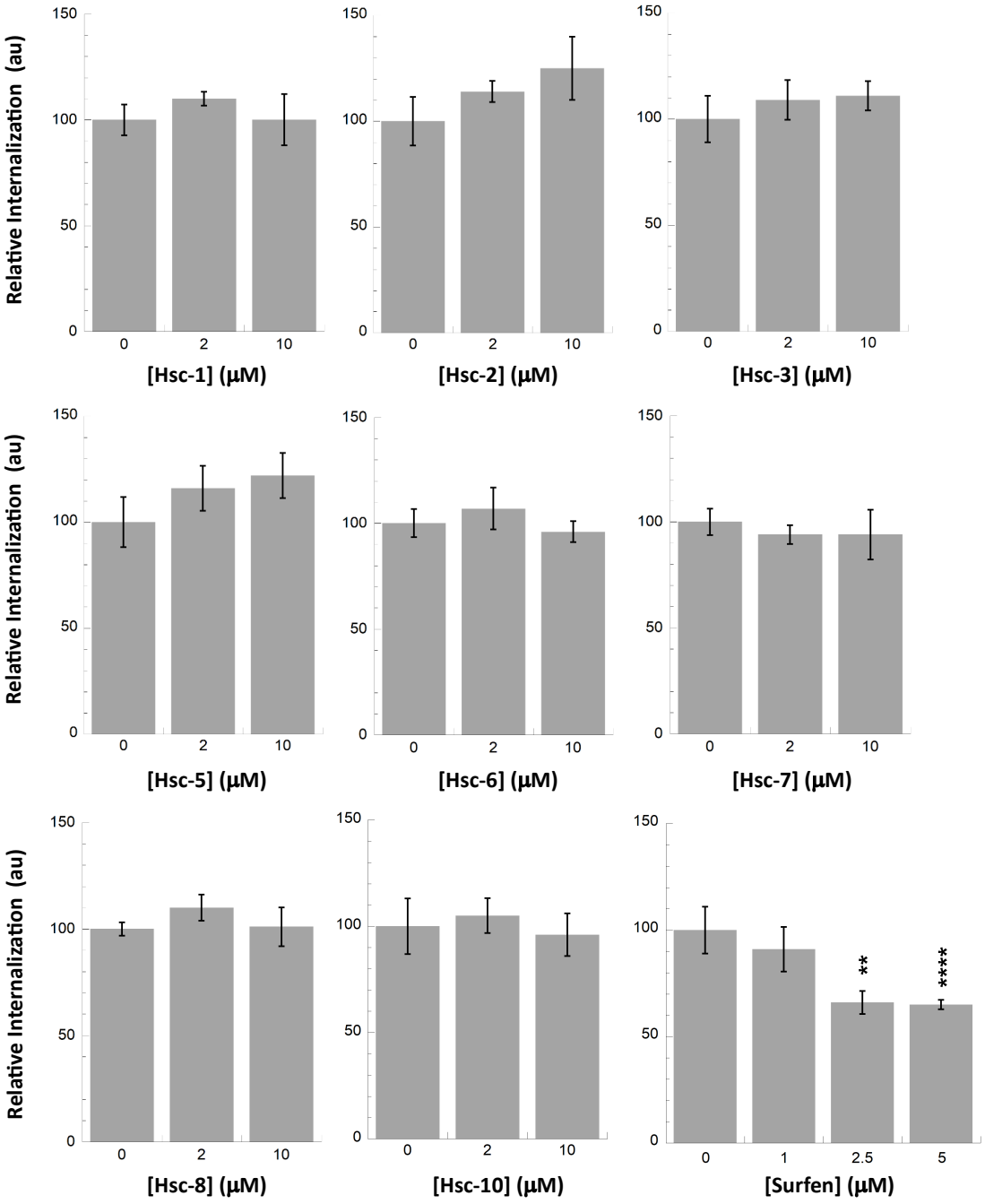

Figure 6. Effect of Hsc70 SBD-derived peptides on αSyn fibrils take-up by Neuro-2a cells. Each Hsc70 SBD-derived peptide (2 or 10 µM) was incubated with Alexa488-

labeled αSyn fibrils (1 μM) in DMEM for 30 min at 37°C. Neuro-2a cells grown in 96-wells plates were exposed to the mixture for 2 hours. After extensive washing trypan blue was added to quench the fluorescence of plasma membrane-bound αSyn fibrils. The amount of internalized αSyn-Alexa488 was measured using a fluorescence plate reader. Means and their associated standard error values were calculated from 3 independent experiments. The same experiment was carried out with Surfen.

Peptide derived from an αSyn fibrils membrane partner, the α3 subunit of the Na^+/K^+-ATPase (NKA)

We previously brought evidence for interaction of fibrillar αSyn with the α3-subunit of the membrane ion pump NKA by pull-down [25]. α3NKA amino acid stretch that interacts with αSyn was identified by cross-linking and mass spectrometry. It consists of the extracellular loop connecting the transmembrane helices 7 and 8 [25]. Interaction of fibrillar αSyn with this extracellular loop of α3NKA was further confirmed by mutagenesis studies [25]. To determine whether NKA derived peptides affect αSyn fibrils binding to and take-up by Neuro-2a cells, we synthesized a 27 amino acid residues long peptide (NKApep) that reproduces this loop within α3NKA (**Figure 7A**). NKApep is soluble in PBS; it is disordered with some β-strand content, as assessed by circular dichroism (**Figures 7B** and **S3C**).

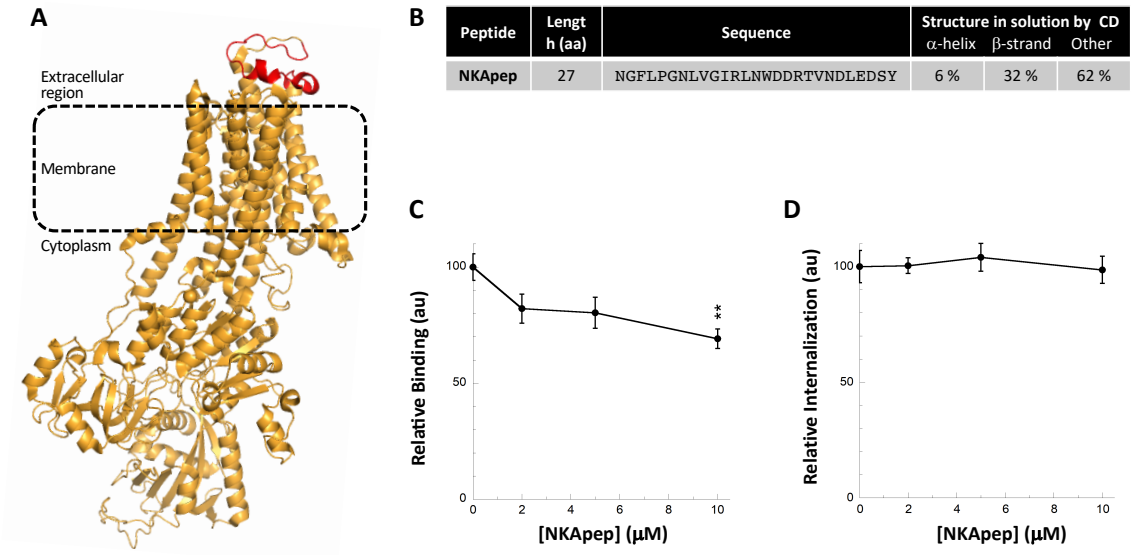

Figure 7

Figure 7. Effect of a peptide derived from the α3 subunit of the NKA on αSyn fibrils binding and take-up by Neuro-2a cells. A, Structure of the α3 subunit of the NKA *Bos taurus* (PDB 4xe5) where the 27 amino acid residues long peptide NKApep corresponding to the extracellular loop previously shown to interact with αSyn fibrils [25] is coloured in red. **B**, Secondary structure content of NKApep determined by circular dichroism. The CD spectra used for deconvolution is shown in Figure S3C. **C,** Effect of NKApep on αSyn fibrils binding to the plasma membrane of Neuro-2a cells. αSyn-Alexa488 fibrils (1 µM) were incubated without or with increasing concentrations of NKApep in DMEM for 30 min at 37°C. Neuro-2a cells were next exposed to the mixture for 30 min. Fluorescence was quantified after extensive washing. Representative images are shown in Figure S1B. For each peptide concentration, the mean percentage of Neuro-2a cells with at least 1 αSyn-Alexa488 fibrils foci and its associated standard error value was calculated from 3 independent experiments. The results and the associated significances are expressed relative to fibrils binding in the absence of peptide. **D,** Effect of NKApep on αSyn fibrils take-up by Neuro-2a cells. αSyn-Alexa488 fibrils (0.5 µM) were incubated with increasing concentrations of NKApep (0-10 µM) in DMEM for 30

min at 37°C. Neuro-2a cells grown in 96-wells plates were exposed to the mixture for 4 hours. After extensive washing trypan blue was added to quench the fluorescence of plasma membrane-bound αSyn fibrils. The amount of internalized αSyn-Alexa488 was measured using a fluorescence plate reader. Means and their associated standard error values were calculated from 4 independent experiments. The results are expressed relative to the internalization in the absence of peptide.

NKApep neither affected αSyn aggregation (not shown) nor bound to preformed αSyn fibrils (**Figure S5D**). Preincubation of preformed αSyn fibrils with NKApep resulted in a dose-dependent reduction in fibrillar αSyn binding to Neuro-2a cells (**Figures 7C** and **S1C**) but did not affect fibrils take-up (**Figure 7D**). Altogether, although designed to affect fibrillar αSyn binding to cells, NKApep acts somewhat differently, possibly through interactions with other membranous components.

Discussion

αSyn fibrils are able to spread from one neuronal cell to another [2–4]. This process is believed to contribute to the spatiotemporal progression of pathology in the central nervous system [2,5]. The binding of αSyn fibrils to naïve cells, after their formation and release from affected counterparts, is key and has been actively documented as it constitutes a potential target for therapeutic interventions [7,13]. We hypothesized that ligands that change the surface properties of αSyn fibrils should affect binding to cell membranes. We previously showed that Hsc70 binding to αSyn fibrils affects the viability of cultured cells of neuronal origin [36]. We demonstrate here that Hsc70 interaction with αSyn fibrils compromises their binding and take-up by cells. The pleiotropic functions of full-length Hsc70 limit its therapeutic potential [42,43]. We therefore generated polypeptides reproducing Hsc70 sub-domains and surfaces that we previously showed to

interact with αSyn through cross-linking studies [37,38] and assessed their effect on αSyn fibrils binding to and take-up by cells of neuronal nature. We show here that two peptides derived from Hsc70 SBD interact with αSyn without affecting, most probably because of their limited affinity, their take-up by Neuro-2a cells [44,45].

We previously identified through unbiased pull-down and cross-linking strategies fibrillar αSyn neuron membrane proteins interactome [25]. Polypeptides reproducing αSyn protein partners may interfere with fibrils binding to their targets. We therefore assessed the shielding propensity of NKApep, an NKA-derived peptide that encompasses a region we showed to interact with fibrillar αSyn [25]. NKApep did not bind to αSyn fibrils under our experimental conditions, nonetheless, we show here that it interferes with fibrillar αSyn binding to cells. This suggests that NKApep affects αSyn fibrils binding to the cell indirectly, possibly through the redistribution of other αSyn fibrils target proteins [21].

Overall, our results suggest that polypeptides that bind αSyn fibrils must have a very high affinity to affect fibrils uptake by cells and hold therapeutic potential. Advantageously, the affinity of polypeptides is amenable to improvements. They can be trimmed and modified by replacing a number of amino acid residues and reassessing affinity in an iterative manner [46]. To limit their folding landscape, they can be stapled using unnatural amino acids bearing alkyl tethers of various lengths at either one or two helix turns [47] or compatible with covalent crosslinking via click chemistry [48], or fused to a scaffolding protein such as thioredoxin [49]. Alternatively, their avidity could be increased by generating tandem repeats of the same or different peptides that bind αSyn fibrils. Many other modifications can be made so that pharmacokinetic properties of polypeptides that interfere with αSyn fibril binding and take-up by cells are improved. Thus, such peptide could yield new therapeutic tools to slow down the progression of synucleinopathies and other neurodegenerative diseases.

Materials and Methods

Expression and purification of αSyn, Hsc70 and Hsc70 subdomains

Recombinant human wild-type αSyn was purified as described [50]. Recombinant His_6-tagged Hsc70 was purified as described [36]. The activity of the purified Hsc70 was assessed using a luciferase refolding assay, as described in [36].

Genes encoding the Hsc70 domain and subdomains SBD, SBDβ and SBD-lid were amplified from the pPRO-EXHTb (Invitrogen) Hsc70 vector [36] and inserted into a pET-M11 vector with an N-terminal 6xHis tag followed by a tobacco etch virus (TEV) protease cleavage site. Recombinant His-tagged proteins were expressed at 37°C in E.coli strain BL21(DE3) (Stratagene, Santa Clara, CA) and purified as follow. Cells were harvested and resuspended in buffer A (30 mM HEPES pH 7.5, 300 mM NaCl, 10% glycerol, 20 mM imidazole). After sonication and centrifugation, lysate supernatants were filtered and loaded onto a 5 mL Talon metal affinity resin column (Clontech, Saint-Germain-en-Laye, France), equilibrated in buffer A. His tagged proteins were eluted with buffer A supplemented with 500 mM imidazole, and then dialysed in PBS. The His tags were cleaved with addition of His-TEV protease, produced using the plasmid pRK1043 (Addgene, Cambridge, MA), at a 1:25 His-TEV:chaperone molar ratio. 100% cleavage, as assessed by SDS-PAGE, was achieved upon incubating the mixtures for 1h at 37 °C. The untagged proteins were purified by collecting the flow through of a 5 mL HisTrap FF column.

Proteins concentrations were determined spectrophotometrically using the following extinction coefficients at 280 nm ($M^{-1}.cm^{-1}$): 5960 for αSyn; 39310 for Hsc70; 12950 for SBD; 2980 for SBDβ; and 9970 for SBD-lid. Pure proteins in PBS were filtered through sterile 0.22-µm filters, aliquoted and stored at -80 °C.

Synthetic peptides and Surfen

All the peptides we designed were purchased from GL Biochem Ltd. (Shanghai, China). Peptides were dissolved in PBS at 0.5 mM, aliquoted, and stored at -20 °C. Surfen (S6951) was purchased from Sigma, dissolved in DMSO at 5 mM, aliquoted, and stored at -20°C.

Circular Dichroism

Far-UV CD spectra were recorded at 20 °C using a JASCO J-810 dichrograph equipped with a thermostated cell holder using a 0.01-cm path length quartz cuvette. Each spectrum was the average of 10 acquisitions recorded in the 260–195 nm range with 0.5-nm steps, a bandwidth of 2 nm, and at a speed of 50 nm/min. All spectra were buffer corrected. The spectra were deconvoluted with the Dichroweb software [51].

Assembly of αSyn into fibrils and labelling

For fibril formation, αSyn was incubated at 200 µM in PBS at 37 °C under continuous shaking in an Eppendorf Thermomixer set at 600 rpm for 2 weeks. The completion of the aggregation reaction was monitored by withdrawing an aliquot (100 µL), subjecting it to centrifugation in a 5415R tabletop centrifuge (Eppendorf) at 20,000 g and 20°C for 30 min and assessing spectrophotometrically the amount of αSyn remaining in the supernatant. The proportion of soluble αSyn was systematically less than 10%. The fibrillar nature of the aggregates obtained at the end of the aggregation reaction was assessed using a Jeol 1400 transmission electron microscope (Jeol Ltd.) following adsorption of the samples onto carbon-coated 200-mesh grids and negative staining with 1% uranyl acetate. The images were recorded with a Gatan Orius CCD camera (Gatan).

For cellular binding and internalization experiments, the fibrils were labeled by addition of the aminoreactive fluorescent dye Alexa 488 (Invitrogen, Carlsbad, CA, USA) using a protein:dye molar ratio of 10:1 based on initial monomer concentration. Labelling was performed following the manufacturer's recommendation. The reaction was stopped by adding Tris-HCl pH 7.5 (20 mM final concentration). Finally, the fibrils were sonicated with an ultrasound sonicator (Hielscher Ultrasonic, Teltow, Germany) set at an amplitude of 75 and 0.5 s cycles for 1 min.

Binding of Hsc70, SBD, SBDβ and SBD-lid to preformed αSyn fibrils and K_D determination

For binding assay, αSyn fibrils (100 µM) alone, Hsc70 alone (10 µM) or αSyn fibrils and Hsc70 (100 and 10 µM, respectively) were incubated for 1h at RT in PBS. Samples were spun for 30 min at 50,000 g and 20°C in a TL100 tabletop ultracentrifuge (Beckman) and the proportion of Hsc70 present in the pellet *vs* the supernatant was analysed by SDS-PAGE.

The K_D for Hsc70, SBD, SBDβ and SBD-lid interaction with αSyn fibrils were measured as follow. Hsc70 and its subdomains were first labeled by addition of the aminoreactive fluorescent dye ATTO488 (Invitrogen, Carlsbad, CA, USA) using a protein:dye molar ratio of 1:5. The reaction was stopped by adding Tris-HCl pH 7.5 (20 mM final concentration). The unreacted fluorophore was removed by NAP5 desalting column. Under these conditions the majority of primary amines unaffected by the labelling as 0.05 to 0.08 dye molecules were incorporated on average within Hsc70 or its subdomains, as assessed by absorbance spectroscopy. Binding of ATTO488-labeled polypeptides to fibrillar αSyn was then followed by a filter retardation assay where fibrils and associated proteins are retained on a membrane [52]. The different ATTO488-labeled polypeptides

were diluted with their unlabeled counterpart (labeled:unlabeled polypeptides ratio of 1:50) at different final concentrations (0-2 µM) and incubated with or without αSyn fibrils (1 µM) in PBS for 1h at RT. 200 µl of each sample were filtered in triplicate through cellulose acetate membranes (0.2 µm pore size, Millipore Corp., Bedford, MA) using a 48-slot slot-blot filtration apparatus (GE Healthcare). The amount of labeled polypeptide retained on the membrane was visualized using a ChemiDocTM MP (BioRad). Images were processed and quantified using Image Lab.

Alternatively, to ensure that the labelling did not affect the binding properties of Hsc70 to αSyn fibrils, a fixed concentration of Hsc70-ATTO488 (0.2 µM) was incubated with increasing concentrations of unlabeled Hsc70 (0-10 µM) and with or without αSyn fibrils (1 µM) in PBS for 1h at RT. The experiment was then performed as above.

Assessment of synthetic peptides effect on αSyn assembly

αSyn (50 µM monomer concentration) was incubated in the absence or in the presence of peptides (50 µM) in PBS at 37 °C under continuous shaking in an Eppendorf Thermomixer set at 600 rpm. Aliquots (10 µL) were withdrawn at different time intervals from the assembly reaction and mixed to a Thioflavin T solution (10 µM; 400 µL). Thioflavin T fluorescence was recorded with a Cary Eclipse spectrofluorimeter (Varian Medical Systems Inc.) using excitation and emission wavelengths set at 440 and 480 nm, respectively. The nature of the fibrils obtained at the end of the aggregation reaction was assessed by electron microscopy as described above. The proportion of αSyn assembled into fibrils was assessed by ultracentifugation in a TL100 tabletop centrifuge (Beckman) at 50,000 g and 20°C for 30 min and analyse of the supernatant and pellet fractions by SDS-PAGE. Following Coomassie staining / destaining the gels were visualized using a ChemiDocTM MP (BioRad). Images were processed and quantified using Image Lab.

Binding of peptides derived from Hsc70 and NKA and Surfen to preformed αSyn fibrils and K_D determination

Hsc70-derived peptides, the NKApep peptide or the Surfen molecule (0 or 200 µM) were incubated with or without αSyn fibrils (100 µM) for 1h at RT in PBS. The samples were centrifuged for 30 min in a 5415R tabletop centrifuge (Eppendorf) at 20,000 g and 20°C. The pellets were first washed by 100 uL of 0.1% TFA and then dissolved for 30 min in 30 µL of pure TFA. After TFA evaporation, the samples were resuspended in 0.1% TFA and stored at -20°C. The composition of each sample was assessed by phase reverse chromatography on a C18 column (Jupiter C18 300A from Phenomenex, Torrance, CA, USA). The solvant composition was 0.1% TFA for solvent A and 80% acetonitrile, 0.09% TFA for solvent B, and the flow was set at 200 µl/min. The column was equilibrated in 5% B. The peptides were eluted by a gradient from 5% to 80% of solvent B. The amount of αSyn-associated ligand present in each sample was determined by comparing their respective absorbance at 215 nm (peptides) or 260 nm (Surfen) to the absorbance of a known amount of the same ligand. For K_D measurements the same experiment was performed using a range of peptide concentrations (0-200 µM).

Cell culture

Murine neuroblastoma Neuro-2a cells (ATCC, Manassas, VA) were culture at 37 °C in humidified air with 5% CO2 in Dulbecco's modified Eagle's medium (DMEM) containing 10% foetal bovine serum, 2 mM glutamine, 100 units.ml^{-1} penicillin and 100 µg.ml^{-1} streptomycin. All materials used for cell culture were from PAA Laboratories GmbH (Pasching, Austria).

Binding of αSyn fibrils to Neuro-2a cells

Alexa488-labeled αSyn fibrils (1 μM equivalent monomer concentration) were first incubated for 30 min at 37°C in DMEM without or with the ligands (Hsc70 or the NKApep peptide) at different concentrations. Neuro-2a cells cultured on ibidi-μ-Dishes (ibidi, Martinsried, Germany) were then incubated for 30 min with this mix. Then, the cells were washed and immediately imaged in serum-free, phenol red-free DMEM on a Zeiss Axio Observer Z1 epifluorescence microscope equipped with an Incubator XLmulti S2 RED LS (Carl Zeiss) and an Orca-R2 camera (Hamamatsu) at a 20x magnification. The percentage of cells with bound Alexa488 foci was estimated by randomly counting at least 500 cells in 10–15 fields and the experiments were reproduced independently 3 times. For each field the number of foci was automatically assessed using the software Fiji [53,54] and an in-house built plugin.

Internalization of αSyn fibrils by Neuro-2a cells

Neuro-2a cells cultured on ibidi-μ-Dishes (ibidi, Martinsried, Germany) were exposed for 4h to Alexa488-labeled αSyn fibrils (1 μM equivalent monomer concentration) at 37°C in DMEM. The cells were washed twice with serum-free, phenol red-free DMEM and 0.1% Trypan Blue (Sigma-Aldrich) was added to quench Alexa488 fluorescence at the plasma membrane. The cells were then imaged and the percentage of cells with internalized Alexa488 foci was estimated as described above.

The uptake of Alexa488-labeled αSyn fibrils (0.5 μM equivalent monomer concentration) pre-incubated or not for 30 min at 37°C in DMEM with the ligands (Hsc70, peptides or Surfen) at different concentrations to Neuro-2A cells was also assessed using a 96-well plate assay. The cells cultured on 96-wells plates were incubated with the fibrils, preincubated or not with the ligands for 30 min at 37°C in DMEM, in 5 independent

wells. After 4 hours the media was removed and Hoechst (Sigma-Aldrich) diluted at 0.2 µg/ml in serum-free, phenol red-free DMEM was added for 30 min. The cells were washed twice with serum-free, phenol red-free DMEM and 0.1% Trypan Blue (Sigma-Aldrich) was added to quench the fluorescence of plasma membrane-bound Alexa488-labeled αSyn fibrils. For each wells Alexa488 and Hoechst fluorescences were recorded on a Clariostar microplate reader (BMG LABTECH GmbH, Germany). For each condition Alexa488 fluorescence value was considered and averaged over the 5 wells only if the Hoescht value was not significantly different from the one of untreated cells.

To assess to role of endocytosis in αSyn fibrils internalization, Neuro-2a cells cultured on 96-wells plates were first incubated with increasing concentrations of chlorpromazine or l'5-N-ethyl-isopropyl-amiloride (EIPA). After 1 hour Alexa488-labeled αSyn fibrils (0.5 µM equivalent monomer concentration) was added. The experiment was then performed as above.

Statistical Significance

Statistical significance was determined through an unpaired student's t-test. Annotations used throughout the manuscript to indicate level of significance are as follows: * $p<0.05$; ** $p<0.01$; *** $p<0.001$; **** $p<0.0001$.

Author Contributions

EM and RM planned the experiments; EM, MB and VR performed experiments; EM and RM analysed data and wrote the paper.

Acknowledgements

We thank Mrs. Tracy Bellande for expert technical assistance. This work was supported by the Centre National de la Recherche Scientifique, the Institut National de la Santé et de la Recherche Médicale, the Région Ile de France through DIM Cerveau et Pensée, the Institut de France-Fondation Simone et Cino Del Duca, the Fondation Pour La Recherche Médicale (contract DEQ. 20160334896), the EC Joint Programme on Neurodegenerative Diseases and Agence Nationale pour la Recherche (TransPathND, ANR-17-JPCD-0002-02 and Protest-70, ANR-17-JPCD-0005-01). This work benefited from the electron microscopy facility Imagerie-Gif.

References

1. Knowles TPJ, Vendruscolo M, Dobson CM. The amyloid state and its association with protein misfolding diseases. Nat Rev Mol Cell Biol. 2014;15: 384–396. doi:10.1038/nrm3810
2. Brundin P, Melki R, Kopito R. Prion-like transmission of protein aggregates in neurodegenerative diseases. Nat Rev Mol Cell Biol. 2010;11: 301–307. doi:10.1038/nrm2873
3. Brundin P, Melki R. Prying into the Prion Hypothesis for Parkinson's Disease. J Neurosci. 2017;37: 9808–9818. doi:10.1523/jneurosci.1788-16.2017
4. Vargas JY, Grudina C, Zurzolo C. The prion-like spreading of α-synuclein: From in vitro to in vivo models of Parkinson's disease. Ageing Res Rev. 2019;50: 89–101. doi:10.1016/j.arr.2019.01.012
5. Jucker M, Walker LC. Propagation and spread of pathogenic protein assemblies in neurodegenerative diseases. Nat Neurosci. 2018;21: 1341–1349. doi:10.1038/s41593-018-0238-6
6. Eisele YS, Monteiro C, Fearns C, Encalada SE, Wiseman RL, Powers ET, et al. Targeting protein aggregation for the treatment of degenerative diseases. Nat Rev Drug Discov. 2015;14: 759–780. doi:10.1038/nrd4593
7. Pemberton S, Melki R. The interaction of Hsc70 protein with fibrillar αSynuclein

and its therapeutic potential in Parkinson disease. Commun Integr Biol. 2012;5: 94–95. doi:10.4161/cib.5.1.18483

8. Xilouri M, Brekk OR, Stefanis L. α-Synuclein and protein degradation systems: a reciprocal relationship. Mol Neurobiol. 2013;47: 537–551. doi:10.1007/s12035-012-8341-2
9. Abounit S, Bousset L, Loria F, Zhu S, de Chaumont F, Pieri L, et al. Tunneling nanotubes spread fibrillar α-synuclein by intercellular trafficking of lysosomes. EMBO J. 2016;35: 2120–2138. doi:10.15252/embj.201593411
10. Deng J, Koutras C, Donnelier J, Alshehri M, Fotouhi M, Girard M, et al. Neurons Export Extracellular Vesicles Enriched in Cysteine String Protein and Misfolded Protein Cargo. Sci Rep. 2017;7: 956. doi:10.1038/s41598-017-01115-6
11. Katsinelos T, Zeitler M, Dimou E, Karakatsani A, Müller HM, Nachman E, et al. Unconventional Secretion Mediates the Trans-cellular Spreading of Tau. Cell Rep. 2018;23: 2039–2055. doi:10.1016/j.celrep.2018.04.056
12. Ren PH, Lauckner JE, Kachirskaia I, Heuser JE, Melki R, Kopito RR. Cytoplasmic penetration and persistent infection of mammalian cells by polyglutamine aggregates. Nat Cell Biol. 2009;11: 219–225. doi:10.1038/ncb1830
13. Monsellier E, Bousset L, Melki R. α-Synuclein and huntingtin exon 1 amyloid fibrils bind laterally to the cellular membrane. Sci Rep. 2016;6: 19180. doi:10.1038/srep19180
14. Han S, Kollmer M, Markx D, Claus S, Walther P, Fändrich M. Amyloid plaque structure and cell surface interactions of β-amyloid fibrils revealed by electron tomography. Sci Rep. 2017;7: 43577. doi:10.1038/srep43577
15. Angot E, Steiner JA, Tomé CM, Ekström P, Mattsson B, Björklund A, et al. Alpha-synuclein cell-to-cell transfer and seeding in grafted dopaminergic neurons in vivo. PLoS One. 2012;7: e39465. doi:10.1371/journal.pone.0039465
16. Münch C, O'Brien J, Bertolotti A. Prion-like propagation of mutant superoxide dismutase-1 misfolding in neuronal cells. Proc Natl Acad Sci. 2011;108: 3548–3553. doi:10.1073/pnas.1017275108
17. Bousset L, Pieri L, Ruiz-Arlandis G, Gath J, Jensen PH, Habenstein B, et al. Structural and functional characterization of two alpha-synuclein strains. Nat Commun. 2013;4: 2575. doi:10.1038/ncomms3575
18. Flavin WP, Bousset L, Green ZC, Chu Y, Skarpathiotis S, Chaney MJ, et al.

Endocytic vesicle rupture is a conserved mechanism of cellular invasion by amyloid proteins. Acta Neuropathol. 2017;134: 629–653. doi:10.1007/s00401-017-1722-x

19. Gidalevitz T, Ben-Zvi A, Ho KH, Brignull HR, Morimoto RI. Progressive disruption of cellular protein folding in models of polyglutamine diseases. Science (80-). 2006;311: 1471–1474. doi:10.1126/science.1124514
20. Holmes BB, Diamond MI. Prion-like properties of Tau protein: The importance of extracellular Tau as a therapeutic target. J Biol Chem. 2014;289: 19855–19861. doi:10.1074/jbc.R114.549295
21. Shrivastava AN, Aperia A, Melki R, Triller A. Physico-Pathologic Mechanisms Involved in Neurodegeneration: Misfolded Protein-Plasma Membrane Interactions. Neuron. 2017;95: 33–50. doi:10.1016/j.neuron.2017.05.026.
22. Trevino RS, Lauckner JE, Sourigues Y, Pearce MM, Bousset L, Melki R, et al. Fibrillar structure and charge determine the interaction of polyglutamine protein aggregates with the cell surface. J Biol Chem. 2012;287: 29722–29728. doi:10.1074/jbc.M112.372474
23. Hamilton A, Zamponi GW, Ferguson SSG. Glutamate receptors function as scaffolds for the regulation of β-amyloid and cellular prion protein signaling complexes. Mol Brain. 2015;8: 18. doi:10.1186/s13041-015-0107-0
24. Shrivastava AN, Redeker V, Pieri L, Bousset L, Renner M, Madiona K, et al. Clustering of Tau fibrils impairs the synaptic composition of α3-Na + /K + -ATPase and AMPA receptors . EMBO J. 2019;38: e99871. doi:10.15252/embj.201899871
25. Shrivastava AN, Redeker V, Fritz N, Pieri L, Almeida LG, Spolidoro M, et al. α-synuclein assemblies sequester neuronal α3-Na+/K+-ATPase and impair Na+ gradient. EMBO J. 2015;34: 2408–2423. doi:10.15252/embj.201591397
26. Mao X, Ou MT, Karuppagounder SS, Kam TI, Yin X, Xiong Y, et al. Pathological α-synuclein transmission initiated by binding lymphocyte-activation gene 3. Science (80-). 2016;353: aah3374. doi:10.1126/science.aah3374
27. Holmes BB, DeVos SL, Kfoury N, Li M, Jacks R, Yanamandra K, et al. Heparan sulfate proteoglycans mediate internalization and propagation of specific proteopathic seeds. Proc Natl Acad Sci. 2013;110: E3138–E3147. doi:10.1073/pnas.1301440110
28. Jacob RS, George E, Singh PK, Salot S, Anoop A, Jha NN, et al. Cell adhesion

on amyloid fibrils lacking integrin recognition motif. J Biol Chem. 2016;291: 5278–5298. doi:10.1074/jbc.M115.678177

29. Kegel KB, Sapp E, Alexander J, Valencia A, Reeves P, Li X, et al. Polyglutamine expansion in huntingtin alters its interaction with phospholipids. J Neurochem. 2009;110: 1585–1597. doi:10.1111/j.1471-4159.2009.06255.x
30. Burke KA, Kauffman KJ, Umbaugh CS, Frey SL, Legleiter J. The interaction of polyglutamine peptides with lipid membranes is regulated by flanking sequences associated with huntingtin. J Biol Chem. 2013;288: 14993–15005. doi:10.1074/jbc.M112.446237
31. Garten M, Prévost C, Cadart C, Gautier R, Bousset L, Melki R, et al. Methyl-branched lipids promote the membrane adsorption of α-synuclein by enhancing shallow lipid-packing defects. Phys Chem Chem Phys. 2015;17: 15589–15597. doi:10.1039/c5cp00244c
32. Evangelisti E, Cecchi C, Cascella R, Sgromo C, Becatti M, Dobson CM, et al. Membrane lipid composition and its physicochemical properties define cell vulnerability to aberrant protein oligomers. J Cell Sci. 2012;125: 2416–2427. doi:10.1242/jcs.098434
33. Bock JE, Gavenonis J, Kritzer JA. Getting in shape: Controlling peptide bioactivity and bioavailability using conformational constraints. ACS Chemical Biology. 2013. pp. 488–499. doi:10.1021/cb300515u
34. Tsomaia N. Peptide therapeutics: Targeting the undruggable space. Eur J Med Chem. 2015;94: 459–470. doi:10.1016/j.ejmech.2015.01.014
35. Usmani SS, Bedi G, Samuel JS, Singh S, Kalra S, Kumar P, et al. THPdb : Database of FDA-approved peptide and protein therapeutics. PLoS One. 2017;12: e0181748. doi:10.1371/journal.pone.0181748
36. Pemberton S, Madiona K, Pieri L, Kabani M, Bousset L, Melki R. Hsc70 protein interaction with soluble and fibrillar α-synuclein. J Biol Chem. 2011;286: 34690–34699. doi:10.1074/jbc.M111.261321
37. Redeker V, Pemberton S, Bienvenut W, Bousset L, Melki R. Identification of protein interfaces between α-synuclein, the principal component of Lewy bodies in Parkinson disease, and the molecular chaperones human Hsc70 and the yeast Ssa1p. J Biol Chem. 2012;287: 32630–32639. doi:10.1074/jbc.M112.387530
38. Nury C, Redeker V, Dautrey S, Romieu A, Van Der Rest G, Renard PY, et al. A novel bio-orthogonal cross-linker for improved protein/protein interaction

analysis. Anal Chem. 2015;87: 1853–1860. doi:10.1021/ac503892c

39. Gao X, Carroni M, Nussbaum-Krammer C, Mogk A, Nillegoda NB, Szlachcic A, et al. Human Hsp70 Disaggregase Reverses Parkinson's-Linked α-Synuclein Amyloid Fibrils. Mol Cell. 2015;59: 781–793. doi:10.1016/j.molcel.2015.07.012
40. Zhu X, Zhao X, Burkholder WF, Gragerov A, Ogata CM, Gottesman ME, et al. Structural Analysis of Substrate Binding by the Molecular Chaperone DnaK. Science (80-). 1996;272: 1606–1614. doi:10.1126/science.272.5268.1606
41. Roan NR, Sowinski S, Münch J, Kirchhoff F, Greene WC. Aminoquinoline surfen inhibits the action of SEVI (Semen-derived Enhancer of Viral Infection). J Biol Chem. 2010;285: 1861–1869. doi:10.1074/jbc.M109.066167
42. Freilich R, Arhar T, Abrams JL, Gestwicki JE. Protein-Protein Interactions in the Molecular Chaperone Network. Acc Chem Res. 2018;51: 940–949. doi:10.1021/acs.accounts.8b00036
43. Rosenzweig R, Nillegoda NB, Mayer MP, Bukau B. The Hsp70 chaperone network. Nat Rev Mol Cell Biol. 2019;20: 665–680. doi:10.1038/s41580-019-0133-3
44. Arispe N, De Maio A. ATP and ADP modulate a cation channel formed by Hsc70 in acidic phospholipid membranes. J Biol Chem. 2000;275: 30839–30843. doi:10.1074/jbc.M005226200
45. Calderwood SK, Theriault J, Gray PJ, Gong J. Cell surface receptors for molecular chaperones. Methods. 2007;43: 199–206. doi:10.1016/j.ymeth.2007.06.008
46. Araghi RR, Bird GH, Ryan JA, Jenson JM, Godes M, Pritz JR, et al. Iterative optimization yields Mcl-1–targeting stapled peptides with selective cytotoxicity to Mcl-1–dependent cancer cells. Proc Natl Acad Sci U S A. 2018;115: E886–E895. doi:10.1073/pnas.1712952115
47. Bernal F, Tyler AF, Korsmeyer SJ, Walensky LD, Verdine GL. Reactivation of the p53 tumor suppressor pathway by a stapled p53 peptide. J Am Chem Soc. 2007;129: 2456–2457. doi:10.1021/ja0693587
48. Jacobsen Ø, Maekawa H, Ge NH, Görbitz CH, Rongved P, Ottersen OP, et al. Stapling of a 310-helix with click chemistry. J Org Chem. 2011;76: 1228–1238. doi:10.1021/jo101670a
49. Reverdatto S, Burz D, Shekhtman A. Peptide Aptamers: Development and Applications. Curr Top Med Chem. 2015;15: 1082–1101.

doi:10.2174/1568026615666150413153143

50. Ghee M, Melki R, Michot N, Mallet J. PA700, the regulatory complex of the 26S proteasome, interferes with α-synuclein assembly. FEBS J. 2005;272: 4023–4033. doi:10.1111/j.1742-4658.2005.04776.x

51. Whitmore L, Wallace BA. DICHROWEB, an online server for protein secondary structure analyses from circular dichroism spectroscopic data. Nucleic Acids Res. 2004;32: W668–W673. doi:10.1093/nar/gkh371

52. Wanker EE, Scherzinger E, Volker H, Sittler A, Eickhoff H, Lehrach H. Membrane Filter Assay for Detection of Amyloid-like Polyglutamine-Containing Protein Aggregates. Methods Enzymol. 1999;309: 375–386.

53. Schindelin J, Arganda-Carreras I, Frise E, Kaynig V, Longair M, Pietzsch T, et al. Fiji: An open-source platform for biological-image analysis. Nature Methods. 2012. pp. 676–682. doi:10.1038/nmeth.2019

54. Rueden CT, Schindelin J, Hiner MC, DeZonia BE, Walter AE, Arena ET, et al. ImageJ2: ImageJ for the next generation of scientific image data. BMC Bioinformatics. 2017;18: 529. doi:10.1186/s12859-017-1934-z

Supporting Information

Figure S1. Representative epifluorescence and phase contrast images for the binding of αSyn fibrils to Neuro-2a cells. A, Dose-dependent binding of αSyn fibrils to the plasma membrane of Neuro-2a cells. Neuro-2a cells were imaged after exposure for 30 min to αSyn-Alexa488 fibrils (0-2 μM equivalent monomer concentration) and extensive washing. **B,** αSyn fibrils binding to the plasma membrane of Neuro-2a cells in the presence or the absence of Hsp70 and NKApep. αSyn-Alexa488 fibrils (1 μM equivalent monomer concentration) were incubated in the absence (top pannels) or in the presence of Hsc70 (10 μM; middle panels) or NKApep (10 μM; bottom panels) in DMEM for 30 min at 37°C. Neuro-2a cells were imaged after exposure to the mixture for 30 min and extensive washing. Scale bars, 20 μM.

Figure S2. Internalization of αSyn fibrils assessed by fluorescence microscopy. Neuro-2a cells were exposed for 4 hours to αSyn-Alexa488 fibrils (1 μM equivalent monomer concentration). The cells were washed twice with serum-free, phenol red-free DMEM then 0.1% Trypan Blue was added to quench the fluorescence of plasma membrane-bound Alexa488-labeled αSyn fibrils. Scale bars, 20 μM.

Figure S3. CD spectra of domains and peptides used throughout this study. A, Hsc70 domains SBD, SBDβ and SBD-lid. **B**, Hsc70 peptides. **C**, NKApep.

Figure S4. Quantification of SBD-ATTO488 (A), SBDβ-ATTO488 (B) and SBD-lid-ATTO488 (C) binding to αSyn fibrils. ATTO488-labelled Hsc70 SBD domain and sub-domains were diluted with the corresponding unlabelled proteins (at a molar ratio 1:50) to different final concentrations (0-5 μM) and incubated with or without aSyn fibrils (1

μM) for 1h at RT. Each sample was then filtered in triplicate through a cellulose acetate membrane and the amount of ATTO488-labelled Hsc70 domain trapped onto the membrane was quantified. In each case a representative experiment is shown. K_D values presented in Figure 4B were derived from 3 independent experiments.

Figure S5. Binding of the peptides Hsc-6 (A), Hsc-7 (B), Hsc-10 (C) and NKApep (D) to αSyn fibrils and K_D determination (E,F). αSyn fibrils (100 μM) were incubated 1h with each peptides (200 μM) at RT. The samples were centrifuged for 30 min at 20.000 g and 20°C. The pellets were dissolved in TFA 100%. After evaporation, the samples were resuspended in TFA 0.1%, and analysed by reversed phase chromatography on a C18 column (bold traces). The elution profile of TFA dissolved αSyn fibrils is depicted (thin traces). The retention time of each peptide was determined by an injection of 1 nmole of the peptide and is indicated by an arrow. Hsc-6 and Hsc-10 co-sediment with αSyn fibrils, whereas Hsc-7 and NKApep do not. E-F, Determination of Hsc-6 and Hsc-10 - αSyn fibrils K_D. Measurements as described above were performed for increasing peptide concentrations (0-200 μM). The amount of αSyn fibrils-bound Hsc-6 and Hsc-10 is plotted against the total peptide concentration. The lines through the data points represent the best fits to a linear function and are drawn for visual guidance only.

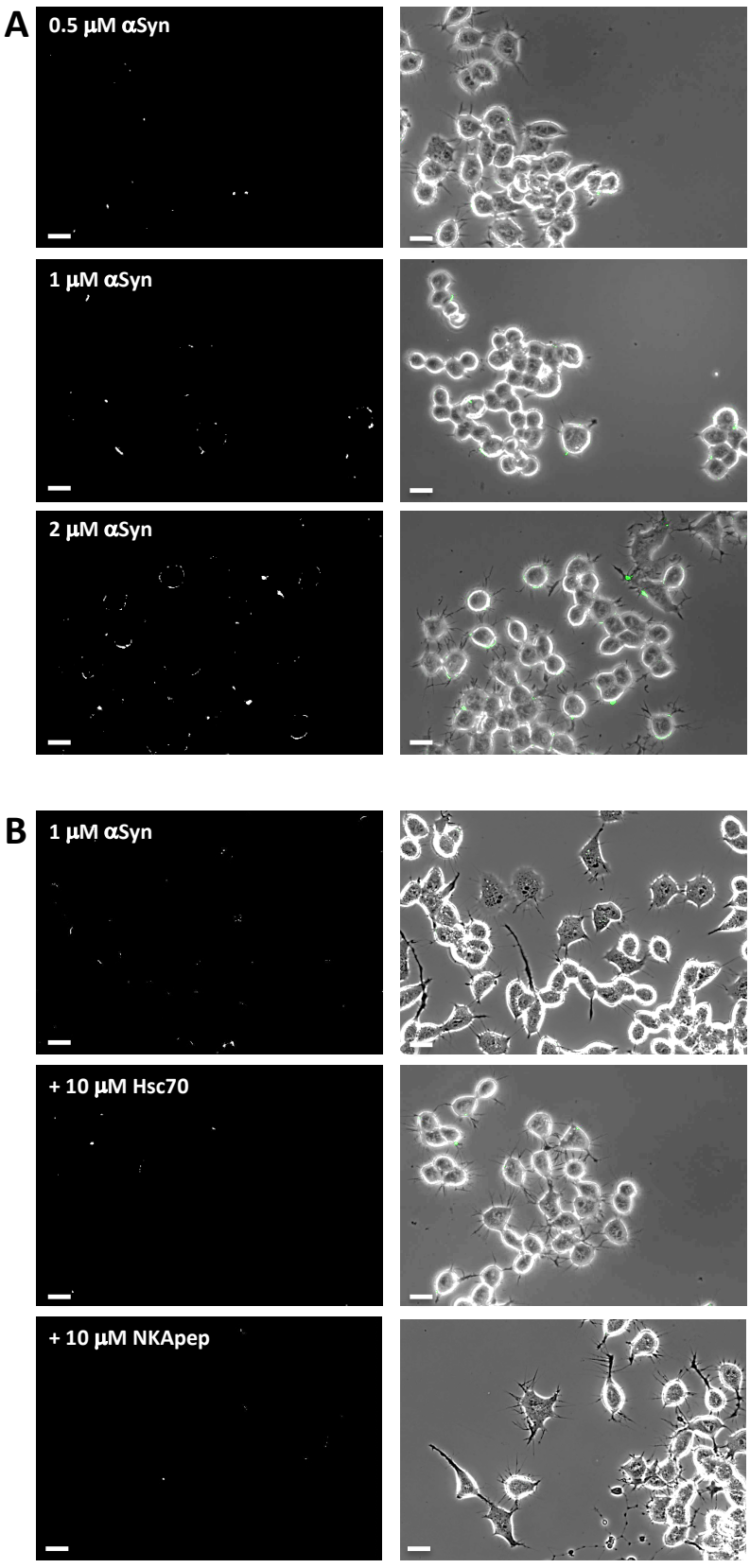
A
0.5 µM αSyn
1 µM αSyn
2 µM αSyn
B
1 µM αSyn
+ 10 µM Hsc70
+ 10 µM NKApep

Figure S1

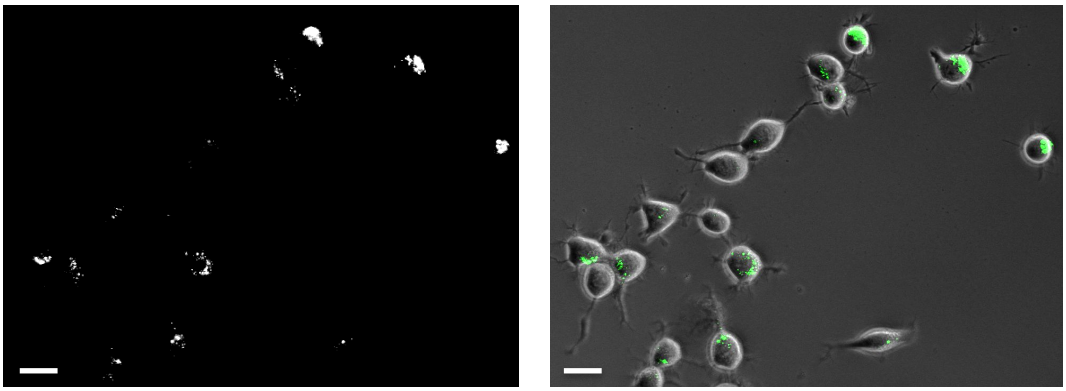

Figure S2

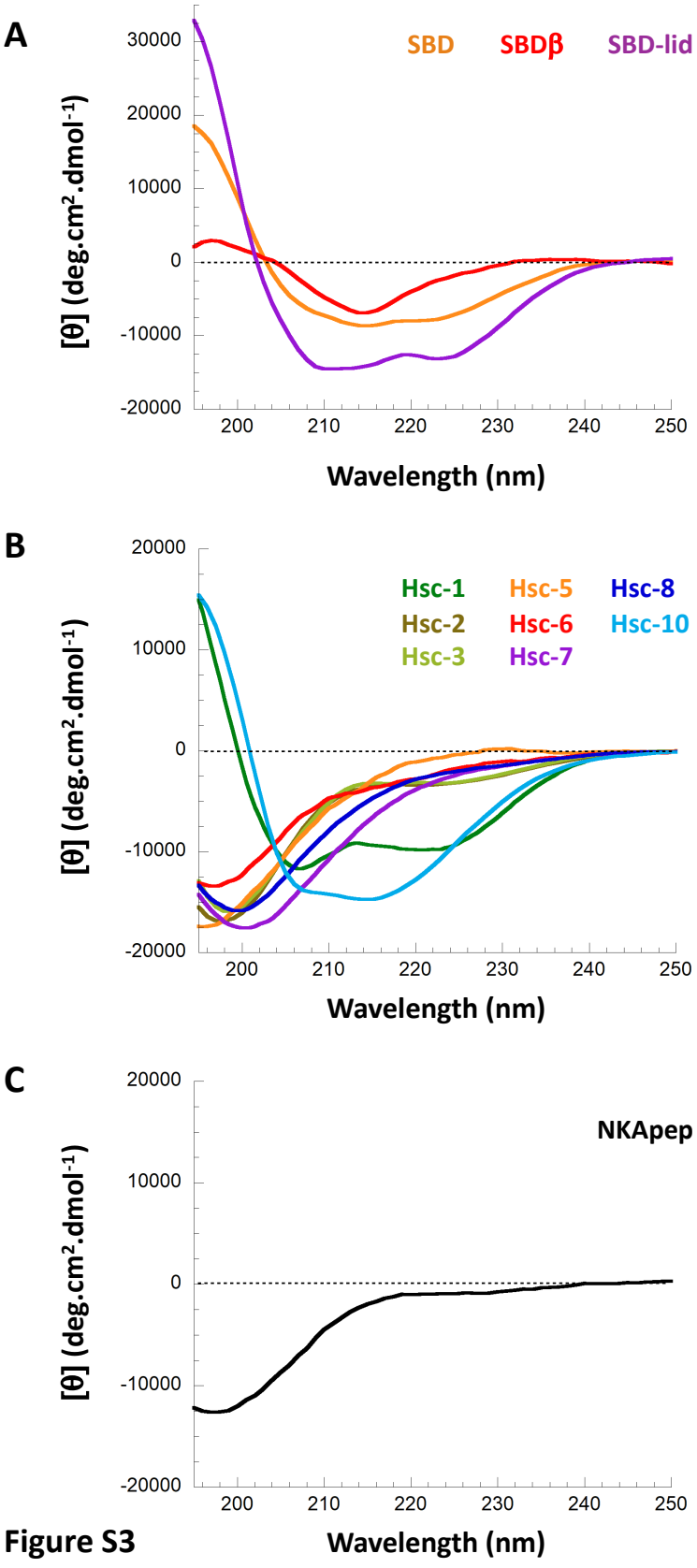
A
SBD
SBDβ
SBD-lid
[θ] (deg.cm².dmol⁻¹)
30000
20000
10000
0
-10000
-20000
200
210
220
230
240
250
Wavelength (nm)
B
Hsc-1
Hsc-5
Hsc-8
Hsc-2
Hsc-6
Hsc-10
Hsc-3
Hsc-7
[θ] (deg.cm².dmol⁻¹)
20000
10000
0
-10000
-20000
200
210
220
230
240
250
Wavelength (nm)
C
NKApep
[θ] (deg.cm².dmol⁻¹)
20000
10000
0
-10000
-20000
200
210
220
230
240
250
Wavelength (nm)

Figure S3

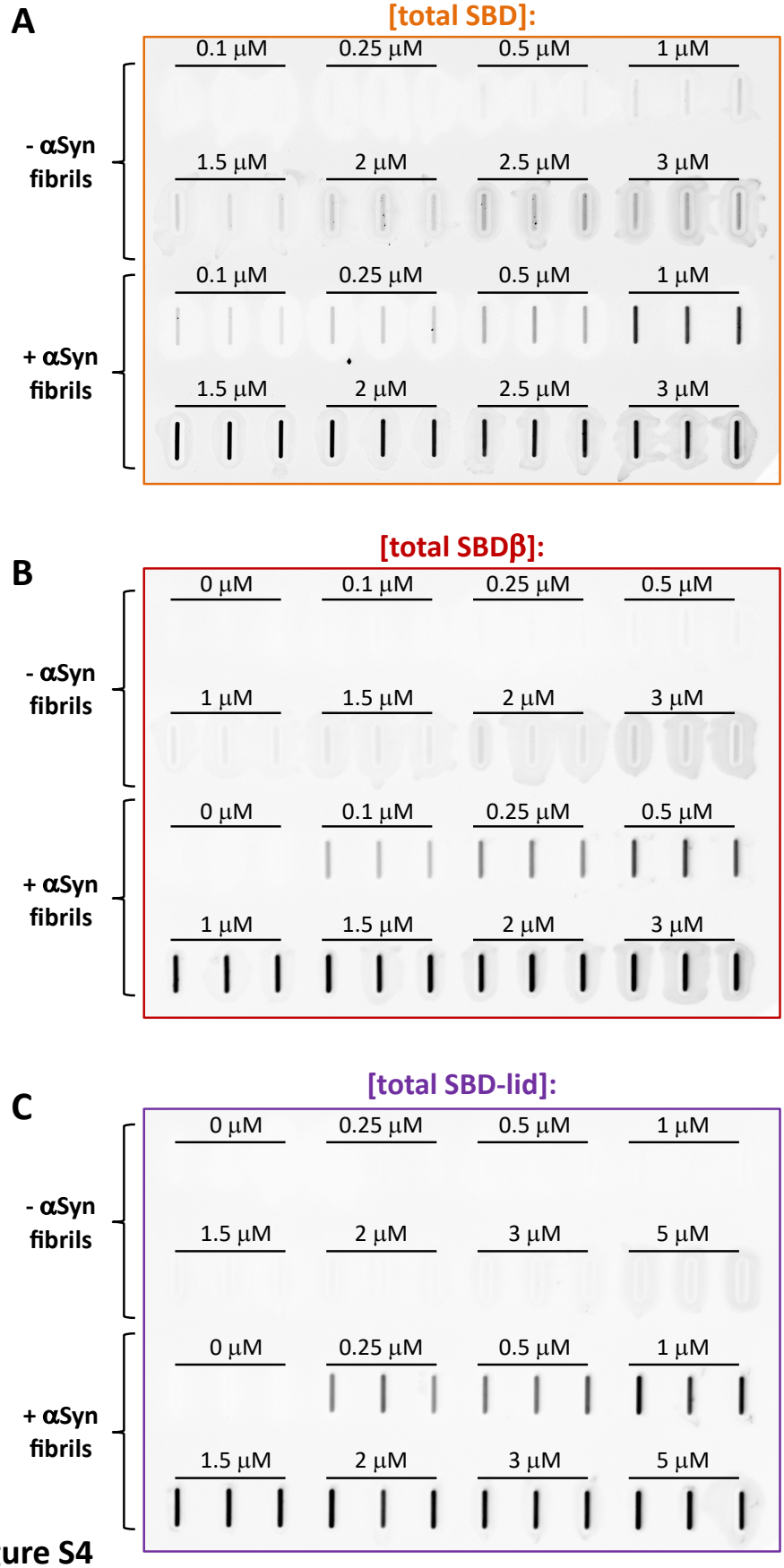
A
[total SBD]:
0.1 µM
0.25 µM
0.5 µM
1 µM
- αSyn fibrils
1.5 µM
2 µM
2.5 µM
3 µM
0.1 µM
0.25 µM
0.5 µM
1 µM
+ αSyn fibrils
1.5 µM
2 µM
2.5 µM
3 µM
B
[total SBDβ]:
0 µM
0.1 µM
0.25 µM
0.5 µM
- αSyn fibrils
1 µM
1.5 µM
2 µM
3 µM
0 µM
0.1 µM
0.25 µM
0.5 µM
+ αSyn fibrils
1 µM
1.5 µM
2 µM
3 µM
C
[total SBD-lid]:
0 µM
0.25 µM
0.5 µM
1 µM
- αSyn fibrils
1.5 µM
2 µM
3 µM
5 µM
0 µM
0.25 µM
0.5 µM
1 µM
+ αSyn fibrils
1.5 µM
2 µM
3 µM
5 µM

Figure S4

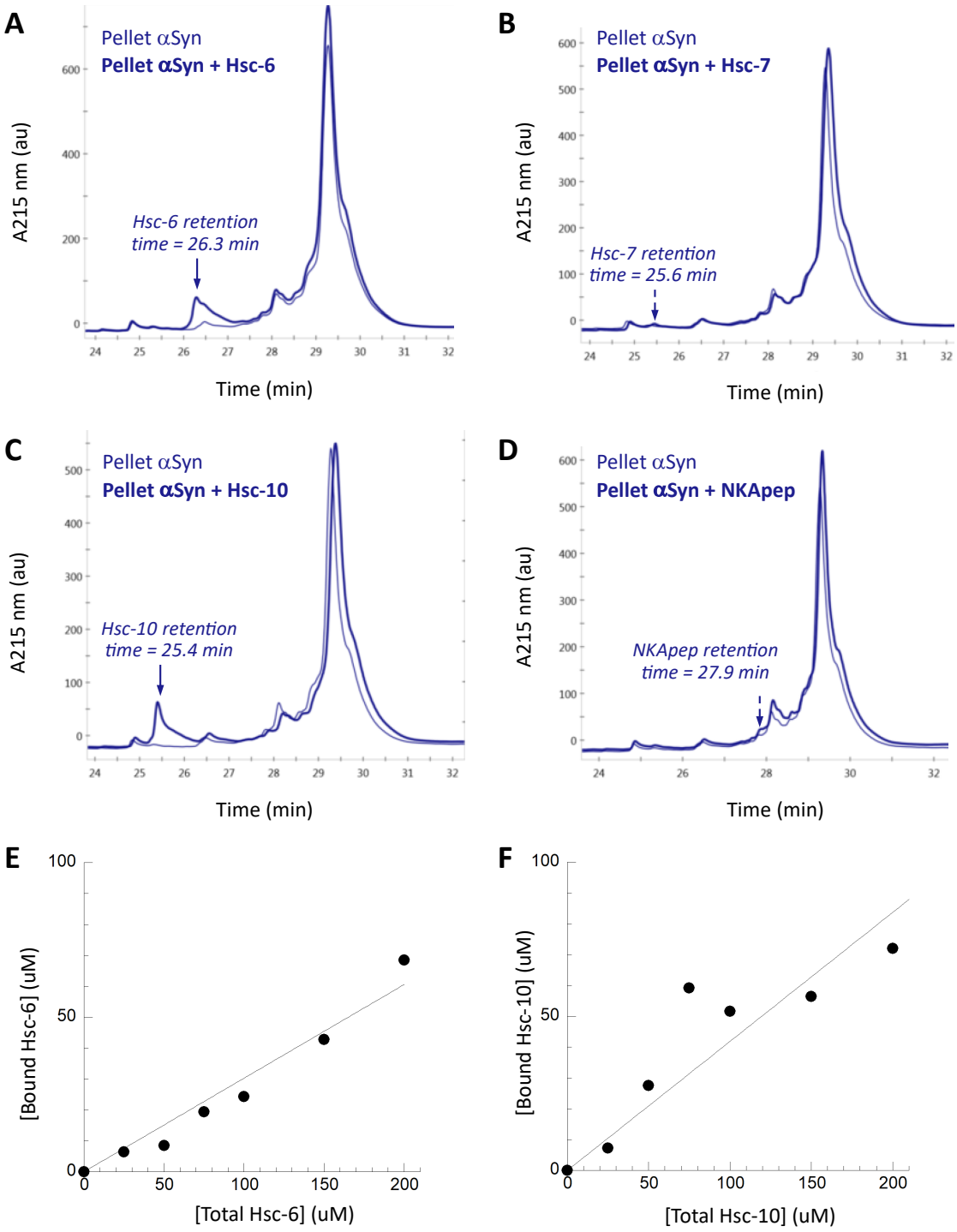
A
Pellet αSyn
Pellet αSyn + Hsc-6
Hsc-6 retention time = 26.3 min
A215 nm (au)
Time (min)
B
Pellet αSyn
Pellet αSyn + Hsc-7
Hsc-7 retention time = 25.6 min
A215 nm (au)
Time (min)
C
Pellet αSyn
Pellet αSyn + Hsc-10
Hsc-10 retention time = 25.4 min
A215 nm (au)
Time (min)
D
Pellet αSyn
Pellet αSyn + NKApep
NKApep retention time = 27.9 min
A215 nm (au)
Time (min)
E
[Bound Hsc-6] (uM)
[Total Hsc-6] (uM)
F
[Bound Hsc-10] (uM)
[Total Hsc-10] (uM)

Figure S5

Chapter 4: Interaction of αBc and CHIP with α-Synuclein fibrils

4.1 Article 2 Preface

The previous work involved polypeptides based on previously identified regions of interest from interacting partners with αSyn monomers or fibrils. In this study, we first identify potential partners of αSyn fibrils whose binding impacts cellular internalization. Then, we use chemical cross-linking to determine regions of interaction. As dictated in section 2.3.3, chemical cross-linking can be accomplished with a large choice of agents. The agents used in this study provided a range of reactivity, spacer arm lengths and reversibility (**Preface Figure 1A**). The mass increments and reactions for the covalent bond formation between proteins and cross-linking agents are shown in **Preface Figure 1A-B.**

The software used in our study was StavroX (Götze et al., 2012). This software has multiple advantages over its alternatives, such as GPMAW, CTB, and MS-Bridge. First off, it can identify cross-links through user-selected amino acids instead of only pre-determined amino acids, which is particularly useful for cross-linking agents such as glutaraldehyde, with poor specificity. Furthermore, it calculates masses of cross-links of multiple amino acids with variable modifications simultaneously, simplifying data analysis. Indeed, StavroX searches for matches based on mass increments between a pre-calculated list of theoretical cross-links, as mentioned above, and precursor ion masses. Nomenclature of cross-linked peptides is given as described previously (Schilling et al., 2003). Finally, StavroX can open MS/MS data, permitting manual verification within the software.

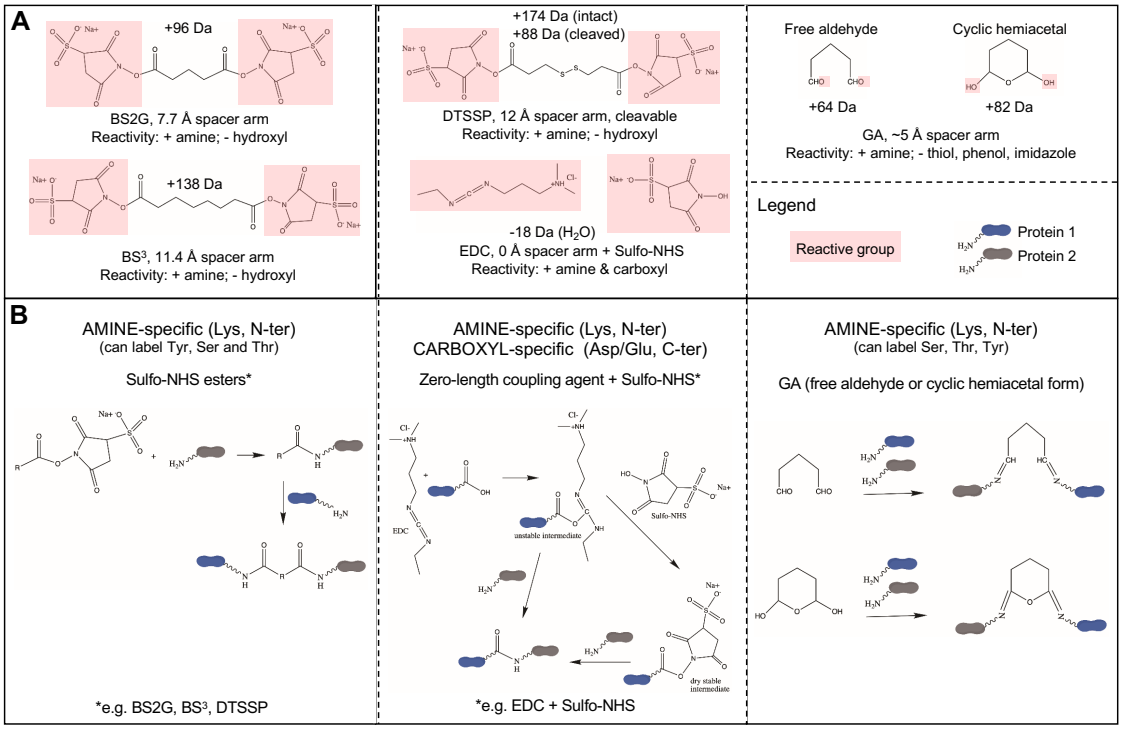

Preface Figure 1: Cross-linking agents and reactions in this study.
A) Agent chemical structures, associated mass increments and legend. **B)** Chemical reactions for crosslinking of amine- and carboxyl-specific chemical cross-linking with the agents in this study. *BS2G* bis(sulfosuccinimidyl) glutarate; *BS*^{3} bis(sulfosuccinimidyl) suberate; *DTSSP* 3,30-dithiobis(sulfosuccinimidylpropionate); *EDC* N-(3-dimethylaminopropyl)-N'-ethylcarbodiimide hydrochloride; *Sulfo-NHS* N-hydroxysulfosuccinimide; *GA* glutaraldehyde.

4.2 Article 2

Article in preparation.

Interaction of the chaperones alpha B-crystallin and CHIP with fibrillar alpha-synuclein: effects on internalization by cells and identification of interacting interfaces.

Maya Bendifallah, Virginie Redeker, Elodie Monsellier, Luc Bousset, Tracy Bellande, Ronald Melki*

** Corresponding author:* ***ronald.melki@cnrs.fr***

CEA, Institut François Jacob (MIRcen) and CNRS, Laboratory of Neurodegenerative Diseases (U9199), 18 Route du Panorama, 92265, Fontenay-aux-Roses, France

Abstract

Fibrillar α-Synuclein (αSyn) is the molecular hallmark of Parkinson's Disease and other synucleinopathies. Its prion-like propagation between cells is linked to disease progression and thus should be targeted. In this study, we looked to molecular chaperones to identify proteins capable of binding αSyn fibrillar aggregates in order to disrupt their propagation. We further assessed the effect of the fibril-binding chaperones on internalization of αSyn fibrils by neuronal cells. We demonstrate that the interaction of aggregating αSyn with αB-crystallin (αBc) or Carboxyl terminus of Hsc70-interacting protein (CHIP) led to the formation of fibrils that are less internalized by cells. Finally, using an optimized chemical cross-linking and mass spectrometry strategy, we identified the interaction areas between fibrillar αSyn and either αBc or CHIP. Our results pave the way for the development of rationally designed polypeptide inhibitors of αSyn fibril propagation.

Introduction

Parkinson's disease and other synucleinopathies are associated with the aggregation of the protein alpha-synuclein (αSyn) into high molecular weight fibrillar aggregates [1,2]. αSyn aggregates traffic between neuronal cells, seed the aggregation of endogenous monomeric αSyn, and amplify [3–5]. This prion-like phenomenon is presumed to contribute to the stereotypic progression of synucleinopathies [5,6]. αSyn aggregates propagate through exosomes [7,8], tunneling nanotubes [9,10] and following their release to the extracellular space through export by living cells or liberation by dying cells [11–13]. The latter aggregates bind to the cell membrane and are internalized, primarily through endocytosis [14,15]. They eventually compromise the endo-lysosomal integrity [16] and reach the cytosol where they amplify by recruiting endogenous monomeric αSyn [17,18]. The resulting aggregates find then their way into naive, unaffected cells, perpetuating the cycle [17,19]. The formation and trafficking of fibrillar αSyn assemblies represent targets for therapeutic interventions [20]. Those assemblies bind to cell membranes through numerous partners, including protein partners [21–24] and lipid partners [25,26], many of which are essential to cell physiology.

αSyn aggregates form in the crowded cellular environment in the presence of a vast number of proteins, including molecular chaperones. Molecular chaperones, the first line of defense in protein homeostasis, interact with aggregating proteins [27]. Extensive research has reported that various chaperones, such as Hsp90, Hsp70, Hsp27 and αlphaB-crystallin (αBc), interfere with the assembly of monomeric αSyn into fibrils [28–33]. Those molecular chaperones may bind aggregated αSyn *in vivo* as they have been shown to be present within αSyn-rich deposits within cells [34–36]. This justifies characterizing thouroughly the interactions between molecular chaperones and αSyn [37–40], demonstrating chaperone binding to αSyn fibrils *in vitro*.

We previously demonstrated that Hsc70 binds fibrillar αSyn with high affinity (Pemberton et al. 2011; Redeker et al. 2012) and that Hsc70-coated αSyn fibrils are less toxic to cells compared to naked fibrils [33]. We further identified inter-molecular surfaces of the interaction between Hsc70 and αSyn [41,42]. In the research presented here, we focused on human sHSP chaperone αBc and human C-terminus Hsc70-interacting protein (CHIP).

αBc is one of the 2 subunits of the chaperone α-crystallin, a prominent component of the human eye lens that prevents aggregation of lens proteins, including itself. It consists of a mixture of oligomers ranging in size from 10 to 40 monomers [43]. αBc colocalizes with Lewy bodies in Parkinson's disease patients' neurons [35]. *In vitro*, αBc slows down the aggregation of many different proteins [28,31,44] and binds to preformed αSyn fibrils [38,39]. Like all sHSPs, the 20 kDa αBc monomer contains a highly conserved α-crystallin domain (αBc-core) flanked by disordered N- and C-terminal domains. Isolated αBc-core is dimeric and retains, *in vitro*, the anti-αSyn aggregation activity of the mother protein [38,45].

CHIP is a human dimeric chaperone of 34.8 kDa per monomer with E3 ubiquitin ligase activity [46]. It colocalizes with αSyn in Lewy bodies in Dementia with Lewy Body patient brains [34]. CHIP also targets αSyn oligomers for degradation and has a rescue effect in αSyn-induced-toxicity in different cellular models [34,47].

We thus assessed the uptake of αSyn fibrils assembled in the presence of αBc and CHIP by Neuro-2a cells. We demonstrated that both chaperones diminish αSyn fibrils take-up by cells. Using an optimized cross-linking and mass spectrometry strategy, we identified the interaction interfaces between αSyn fibrils and αBc or CHIP. The two chaperones bind different αSyn polypeptides exposed at the surface of fibrils: at a flexible segment located just before the fibrillar core for αBc, and at a solvent accessible surface of the

fibrillar core itself for CHIP. Our results may allow for the development of peptide ligands that can interfere with αSyn fibril prion-like propagation and subsequent disease progression.

Methods

Cloning

A synthetic gene encoding αBc was purchased from GeneArt (Thermo Fisher Scientific). The vector allowing the bacterial expression of αBc was obtained by subcloning the corresponding synthetic gene into a pET14b vector (Novagen) at the NcoI-XhoI restriction sites. The pET151/D-TOPO vector (Invitrogen) allowing the bacterial expression of His_6, N-terminal-tagged CHIP with a V5 epitope was a gift from Jeffrey L. Brodsky. The His_6 tag is followed by a tobacco etch virus (TEV) protease cleavage site. Constructs were verified by DNA sequencing (Eurofins Genomics).

Expression & purification of recombinant proteins

Recombinant human wild-type α-Synuclein (αSyn) was expressed and purified as described [48].

Recombinant human wild-type αBc was expressed at 37 °C in *E.coli* strain BL21(DE3) (Stratagene) upon induction with IPTG (0.5 mM) for 3 hours. Cells were harvested and resuspended in buffer A (50 mM Tris-HCl pH 8.5, 1 mM EDTA). After sonication and centrifugation, lysate supernatants were subjected to PEI precipitation (0.12% v/v). The supernatants were filtered and loaded onto a Q-sepharose FF column (GE Healthcare Lifesciences) equilibrated with buffer A, and eluted with buffer B (50 mM Tris-HCl pH 8.5, 1 mM EDTA, 100 mM NaCl). Fractions containing αBc were pooled and concentrated with a 3 kDa cutoff (Millipore), then loaded onto a size exclusion chromatography column (Superose 6 10/300 GL, GE Healthcare Lifesciences). αBc was

eluted with an apparent molecular weight corresponding to a multimer of 20-35 monomers. Gel filtration standards from Sigma-Aldrich (MWGF1000) were used for apparent molecular weight determination.

Recombinant His_6, N-terminal-tagged CHIP was expressed at 30 °C in *E.coli* strain BL21(DE3). Protein expression was induced by IPTG (0.5 mM) for 2 hours. The cells were harvested and resuspended in buffer D (50 mM $NaPO_4$ pH 8.0, 300 mM NaCl, 3 mM β-mercaptoethanol [βME]). After sonication and centrifugation, lysate supernatants were filtered and loaded onto a 5 mL Talon metal affinity resin column (Clontech), equilibrated in buffer D. The protein was eluted in buffer D supplemented with 200 mM imidazole, then dialyzed in PBS. The His_6-tag was cleaved by addition of His_6-tagged TEV (His-TEV) protease, produced using the plasmid pRK793 (Addgene), at a 1:20 His-TEV:chaperone molar ratio. 100% cleavage, as assessed by SDS-PAGE, was achieved upon incubating the mixtures for 1 hour at 37 °C. The untagged proteins were purified by collecting the flow through of a 5 mL Talon metal affinity resin column.

After purification, all proteins were immediately filtered through sterile 0.22 µm filters, aliquoted and stored at -80 °C. The purity of all proteins was confirmed by SDS-PAGE and MALDI mass spectrometry (not shown). Protein concentrations were determined spectrophotometrically using the following extinction coefficients at 280 nm ($M^{-1}.cm^{-1}$): 5960 for αSyn; 13980 for αBc and 29380 for CHIP.

Assembly of αSyn into fibrils and labeling

For kinetics and internalization experiments, monomeric αSyn was labeled by addition of the aminoreactive fluorescent dye Alexa Fluor 488 (Alexa488, Invitrogen) using a protein:dye molar ratio of 10:1 based on initial monomer concentration. Labelling was

performed following the manufacturer's recommendation. The reaction was quenched with Tris-HCl pH 7.5 (40 mM final concentration).

αSyn (100 μM monomer concentration) was incubated with increasing concentrations of αBc or CHIP (0-100 μM) in PBS at 37 °C under continuous shaking in an Eppendorf Thermomixer set at 600 rpm for 2 weeks. Aliquots were withdrawn at different time intervals from the assembly reactions and mixed with a primuline solution (10 μM). Primuline fluorescence was recorded with a Cary Eclipse spectrofluorimeter (Varian Medical Systems, Inc.) using excitation and emission wavelengths set at 400 and 480 nm, respectively. The nature of the fibrils obtained at the end of the aggregation reaction was assessed by transmission electron microscopy (TEM) as described below. The proportion of αSyn assembled into fibrils was assessed through a partition assay by ultracentrifugation. To this aim, aliquots were withdrawn, subjected to centrifugation in an Eppendorf 5415R centrifuge at 20,000 g and 20 °C, and the amount of protein in the supernatant and pellet fraction determined by SDS-PAGE analysis.

Transmission electron microscopy (TEM)

Fibrils were imaged by TEM in a Jeol 1400 transmission electron microscope (Jeol SAS) after adsorption onto carbon-coated 200 mesh grids and negative staining with 1% uranyl acetate. The images were recorded with a Gatan Orius CCD camera (Gatan, Inc.).

Cell culture and internalization

Murine neuroblastoma Neuro-2a cells (ATCC) were cultured at 37 °C in humidified air with 5% CO2 in Dulbecco's modified Eagle's medium (DMEM, Sigma-Aldrich) containing 10% fetal bovine serum (Gibco, Thermo Fisher Scientific), 2 mM glutamine,

100 units.ml^{-1} penicillin (PAA Laboratories) and 100 µg.ml^{-1} streptomycin (PAA Laboratories). All materials used for cell culture were from PAA Laboratories.

The internalization of Alexa488-labeled αSyn (1 µM equivalent monomer concentration) assembled in the presence or absence of αBc or CHIP was assessed. All fibrils were sonicated for 20 min in a VialTweeter powered by an ultrasonic processor UIS250v (250 W, 2.4 kHz; Hielscher Ultrasonic) set at 75% amplitude, 0.5 s pulses before dilution in DMEM. Neuro-2a cells cultured on 96-well plates were then incubated with these mixtures distributed in 5 independent wells. After 2 hours, the medium was removed and Hoescht (Sigma-Aldrich), diluted at 0.2 µg/ml in serum-free, phenol red-free DMEM, was added for 30 min. The cells were washed twice and 0.1% Trypan Blue (Sigma-Aldrich) was added to quench the fluorescence of Alexa488-labeled αSyn fibrils that were plasma membrane-bound. For each well, Alexa488 and Hoechst fluorescence values were recorded on a Clariostar microplate reader (BMG LABTECH). For each condition, the Alexa488 fluorescence value was considered and averaged over the 5 wells only if the Hoescht value was not significantly different from the one of untreated cells. Three independent experiments were conducted.

Chemical cross-linking and western blotting

Cross-linking experiments of chaperones with fibrillar αSyn were performed in PBS using αSyn alone (100 µM), chaperones alone (either 50 µM for αBc, or 33 µM for CHIP), or αSyn (100 µM) assembled into fibrils in the presence of chaperones (either 50 µM of αBc, corresponding to an αSyn:αBc molar ratio of 2:1; or 33 µM of CHIP, corresponding to an αSyn:CHIP molar ratio of 3:1) as described above. After 2 weeks of assembly, fibrillar αSyn samples were centrifuged at 100,000 g in a TL100 tabletop ultracentrifuge (Hitachi) for 30 minutes at 20 °C. The pellets were allowed to swell in PBS overnight

before gentle resuspension. The final concentrations of αSyn fibrillar material and chaperones in the pellets were assessed by a partition assay by ultracentrifugation as described above.

The samples were exposed to various crosslinkers: glutaraldehyde (GA, ~5 Å spacer arm for monomeric glutaraldehyde, Sigma-Aldrich); bis(sulfosuccinimidyl) glutarate (BS2G, 7.7 Å spacer arm, Pierce); bis(sulfosuccinimidyl) suberate (BS^3, 11.4 Å spacer arm, Pierce); 3,30-dithiobis(sulfosuccinimidylpropionate) (DTSSP, 12 Å spacer arm, Pierce); or N-(3-dimethylaminopropyl)-N'-ethylcarbodiimide hydrochloride (EDC) with N-hydroxysulfosuccinimide (Sulfo-NHS) (0 Å spacer arm, Thermo Fisher Scientific) at a 1:1.25 EDC:Sulfo-NHS molar ratio. For GA, BS2G, BS^3 and DTSSP, reactions were quenched with the addition of Tris-HCl pH 7.5 (50 mM final concentration). For EDC/Sulfo-NHS, reactions were quenched with the addition of βME (20 mM final concentration) and Tris-HCl pH 8.2 (50 mM final concentration).

A specific αSyn-αBc cross-linked complex was obtained with GA exposition for 30 min at RT using a total protein:GA molar ratio of 1:1, corresponding to the following GA concentrations: 32 µM for αBc alone; 88 µM for αSyn fibrils alone; and 100 µM for αSyn fibrils formed in the presence of αBc. Total protein:GA molar ratios of 1:2 and 1:5, corresponding to 77/82/100 µM and 192/408/500 µM GA, led to the formation of higher order intermolecular cross-links among chaperones and fibrils alone.

A specific αSyn-CHIP cross-linked complex was obtained with EDC/Sulfo-NHS exposition for 30 min at RT using a total protein:EDC:Sulfo-NHS molar ratio of 1:10:12.5, corresponding to the following EDC/Sulfo-NHS concentrations: 320/400 µM for CHIP alone; 823/1029 µM for αSyn fibrils alone; 1178/1473 µM for αSyn fibrils formed in the presence of CHIP. A total protein:EDC:Sulfo-NHS molar ratio of 1:20:25 or at fixed concentrations of 2945/3683 µM (corresponding to total protein:EDC:Sulfo-

NHS molar ratios of 1:91:115, 1:36:45 and 1:25:31, respectively) led to the formation of higher order intermolecular cross-links among chaperones and fibrils alone.

In order to solubilize protein samples before SDS-PAGE analysis, all samples were first vacuum-dried then dissociated by addition of 10 to 20 µl of pure hexafluoroisopropanol (HFIP, Sigma-Aldrich). After incubation for 1 hour in HFIP at RT, samples were evaporated before resuspension in denaturing Laemmli buffer, with the exception of DTSSP cross-linked samples which were resuspended in the same buffer without βME. Samples were heated for 5 min at 80˚C and loaded onto 7.5% Tris-Tricine gels.

For western blot analysis, proteins separated by SDS-PAGE were transferred to nitrocellulose membranes (GE Healthcare). The membranes were first analyzed using an anti-αSyn antibody, stripped, and then revealed with an anti-αBc or anti-CHIP antibody. Briefly, the membranes were blocked in 3% skim milk in TBS-Tween 0.5%, probed with a primary then secondary antibody and developed with the enzyme-coupled luminescence technique (ECL, Thermo Fisher Scientific) using a ChemiDoc™ MP Imaging System (BioRad). The primary and secondary antibodies combinations used were the following: SYN1 antibody (1/5000, 610787 BD Biosciences) followed by anti-mouse-HRP (1/5000, GTX 213111-01 Genetex) for αSyn detection, and generated, in-house-immunopurified rabbit polyclonal antibodies (1/5000, Covalab) followed by anti-rabbit-HRP (1/5000, A120-101P Bethyl) for αBc or CHIP detection. For polyclonal antibody immunopurification, 1-10 mg of purified antigen protein was separated into a 15% SDS-PAGE gel and further transferred to a nitrocellulose membrane (GE Healthcare). The antigen-containing membrane was pre-incubated with 100 mM glycine pH 2.5 for 10 minutes before being blocked with 5% skim milk in TBS-Tween 0.05% and further incubated overnight in the anti-αBc or anti-CHIP antibody-containing serum. Polyclonal antibodies against αBc or CHIP were eluted with 2 mL 100 mM glycine pH 2.5 for 2

minutes. After immediate neutralization with addition of Tris-HCl pH 8.5, the immunopurified antibodies were dialyzed into PBS pH 7.4, 30% glycerol. Stripping of the membrane between two immunodetections was achieved with 100 mM βME, 62.5 mM Tris-HCl pH 6.8, 2% SDS for 1 hour at 50 ˚C.

Peptide preparation and NanoLC-MS/MS identification of cross-linked peptides

Bands of interest were excised and cut in pieces of about 2 mm^2. Each band was subjected to washing and in-gel tryptic digestion as described [49], without reduction and alkylation. Tryptic digestion was performed overnight at 37 °C using Trypsin Gold (Promega) at a concentration of 10 ng/µl in 25 mM ammonium bicarbonate. Tryptic peptides were extracted using two volumes of 60% acetonitrile (ACN), 0.1% formic acid for 1 hour. The supernatant was recovered and a second extraction was performed by addition of one volume of 100% ACN for 30 min. The two supernatants of extracted peptides were pooled and vacuum dried. Tryptic peptides were resuspended in 0.1% formic acid (v/v) prior to nanoLC-MS/MS analysis.

Tryptic peptides were analyzed with a Data Dependent acquisition method by selecting the 20 most intense precursors for CID fragmentation using a Triple-TOF 4600 mass spectrometer (ABSciex) coupled to a nanoRSLC ultra performance liquid chromatography (UPLC) system (Dionex, Thermo Fisher Scientific) as previously described [50], with the following exceptions: The analytical column was an Acclaim PepMap RSLC C18 (75 µm i.d.× 50 cm, 2 µm, 100 Å, Thermo Fisher Scientific). Peptides were loaded at 6 µl/min and separated with a gradient of 5 to 35% 0.1% formic acid in 100% ACN.

NanoLC-MS/MS data analysis

NanoLC-MS/MS raw data were converted into mgf data files using the MS Data Converter software (Peakview, ABSciex). Sequence coverage of the proteins was determined through database searching using the Mascot search engine (Matrix Science; version 2.6) with the SwissProt mammalian database (SwissProt_2018_10 database release) together with a decoy database search. Only peptides with a mascot score above 20 were considered. Inter-molecular cross-linked peptides between αSyn and chaperones were searched using the StavroX software (version 3.6.6.6) [51]. For GA, which exists as a mixture of monomers (free aldehyde or cyclic hemiacetal forms) or different polymers [52], we set the mass modification to 64.031 or 82.042 to search for inter-protein peptides cross-linked by a free aldehyde or a cyclic hemiacetal GA, respectively, on a list of potentially reactive amino acids for sites 1 and 2 as reported in the literature, or as indicated by their physico-chemical properties (Lysine, Serine, Threonine, Tyrosine, Arginine, Tryptophan, Phenylalanine, Proline, and N-terminus). One interprotein cross-link by a cyclic hemiacetal monomer of GA was identified and confirmed. For EDC, mass modification was set to 18.01 Da for interprotein cross-linked peptides modified on Lysine, Serine, Threonine, Tyrosine, and N-terminus for site 1 and Aspartate, Glutamate and C-terminus for site 2. For both Mascot and StavroX searches, the parent and fragment ion mass tolerances were 25 ppm and 0.05 Da, respectively, oxidation of methionine was set as a variable modification, and trypsin cleavage was semi-specific. Candidate cross-linked peptides were validated after confirmation of their absence in the control samples and manual analysis of their MS/MS spectra.

Results

Extensive studies have reported that chaperones interact with amyloid-forming proteins and are thus good candidates to prevent either the aggregation reaction or the interaction

of the resulting amyloids with binding partners within the cytosol or at the plasma membrane. Previous work in our laboratory showed that the molecular chaperone Hsc70 reduces αSyn assembly and affects preformed fibril-induced toxicity (Pemberton *et al.* 2011).

We wanted to assess if the ability to bind preformed αSyn fibrils is a generic property of molecular chaperones, in the perspective of expanding our arsenal of chaperones able to modify αSyn fibril surfaces and interfere with their cell-to-cell propagation. We selected two different molecular chaperones that we considered promising based on previous data demonstrating their association or colocalization with aggregated αSyn, either *in vitro* or in pathological lesions or inclusions observed in the brains of patients with synucleinopathies [31,34,35,38,39,47]: the human sHSP chaperone αBc and human E3 ubiquitin ligase CHIP.

Effect of αBc and CHIP on αSyn fibrils take-up by Neuro-2a cells

We first assessed the effect of αBc and CHIP on the assembly of αSyn into fibrils at different αSyn:molecular chaperone molar ratios (**Figure 1**). We used Alexa488-labeled monomeric αSyn for these assembly reactions, in order to obtain labeled αSyn fibrils in complexes with unlabeled chaperones and assess the uptake of the resulting fibrils by Neuro-2a cells. The kinetics of aggregation were followed by primuline fluorescence. Notably, the assembly kinetics of unlabeled and Alexa488-labeled αSyn into fibrils, as well as the fibrils' abilities to seed, are comparable [53]. The resulting fibrils display similar morphologies undistinguishable by transmission electron microscopy (**Figure S1**).

Fibrillation kinetics of αSyn in presence of increasing concentrations of αBc show that αBc significantly slows down αSyn aggregation, starting from an αSyn:αBc molar ratio

of 10:1 (**Figure 1A, C**). At a 2:1 αSyn:αBc molar ratio, αBc did not significantly modify neither the amount (**Figure 1E**) nor the morphology (**Figure 1H**) of fibrillar αSyn. While CHIP had no significant effect either on αSyn kinetics of aggregation (**Figure 1B,D**) or on the amount (**Figure 1F**) of aggregated αSyn, it had an effect on the morphology of fibrils. They appeared more twisted than those formed without molecular chaperones (**Figure 1I**). Increases of αBc or CHIP concentrations induced an increase of the amount of chaperones bound to αSyn fibrils, as identified through a sedimentation assay (**Figure 1E, F**).

We next assessed the internalization of αSyn fibrils formed in the presence of αBc or CHIP by Neuro-2a cells (**Figure 2A and B,** respectively). Neuro-2a cells, in 96-well plates, were exposed for 2 hours to Alexa488-labeled αSyn fibrils (1 μM Cf) formed in absence or presence of αBc (1 or 0.5 μM Cf) or CHIP (0.3 or 0.1 μM Cf), prior to Trypan blue addition and quantification of Alexa488 fluorescence in a plate-reader. αSyn fibril fluorescence quenching by Trypan blue allowed us to determine accurately the amount of internalized fibrils in a dose-dependent manner. We used Hoescht staining to ascertain that the number of cells remained constant (see Material & Methods). As a positive control for this experiment, we examined the effect of heparin, a ligand of cell membrane heparan sulfate proteoglycans that have been implicated in αSyn internalization [21]. When preformed αSyn-Alexa488 fibrils (1 μM) were pre-incubated with 0.2 μg/mL heparin, we observed an 83% reduction of their internalization (**Figure S2**), in agreement with previous reports [21]. αSyn-Alexa488 fibrils assembled in presence of increasing amounts of αBc or CHIP take-up by Neuro-2a cells decreased in a chaperone concentration-dependent manner (**Figure 2**). We conclude from these experiments that αBc or CHIP affect fibrillar αSyn uptake by Neuro-2a cells, most probably by binding the fibrils and changing their surface properties.

Figure 1

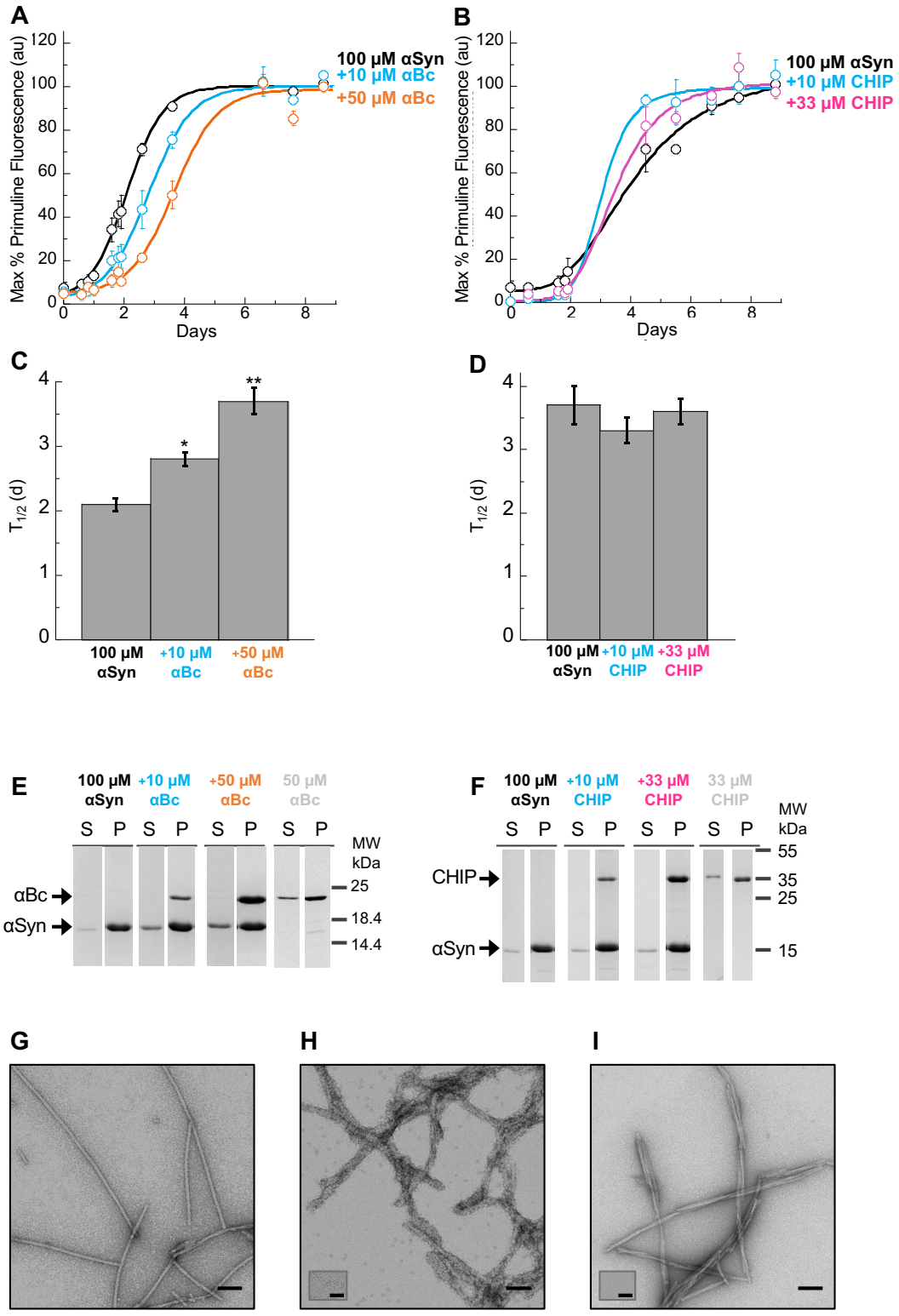

Figure 1: αSyn fibrillation in presence of chaperones. (A-B) Time-course fibrillation of αSyn-Alexa488 (100 µM) in the presence of increasing concentrations of αBc (**A**) or

CHIP (**B**) was followed by primuline fluorescence. Chaperone concentrations of 0 μM, 10 μM, 20 μM, 33 μM, 50 μM are represented as αSyn:chaperone molar ratios of 1:0 (black), 10:1 (blue), 3:1 (pink) or 2:1 (orange) respectively. Means and their associated standard error values were calculated from three independent experiments. Lines through the data points are the best sigmoidal fit. **(C-D)** Half-time ($t_{1/2}$) of αSyn-Alexa488 aggregation in the presence of increasing concentrations of αBc (**C**) or CHIP (**D**). For each independent experiment, the $t_{1/2}$ parameter was extracted from the best fit to a sigmoid function. Means and their associated standard error values were calculated from three independent experiments. Statistical significance was determined through an unpaired student's t-test with equal variance. Annotations indicating level of significance are as follows: *p<0.05; **p<0.01. Legends state αSyn:chaperone molar ratios. **(E-F)** Supernatant and pellet samples at the end of the aggregation reactions in absence or presence of αBc (**E**) or CHIP (**F**) resolved by SDS-PAGE and Coomassie blue staining. Legends state αSyn and chaperone concentrations. **(G-I)** TEM micrographs of αSyn-Alexa488 fibrils formed alone (**G**), fibrils formed in presence of αBc (2:1 αSyn:αBc molar ratio (**H**)), and fibrils formed in presence of CHIP (3:1 αSyn:CHIP molar ratio (**I**)). Gray insets are of chaperones alone. Scale bars: 100 nm.

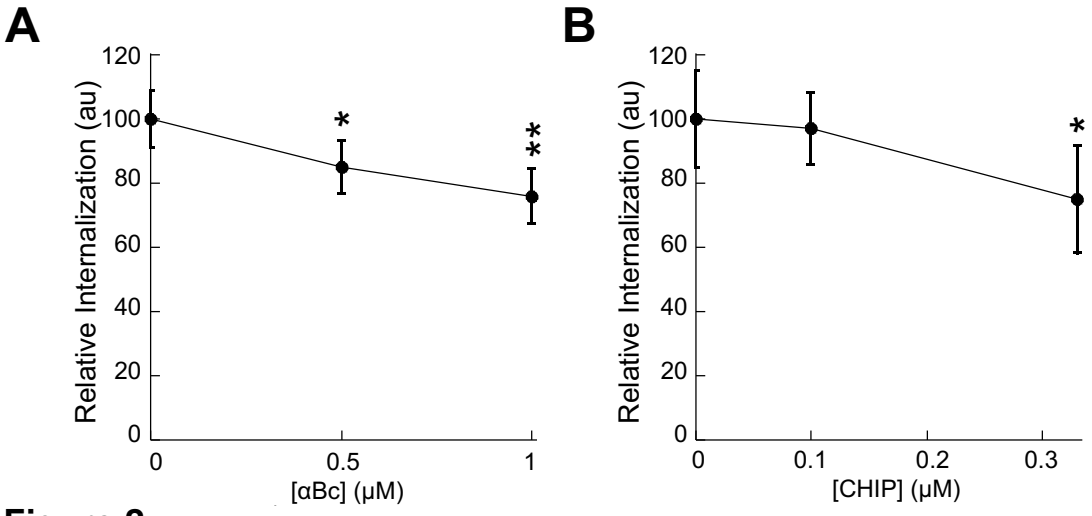

Figure 2

Figure 2: Effect of αBc and CHIP on αSyn fibril uptake by Neuro-2a cells. αSyn-Alexa488 fibrils were assembled at 100 µM in the absence or in the presence of 50 or 100 µM αBc or 10 or 33 µM CHIP. After 2 weeks of fibril formation, the mixture was diluted 100x in DMEM and incubated for 30 min at 37 °C. Neuro-2a cells in 96-well plates were exposed for 2 hours to αSyn-Alexa488 fibrils assembled in the presence of αBc (**A**) or CHIP (**B**). Trypan blue was added after extensive washing to quench the fluorescence of plasma membrane-bound αSyn-Alexa488 fibrils. The amount of internalized αSyn-Alexa488 was measured on a fluorescence plate reader. Means and their associated standard deviation values were calculated over 5 wells. In each case, we performed three independent experiments; one representative experiment is shown. The results and the associated significances are reported relative to the internalization in the absence of chaperone. Statistical significance was determined through an unpaired student's t-test with equal variance. Annotations indicating level of significance are as follows: *$p<0.05$; **$p<0.01$; ***$p<0.001$.

Identification of interaction surfaces between fibrillar αSyn, αBc and CHIP through chemical cross-linking

We next mapped the surface interfaces between αBc or CHIP and fibrillar αSyn to further characterize the interactions. We used chemical cross-linking and mass spectrometric identification of cross-linked peptides to this aim [41,42,54,55].

αSyn fibrils (100 µM) formed in presence or absence of αBc (50 µM) or CHIP (33 µM) were exposed to different cross-linkers at different total protein to cross-linker molar ratios. αSyn fibrils, αBc and CHIP were exposed individually to the cross-linkers in control reactions. The cross-linkers we used had distinct structural-chemical characteristics. Three homobifunctional water soluble NHS-ester cross-linkers specific to

nucleophilic groups (predominantly primary amines e.g. proteins' N-terminus and Lysine residues, but also Tyrosine, Serine and Threonine) with varying spacer arm lengths: 7.7, 11.4 and 12 Å for BS2G, BS^3 and DTSSP, respectively, were used. We further used the heterobifunctional zero length carbodiimide cross-linker EDC that cross-links primary amines to carboxyl groups (e.g. Glu, Asp and proteins C-terminus) in the presence of Sulfo-NHS. Finally, we also used GA, known for its efficiency, but also its limited specificity and molecular heterogeneity with a ~5Å spacer arm for the monomer [52]. The cross-linking reactions products were analyzed by SDS-PAGE to identify fibrillar αSyn-αBc or fibrillar αSyn-CHIP complexes, observed neither in the fibrillar αSyn nor in the chaperone control samples subjected to identical cross-linking conditions. The total protein to cross-linker ratio was optimized. A 1:1 and 1:10:12.5 total protein to cross-linker ratios were selected for fibrillar αSyn-αBc cross-linking with GA and for fibrillar αSyn-CHIP cross-linking with EDC/Sulfo-NHS, respectively. Finally, as the reaction involved cross-linking fibrillar αSyn to the molecular chaperones, the cross-linked high molecular weight complexes were dissociated to allow their analysis by SDS-PAGE.

Specific cross-linked complexes were observed with GA and fibrillar αSyn with αBc (**Figure 3A**) upon staining the polyacrylamide gel with Coomassie blue and on western blots using antibodies directed against αSyn and αBc. The exposure of αSyn fibrils alone to GA yielded protein bands representing monomers, dimers, trimers and tetramers, while that of αBc alone did not affect the intensity of the dimeric form of the protein. Higher concentrations of GA led to the formation of cross-linked higher molecular weight αSyn and αBc species (**Figure S2A**). When an αSyn-αBc complex was cross-linked with GA, a unique and specific protein band appeared at around 40 kDa (arrow). Western blot analyses with antibodies directed against αSyn and αBc confirmed that this specific band contains both proteins and thus corresponds to a covalent αSyn-αBc complex. Its apparent

molecular mass of 40 kDa suggested it was formed of one αSyn and one αBc monomer. The band of interest corresponding to the αSyn-αBc complex was thus cut off the gel and subjected to trypsin digestion. The resulting peptides were analyzed by nanoliquid chromatography coupled to tandem mass spectrometry (nanoLC-MS/MS). For the αSyn-αBc complex, using database searching as described in Materials & Methods, we obtained a sequence coverage of 100% for αSyn and 97% for αBc. Using the StavroX software [51], we identified one αSyn-αBc inter-protein cross-linked peptide that was absent from control bands (monomeric or dimeric αSyn or αBc with or without GA cross-linking) and was validated manually. This peptide was identified as a quadruple peptide ion with a mass-to-charge of 622.847, consistent with an inter-peptide cross-link that covalently binds two peptide sequences and thus is highly charged (**Figure 3B**). Its fragmentation spectrum, presented in **Figure 3B,** identified the cross-linked peptides and sites. The y and b fragments ions series reported in **Figure 3C** identified the αSyn [33-43] and αBc [153-163] sequences of the cross-linked peptide with a cross-link between Lys-34 from αSyn and Thr-162 from αBc. The mass deviation of -3.02 ppm measured between the experimental and the theoretical mass of this cross-linked peptide further validated the identification. Interestingly, the αBc peptide [153-163] ,in which Thr-162 (in purple, space fill, **Figure 3D**) is cross-linked to αSyn fibrils, is located in the flexible, unstructured C-terminus of the chaperone [44], and the αSyn peptide [33-43], in which Lys-34 (in red, **Figure 3E**) is cross-linked to αBc, is located within a flexible loop and is exposed to the solvent in the fibrillar structures of αSyn (PBD code 6rt0 and 6rtb) we recently solved [56].

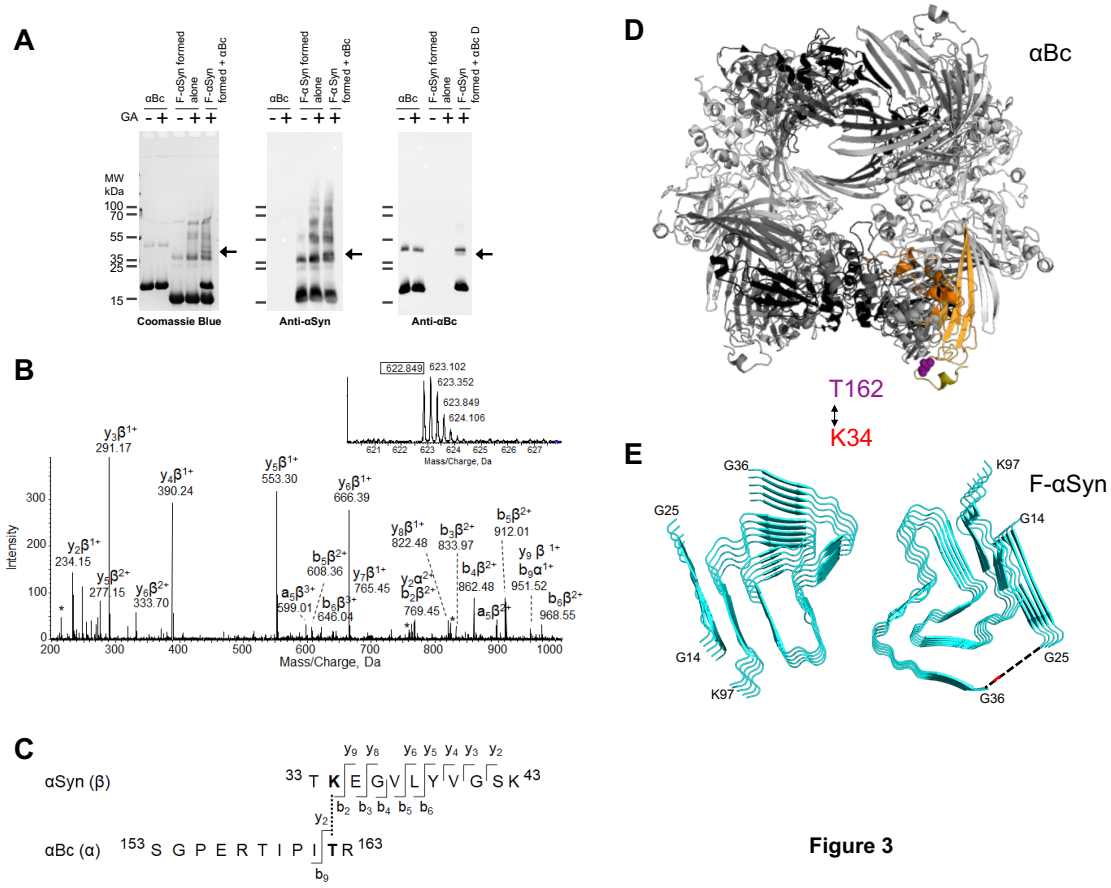

Figure 3

Figure 3: Cross-linking of αBc to αSyn fibrils by glutaraldehyde.

(A) Cross-linked reaction protein products were separated on a 7.5% Tris-Tricine SDS-PAGE and detected by Coomassie blue staining and immunodetection by western blot using detections with either SYN1 anti-αSyn or in-house-immunopurified rabbit polyclonal anti-αBc antibodies. αBc alone, αSyn fibrils (F-αSyn) alone or αSyn fibrils formed in the presence of αBc (2:1 αSyn:αBc molar ratio) were exposed to the glutaraldehyde (GA) cross-linker at the same total protein:GA molar ratio (1:1). The arrows show the band of the αSyn-αBc complex of interest. **(B-C)** NanoLC-MSMS analysis and data analysis using the StavroX software identified the peptide [153-163] from αBc cross-linked with peptide [33-43] from αSyn fibrils. In **B**, the fragmentation spectrum of the quadruple-charged cross-linked precursor ion at the monoisotopic m/z 622.847 (on the top) is annotated with the identified fragments and their charge state. Loss of water (asterisks) and internal fragments (i) are indicated. In **C**, the identified

fragments are indicated on the cross-linked sequences. The α and β sequences correspond to the αBc [153-163] and αSyn [33-43] peptides, respectively. The identified cross-link involves residues Thr-162 and Lys-34 from αBc and αSyn, respectively. **(D)** Location of the cross-linked Threonine in a model structure of an αBc 24-mer (PDB accession number 2ygd, 9.4 Å resolution). Thr-162 (T162) is represented by a purple sphere. (**E**) Location of the cross-linked Lysine in αSyn fibrils (PDB accession number 6rt0). Lys-34 (K34) is in a flexible portion of the sequence, not resolved by cryo-EM, and sketched by a dotted black line; K34 itself is represented by a red line. Figures **D-E** were generated with PYMOL (**http://www.pymol.org**).

Fibrillar αSyn-CHIP cross-links obtained using EDC/Sulfo-NHS were resolved by SDS-PAGE and detected both by Coomassie blue staining and western blot using antibodies against αSyn and CHIP (**Figure 4A**). A dimeric form of CHIP was observed upon treatment of the protein with EDC/Sulfo-NHS, confirming its dimeric state. Higher concentrations of EDC/Sulfo-NHS led to the formation of cross-linked higher molecular weight αSyn and CHIP (**Figure S2B**). When an αSyn-CHIP complex was cross-linked with EDC, a unique and specific protein band appeared at an apparent molecular mass around 55 kDa (arrow). Western blot analyses with antibodies directed against αSyn and CHIP confirmed that this specific additional band contained both proteins and thus corresponded to a covalent αSyn-CHIP complex. Its apparent molecular mass of about 55 kDa suggested it was constituted by one αSyn and one CHIP monomer. The band of interest corresponding to the αSyn-CHIP covalent complex was cut off the gel and in-gel digested using trypsin and the resulting peptides were further analyzed by nanoLC-MS/MS as described above. By database search as described in Material and Methods, we obtained a sequence coverage of 100% for αSyn and 85% for CHIP. Using the

StavroX software [51], we identified one αSyn-CHIP inter-protein cross-linked peptide that was absent from control bands (monomeric or dimeric αSyn or CHIP with or without EDC cross-linking) and was validated manually. This peptide was identified as a quadruple charged ion with a mass-to-charge of 616.136 (**Figure 4B**). Its fragmentation spectrum, presented in **Figure 4B,** identified the cross-linked peptides and sites. The y and β fragments ions, reported in **Figure 4C,** identified the αSyn [61-80] and CHIP [254-262] sequences of the cross-linked peptide with a cross-link between Glu-61 from αSyn and Lys-254 from CHIP. Finally, the mass deviation of 4.17 ppm measured between the experimental and the theoretical mass of this cross-linked peptide further validated the identification. Interestingly, CHIP peptide [254-262], in which Lys-254 (in purple, space fill, **Figure 4D**) was cross-linked to fibrillar αSyn, is located within the CHIP U-box domain [46] while αSyn peptide [61-80], in which Glu-61 (red sphere, **Figure 4E**) was cross-linked to CHIP, is located in the non-amyloid component (NAC) region and is accessible to the solvent in the fibrillar structures of αSyn (PBD code 6rt0 and 6rtb) we recently solved [56].

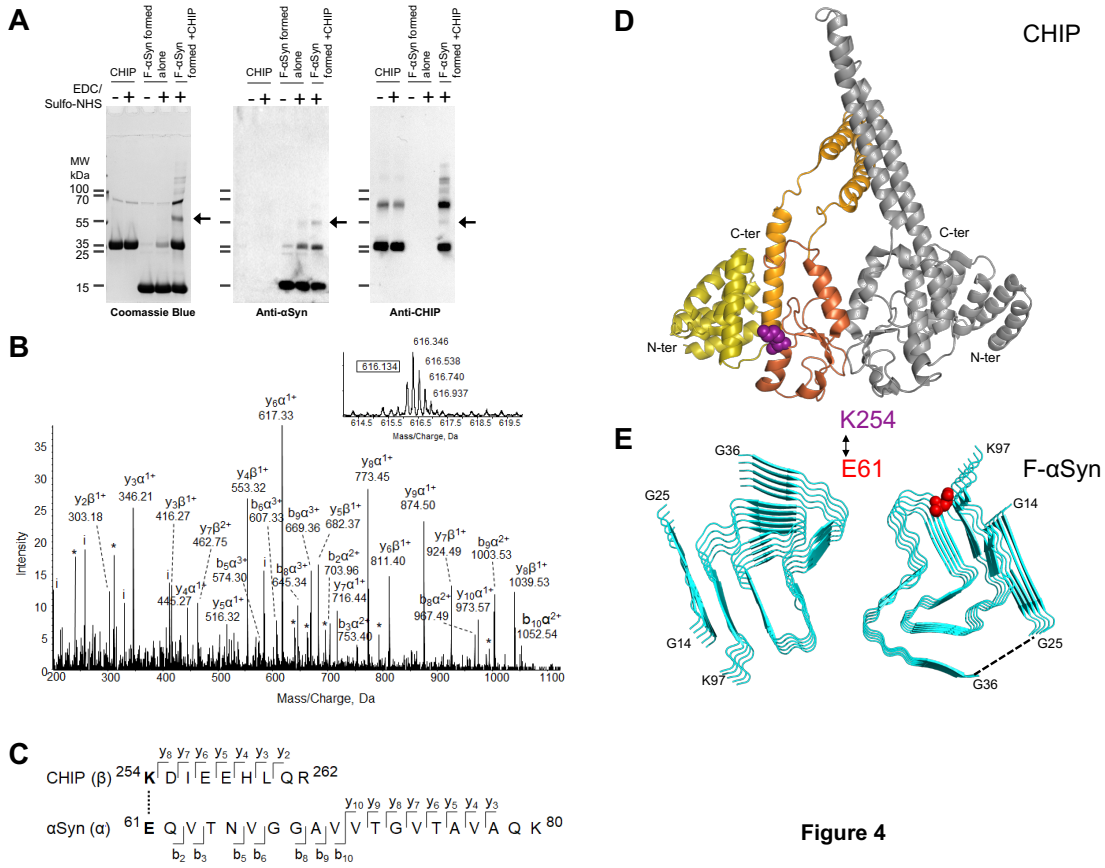

Figure 4

Figure 4: Cross-linking of CHIP to αSyn fibrils by EDC/SulfoNHS-ester.

(A) Cross-linked reaction protein products were separated on a 7.5% Tris-Tricine SDS-PAGE and detected by Coomassie blue staining and immunodetection by western blot using detections with either SYN1 anti-αSyn or in-house-immunopurified rabbit polyclonal anti-CHIP antibodies. CHIP alone, αSyn fibrils alone or αSyn fibrils formed in the presence of CHIP (3:1 αSyn:CHIP molar ratio) were exposed with EDC/SulfoNHS-ester cross-linker at same total protein:EDC:Sulfo-NHS molar ratio (1:10:12.5). The arrows show the band of the αSyn-CHIP complex of interest. **(B-C)** NanoLC-MSMS analysis and data analysis using the StavroX software identified the peptide [254–262] from CHIP cross-linked with peptide [61-80] from αSyn fibrils. In **B**, the fragmentation spectrum of the quintuple-charged cross-linked precursor ion at the monoisotopic m/z 616.136 (on the top) is annotated with the identified fragments and their charge state. Loss of water (asterisks) and internal fragments (i) are indicated. In **C**, the identified

fragments are indicated on the cross-linked sequences. The α and β sequences correspond to the αSyn [61-80] and CHIP [254-262] peptides, respectively. The cross-link involves residues Lys-254 and Glu-61 from CHIP and fibrillary αSyn, respectively. **(D)** Location of the cross-linked Lysine in a CHIP dimer (Protein Data Bank accession number 2C2L, of murine CHIP, sharing 98% sequence identity with human CHIP). Lys-254 (K254) is represented by a purple sphere. The helical hairpin domains are in light orange, the tetratricopeptide repeat (TPR) domains are in yellow; the U-box domains are in bright orange. (**E**) Location of the cross-linked Glutamate in αSyn fibrils (PDB accession number 6rt0). Glu-61 (E61) is represented by a red sphere. Figures **D-E** were generated with PYMOL (**http://www.pymol.org**).

Discussion

The aggregation of distinct proteins is the hallmark of neurodegenerative diseases [27]. Molecular chaperones interfere with this process and/or are a component of the resulting aggregates [27,31,34,35,44,57,58]. αSyn fibrillar aggregates are capable of propagating between neuronal cells and consequently contribute to disease progression in synucleinopathies [3,4]. Therefore, identifying the contribution of molecular chaperones within this process and determining whether they bind αSyn fibrils and affect their propagation is of particular interest. In that regard, it has been previously shown that Hsc70 not only reduces aggregation of αSyn [33] into fibrils, but also binds the fibrils and affects their toxicity [33]. Furthermore, we also identified inter-molecular interaction surfaces between Hsc70 and αSyn using covalent cross-linking and mass spectrometry [41,42].

The binding of molecular chaperones to preformed αSyn fibrils has been assessed on rare occasions [37–40]. In particular, the molecular chaperone αBc that we used here has been

shown to bind to preformed αSyn fibrils [38,39]. This clearly raises the need for further investigation, as the propagating αSyn aggregates form within the cells, in the presence of cytosolic molecular chaperones. Here, we thus went further and assessed the take-up by cultured cells of neuronal origin of fibrillar αSyn assembled in the presence of molecular chaperones. We showed that the molecular chaperones αBc and CHIP bind efficiently to αSyn fibrils generated in their presence and affect their take-up by Neuro-2a cells. Also, we further identified the inter-molecular interaction interfaces between fibrillar αSyn and αBc or CHIP.

Our cross-linking studies show that αBc interacts with αSyn fibrils. A unique intermolecular peptide was identified, where Thr-162 from αBc and Lys-34 from αSyn fibrils were cross-linked by GA. Lys-34 from αSyn is located within a flexible loop exposed to the solvent and αSyn fibril binders in the αSyn fibrillar structures (PBD code 6rt0 and 6rtb) we recently solved (**Figure 3E**) [56]. Thr-162 from αBc lies in the unstructured C-terminal domain of αBc (**Figure 3D)**. αBc has been shown to interact with monomeric αSyn through a different region, namely a conserved β4/β8 surface lying within its core [59]. Indeed, αBc-core prevents the aggregation of αSyn [38,45]. Another heat shock protein, Hsp27, prevents the aggregation of αSyn and binds αSyn fibrils [38,60]. Interestingly, and in contrast with the whole protein, truncated Hsp27 containing only the conserved β4/β8 α-crystallin core domain loses its ability to bind αSyn fibrils [60]. Furthermore, dimeric, untruncated mutant Hsp27 binds αSyn fibrils, suggesting that residues outside of the core region of the conserved α-crystallin domain play a role in αSyn fibril binding [60].

As in the case of αBc, we mapped the interfaces between αSyn fibrils and the molecular chaperone CHIP. One inter-molecular peptide was identified, where Lys-254 from CHIP and Glu-61 from αSyn fibrils were cross-linked by EDC. Glu-61 from αSyn is located at

one tip of the αSyn non-amyloid component (NAC) region and is exposed to the solvent (**Figure 4E**) [56]. Lys-254 from CHIP is located in the C-terminal U-box domain of the chaperone (**Figure 4D)**, responsible for CHIP binding to ubiquitin-conjugating enzymes [46]. This result is coherent with previously published data. Indeed, a CHIP variant devoid of the Hsp70-binding N-terminal tetratricopeptide repeat domain (TPR, in yellow in **Figure 4D**) but in which the U-box domain was still present, was able to immunoprecipitate αSyn [47].

It is worth noting that the interaction areas we identified within the αBc-αSyn fibril or CHIP-αSyn fibril complexes are not exhaustive as the cross-linking coupled with mass spectrometry strategy we applied to fibrillar assemblies remains challenging. Nonetheless, identifying polypeptides derived from molecular chaperones at close proximity with exposed polypeptide stretches at αSyn fibril surfaces may pave the way for the development of finely targeted ligands. Notably, peptides are tunable: their affinity for their protein targets can be optimized and their pharmacokinetics properties can be adjusted [61]. Such flexibility holds promise for ligands that can interfere with αSyn fibril prion-like propagation and subsequent disease progression.

Author Contributions

EM, VR and RM planned the experiments; MB, VR, LB and TB performed experiments; MB, EM, VR and RM analyzed data and wrote the paper.

Acknowledgements

We thank David Cornu for expert assistance in MS. This work was supported by the Centre National de la Recherche Scientifique, the Institut National de la Santé et de la Recherche Médicale, the Région Ile de France through DIM Cerveau et Pensée and the EC Joint Programme on Neurodegenerative Diseases and Agence Nationale pour la Recherche (TransPathND, ANR-17-JPCD-0002-02 and Protest-70, ANR-17-JPCD-0005-01). This work also received support from the EU/EFPIA/Innovative Medicines Initiative 2 Joint Undertaking (IMPRiND grant No. 116060 and PD-MitoQUANT grant No. 821522). This work benefited from the electron microscopy facility Imagerie-Gif and the proteomic facility SICaPS.

Bibliography

1 Spillantini MG, Crowther AR, Jakes R, Cairns NJ, Lantos PL & Goedert M (1998) Filamentous α-synuclein inclusions link multiple system atrophy with Parkinson's disease and dementia with Lewy bodies. *Neurosci. Lett.* **251**, 205–208.

2 Spillantini MG, Crowther AR, Jakes R, Hasegawa M & Goedert M (1998) Alpha-Synuclein in filamentous inclusions of Lewy bodies from Parkinson's disease and dementia with Lewy bodies. *Proc. Natl. Acad. Sci.* **95**, 6469–6473.

3 Davis AA, Leyns CEG & Holtzman DM (2018) Intercellular Spread of Protein Aggregates in Neurodegenerative Disease. *Annu. Rev. Cell Dev. Biol.* **34**, 545–68.

4 Brundin P, Melki R & Kopito R (2010) Prion-like transmission of protein aggregates in neurodegenerative diseases. *Nat. Rev. Mol. Cell Biol.* **11**, 301–7.

5 Brundin P & Melki R (2017) Prying into the Prion Hypothesis for Parkinson's Disease. *J. Neurosci.* **37**, 9808–9818.

6 Braak H, Del Tredici K, Rüb U, De Vos RAI, Jansen Steur ENH & Braak E (2003) Staging of brain pathology related to sporadic Parkinson's disease. *Neurobiol. Aging* **24**, 197–211.

7 Ngolab J, Trinh I, Rockenstein E, Mante M, Florio J, Trejo M, Masliah D, Adame A, Masliah E & Rissman RA (2017) Brain-derived exosomes from dementia with Lewy bodies propagate α-synuclein pathology. *Acta Neuropathol. Commun.* **5**, 46.

8 Emmanouilidou E, Melachroinou K, Roumeliotis T, Garbis SD, Ntzouni M, Margaritis LH, Stefanis L & Vekrellis K (2010) Cell-Produced a-Synuclein Is Secreted in a Calcium-Dependent Manner by Exosomes and Impacts Neuronal Survival. *J. Neurosci.* **30**, 6838–6851.

9 Abounit S, Bousset L, Loria F, Zhu S, de Chaumont F, Pieri L, Olivo-Marin J, Melki

R & Zurzolo C (2016) Tunneling nanotubes spread fibrillar α-synuclein by intercellular trafficking of lysosomes. *EMBO J.* **35**, 2120–2138.

10 Rostami J, Holmqvist S, Lindström V, Sigvardson J, Westermark GT, Ingelsson M, Bergström J, Roybon L & Erlandsson A (2017) Human Astrocytes Transfer Aggregated Alpha-Synuclein via Tunneling Nanotubes. *J. Neurosci.* **37**, 11835–11853.

11 Brahic M, Bousset L, Bieri G, Melki R & Gitler AD (2016) Axonal transport and secretion of fibrillar forms of α-synuclein, Aβ42 peptide and HTTExon 1. *Acta Neuropathol.* **131**, 539–548.

12 Lee H-J, Patel S & Lee S-J (2005) Intravesicular Localization and Exocytosis of a-Synuclein and its Aggregates. *J. Neurosci.* **25**, 6016–6024.

13 Desplats P, Lee H-J, Bae E-J, Patrick C, Rockenstein E, Crews L, Spencer B, Masliah E & Lee S-J (2009) Inclusion formation and neuronal cell death through neuron-to-neuron transmission of a-synuclein. *Proc. Natl. Acad. Sci.* **106**, 13010–13015.

14 Rodriguez L, Marano MM & Tandon A (2018) Import and export of misfolded α-synuclein. *Front. Neurosci.* **12**, 1–9.

15 Grozdanov V & Danzer KM (2018) Release and uptake of pathologic alpha-synuclein. *Cell Tissue Res.* **373**, 175–182.

16 Flavin WP, Bousset L, Green ZC, Chu Y, Skarpathiotis S, Chaney MJ, Kordower JH, Melki R & Campbell EM (2017) Endocytic vesicle rupture is a conserved mechanism of cellular invasion by amyloid proteins. *Acta Neuropathol.* **134**, 629–653.

17 Jucker M & Walker LC (2013) Self-propagation of pathogenic protein aggregates in neurodegenerative diseases. *Nature* **501**, 45–51.

18 Peelaerts W, Bousset L, Baekelandt V & Melki R (2018) α-Synuclein strains and seeding in Parkinson's disease, incidental Lewy body disease, dementia with Lewy bodies and multiple system atrophy: similarities and differences. *Cell Tissue Res.* **373**, 195–212.

19 Tyson T, Steiner JA & Brundin P (2016) Sorting Out Release, Uptake and Processing of Alpha-Synuclein During Prion-Like Spread of Pathology. *J Neurochem* **139**, 275–289.

20 Pemberton S & Melki R (2012) The interaction of Hsc70 protein with fibrillar alpha-Synuclein and its therapeutic potential in Parkinson's disease. *Commun Integr Biol* **5**, 94–95.

21 Stopschinski BE, Holmes BB, Miller GM, Manon VA, Vaquer-Alicea J, Prueitt WL, Hsieh-Wilson LC & Diamond MI (2018) Specific glycosaminoglycan chain length and sulfation patterns are required for cell uptake of tau versus α-synuclein and β-amyloid aggregates. *J. Biol. Chem.* **293**, 10826–10840.

22 Mao X, Ou MT, Karuppagounder SS, Kam T-I, Yin X, Xiong Y, Ge P, Umanah GE, Brahmachari S, Shin J-H, Kang HC, Zhang J, Xu J, Chen R, Park H, Andrabi SA, Kang SU, Goncalves RA, Liang Y, Zhang S, Qi C, Lam S, Keiler JA, Tyson J, Kim D, Panicker N, Yun SP, Workman CJ, Vignali DAAA, Dawson VL, Ko HS & Dawson TM (2016) Pathological a-synuclein transmission initiated by binding lymphocyte-activation gene 3. *Science* **353**, aah3374-1-aah3374-12.

23 Shrivastava AN, Redeker V, Fritz N, Pieri L, Almeida LG, Spolidoro M, Liebmann T, Bousset L, Renner M, Léna C, Aperia A, Melki R, Triller A, Lena C, Aperia A, Melki R & Triller A (2015) α-synuclein assemblies sequester neuronal α3-Na+/K+-ATPase and impair Na+ gradient. *EMBO J.* **34**, 2408–2423.

24 Shrivastava AN, Aperia A, Melki R & Triller A (2017) Physico-Pathologic Mechanisms Involved in Neurodegeneration: Misfolded Protein-Plasma Membrane Interactions. *Neuron* **95**, 33–50.

25 Grey M, Linse S, Nilsson H, Brundin P & Sparr E (2011) Membrane interaction of α-synuclein in different aggregation states. *J. Parkinsons. Dis.* **1**, 359–371.

26 Trevino RS, Lauckner JE, Sourigues Y, Pearce MM, Bousset L, Melki R & Kopito RR (2012) Fibrillar structure and charge determine the interaction of polyglutamine protein aggregates with the cell surface. *J. Biol. Chem.* **287**, 29722–29728.

27 Wentink A, Nussbaum-Krammer C & Bukau B (2019) Modulation of Amyloid States by Molecular Chaperones. *Cold Spring Harb. Perspect. Biol.* **11**, a033969.

28 Bruinsma IB, Bruggink KA, Kinast K, Versleijen AAM, Segers-Nolten IMJ, Subramaniam V, Bea Kuiperij H, Boelens W, de Waal RMW & Verbeek MM (2011) Inhibition of α-synuclein aggregation by small heat shock proteins. *Proteins Struct. Funct. Bioinforma.* **79**, 2956–2967.

29 Falsone SF, Kungl AJ, Rek A, Cappai R & Zangger K (2009) The molecular chaperone Hsp90 modulates intermediate steps of amyloid assembly of the Parkinson-related protein α-synuclein. *J. Biol. Chem.* **284**, 31190–31199.

30 Dedmon MM, Christodoulou J, Wilson MR & Dobson CM (2005) Heat shock protein 70 inhibits α-synuclein fibril formation via preferential binding to prefibrillar species. *J. Biol. Chem.* **280**, 14733–14740.

31 Rekas A, Adda CG, Andrew Aquilina J, Barnham KJ, Sunde M, Galatis D, Williamson NA, Masters CL, Anders RF, Robinson C V., Cappai R & Carver JA (2004) Interaction of the molecular chaperone aB-crystallin with a-Synuclein: Effects on amyloid fibril formation and chaperone activity. *J. Mol. Biol.* **340**, 1167–1183.

32 Roodveldt C, Bertoncini CW, Andersson A, Van Der Goot AT, Hsu S Te, Fernández-Montesinos R, De Jong J, Van Ham TJ, Nollen EA, Pozo D, Christodoulou J & Dobson CM (2009) Chaperone proteostasis in Parkinson's disease: Stabilization of the Hsp70/α-synuclein complex by Hip. *EMBO J.* **28**, 3758–3770.

33 Pemberton S, Madiona K, Pieri L, Kabani M, Bousset L & Melki R (2011) Hsc70 Protein Interaction with Soluble and Fibrillar α-Synuclein. *J. Biol. Chem.* **286**, 34690–34699.

34 Shin Y, Klucken J, Patterson C, Hyman BT & McLean PJ (2005) The Co-chaperone carboxyl terminus of Hsp70-interacting protein (CHIP) mediates a-synuclein degradation decisions between proteasomal and lysosomal pathways. *J. Biol. Chem.* **280**, 23727–23734.

35 Braak H, Del Tredici K, Sandmann-Keil D, Rüb U & Schultz C (2001) Nerve cells expressing heat-shock proteins in Parkinson's disease. *Acta Neuropathol.* **102**, 449–454.

36 McLean PJ, Kawamata H, Shariff S, Hewett J, Sharma N, Ueda K, Breakefield XO & Hyman BT (2002) TorsinA and heat shock proteins act as molecular chaperones: suppression of a-synuclein aggregation. *J Neurochem* **83**, 846–854.

37 Gao X, Carroni M, Nussbaum-Krammer C, Mogk A, Nillegoda NB, Szlachcic A, Guilbride DL, Saibil HR, Mayer MP & Bukau B (2015) Human Hsp70 Disaggregase Reverses Parkinson's-Linked α-Synuclein Amyloid Fibrils. *Mol. Cell* **59**, 781–793.

38 Cox D, Selig E, Griffin MDW, Carver JA & Ecroyd H (2016) Small Heat-shock Proteins Prevent α-synuclein aggregation via transient interactions and their efficacy is affected by the rate of aggregation. *J. Biol. Chem.* **291**, 22618–22629.

39 Waudby CA, Knowles TPJ, Devlin GL, Skepper JN, Ecroyd H, Carver JA, Welland ME, Christodoulou J, Dobson CM & Meehan S (2010) The interaction of αB-crystallin with mature α-synuclein amyloid fibrils inhibits their elongation. *Biophys. J.* **98**, 843–851.

40 Aprile FA, Arosio P, Fusco G, Chen SW, Kumita JR, Dhulesia A, Tortora P, Knowles TPJ, Vendruscolo M, Dobson CM & Cremades N (2017) Inhibition of α-Synuclein Fibril Elongation by Hsp70 Is Governed by a Kinetic Binding Competition between α-Synuclein Species. *Biochemistry* **56**, 1177–1180.

41 Redeker V, Pemberton S, Bienvenut W, Bousset L & Melki R (2012) Identification of protein interfaces between α-synuclein, the principal component of Lewy bodies in Parkinson disease, and the molecular chaperones human Hsc70 and the yeast Ssa1p. *J. Biol. Chem.* **287**, 32630–32639.

42 Nury C, Redeker V, Dautrey S, Romieu A, Van Der Rest G, Renard PY, Melki R & Chamot-Rooke J (2015) A novel bio-orthogonal cross-linker for improved protein/protein interaction analysis. *Anal. Chem.* **87**, 1853–1860.

43 Aquilina JA, Benesch JLP, Bateman OA, Slingsby C & Robinson C V. (2003) Polydispersity of a mammalian chaperone: Mass spectrometry reveals the population of oligomers in B-crystallin. *Proc. Natl. Acad. Sci.* **100**, 10611–10616.

44 Mainz A, Peschek J, Stavropoulou M, Back KC, Bardiaux B, Asami S, Prade E, Peters C, Weinkauf S, Buchner J & Reif B (2015) The chaperone αB-crystallin uses different interfaces to capture an amorphous and an amyloid client. *Nat. Struct. Mol. Biol.* **22**, 898–905.

45 Hochberg GK a, Ecroyd H, Liu C, Cox D, Cascio D, Sawaya MR, Collier MP, Stroud J, Carver J a, Baldwin AJ, Robinson C V, Eisenberg DS, Benesch JLP & Laganowsky A (2014) The structured core domain of B-crystallin can prevent amyloid fibrillation and associated toxicity. *Proc. Natl. Acad. Sci.* **111**, E1562–E1570.

46 Zhang M, Windheim M, Roe SM, Peggie M, Cohen P, Prodromou C & Pearl LH (2005) Chaperoned Ubiquitylation—Crystal Structures of the CHIP U Box E3 Ubiquitin Ligase and a CHIP-Ubc13-Uev1a Complex. *Mol. Cell* **20**, 525–538.

47 Tetzlaff JE, Putcha P, Outeiro TF, Ivanov A, Berezovska O, Hyman BT & McLean PJ (2008) CHIP Targets Toxic α-Synuclein Oligomers for Degradation. *J. Biol. Chem.* **283**, 17962–17968.

48 Ghee M, Melki R, Michot N & Mallet J (2005) PA700, the regulatory complex of the 26S proteasome, interferes with α-synuclein assembly. *FEBS J.* **272**, 4023–

4033.

49 Shevchenko A, Wilm M, Vorm O & Mann M (1996) Mass spectrometric sequencing of proteins from silver-stained polyacrylamide gels. *Anal. Chem.* **68**, 850–858.

50 Shrivastava AN, Redeker V, Pieri L, Bousset L, Renner M, Madiona K, Mailhes-Hamon C, Coens A, Buée L, Hantraye P, Triller A & Melki R (2019) Clustering of Tau fibrils impairs the synaptic composition of α3-Na + /K + -ATPase and AMPA receptors. *EMBO J.* **38**, e99871.

51 Götze M, Pettelkau J, Schaks S, Bosse K, Ihling CH, Krauth F, Fritzsche R, Kühn U & Sinz A (2012) StavroX-A software for analyzing crosslinked products in protein interaction studies. *J. Am. Soc. Mass Spectrom.* **23**, 76–87.

52 Migneault I, Dartiguenave C, Bertrand MJ & Waldron KC (2004) Glutaraldehyde: behavior in aqueous solution, reaction with proteins, and application to enzyme crosslinking. *Biotechniques* **37**, 790–802.

53 Hansen C, Angot E, Bergström A, Steiner J a, Pieri L, Paul G, Outeiro TF, Melki R, Kallunki P & Fog K (2011) α-Synuclein propagates from mouse brain to grafted dopaminergic neurons and seeds aggregation in cultured human cells. *J. Clin. Invest.* **121**, 715–725.

54 Monsellier E, Redeker V, Ruiz-Arlandis G, Bousset L & Melki R (2015) Molecular interaction between the chaperone Hsc70 and the N-terminal flank of huntingtin exon 1 modulates aggregation. *J. Biol. Chem.* **290**, 2560–2576.

55 Redeker V, Bonnefoy J, Le Caer JP, Pemberton S, Laprévote O & Melki R (2010) A region within the C-terminal domain of Ure2p is shown to interact with the molecular chaperone Ssa1p by the use of cross-linkers and mass spectrometry. *FEBS J.* **277**, 5112–5123.

56 Guerrero-Ferreira R, Taylor NMI, Arteni A-A, Kumari P, Mona D, Ringler P, Britschgi M, Lauer ME, Makky A, Verasdonck J, Riek R, Melki R, Meier BH, Böckmann A, Bousset L & Stahlberg H (2019) Two new polymorphic structures of human full-length alpha-synuclein fibrils solved by cryo-electron microscopy. *Elife* **8**, 654582.

57 Lindberg I, Shorter J, Wiseman RL, Chiti F, Dickey CA & McLean PJ (2015) Chaperones in Neurodegeneration. *J. Neurosci.* **35**, 13853–13859.

58 Dimant H, Ebrahimi-Fakhari D & McLean PJ (2012) Molecular chaperones and co-chaperones in parkinson disease. *Neuroscientist* **18**, 589–601.

59 Liu Z, Wang C, Li Y, Zhao C, Li T, Li D, Zhang S & Liu C (2018) Mechanistic insights into the switch of αB-crystallin chaperone activity and self-multimerization. *J. Biol. Chem.* **293**, 14880–14890.

60 Cox D, Whiten DR, Brown JWP, Horrocks MH, San Gil R, Dobson CM, Klenerman D, van Oijen AM & Ecroyd H (2018) The small heat shock protein Hsp27 binds α-synuclein fibrils, preventing elongation and cytotoxicity. *J. Biol. Chem.* **293**, 4486–4497.

61 Di L (2015) Strategic Approaches to Optimizing Peptide ADME Properties. *AAPS J.* **17**, 134–143.

Supporting Information

Figure S1

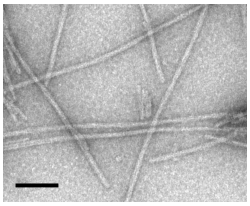

Figure S1: TEM micrograph of unlabeled αSyn fibrils. αSyn fibrils were assembled at 100 µM. Scale bar: 100 nm.

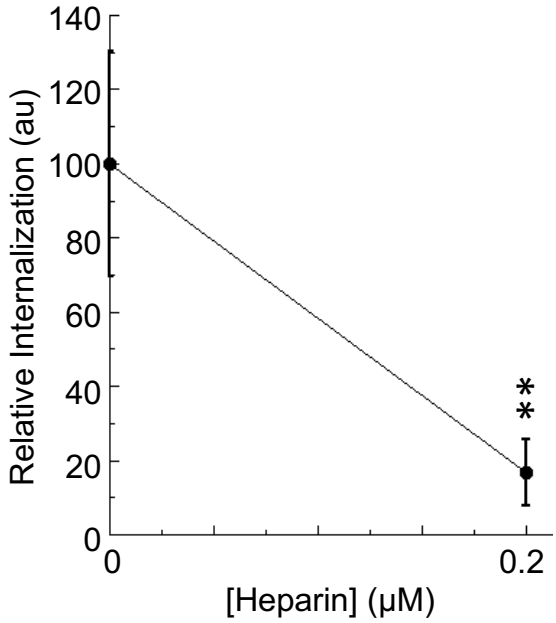

Figure S2: Internalization of preformed αSyn-Alexa488 fibrils preincubated with heparin. αSyn fibrils were assembled at 100 µM. After two weeks of fibril formation, the fibrils were labeled with Alexa488 before a 100x dilution in DMEM followed by incubation for 30 min at 37 °C with 0 or 0.2 µM heparin. Neuro-2a cells in 96-well plates were exposed for 2 hours to αSyn-Alexa488 fibrils in absence or presence of heparin. Trypan blue was added after extensive washing to quench the fluorescence of plasma membrane-bound αSyn-Alexa488 fibrils. The amount of internalized αSyn-Alexa488 was measured on a fluorescence plate reader. Means and their associated standard deviation values were calculated over 5 wells. The results and the associated significances

were reported relative to the internalization in the absence of heparin. Statistical significance was determined through an unpaired student's t-test with equal variance. Annotations indicating level of significance are as follows: **p<0.01.

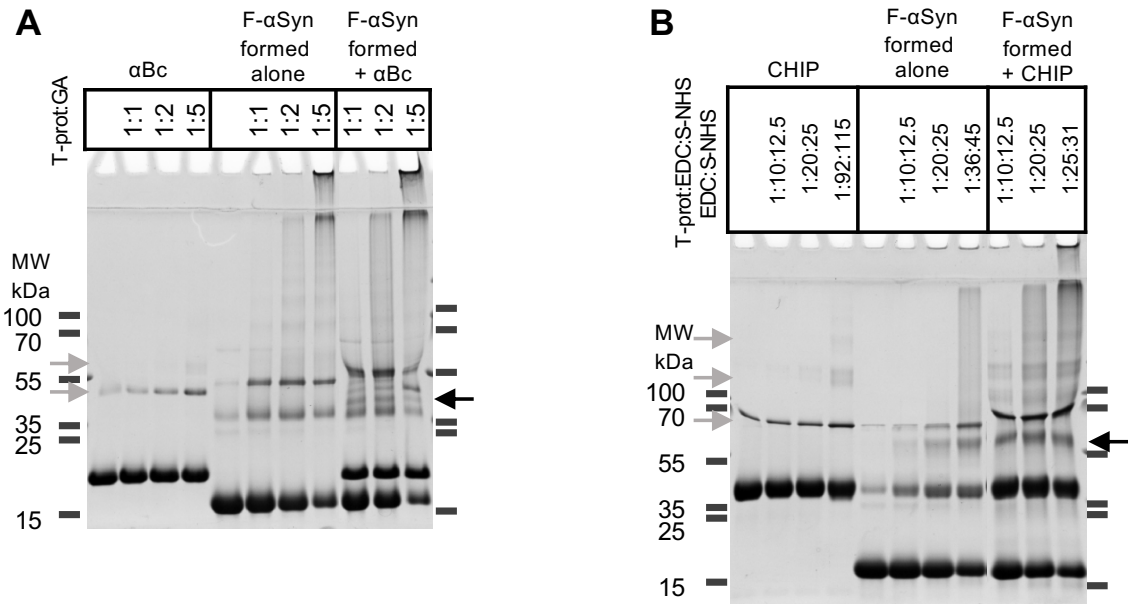

Figure S3: Cross-linking at higher concentrations of αBc or CHIP to αSyn fibrils by glutaraldehyde or EDC/SulfoNHS-ester.

(A, B) Cross-linked reaction protein products were separated on a 7.5% Tris-Tricine SDS-PAGE and detected by Coomassie blue staining. The black arrows show the band of the αSyn-chaperone complexes of interest while the gray arrows show the bands of oligomeric cross-linked chaperones. **(A)** αBc alone, αSyn fibrils (F-αSyn) alone or αSyn fibrils formed in the presence of αBc (2:1 αSyn:αBc molar ratio) were exposed to the glutaraldehyde (GA) cross-linker at the same total protein:GA molar ratios (1:1, 1:2, 1:5). **(B)** CHIP alone, αSyn fibrils alone or αSyn fibrils formed in the presence of CHIP (3:1 αSyn:CHIP molar ratio) were exposed with EDC/SulfoNHS-ester cross-linker at same total protein:EDC:Sulfo-NHS molar ratio (1:10:12.5; 1:20:25) or the same fixed concentration (2945/3683 μM, corresponding to total protein:EDC:Sulfo-NHS molar ratios of 1:91:115, 1:36:45 and 1:25:31, respectively).

Chapter 5: Complementary results

5.1 Chaperone binding to preformed αSyn amyloid fibrils

Introduction

In Chapter 4, we characterized the binding between chaperones and fibrils formed in their presence. However, the binding of molecular chaperones to preformed αSyn fibrils have been tested only on rare occasions and for few chaperones (Aprile et al., 2017; Cox et al., 2016; Gao et al., 2015; Waudby et al., 2010). In this work, we examined binding to preformed αSyn fibrils to an expanded number of chaperones in order to design new molecular tools able to interfere with the propagation process of αSyn fibrils. We selected the two chaperones discussed in Chapter 4, αBc and CHIP, as well as the core domain of αBc, the bacterial chaperone CsgC, and a truncated version of the neurosecreted chaperone proSAAS (proSSAS$_{62\text{-}180}$), altogether chosen for their limited sizes, diverse origins, various oligomeric states, and the promising research previously published, discussed for αBc and CHIP in Chapter 4. The highly conserved α-crystallin domain of αBc, or αBc-core, has been shown to be dimeric and retains the *in vitro* anti-aggregation activity of the mother protein against αSyn assembly into fibrils (Cox et al., 2016; Hochberg et al., 2014). CsgC is a 11.3 kDa monomeric bacterial chaperone that inhibits CsgA amyloid fibrillation in the curli system (Taylor et al., 2016). *In vitro*, it fully inhibits αSyn fibril formation at sub-stoichiometrical ratios (Chorell et al., 2015; Evans et al., 2015). Lastly, proSAAS is a 19 kDa small secretory neuronal peptide precursor that colocalizes with Lewy bodies of Parkinson's disease patient brains (Jarvela et al., 2016). The truncated variant proSAAS$_{62\text{-}180}$ has a stronger chaperone ability on αSyn fibrillation than the whole protein (Jarvela et al., 2016).

Methods

Cloning

Synthetic genes encoding for the α-crystallin core of αBc (αBc-core, encompassing residues 68-153 of αBc), a truncated version of proSAAS (proSAAS$_{62-180}$) and CsgC were purchased from GeneArt (Thermo Fisher Scientific). The vector allowing the bacterial expression of αBc was obtained by subcloning the corresponding synthetic gene into a pET14b vector (Novagen) at the NcoI-XhoI restriction sites. The vector allowing the bacterial expression of His$_6$, N-terminal-tagged αBc-core was obtained by subcloning the corresponding synthetic gene into a pET22b+ vector (Novagen) at the NdeI-XhoI restriction sites. The vectors allowing the bacterial expression of His$_6$, N-terminal-tagged CsgC and proSAAS$_{62-180}$ were obtained by subcloning the corresponding synthetic genes into a pETM-11 vector (EMBL) at the NcoI-XhoI or NcoI-BamHI restriction sites, respectively. All His$_6$ tags are followed by a tobacco etch virus (TEV) protease cleavage site. Cloning for αBc and CHIP were as described in Chapter 4. Constructs were verified by DNA sequencing (Eurofins Genomics).

Expression & purification of recombinant proteins

Recombinant human wild-type αSyn, αBc and CHIP were expressed and purified as described in Chapter 4.

Recombinant His$_6$, N-terminal-tagged αBc-core and proSAAS$_{68-180}$ were expressed at 37 °C in *E.coli* strain BL21(DE3). After three hours of induced protein expression, cells were harvested and resuspended in buffer C (50 mM Tris-HCl pH 7.5, 200 mM KCl, 10% glycerol, 10 mM imidazole). After sonication and centrifugation, lysate supernatants were filtered and loaded onto a 5 mL Talon metal affinity resin column (Clontech, Saint-

Germain-en-Laye, France), equilibrated in buffer C. His_6-tagged proteins were eluted with a gradient of 10 – 500 mM imidazole and then dialyzed in PBS. The His_6-tags were cleaved with addition of His_6-tagged tobacco etch virus (His-TEV) protease, produced using the plasmid pRK793 (Addgene), at a 1:20 His-TEV:chaperone molar ratio. 100% cleavage, as assessed by SDS-PAGE, was achieved upon incubating the mixtures for 1 h at 37 °C. The untagged proteins were purified by collecting the flowthrough of a 5 mL Talon metal affinity resin column.

Recombinant His_6, N-terminal-tagged CsgC was expressed at 18 °C in *E.coli* strain BL21(DE3). After 16 hours of induced protein expression, cells were harvested and resuspended in buffer C. Purification of the of the His_6-tagged protein, His_6-tag cleavage and purification of the His_6-tag cleaved protein was then performed as described for αBc-core and $proSAAS_{68\text{-}180}$.

Assembly of αSyn into fibrils

Fibrils were formed as described in Chapter 4.

Binding of the chaperones to preformed αSyn fibrils & K_D determination

Binding of αBc, αBc-core, CHIP, CsgC or $proSAAS_{62\text{-}180}$ to αSyn fibrils was assessed by a supernatant pellet partition assay. For each chaperone / αSyn fibrils pair, αSyn fibrils alone (50 μM), chaperone alone (15 μM) or αSyn fibrils and chaperone (50 and 15 μM, respectively) were incubated for 2 h in PBS at RT. Samples were subjected to ultracentrifugation at 100,000 g in a TL100 tabletop ultracentrifuge (Hitachi, Tokyo, Japan) for 30 min at 20°C. The pellet was resuspended in denaturating Laemmli buffer and the supernatant was diluted v/v in the same buffer. The proportion of chaperone

present in the pellet vs the supernatant was analyzed by SDS-PAGE. Following Coomassie blue staining / destaining, the gels were visualized using a ChemiDoc™ MP Imaging System (BioRad). Images were processed and the intensity of each protein band was quantified using Image Lab (BioRad). For K_D measurements, the same experiment was performed using 20 µM αSyn fibrils and a range of chaperone concentrations (0 – 130 µM).

The truncated chaperone proSAAS$_{62-180}$ migrates at the same apparent molecular weight as αSyn by SDS-PAGE (not shown). Thus, binding of proSAAS$_{62-180}$ to αSyn fibrils was examined following the same partition assay as described above, except that the presence of proSAAS$_{62-180}$ in the supernatant and in the pellet was assessed by dot blot analysis using a generated, in-house-immunopurified rabbit polyclonal antibody against proSAAS$_{62-180}$ (1/5000, Covalabs) followed by anti-rabbit-HRP antibody (1/5000, Bethyl). Polyclonal antibody immunopurification was done as indicated in Chapter 4.

Results & Discussion

Different chaperones display various binding abilities to preformed αSyn fibrils

Using a sedimentation assay, we tested the binding ability of five various chaperones to preformed αSyn fibrils. Chaperones were incubated for 2 hours with or without preformed fibrils. The samples were centrifuged and the supernatant and pellet fractions analyzed by SDS-PAGE (αBc, αBc-core CHIP, CsgC) or dot blot (proSAAS$_{62-180}$) (**Comp. Results Figure 1A)**. The amount of pelleted chaperone in presence minus in absence of fibrils is defined as bound chaperone and is represented. αBc and CHIP significantly bind to αSyn fibrils. Strikingly, αBc-core completely loses this fibril binding ability. Finally, CsgC and proSAAS$_{62-180}$ are not able to bind αSyn fibrils neither. Thus, the capacity to bind αSyn fibrils is not an innate property of molecular chaperones.

Hsp27, an HSP like αBc, also required its NTE and/or CTE for αSyn fibril binding (Cox et al., 2018), suggesting that the regions in these HSPs, and potentially other HSPs, that are responsible for binding aggregating amyloidogenic proteins and fully formed amyloid fibrils are separate.

To further characterize the interaction between αBc or CHIP and αSyn fibrils, the same experiment was performed at different chaperones concentrations and the dissociation constants (K_D) were retrieved (**Comp. Results Figure 1B,C**). We measured an affinity of αBc for preformed αSyn fibrils of 31 ± 8 μM (**Comp. Results Figure 1B**). The affinity of CHIP for αSyn fibrils was 37 ± 1 μM (**Comp. Results Figure 1C**). Binding of αBc to preformed αSyn fibrils has been already reported (Cox et al., 2016; Waudby et al., 2010). We show for the first time a direct, although moderate, *in vitro* binding between CHIP and αSyn fibrils.

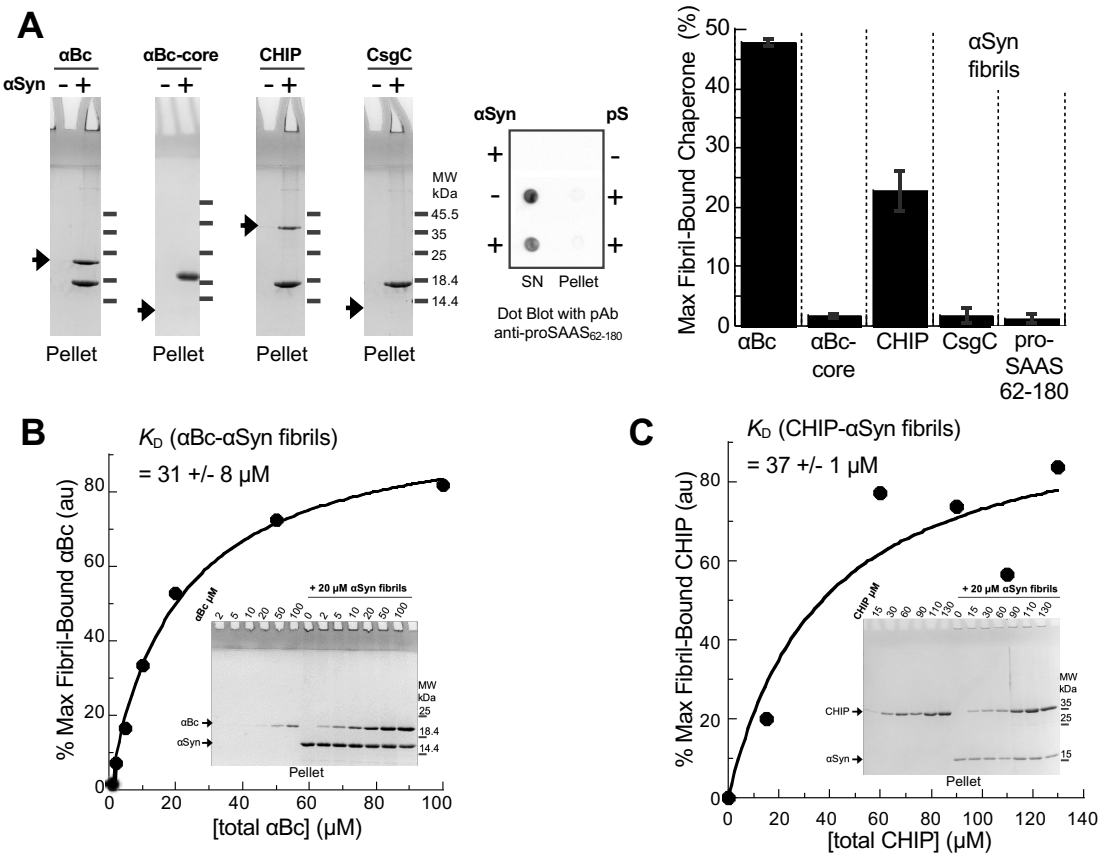

Comp. Results Figure 1: Chaperone binding abilities to αSyn fibrils.
(A) Chaperones αBc, αBc-core, CHIP, CsgC and proSAAS$_{62\text{-}180}$ (15 μM) were incubated with or without preformed αSyn fibrils (50 μM equivalent monomeric protein concentrations) for 2 hours at RT before centrifugation and supernatant pellet partition. Shown are SDS-PAGE gels from one representative experiment of the amount of bound chaperone, determined by sedimentation and densitometry quantification of the pelleted chaperones, alongside quantifications from two independent experiments. **(B-C)** αBc (**B**) or CHIP (**C**) were incubated for 2 hours at different final concentrations with or without αSyn fibrils (20 μM) before centrifugation, supernatant pellet partition and quantification of the pelleted fibril-bound chaperones. One representative K_D determination experiment is shown with the fibril-bound chaperone plotted against the total chaperone concentration and a representative SDS-PAGE gel in the inset. K_D values and their associated standard errors are calculated from three (**B**) or two (**C**) independent experiments.

5.2 Internalization of preformed αSyn fibrils in presence of αBc or CHIP

Introduction

We previously demonstrated that Hsc70 binds to αSyn fibrils with high affinity, preventing their interaction with the plasma membrane and their uptake by cultured cells. We concluded that the binding of the chaperone to the fibrils modified their surface properties and shielded them from interacting with their partners at the plasma membrane (**Chapter 3, Figures 2B,F**). We thus tested if the binding of αBc or CHIP to preformed αSyn fibrils could have the same effect.

Methods

Assembly of αSyn into fibrils and labeling

Fibrils were formed as described in Chapter 4. Fibrillar αSyn was labeled by addition the aminoreactive fluorescent dye Alexa Fluor 488 (Alexa488, Invitrogen) using a protein:dye molar ratio of 10:1 based on initial monomer concentration. Labelling was performed following the manufacturer's recommendation. The reaction was quenched with Tris-HCl pH 7.5 (40 mM final concentration).

Cell culture and internalization

Cell culture was done as described in Chapter 4. Fibril internalization assays were done as described in Chapter 4 with the following exception: preformed Alexa488-labeled αSyn fibrils (1 μM equivalent monomer concentration) were preincubated for 30 min at 37 °C in DMEM in the absence or in the presence of 2 or 10 μM αBc or CHIP.

Results & Discussion

Pre-incubation of αSyn fibrils with αBc or CHIP does not affect their uptake by cultured cells

Neuro-2a cells, in 96-well plates, were exposed for 2 hours to Alexa488-labeled αSyn fibrils (1 µM) pre-incubated or not with αBc or CHIP (0, 2 and 10 µM), prior to Trypan blue addition and quantification of Alexa488 fluorescence in a plate-reader. αSyn fibril fluorescence quenching by Trypan blue allowed us to determine accurately the amount of internalized fibrils in a dose-dependent manner (**Chapter 3, Figure 2C**). We used Hoescht staining to ascertain that the number of cells remained constant (see Materials and Methods).

Neither αBc (**Comp. Results Figure 2A**) nor CHIP (**Comp. Results Figure 2B**) were able to significantly decrease the internalization of αSyn-Alexa488 fibrils (1 µM) after pre-incubation with 2 µM or 10 µM chaperones. Considering that the protein concentrations used in this experiment are well below the K_Ds we measured for these interactions, these results were expected.

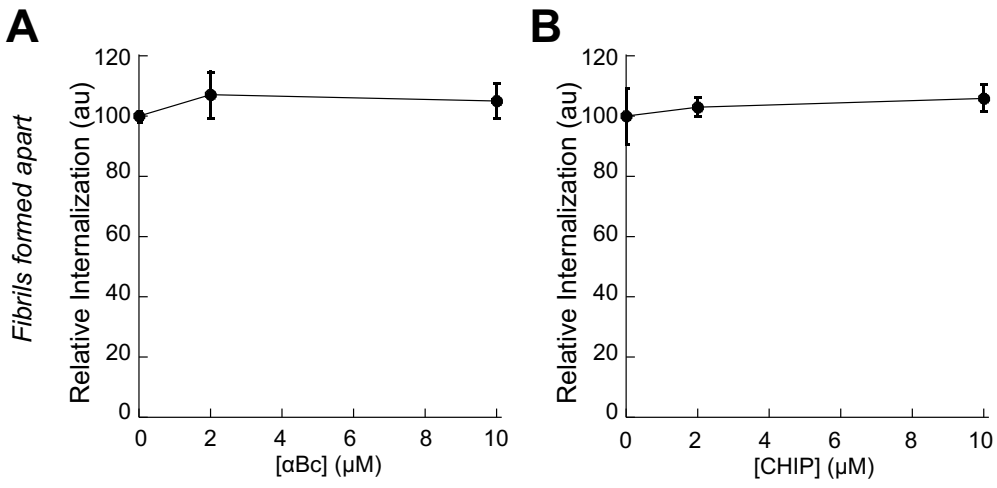

Comp. Results Figure 2: Effect of αBc and CHIP on αSyn fibril uptake by Neuro-2a cells.
Internalization of αSyn fibrils was measured after pre-incubation of αSyn fibrils with αBc (**A**) and CHIP (**B**). Preformed αSyn-Alexa488 fibrils (1 µM equivalent monomer

concentration) were incubated with increasing concentrations of αBc (**A**) or CHIP (**B**) (0-10 μM) in DMEM for 30 min at 37 °C. Neuro-2a cells in 96-well plates were exposed for 2 hours to the mixture. Trypan blue was added after extensive washing to quench the fluorescence of plasma membrane-bound αSyn fibrils. The amount of internalized αSyn-Alexa488 was measured on a fluorescence plate reader. Means and their associated standard deviation values were calculated over 5 wells. In each case we performed three independent experiments; one representative experiment is shown. The results and the associated significances are reported relative to the internalization in the absence of chaperone.

5.3 Exploring the structure of fibrils formed with chaperones

Introduction

Chapter 5.2 demonstrated that preformed αSyn fibrils preincubated with αBc or CHIP were internalized at similar rates as fibrils alone by Neuro-2a cells. This is likely due to the moderate affinity of the chaperones for αSyn fibrils, under our experimental conditions. However, αSyn fibrils formed with αBc or CHIP were less internalized than αSyn fibrils formed alone. The first explanation for this difference is that the chaperones alone could indirectly block internalization of fibrils. This is the case for the NKA peptide from Chapter 3, as it was demonstrated to not bind αSyn fibrils yet reduced αSyn fibril membrane binding. In the experiments with fibrils formed in presence of chaperones, the chaperones were significantly less concentrated than during the experiments with preformed fibrils preincubated with chaperones, implying that there is no indirect reduction of internalization.

Another explanation for this difference is that the chaperones induce structural changes in the fibrils, therefore affecting their ability to bind the cell membrane and subsequent internalization. Structural differences, as seen for fibrils and ribbons, for example, displayed unique permeabilization and toxic properties (Bousset et al., 2013). The phenomenon of chaperone-induced structural changes was observed previously for

HTTExon1Q48 fibrils formed with Hsc70. Hsc70 incubation during fibrillation led HTTExon1Q48 fibrils to display less amyloid β-sheet levels than HTTExon1Q48 fibrils formed alone. Indeed, the FT-IR signal of HTTExon1Q48 fibrils formed in the presence of Hsc70 was more similar to the one of fibrils formed from a non-pathological variant of HTTExon1, HTTExon1Q25 (**Comp. Results Figure 3)**. In addition, Hsc70-formed-HTTExon1Q48 fibrils were less capable of inducing seeding, when added to αSyn-CherryFP-expressing cells, than fibrils formed alone (Monsellier et al., 2015). However, these experiments were possible because Hsc70 does not bind to fibrils, therefore permitting isolation of the fibrils for structural studies. In the current experiments, on the other hand, both αBc and CHIP bind αSyn fibrils, rendering further pursuit of fibril structural studies challenging.

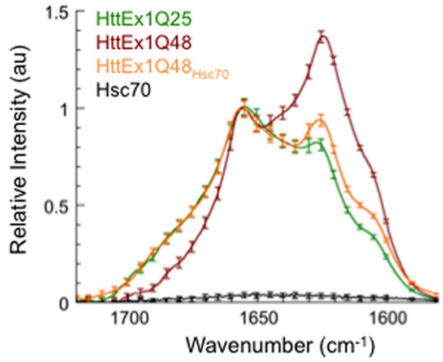

Secondary structure content of different types of HttEx1Qn fibrils estimated from FTIR spectroscopy measurements

Secondary structure	HttEx1Q25 fibrils	HttEx1Q48 fibrils	HttEx1Q48 fibrils formed in the presence of Hsc70
	%	%	%
Lateral chains	9	13	13
Amyloid	28	43	30
β-Sheets (non-amyloid)	16	3	14
α-Helices	13	12	12
Others	34	31	29

Comp. Results Figure 3: HTTExon1Q48 fibrils have different secondary structures when formed in presence of Hsc70.
FT-IR spectrum and associated measurements from various mHTT fibrils formed in absence or presence of Hsc70. HTTExon1Q48 fibrils formed in presence of Hsc70 more closely resemble the spectrum of HTTExon1Q25 fibrils than those of HTTExon1Q48 fibrils formed alone. Figure from Monsellier et al., 2015.

Nonetheless, multiple techniques can be used to elucidate structural differences between αSyn fibrils formed alone or in presence of chaperones. First, high magnification TEM can discern obvious morphological differences, such as straight or twisted filaments, as seen with αSyn fibrils and ribbons (Bousset et al., 2013). The morphology of fibrils

formed with αBc could not be elucidated, possibly due to coating by large oligomers or differential coloration (**Chapter 4, Figure 1H**). On the other hand, more twisted filaments were observed for fibrils formed in the presence of CHIP compared to fibrils formed alone (**Chapter 4, Figure 1I**).

More specific details about the secondary structure of fibrils can be obtained by other means, such as spectroscopic methods like CD and FT-IR. However, CD is not adapted to β-rich samples (Kelly et al., 2005), and FT-IR requires a significant amount of material. In both cases, if the chaperone undergoes any structural changes upon binding to the fibrils, its spectra could not be removed from the spectra of fibrils formed in presence of chaperones and thus would leave the results inconclusive. To avoid chaperone spectra and to obtain results with better precision, ss-NMR with isotopically labelled αSyn fibrils could be deployed.

Lastly, another common, more accessible way to identify structural differences is through limited proteolysis and western blots, as fibrils with different structures will have unique regions exposed to the solvent, leading to individual limited proteolysis profiles (Bousset et al., 2013).

Methods

Limited proteolysis

αSyn fibrils at 100µM, formed for two weeks in absence or presence of either 100µM αBc or 33µM CHIP, were digested by proteinase-K (pK) at a 1:0.038 total protein:pK molar ratio for 0, 1, 5, 15 and 60 minutes at 37˚C before stopping the reaction with the addition of 100µM Cf of the protease inhibitor phenylmethylsulfonyl fluoride. Samples were then vacuum-dried before solubilization by addition of 20 µl of pure HFIP. After 1 hour of incubation in HFIP at RT, samples were evaporated before resuspension in

denaturing Laemmli buffer, heating at 80˚C for 5 minutes and loading onto 12% Tris Glycine SDS-PAGE gels. Gels were then transferred onto nitrocellulose membranes for western blots, as described in Chapter 4, in order to see the proteolytic profiles of αSyn fibrils and chaperones separately.

Results & Discussion

αSyn fibrils formed in presence of αBc and CHIP have different limited proteolyic profiles than fibrils formed alone

Limited proteolysis over 1 hour of αSyn fibrils formed alone and formed in presence of αBc reveals similar profiles until 60 minutes (**Comp. Results Figure 4A**). As seen by antibody recognition of residues 91-99, profiles are strikingly similar from the 0- to 15-minute time points. Full length αSyn resists degradation until before 60 minutes in both cases. At 60 minutes, however, a small peptide with an apparent molecular mass below 10 kDa is observed for fibrils formed alone but not for fibrils formed with αBc. Furthermore, a peptide around 12 kDa is more intense for fibrils formed in presence of αBc than fibrils formed alone. αBc epitopes recognized by the polyclonal antibodies, are not fully degraded until after the 15-minute time point, likely due to the chaperone's oligomeric state.

In contrast, limited proteolysis of αSyn fibrils formed in presence of CHIP reveals significant differences (**Comp. Results Figure 5B**). Full length αSyn remained intact for longer than 15 minutes for both types of fibrils. However, starting at the 1-minute time point, substantially fewer polypeptides with intact epitopes were formed. In contrast, the epitopes recognized by the polyclonal antibodies against CHIP are no longer present before 5 minutes.

Thus, proteolytic profile differences for fibrils formed in presence of αBc and more so in presence of CHIP lead to two possible hypotheses: (i) αSyn fibrils formed in presence of chaperones do not have the same structure as αSyn fibrils formed alone, as the regions accessible to pK are different, or (ii) chaperone binding to αSyn fibrils interferes with pK cleavage, for example by protecting some cleavage sites or by interacting with the enzyme.

While the first hypothesis is probable given the morphological differences visible to TEM, it still needs to be confirmed through other complementary methods, especially due to the presence of chaperones during the limited proteolysis. Thus, to further address the first hypothesis would require separation of the bound chaperones from the fibrils, through use of high salt buffers, for example. However, this could potentially alter the structure of the fibrils, instigating doubt in the relevance of the results. A potential way to address the second hypothesis would be to examine limited proteolysis profiles of preformed fibrils pre-incubated with chaperones. If the profiles are identical to those shown here, we could conclude that the different profiles could be due to chaperone binding impeding access to fibrils by pK or by chaperones interacting with the enzyme and not due to induced structural changes. However, if the profiles are different from what is shown here, we would still be unable to differentiate between the two hypotheses, as binding to fibrils formed in presence of chaperones may be different from fibrils formed apart.

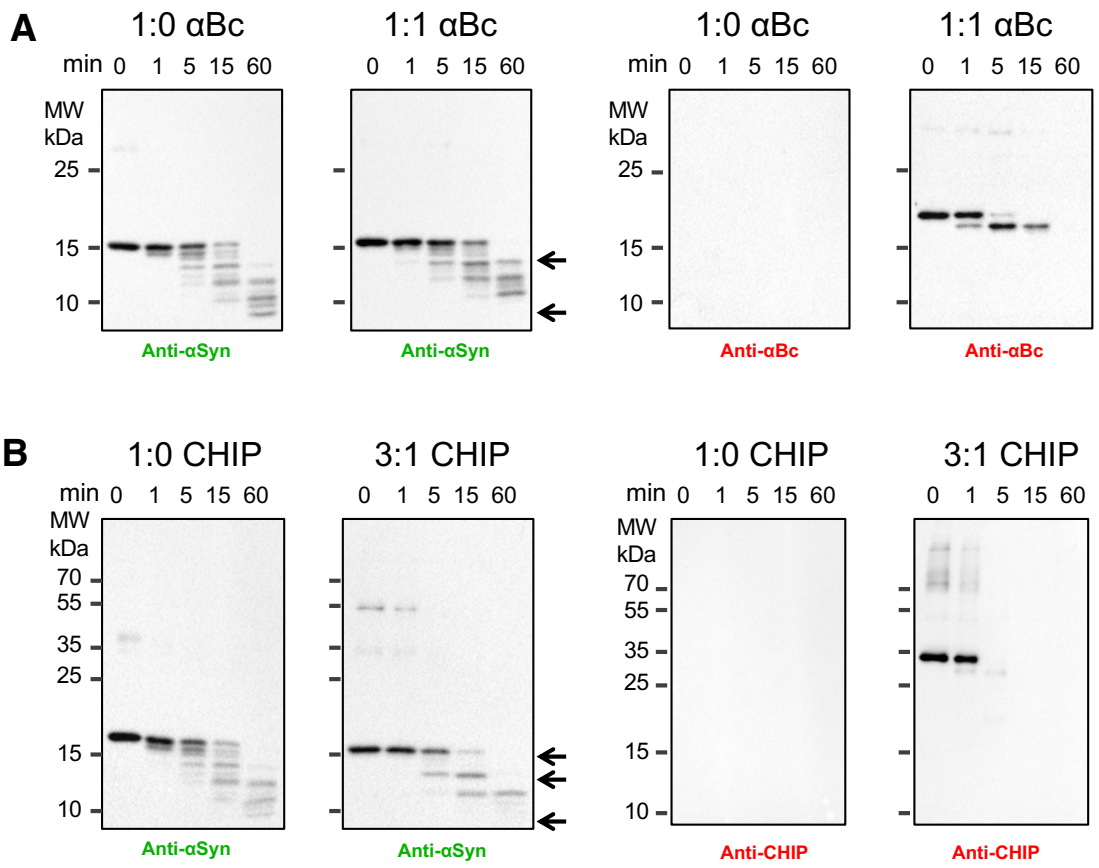

Comp. Results Figure 6: Proteinase-K limited proteolysis profiles for αSyn fibrils formed in presence of αBc and CHIP.
(A) Western blots against αSyn or αBc of proteinase-K limited proteolysis products of 100µM αSyn fibrils formed in presence of 0 or 100µM αBc (1:0 or 1:1 αBc). **(B)** Western blots against αSyn or CHIP of proteinase-K limited proteolysis products of 100µM αSyn fibrils formed in presence of 0 or 33µM CHIP (1:0 or 3:1 CHIP). The arrows point to the divergent proteolysis products for αSyn fibrils formed in presence of chaperones. For both **A** and **B**, the membranes were stripped between αSyn and chaperone western blots.

5.4 Chaperone binding to preformed Tau and HTTExon1Q48 amyloid fibrils

Introduction

The fibril binding properties of five different molecular chaperones to αSyn fibrils were tested in Chapter 5.1. Previously, work with chaperones and Tau or mHTT fibrils has shown that Hsp70 bound fibrillar Tau with nanomolar affinity, as identified through total internal reflection fluorescence (TIRF) microscopy (Kundel et al., 2018). Furthermore, DNJ-13, HSP-1 and HSP-110 chaperones bound fibrillar HTTExon1Q48 (Scior et al.,

2018), however the binding was less characterized as it was only identified through immunogold labelling and TEM. On the contrary, Hsc70 did not bind to preformed HTTExon1Q48 fibrils (Monsellier et al., 2015). It is thus of interest to expand the reservoir of known chaperones capable of binding Tau and mHTT amyloid fibrils for the development of fibril propagation strategies. Consequently, this chapter looks at testing the original range of chaperones for binding to Tau 1N4R and HTTExon1Q48 amyloid fibrils.

Methods

Expression & purification of recombinant proteins

Recombinant human wild-type Tau 1N4R (Tau) was expressed and purified as previously described (Tardivel et al., 2016). Likewise, recombinant human exon 1 of the huntingtin protein with a 48-residues-long poly-glutamine expansion (HTTExon1Q48) was expressed and purified as previously described (Monsellier et al., 2015).

Assembly of Tau and HTTExon1Q48 into fibrils

Tau was incubated in PBS and 1 mM DTT with a Tau:Heparin molar ratio of 4:1 at 37 °C under continuous shaking in an Eppendorf Thermomixer set at 600 rpm for 5 days. HTTExon1Q48 was incubated overnight in PBS at 37 °C without shaking. For Tau, the completion of the aggregation reactions was monitored by withdrawing aliquots, subjecting them to centrifugation in an Eppendorf 5415R centrifuge at 20,000 g and 20 °C, and assessing spectrophotometrically the amount of remaining protein in the supernatant. For HTTExon1Q48, the completion of the aggregation reaction was monitored by withdrawing aliquots and assessing the amount of soluble material by SDS-PAGE as described in (Monsellier et al, 2015).

Binding of the chaperones to preformed fibrils & K_D determination

These experiments were done as stated in Chapter 4. For HTTExon1Q48 fibrils, gels were stained with SYPRO Orange (1/5000 for 1h, Thermo Fisher).

Results & Discussion

αBc binds to preformed mHTT and Tau fibrils

Using a sedimentation assay, we tested whether these various chaperones could bind to Tau or HTTExon1Q48 fibrils. Chaperones were incubated for 2 hours with or without preformed fibrils. The fibrils were centrifuged and the supernatant and pellet fractions analyzed by SDS-PAGE (**Comp. Results Figure 7B-C**). The amount of pelleted chaperone in presence minus in absence of fibrils is defined as bound chaperone and is represented in **Comp. Results Figure 8A**. αBc was shown to significantly bind to both Tau and HTTExon1Q48 fibrils. NMR studies demonstrated that αBc binds to Tau K19 (244-372; 3R) and αSyn (Liu et al., 2018) through the β4 (residues 88-94) and β8 (residues 133-6) strands of αBc-core. However, at least in the case of αSyn, αBc binds to fibrils through its C-terminus, not present in αBc-core, which correlates with the lack of binding of αBc-core to αSyn fibrils. It is thus not surprising that αBc-core loses αBc's Tau fibril binding ability. Thus, the dual binding mode for aggregating and fibrillated proteins might apply to Tau as well as αSyn. CHIP, to a weak extent, binds Tau and even less so HTTExon1Q48 fibrils. Finally, CsgC and proSAAS$_{62\text{-}180}$ are not able to bind either of the preformed fibrils tested.

To further characterize the interaction between αBc and Tau or HTTExon1Q48 fibrils, the same experiment was performed at different chaperone concentrations and the dissociation constants (K_D) were retrieved (**Comp. Results Figure 9**). We measured an affinity of αBc for preformed Tau or HTTExon1Q48 fibrils of 72 ± 13 μM or 78 ± 10

μM, respectively. These dissociation constants are of the same order of magnitude as those calculated for αSyn fibrils. Thus, αBc appears to have moderate affinity for three types of amyloid fibrils.

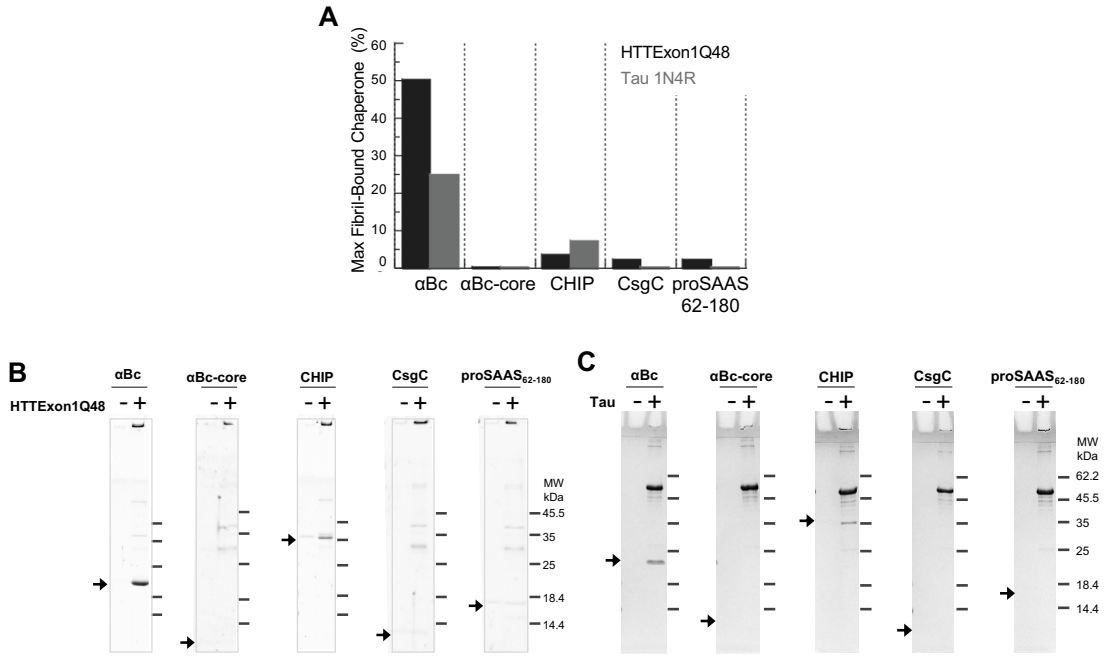

Comp. Results Figure 10: Chaperone binding to Tau and HTTExon1Q48 fibrils. **(A-C)** Chaperones αBc, αBc-core, CHIP, CsgC and proSAAS$_{62\text{-}180}$ (15 μM) were incubated with or without preformed Tau and HTTExon1Q48 fibrils (50 μM equivalent monomeric protein concentrations) for 2 hours at RT before centrifugation and supernatant pellet partition. SDS-PAGE gels with pellet samples from one representative experiment as well as quantification of the amount of bound chaperone from two independent experiments, determined by sedimentation and densitometry quantification of the pelleted chaperones, are shown. HTTExon1Q48 aggregates are found in the well (Monsellier et al, 2015). Gels for Tau and HTTExon1Q48 were colored with Coomassie blue and SYPRO Orange, respectively.

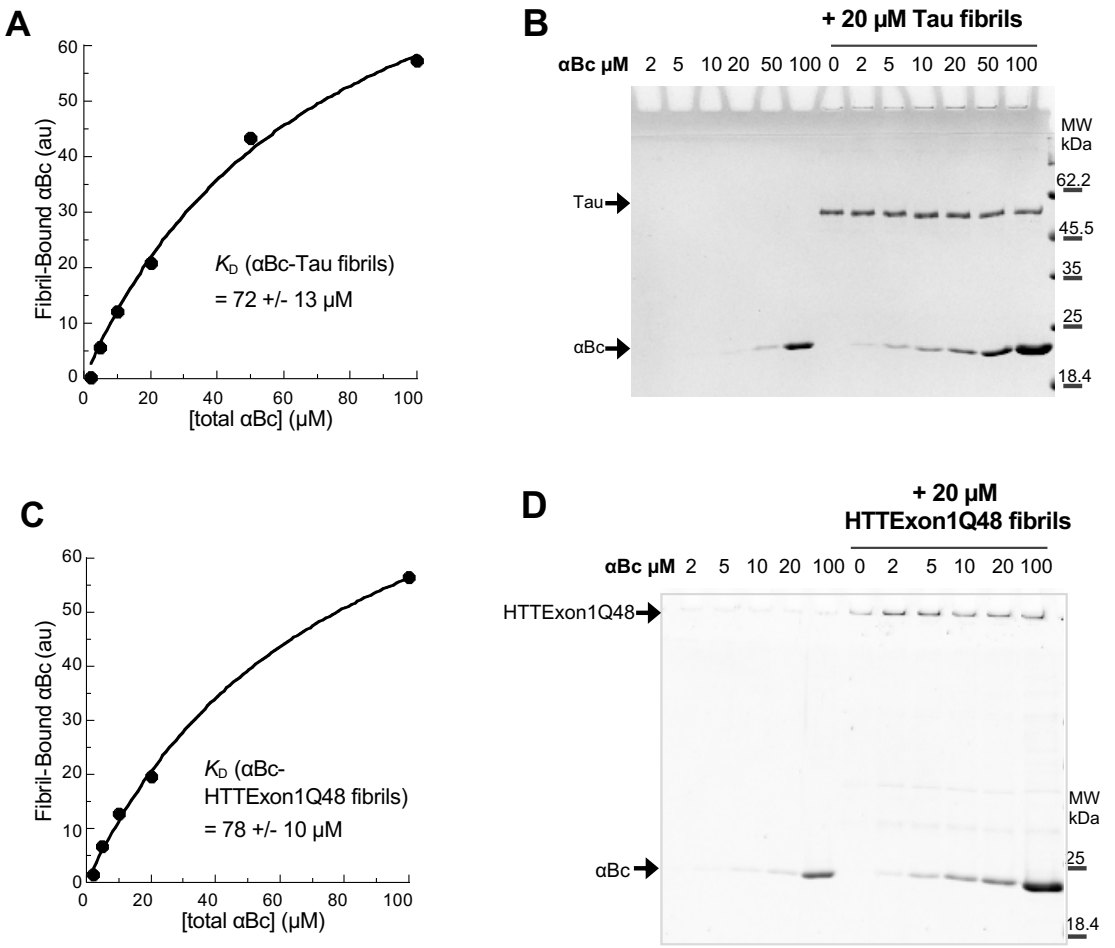

Comp. Results Figure 11: αBc binding abilities to Tau and HTTExon1Q48 fibrils. **(A-B)** αBc (2-100 μM) was incubated with or without preformed Tau fibrils (20 μM equivalent monomeric protein concentrations) for 2 hours at RT before centrifugation and supernatant pellet partition. Shown are SDS-PAGE gels with pellet samples from one representative experiment as well as the calculation for the K_D through sedimentation and densitometry quantification of the pelleted chaperones. **(C-D)** The experiments were done as above, but with HTTExon1Q48 fibrils. HTTExon1Q48 aggregates are found in the well (Monsellier et al, 2015). Gels for Tau and HTTExon1Q48 were colored with Coomassie blue and SYPRO Orange, respectively.

PART 3:

CONCLUSIONS &

PERSPECTIVES

A multitude of studies have demonstrated that various amyloid fibrils implicated in NDs are capable of propagating between cells and this propagation correlates with disease progression. During my PhD, I contributed to studies aimed at identifying polypeptide binders of αSyn fibrils that, when bound to the surface of fibrils, lead to a reduction in cell entry. The common approach of the studies is the following: after protein partners of fibrils were identified, they were tested for their effect on αSyn fibril membrane binding and/or internalization by neuronal cells. Furthermore, the interaction zones implicated in the partner-αSyn fibril binding were elucidated. Finally, peptides from these partners were rationally designed based on the interaction zones.

Molecular chaperones, known to interact with aggregating and aggregated species, were investigated as potential αSyn fibril binding partners. Some, but not all molecular chaperones were able to bind αSyn fibrils. When the affinity between chaperones and αSyn fibrils was high, such as for Hsc70, pre-incubation of fibrils with chaperones led to reduced membrane binding and internalization. On the other hand, the low affinity between the chaperones αBc and CHIP and αSyn fibrils explains the absence of a fibril internalization neutralization by the chaperones. An alternative mode of interaction, with fibrils formed in presence of the chaperones αBc and CHIP, led to fibrils that were less internalized than those formed alone. Some potential reasons behind this effect were discussed in Chapter 5. Notably, additional studies could explore in more detail the structure of fibrils formed in presence of chaperones.

Furthermore, interaction zones between the oligomeric chaperones αBc or CHIP and αSyn fibrils were elucidated through an optimized chemical cross-linking and mass spectrometry strategy. This led to the identification of residues implicated in chaperone-fibril binding, which could be used to develop polypeptidic mini-chaperones potentially capable of inhibiting αSyn fibril propagation. Some Hsc70-derived peptides retained

αSyn binding properties of the parent protein, albeit with weaker affinity, supporting the validity of this approach. Although I showed that these peptides were unable to affect fibril internalization, peptides with improved affinity for αSyn fibrils would likely have an effect.

The primary perspectives from these studies are to create a range of peptides containing the αSyn fibril binding sites from αBc and CHIP and test them as was done in the first study with Hsc70-derived peptides. Then, retained peptide candidates, along with the two Hsc70-derived peptides of interest, can be optimized for affinity and stability. Point mutations and variations on peptide length can be tested for improved affinity. In addition, multiple peptides can be linked together to increase the fibril-binding surface area and subsequent avidity. Importantly, improving stability also contributes to affinity and can be accomplished through multiple measures. Secondary structural features like α-helices can be stabilized through hydrogen-bond surrogates, turn-inducers and/or carbon stapling through the use of unnatural amino acids (Ali et al., 2019; Cunningham et al., 2017; Góngora-Benítez et al., 2014; Tsomaia, 2015).

These approaches could be of particular interest in the case of the NKApep from the first study. It was derived from the α3-subunit of the Na^+/K^+-ATPase, identified as a binding partner of αSyn fibrils in an unbiased mass-spectrometry pulldown from primary neuronal cultures. The isolated peptide, however, was unable to bind αSyn fibrils. This could potentially be due to the adoption of a different secondary structure, as illustrated by its β-sheet and α-helix content compared to the peptide in the parent protein.

Once optimized for affinity and/or avidity, peptides derived from fibril binding partners could be further tested in cells to see how their binding affects αSyn fibril membrane binding, internalization, seeding and toxicity in neuronal cells. Eventually, candidate peptides could be modified for improved pharmacokinetics for *in vivo* studies,

notably improving half-life via lipidation or addition of polymers (Weinstock et al., 2012; Witt et al., 2001) and blood brain barrier permeability through CPPs (Heitz et al., 2009; Neves-Coelho et al., 2017), for example.

In addition, our optimized chemical cross-linking and mass spectrometry strategy for amyloid fibrils could be applied to more chaperone-fibril pairs. First, αBc and Tau or HTTExon1Q48 fibrils, which I showed bind with similar affinity as αBc and αSyn fibrils, would be of interest. Furthermore, cross-linking with different agents could be performed with CHIP and αSyn fibrils in order to identify other binding sites located at longer distances than what was identified with the zero-angstrom cross-linker. Lastly, applying this approach to chaperone-fibril pairs such as Hsp27 and αSyn would be of particular interest due to previous data demonstrating the lateral binding of the chaperone along the fibrils (Cox et al., 2018).

APPENDIX

Scientific production

Journal Articles

→ Polypeptides derived from α-Synuclein binding partners to prevent α-Synuclein fibrils interaction with and take-up by cells.

Elodie Monsellier, **Maya Bendifallah**, Virginie Redeker and Ronald Melki. CEA, Institut François Jacob (MIRcen) and CNRS, Laboratory of Neurodegenerative Diseases (U9199), 18 Route du Panorama, 92265, Fontenay-aux-Roses, France. Submitted to PLOS One.

→ Interaction of the chaperones alphaB-crystallin and CHIP with fibrillar alpha-synuclein: effects on internalization by cells and identification of interacting interfaces.

Maya Bendifallah, Virginie Redeker, Elodie Monsellier, Luc Bousset, and Ronald Melki. CEA, Institut François Jacob (MIRcen) and CNRS, Laboratory of Neurodegenerative Diseases (U9199), 18 Route du Panorama, 92265, Fontenay-aux-Roses, France. In preparation.

Conference Posters

Development of mini-chaperones to prevent amyloid fibril propagation.

Maya Bendifallah, Elodie Monsellier, Virginie Redeker and Ronald Melki. CEA, Institut François Jacob (MIRcen) and CNRS, Laboratory of Neurodegenerative Diseases (U9199), 18 Route du Panorama, 92265, Fontenay-aux-Roses, France.

March **2019**, 20th International AD/PD Conference, Lisbon, Portugal.

September **2019**, 4th biennial Synuclein Meeting, Ofir, Portugal.

Résumé en français

Les protéinopathies sont des maladies caractérisées par des protéines mépliées dont l'agrégation dans le système nerveux central est la cause de plus d'une vingtaine de maladies neurodégénératives. Les fibres amyloïdes composées des protéines αSyn, Tau et mHTT, impliquées respectivement dans les synucleinopathies comme la maladie de Parkinson, dans les Tauopathies comme la maladie d'Alzheimer, et dans la maladie d'Huntington, toutes des maladies incurables, sont capables de se propager entre les cellules neuronales d'une manière spatio-temporelle spécifique à chaque protéine et maladie. Par conséquent, inhiber d'une façon appropriée la propagation des fibres pourrait aider à ralentir la progression de telles maladies. En effet, le cycle de propagation comprend la liaison à la membrane cellulaire puis l'entrée dans la cellule, le recrutement des protéines endogènes et leur intégration parmi les fibres amyloïdes, puis encore l'export des agrégats et ainsi de suite. Cibler la première étape dans ce cycle, c'est-à-dire la liaison des fibres amyloïdes extracellulaires à la membrane, est ainsi une stratégie viable dans une perspective thérapeutique. De surcroît, puisque les fibres amyloïdes peuvent interagir avec une multitude de partenaires protéiques et lipidiques au niveau de la membrane cellulaire, l'inhibition de la propagation pourrait être entreprise par la liaison d'agents qui altèreraient les propriétés de surface des fibres, dès lors perturbant leurs interactions avec une grande gamme de partenaires potentiels.

Les chaperons moléculaires, éléments du système de contrôle de qualité des protéines dans la cellule dont le but spécifique est d'empêcher ou éliminer les agrégats protéiques, sont de bons points de départ pour l'identification de partenaires capables de se lier aux fibres. Bien que certains chaperons moléculaires se soient avérés capables de se lier à certaines des fibres amyloïdes, de telles liaisons n'ont pas toujours été bien caractérisées et leurs effets sur la propagation n'ont pas encore été testés dans des modèles

cellulaires. D'un point de vue thérapeutique, les chaperons entiers ne sont malheureusement pas de bons candidats à cause de leurs rôles cellulaires pléiotropiques. Afin donc d'éviter les interactions hors-cible, les chaperons moléculaires entiers doivent être réduits à des sous-domaines ou à des dérivés peptidiques bioactifs.

Dans la première phase de cette recherche, le chaperon moléculaire Hsc70, trois de ses domaines et huit de ses dérivés peptidiques ont été testés dans le cadre d'une combinaison d'expériences concernant l'inhibition de la fibrillation d'αSyn, la liaison aux fibres d'αSyn et/ou l'inhibition de la propagation des fibres d'αSyn -- cette dernière série d'expériences comprenant celles auxquelles j'ai personnellement contribué. En outre, nous avons également testé un peptide dérivé de la sous-unité α3 de la pompe sodium/potassium Na^+/K^+-ATPase (NKApep), dont l'interaction avec l'αSyn fibrillaire dans des cultures de neurones primaires avait déjà été élucidée. Alors que tous les trois sous-domaines de Hsc70 ont retenu leurs capacités de liaison aux fibres, seuls deux peptides dérivés de Hsc70 ont d'une part affecté la cinétique de la formation de fibres et d'autre part se sont liés aux fibres d'αSyn, quoiqu'avec une affinité significativement plus faible que celles des sous-domaines ou de la protéine mère. De surcroît, la pré-incubation des peptides n'a eu aucun effet sur l'internalisation des fibres d'αSyn, ce à quoi il fallait bien s'attendre avec des affinités aussi basses. Quant au NKApep, il n'a pas pu se lier aux fibres d'αSyn. Cependant, il a pu quand même réduire la liaison des fibres d'αSyn à la membrane de manière indirecte, mais sans effet sur leur internalisation. En résumé de la première partie de cette recherche, des partenaires protéiques divers d'αSyn ont mené au développement de peptides qui sont capables d'interagir avec les fibres d'αSyn mais qui nécessiteront davantage de modifications afin d'améliorer leurs niveaux d'affinité et permettre un effet cellulaire significatif.

Dans la deuxième partie de cette recherche, qui a constitué mon projet de thèse principal, plusieurs chaperons moléculaires de petite taille et d'origines et statuts oligomériques divers ont été testés pour leurs capacités de liaison aux fibres amyloïdes d'αSyn, et les constantes de dissociation ont été estimées pour les candidats retenus. Des fibres d'αSyn préformées et pré-incubées avec deux de ces chaperons, αB-crystallin (αBc) et CHIP, ont été internalisées de manière similaire aux fibres laissées seules dans une lignée cellulaire neuronale. En revanche, les fibres d'αSyn formées en présence de l'un ou l'autre chaperon ont été moins internalisées que les fibres formées seules. Il a fallu dès lors identifier les résidus responsables de cet effet cellulaire. De ce fait, une stratégie optimisée du pontage chimique entre αBc ou CHIP et les fibres d'αSyn formées en présence des chaperons, couplé à la spectrométrie de masse, a permis l'identification des résidus impliqués dans l'interaction fibres-chaperons. Dans le cas d'αBc, c'est son C-terminus flexible qui s'est avéré impliqué dans la liaison aux fibres, alors que son noyau structuré avait été précédemment impliqué dans l'inhibition de la fibrillation d'αSyn, ce qui indique un double mode de liaison du chaperon pour αSyn, tant agrégeant que fibrillaire. Cette approche a également permis d'identifier un site de liaison aux fibres d'αSyn dans le domaine U-box de CHIP. Donc tant αBc que CHIP se liaient aux fibres d'αSyn, mais le premier en amont du cœur fibrillaire et le deuxième en son centre. Ces sites de liaison peuvent donc être utilisés pour le développement de mini-chaperons peptidiques potentiellement capables d'inhiber la propagation des fibres d'αSyn.

Enfin, la gamme originale des chaperons a été testée pour leur liaison aux fibres amyloïdes de Tau ou HTTExon1Q48 et seul αBc s'est avéré capable de se lier à ces deux types de fibres amyloïdes, avec des constantes de dissociation similaires à celle des fibres amyloïdes d'αSyn. Les études cellulaires et de pontage chimique couplé à la

spectrométrie de masse décrites au-dessus pourraient donc être conduites fructueusement sur les fibres amyloïdes de Tau et HTTExon1Q48 avec αBc.

Appendix figures

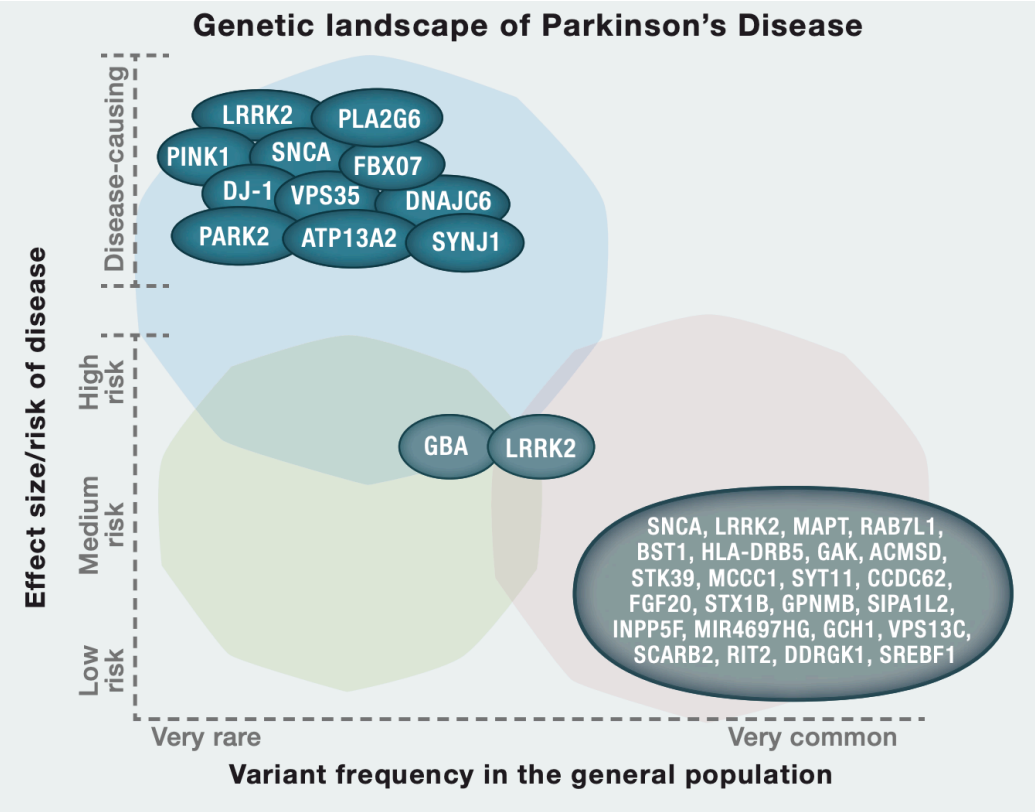

Appendix 1: Genetic risk factors for PD.
From (Brás et al., 2015).

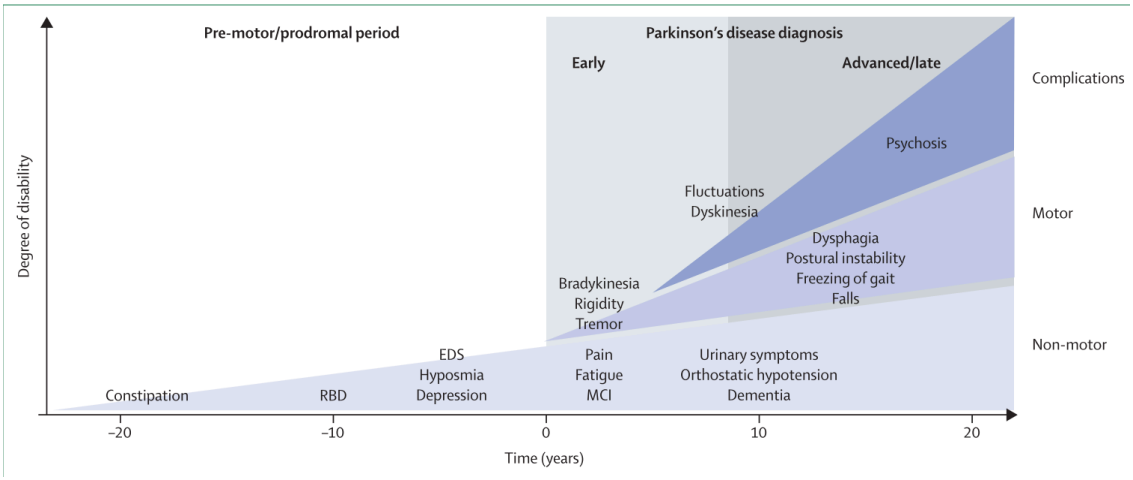

Appendix 2: Time course of PD clinical symptoms.
EDS=excessive daytime sleepiness. MCI=mild cognitive impairment. RBD=Rapid eye movement (REM) sleep behavior disorder. From Kalia and Lang, 2015.

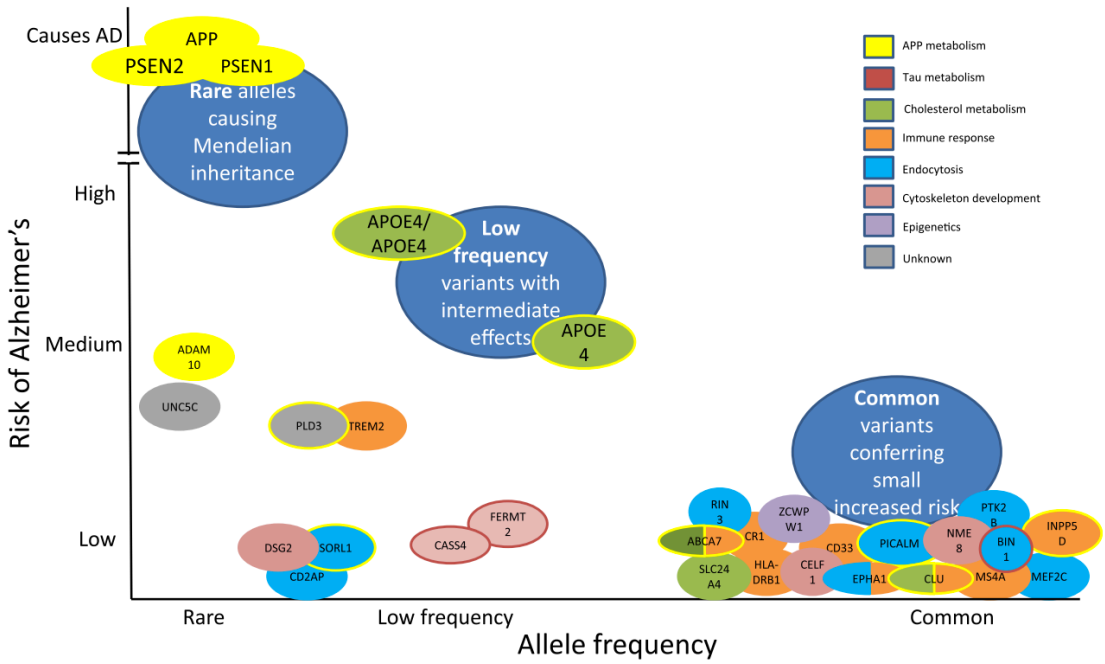

Appendix 3: Risk genes associated with AD.

From (Barragán Martínez et al., 2019). Their internal color dictates the pathway associated with the gene while the outside color indicates potential implicated pathways.

Alzheimer’s disease
Amyotrophic lateral sclerosis and parkinsonism-dementia complex
Argyrophilic grain disease
Chronic traumatic encephalopathy
Corticobasal degeneration
Diffuse neurofibrillary tangles with calcification
Down’s syndrome
Familial British dementia
Familial Danish dementia
Frontotemporal dementia and parkinsonism linked to chromosome 17
(caused by MAPT mutations)
Frontotemporal lobar degeneration (some cases caused by C90RF72 mutations)
GerstmanneSträusslereScheinker disease
Guadeloupean parkinsonism
Myotonic dystrophy
Neurodegeneration with brain iron accumulation
Niemann-Pick disease, type C
Non-Guamanian motor neuron disease with neurofibrillary tangles
Pick’s disease
Postencephalitic parkinsonism
Prion protein cerebral amyloid angiopathy
Progressive subcortical gliosis
Progressive supranuclear palsy
SLC9A6-related mental retardation
Subacute sclerosing panencephalitis
Tangle-only dementia
White matter Tauopathy with globular glial inclusions

Appendix 4: Tauopathies.
From (Clavaguera et al., 2014).

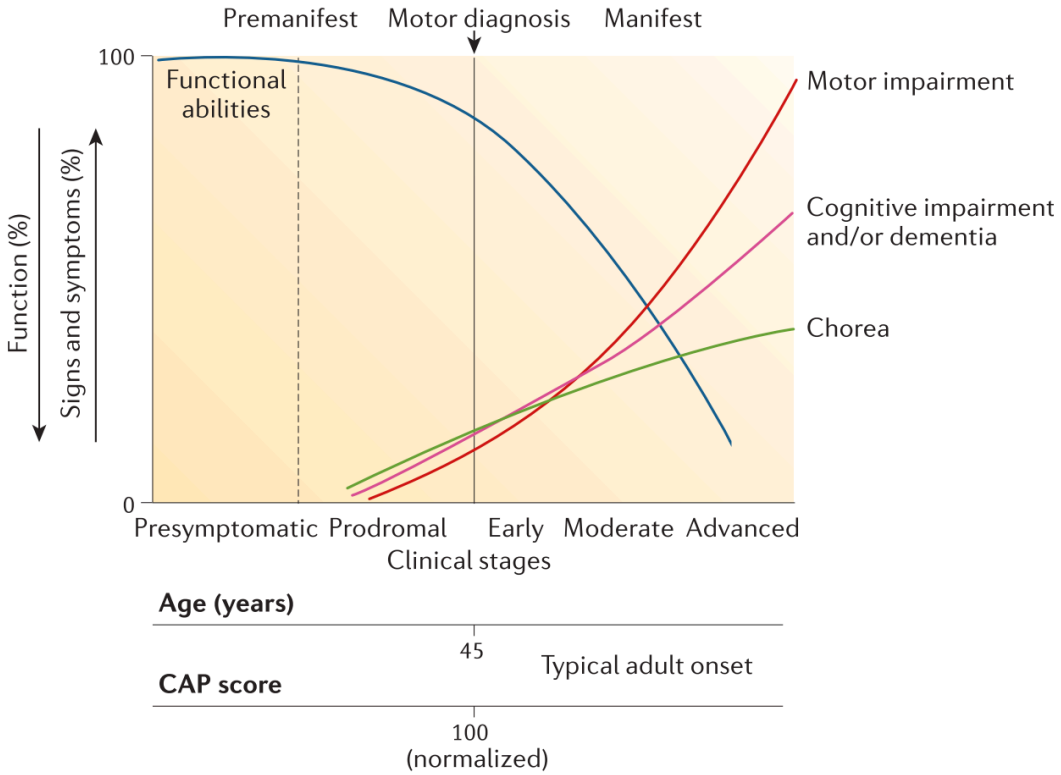

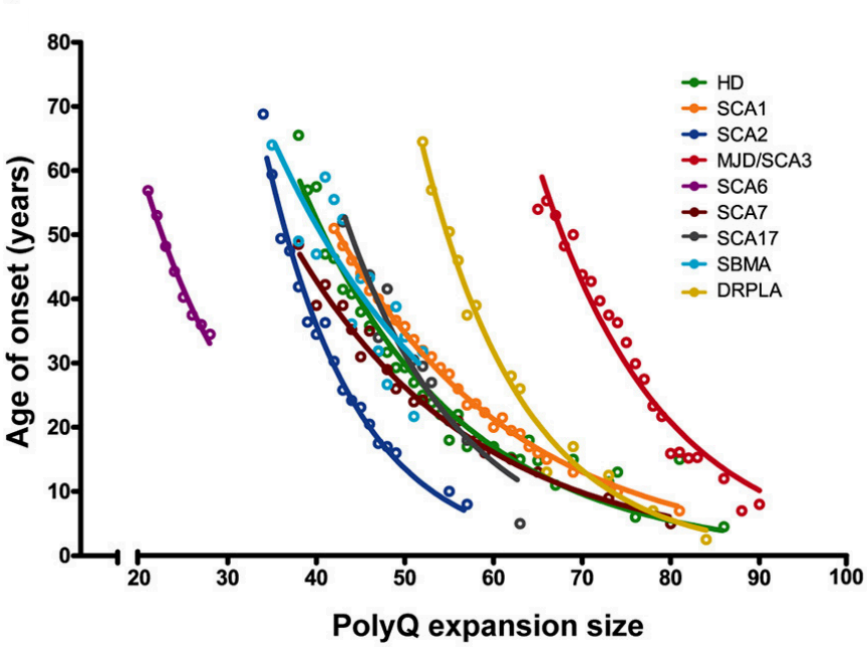

Appendix 5: HD evolution & influence of polyQ length.
CAP score CAG age product. Correlation between polyQ length and age of onset. (Bates et al., 2015; Kuiper et al., 2017)

αSyn AB	Remarks	Tau AB	Remarks	mHTT AB	Remarks
EP1536Y	pSer129	MC1	Conformation dependent antibody (AA 312-322)	EM48	mHTT aggregates (AA 1-256)
MJF-R13	pSer129	MC6	pSer235	MW7	Proline-rich domain, high MW mHTT structures
81a	pSer129	PHF-1	pSer396/pSer404		
pSyn#64	pSer129	PG5	pSer409		
5038	pSer129	TG3	PHF-Tau (pThr231, conformation specific)		
		AT8	pSer202/pSer208/pThr205		
		AT100	pThr212/pSer214; detects fibrils		
		Gallyas silver	Stains most pathological fibrillar tau structures		

Appendix 6: Antibodies for propagation studies.
A non-exhaustive list of antibodies used for propagation studies. The above antibodies are those used in the papers from **Table 2**. (Delic et al., 2018; Falcon et al., 2015; Jicha et al., 2002; Ko et al., 2018; Kovacs, 2015; Li and Li, 1998; Lin et al., 2017).

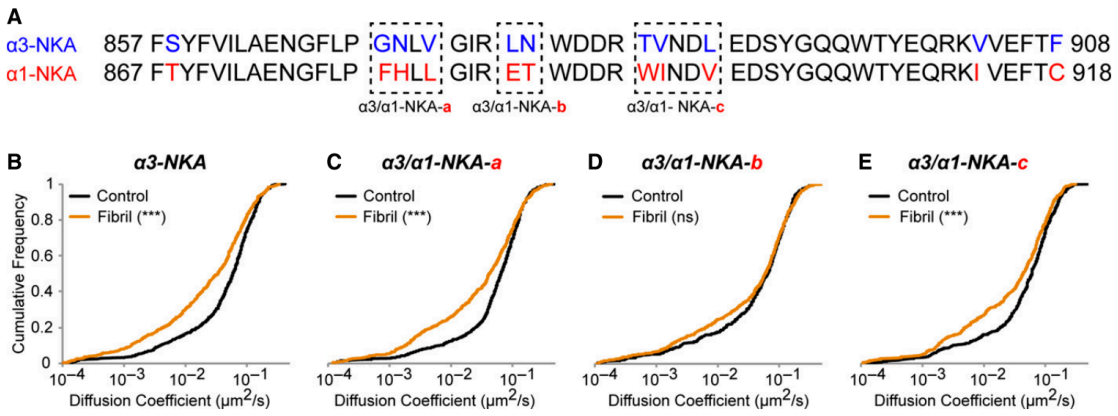

Appendix 7: Residues in the α3 subunit of NKA involved in αSyn fibril binding.
(**A**) α3 and α1 sequences for the transmembrane 7-8 extracellular loops. α1/α3 chimeras are represented by the boxes. (**B–E**) Single particle tracking experiments using quantum dots on α3-NKA (non-chimeric) and chimeric α3-NKA-a/b/c. From (Shrivastava et al., 2015).

BIBLIOGRAPHY

Abeliovich, A., Schmitz, Y., Fariñas, I., Choi-Lundberg, D., Ho, W.H., Castillo, P.E., Shinsky, N., Garcia Verdugo, J.M., Armanini, M., Ryan, A., Hynes, M., Phillips, H., Sulzer, D., Rosenthal, A., 2000. Mice lacking α-synuclein display functional deficits in the nigrostriatal dopamine system. Neuron 25, 239–252.

Abounit, S., Bousset, L., Loria, F., Zhu, S., de Chaumont, F., Pieri, L., Olivo-Marin, J., Melki, R., Zurzolo, C., 2016. Tunneling nanotubes spread fibrillar α-synuclein by intercellular trafficking of lysosomes. EMBO J. 35, 2120–2138.

Adams, D., Gonzalez-Duarte, A., O'Riordan, W.D., Yang, C.-C., Ueda, M., Kristen, A. V., Tournev, I., Schmidt, H.H., Coelho, T., Berk, J.L., Lin, K.-P., Vita, G., Attarian, S., Planté-Bordeneuve, V., Mezei, M.M., Campistol, J.M., Buades, J., Brannagan, T.H., Kim, B.J., Oh, J., Parman, Y., Sekijima, Y., Hawkins, P.N., Solomon, S.D., Polydefkis, M., Dyck, P.J., Gandhi, P.J., Goyal, S., Chen, J., Strahs, A.L., Nochur, S. V., Sweetser, M.T., Garg, P.P., Vaishnaw, A.K., Gollob, J.A., Suhr, O.B., 2018. Patisiran, an RNAi Therapeutic, for Hereditary Transthyretin Amyloidosis. N. Engl. J. Med. 379, 11–21.

Aldaz, T., Nigro, P., Sánchez-Gómez, A., Painous, C., Planellas, L., Santacruz, P., Cámara, A., Compta, Y., Valldeoriola, F., Martí, M.J., Muñoz, E., 2019. Non-motor symptoms in Huntington's disease: a comparative study with Parkinson's disease. J. Neurol. 266, 1340–1350.

Ali, A.M., Atmaj, J., Van Oosterwijk, N., Groves, M.R., Dömling, A., 2019. Stapled Peptides Inhibitors: A New Window for Target Drug Discovery. Comput. Struct. Biotechnol. J. 17, 263–281.

Allocca, S., Ciano, M., Ciardulli, M.C., D'Ambrosio, C., Scaloni, A., Sarnataro, D., Caporaso, M.G., D'Agostino, M., Bonatti, S., 2018. An αB-crystallin peptide rescues compartmentalization and trafficking response to cu overload of ATP7B-H1069Q, the most frequent cause of Wilson disease in the Caucasian population. Int. J. Mol. Sci. 19.

Alo, Y.O., Kitat, B.M., Zhai, R.G., 2011. Dealing with Misfolded Proteins: Examining the Neuroprotective Role of Molecular Chaperones in Neurodegeneration. Molecules 15, 1–26.

Alonso, A.D.C., Zaidi, T., Novak, M., Grundke-Iqbal, I., Iqbal, K., 2001. Hyperphosphorylation induces self-assembly of into tangles of paired helical filaments/straight filaments. Proc. Natl. Acad. Sci. 98, 6923–6928.

Alza, N.P., Iglesias González, P.A., Conde, M.A., Uranga, R.M., Salvador, G.A., 2019. Lipids at the crossroad of α-synuclein function and dysfunction: Biological and pathological implications. Front. Cell. Neurosci. 13, 1–17.

Alzheimer Association, 2019. 2019 Alzheimer's disease facts and figures. Alzheimer's Dement. 15, 321–387.

Anckar, J., Sistonen, L., 2007. Heat Shock Factor 1 as a Coordinator of Stress and Developmental Pathways. In: Molecular Aspects of the Stress Response: Chaperones, Membranes and Networks. Springer New York, New York, NY, pp. 78–88.

Angot, E., Steiner, J.A., Tomé, C.M., Ekström, P., Mattsson, B., Björklund, A., Brundin, P., 2012. Alpha-synuclein cell-to-cell transfer and seeding in grafted dopaminergic neurons in vivo. PLoS One 7, 23–27.

Aprile, F.A., Arosio, P., Fusco, G., Chen, S.W., Kumita, J.R., Dhulesia, A., Tortora, P., Knowles, T.P.J., Vendruscolo, M., Dobson, C.M., Cremades, N., 2017. Inhibition of α-Synuclein Fibril Elongation by Hsp70 Is Governed by a Kinetic Binding Competition between α-Synuclein Species. Biochemistry 56, 1177–1180.

Aquilina, J.A., Shrestha, S., Morris, A.M., Ecroyd, H., 2013. Structural and functional aspects of hetero-oligomers formed by the small heat shock proteins aB-crystallin and HSP27. J. Biol. Chem. 288, 13602–13609.

Armstrong, M.J., Litvan, I., Lang, A.E., Bak, T.H., Bhatia, K.P., Borroni, B., Boxer, A.L., Dickson, D.W., Grossman, M., Hallett, M., Josephs, K.A., Kertesz, A., Lee, S.E., Miller, B.L., Reich, S.G., Riley, D.E., Tolosa, E., Troster, A.I., Vidailhet, M., Weiner, W.J., 2013. Criteria for the diagnosis of corticobasal degeneration. Neurology 80, 496–503.

Arotcarena, M., Bourdenx, M., Dutheil, N., Thiolat, M., Doudnikoff, E., Dovero, S., Ballabio, A., Fernagut, P., Meissner, W.G., Bezard, E., Dehay, B., 2019. Transcription factor EB overexpression prevents neurodegeneration in experimental synucleinopathies. JCI Insight 4.

Augusteyn, R.C., 2004. Dissociation is not required for alpha-crystallin's chaperone function. Exp. Eye Res. 79, 781–4.

Aylward, E.H., Sparks, B.F., Field, K.M., Yallapragada, V., Shpritz, B.D., Rosenblatt, A., Brandt, J., Gourley, L.M., Liang, K., Zhou, H., Margolis, R.L., Ross, C.A., 2004. Onset and rate of striatal atrophy in preclinical Huntington disease. Neurology 63, 66–72.

Baba, M., Nakajo, S., Tu, P.H., Tomita, T., Nakaya, K., Lee, V.M.Y., Trojanowski, J.Q., Iwatsubo, T., 1998. Aggregation of α-synuclein in Lewy bodies of sporadic Parkinson's disease and dementia with Lewy bodies. Am. J. Pathol. 152, 879–884.

Bae, E.-J., Lee, H.-J., Rockenstein, E., Ho, D.-H., Park, E.-B., Yang, N.-Y., Desplats, P., Masliah, E., Lee, S.-J., 2012. Antibody-Aided Clearance of Extracellular α-Synuclein Prevents Cell-to-Cell Aggregate Transmission. J. Neurosci. 32, 13454–69.

Ballinger, C.A., Connell, P., Wu, Y., Hu, Z., Thompson, L.J., Yin, L.-Y., Patterson, C., 1999. Identification of CHIP, a Novel Tetratricopeptide Repeat-Containing Protein That Interacts with Heat Shock Proteins and Negatively Regulates Chaperone Functions. Mol. Cell. Biol. 19, 4535–4545.

Banerjee, P.R., Pande, A., Shekhtman, A., Pande, J., 2015. Molecular mechanism of the chaperone function of mini-a-crystallin, a 19-residue peptide of human a-crystallin. Biochemistry 54, 505–515.

Barragán Martínez, D., García Soldevilla, M.A., Parra Santiago, A., Tejeiro Martínez, J., 2019. Alzheimer's disease. Med. 12, 4338–4346.

Barrett, P.J., Timothy Greenamyre, J., 2015. Post-translational modification of α-synuclein in Parkinson′s disease. Brain Res. 1628, 247–253.

Bartels, T., Choi, J.G., Selkoe, D.J., 2011. α-Synuclein occurs physiologically as a helically folded tetramer that resists aggregation. Nature 477, 107–111.

Bateman, R.J., Aisen, P.S., De Strooper, B., Fox, N.C., Lemere, C.A., Ringman, J.M., Salloway, S., Sperling, R.A., Windisch, M., Xiong, C., 2011. Autosomal-dominant Alzheimer's disease: A review and proposal for the prevention of Alzheimer's disease. Alzheimer's Res. Ther. 2, 1–13.

Bates, G.P., Dorsey, R., Gusella, J.F., Hayden, M.R., Kay, C., Leavitt, B.R., Nance, M., Ross, C.A., Scahill, R.I., Wetzel, R., Wild, E.J., Tabrizi, S.J., 2015. Huntington disease. Nat. Rev. Dis. Prim. 1, 15005.

Baughman, H.E.R., Clouser, A.F., Klevit, R.E., Nath, A., 2018. HspB1 and Hsc70 chaperones engage distinct tau species and have different inhibitory effects on amyloid formation. J. Biol. Chem. 293, 2687–2700.

Berriman, J., Serpell, L.C., Oberg, K.A., Fink, A.L., Goedert, M., Crowther, R.A., 2003. Tau filaments from human brain and from in vitro assembly of recombinant protein show cross-beta structure. Proc. Natl. Acad. Sci. 100, 9034–9038.

Bhattacharyya, J., Padmanabha Udupa, E.G., Wang, J., Sharma, K.K., 2006. Mini-alphaB-

crystallin: a functional element of alphaB-crystallin with chaperone-like activity. Biochemistry 45, 3069–3076.

Biancalana, M., Koide, S., 2010. Molecular mechanism of Thioflavin-T binding to amyloid fibrils. Biochim. Biophys. Acta - Proteins Proteomics 1804, 1405–1412.

Biemann, K., 1988. Contributions of mass spectrometry to peptide and protein structure. Biol. Mass Spectrom. 16, 99–111.

Biemann, K., 1992. Mass Spectrometry of Peptides and Proteins. Annu. Rev. Biochem. 61, 977–1010.

Bieri, G., Gitler, A.D., Brahic, M., 2018. Internalization, axonal transport and release of fibrillar forms of alpha-synuclein. Neurobiol. Dis. 109, 219–225.

Binger, K.J., Ecroyd, H., Yang, S., Carver, J.A., Howlett, G.J., Griffin, M.D.W., 2013. Avoiding the oligomeric state: αB-crystallin inhibits fragmentation and induces dissociation of apolipoprotein C-II amyloid fibrils. FASEB J. 27, 1214–1222.

Binukumar, B., Shukla, V., Amin, N.D., Grant, P., Bhaskar, M., Skuntz, S., Steiner, J., Pant, H.C., 2015. Peptide TFP5/TP5 derived from Cdk5 activator P35 provides neuroprotection in the MPTP model of Parkinson's disease. Mol. Biol. Cell 26, 4478–4491.

Binukumar, B., Skuntz, S., Prochazkova, M., Kesavapany, S., Amin, N.D., Shukla, V., Grant, P., Kulkarni, A.B., Pant, H.C., 2019. Overexpression of the Cdk5 inhibitory peptide in motor neurons rescue of amyotrophic lateral sclerosis phenotype in a mouse model. Hum. Mol. Genet. 1, 1–38.

Blennow, K., Biscetti, L., Eusebi, P., Parnetti, L., 2016. Cerebrospinal fluid biomarkers in Alzheimer's and Parkinson's diseases-From pathophysiology to clinical practice. Mov. Disord. 31, 836–847.

Blennow, K., de Leon, M.J., Zetterberg, H., 2006. Alzheimer's disease. Lancet 368, 387–403.

Bonifati, V., 2014. Genetics of Parkinson's disease - state of the art, 2013. Park. Relat. Disord. 20, S23–S28.

Borghi, R., Marchese, R., Negro, A., Marinelli, L., Forloni, G., Zaccheo, D., Abbruzzese, G., Tabaton, M., 2000. Full length α-synuclein is present in cerebrospinal fluid from Parkinson's disease and normal subjects. Neurosci. Lett. 287, 65–67.

Bousset, L., Pieri, L., Ruiz-Arlandis, G., Gath, J., Jensen, P.H., Habenstein, B., Madiona, K., Olieric, V., Böckmann, A., Meier, B.H., Melki, R., 2013. Structural and functional characterization of two alpha-synuclein strains. Nat. Commun. 4, 2575.

Braak, H., Alafuzoff, I., Arzberger, T., Kretzschmar, H., Tredici, K., 2006a. Staging of Alzheimer disease-associated neurofibrillary pathology using paraffin sections and immunocytochemistry. Acta Neuropathol. 112, 389–404.

Braak, H., Braak, E., Bohl, J., 1993. Staging of Alzheimer-Related Cortical Destruction. Eur. Neurol. 33, 403–408.

Braak, H., De Vos, R.A.I., Bohl, J., Del Tredici, K., 2006b. Gastric α-synuclein immunoreactive inclusions in Meissner's and Auerbach's plexuses in cases staged for Parkinson's disease-related brain pathology. Neurosci. Lett. 396, 67–72.

Braak, H., Del Tredici, K., 2008. Assessing fetal nerve cell grafts in Parkinson's disease. Nat. Med. 14, 483–485.

Braak, H., Del Tredici, K., 2016. Potential pathways of abnormal tau and α-synuclein dissemination in sporadic Alzheimer's and Parkinson's diseases. Cold Spring Harb. Perspect. Biol. 8, 1–23.

Braak, H., Del Tredici, K., 2017. Neuropathological Staging of Brain Pathology in Sporadic Parkinson's disease: Separating the Wheat from the Chaff. J. Parkinsons. Dis. 7, S73–S87.

Braak, H., Del Tredici, K., Rüb, U., De Vos, R.A.I., Jansen Steur, E.N.H., Braak, E., 2003a. Staging of brain pathology related to sporadic Parkinson's disease. Neurobiol. Aging 24, 197–211.

Braak, H., Del Tredici, K., Sandmann-Keil, D., Rüb, U., Schultz, C., 2001. Nerve cells expressing heat-shock proteins in Parkinson's disease. Acta Neuropathol. 102, 449–454.

Braak, H., Ghebremedhin, E., Rüb, U., Bratzke, H., Del Tredici, K., 2004. Stages in the development of Parkinson's disease-related pathology. Cell Tissue Res. 318, 121–134.

Braak, H., Rüb, U., Del Tredici, K., 2006c. Cognitive decline correlates with neuropathological stage in Parkinson's disease. J. Neurol. Sci. 248, 255–258.

Braak, H., Rüb, U., Gai, W.P., Del Tredici, K., 2003b. Idiopathic Parkinson's disease: Possible routes by which vulnerable neuronal types may be subject to neuroinvasion by an unknown pathogen. J. Neural Transm. 110, 517–536.

Brahic, M., Bousset, L., Bieri, G., Melki, R., Gitler, A.D., 2016. Axonal transport and secretion of fibrillar forms of α-synuclein, Aβ42 peptide and HTTExon 1. Acta Neuropathol. 131, 539–548.

Brás, J., Guerreiro, R., Hardy, J., 2015. SnapShot: Genetics of Parkinson's disease. Cell 160, 570-570.e1.

Braun, N., Zacharias, M., Peschek, J., Kastenmuller, A., Zou, J., Hanzlik, M., Haslbeck, M., Rappsilber, J., Buchner, J., Weinkauf, S., 2011. Multiple molecular architectures of the eye lens chaperone B-crystallin elucidated by a triple hybrid approach. Proc. Natl. Acad. Sci. 108, 20491–20496.

Brehme, M., Voisine, C., Rolland, T., Wachi, S., Soper, J.H., Zhu, Y., Orton, K., Villella, A., Garza, D., Vidal, M., Ge, H., Morimoto, R.I., 2014. A chaperome subnetwork safeguards proteostasis in aging and neurodegenerative disease. Cell Rep. 9, 1135–1150.

Broome, B.M., Hecht, M.H., 2000. Nature disfavors sequences of alternating polar and non-polar amino acids: Implications for amyloidogenesis. J. Mol. Biol. 296, 961–968.

Bruinsma, I.B., Bruggink, K.A., Kinast, K., Versleijen, A.A.M., Segers-Nolten, I.M.J., Subramaniam, V., Bea Kuiperij, H., Boelens, W., de Waal, R.M.W., Verbeek, M.M., 2011. Inhibition of α-synuclein aggregation by small heat shock proteins. Proteins Struct. Funct. Bioinforma. 79, 2956–2967.

Brundin, P., Li, J.Y., Holton, J.L., Lindvall, O., Revesz, T., 2008. Research in motion: The enigma of Parkinson's disease pathology spread. Nat. Rev. Neurosci. 9, 741–745.

Brundin, P., Melki, R., 2017. Prying into the Prion Hypothesis for Parkinson's Disease. J. Neurosci. 37, 9808–9818.

Brundin, P., Melki, R., Kopito, R., 2010. Prion-like transmission of protein aggregates in neurodegenerative diseases. Nat. Rev. Mol. Cell Biol. 11, 301–7.

Buée, L., Bussière, T., Buée-Scherrer, V., Delacourte, A., Hof, P.R., 2000. Tau protein isoforms, phosphorylation and role in neurodegenerative disorders. Brain Res. Rev. 33, 95–130.

Bunka, D.H.J., Stockley, P.G., 2006. Aptamers come of age - At last. Nat. Rev. Microbiol. 4, 588–596.

Burke, K.A., Kauffman, K.J., Umbaugh, C.S., Frey, S.L., Legleiter, J., 2013. The interaction of polyglutamine peptides with lipid membranes is regulated by flanking sequences associated with huntingtin. J. Biol. Chem. 288, 14993–15005.

Burré, J., Sharma, M., Südhof, T.C., 2018. Cell Biology and Pathophysiology of α-Synuclein. Cold Spring Harb. Perspect. Med. 8, a024091.

Burré, J., Sharma, M., Tsetsenis, T., Buchman, V., Etherton, M.R., Südhof, T.C., 2010. α-Synuclein promotes SNARE-complex assembly in vivo and in vitro. Science 329, 1663–

1667.

Burré, J., Vivona, S., Diao, J., Sharma, M., Brunger, A.T., Südhof, T.C., 2013. Properties of native brain α-synuclein. Nature 498, 1–6.

Bushman, D.M., Kaeser, G.E., Siddoway, B., Westra, J.W., Rivera, R.R., Rehen, S.K., Yung, Y.C., Chun, J., 2015. Genomic mosaicism with increased amyloid precursor protein (APP) gene copy number in single neurons from sporadic Alzheimer's disease brains. Elife 4, 1–26.

Byler, M., Susi, H., 1986. Examination of the Secondary Structure.

Calabrese, A.N., Radford, S.E., 2018. Mass spectrometry-enabled structural biology of membrane proteins. Methods 147, 187–205.

Calafate, S., Flavin, W., Verstreken, P., Moechars, D., 2016. Loss of Bin1 Promotes the Propagation of Tau Pathology. Cell Rep. 17, 931–940.

Cali, I., Cohen, M.L., Haik, S., Parchi, P., Giaccone, G., Collins, S.J., Kofskey, D., Wang, H., McLean, C.A., Brandel, J.P., Privat, N., Sazdovitch, V., Duyckaerts, C., Kitamoto, T., Belay, E.D., Maddox, R.A., Tagliavini, F., Pocchiari, M., Leschek, E., Appleby, B.S., Safar, J.G., Schonberger, L.B., Gambetti, P., 2018. Iatrogenic Creutzfeldt-Jakob disease with Amyloid-β pathology: an international study. Acta Neuropathol. Commun. 6, 5.

Campioni, S., Monsellier, E., Chiti, F., 2010. Why Proteins Misfold. In: Protein Misfolding Diseases. John Wiley & Sons, Inc., Hoboken, NJ, USA, pp. 1–20.

Cantley, W.L., Du, C., Lomoio, S., DePalma, T., Peirent, E., Kleinknecht, D., Hunter, M., Tang-Schomer, M.D., Tesco, G., Kaplan, D.L., 2018. Functional and Sustainable 3D Human Neural Network Models from Pluripotent Stem Cells. ACS Biomater. Sci. Eng. 4, 4278–4288.

Carra, S., Sivilotti, M., Chávez Zobel, A.T., Lambert, H., Landry, J., 2005. HspB8, a small heat shock protein mutated in human neuromuscular disorders, has in vivo chaperone activity in cultured cells. Hum. Mol. Genet. 14, 1659–1669.

Cavaliere, F., Cerf, L., Dehay, B., Ramos-Gonzalez, P., De Giorgi, F., Bourdenx, M., Bessede, A., Obeso, J.A., Matute, C., Ichas, F., Bezard, E., 2017. In vitro α-synuclein neurotoxicity and spreading among neurons and astrocytes using Lewy body extracts from Parkinson disease brains. Neurobiol. Dis. 103, 101–112.

Chafekar, S.M., Duennwald, M.L., 2012. Impaired heat shock response in cells expressing full-length polyglutamine-expanded Huntingtin. PLoS One 7, 1–11.

Chan, P.-C., Lee, H.-H., Hong, C.-T., Hu, C.-J., Wu, D., 2018. REM Sleep Behavior Disorder (RBD) in Dementia with Lewy Bodies (DLB). Behav. Neurol. 2018, 1–10.

Chan, D.K.Y., Xu, Y.H., Chan, L.K.M., Braidy, N., Mellick, G.D., 2017. Mini-review on initiatives to interfere with the propagation and clearance of alpha-synuclein in Parkinson's disease. Transl. Neurodegener. 6, 33.

Chanpimol, S., Seamon, B., Hernandez, H., Harris-love, M., Blackman, M.R., 2016. Novel treatment strategies targeting alpha-synuclein in multiple system atrophy as a model of synucleinopathy. Neuropathol. Appl. Neurobiol. 42, 95–106.

Chatellier, J., Hill, F., Lund, P.A., Fersht, A.R., 1998. In vivo activities of GroEL minichaperones. Proc. Natl. Acad. Sci. 95, 9861–9866.

Chen, S., Brown, I.R., 2007. Neuronal expression of constitutive heat shock proteins: implications for neurodegenerative diseases. Cell Stress Chaperones 12, 51–8.

Chen, C., Dong, X.P., 2016. Epidemiological characteristics of human prion diseases. Infect. Dis. Poverty 5, 1–10.

Chen, J., Yagi, H., Sormanni, P., Vendruscolo, M., Makabe, K., Nakamura, T., Goto, Y., Kuwajima, K., 2012. Fibrillogenic propensity of the GroEL apical domain: A Janus-faced

minichaperone. FEBS Lett. 586, 1120–1127.

Cheng, B., Gong, H., Xiao, H., Petersen, R.B., Zheng, L., Huang, K., 2013. Inhibiting toxic aggregation of amyloidogenic proteins: A therapeutic strategy for protein misfolding diseases. Biochim. Biophys. Acta - Gen. Subj. 1830, 4860–4871.

Cheng, H.-C., Ulane, C.M., Burke, R.E., 2010. Clinical progression in Parkinson disease and the neurobiology of axons. Ann. Neurol. 67, 715–725.

Chi, E.Y., Frey, S.L., Lee, K.Y.C., 2007. Ganglioside GM1 -Mediated Amyloid-beta Fibrillogenesis and Membrane Disruption. Biochemistry 46, 1913–1924.

Chiti, F., Dobson, C.M., 2006. Protein Misfolding, Functional Amyloid, and Human Disease. Annu. Rev. Biochem. 75, 333–366.

Choi, S.H., Kim, Y.H., Hebisch, M., Sliwinski, C., Lee, S., D'Avanzo, C., Chen, H., Hooli, B., Asselin, C., Muffat, J., Klee, J.B., Zhang, C., Wainger, B.J., Peitz, M., Kovacs, D.M., Woolf, C.J., Wagner, S.L., Tanzi, R.E., Kim, D.Y., 2014. A three-dimensional human neural cell culture model of Alzheimer's disease. Nature 515, 274–278.

Chorell, E., Andersson, E., Evans, M.L., Jain, N., Götheson, A., Åden, J., Chapman, M.R., Almqvist, F., Wittung-Stafshede, P., 2015. Bacterial Chaperones CsgE and CsgC Differentially Modulate Human α-Synuclein Amyloid Formation via Transient Contacts. PLoS One 10, e0140194.

Cicchetti, F., Lacroix, S., Cisbani, G., Vallières, N., Saint-Pierre, M., St-Amour, I., Tolouei, R., Skepper, J.N., Hauser, R.A., Mantovani, D., Barker, R.A., Freeman, T.B., 2014. Mutant huntingtin is present in neuronal grafts in huntington disease patients. Ann. Neurol. 76, 31–42.

Cicchetti, F., Saporta, S., Hauser, R.A., Parent, M., Saint-Pierre, M., Sanberg, P.R., Li, X.J., Parker, J.R., Chu, Y., Mufson, E.J., Kordower, J.H., Freeman, T.B., 2009. Neural transplants in patients with Huntington's disease undergo disease-like neuronal degeneration. Proc. Natl. Acad. Sci. 106, 12483–12488.

Cicchetti, F., Soulet, D., Freeman, T.B., 2011. Neuronal degeneration in striatal transplants and Huntington's disease: potential mechanisms and clinical implications. Brain 134, 641–652.

Clavaguera, F., Akatsu, H., Fraser, G., Crowther, R.A., Frank, S., Hench, J., Probst, A., Winkler, D.T., Reichwald, J., Staufenbiel, M., Ghetti, B., Goedert, M., Tolnay, M., 2013. Brain homogenates from human tauopathies induce tau inclusions in mouse brain. Proc. Natl. Acad. Sci. 110, 9535–9540.

Clavaguera, F., Bolmont, T., Crowther, R.A., Abramowski, D., Frank, S., Probst, A., Fraser, G., Stalder, A.K., Beibel, M., Staufenbiel, M., Jucker, M., Goedert, M., Tolnay, M., 2009. Transmission and spreading of tauopathy in transgenic mouse brain. Nat. Cell Biol. 11, 909–913.

Clavaguera, F., Grueninger, F., Tolnay, M., 2014. Intercellular transfer of tau aggregates and spreading of tau pathology: Implications for therapeutic strategies. Neuropharmacology 76, 9–15.

Cliffe, R., Sang, J.C., Kundel, F., Finley, D., Klenerman, D., Ye, Y., 2019. Filamentous Aggregates Are Fragmented by the Proteasome Holoenzyme. Cell Rep. 26, 2140-2149.e3.

Colby, D.W., Prusiner, S.B., 2011. Prions. Cold Spring Harb. Perspect. Biol. 3, a006833–a006833.

Corbi-Verge, C., Garton, M., Nim, S., Kim, P.M., 2017. Strategies to Develop Inhibitors of Motif-Mediated Protein-Protein Interactions as Drug Leads. Annu. Rev. Pharmacol. Toxicol. 57, 39–60.

Cornwell, O., Radford, S.E., Ashcroft, A.E., Ault, J.R., 2018. Comparing Hydrogen Deuterium Exchange and Fast Photochemical Oxidation of Proteins: a Structural Characterisation of Wild-Type and ΔN6 β2-Microglobulin. J. Am. Soc. Mass Spectrom. 29, 2413–2426.

Costanzo, M., Abounit, S., Marzo, L., Danckaert, A., Chamoun, Z., Roux, P., Zurzolo, C., 2013. Transfer of polyglutamine aggregates in neuronal cells occurs in tunneling nanotubes. J. Cell Sci. 126, 3678–3685.

Coughlin, D., Irwin, D.J., 2017. Emerging Diagnostic and Therapeutic Strategies for Tauopathies. Curr. Neurol. Neurosci. Rep. 17, 1–23.

Cox, D., Ecroyd, H., 2017. The small heat shock proteins αB-crystallin (HSPB5) and Hsp27 (HSPB1) inhibit the intracellular aggregation of α-synuclein. Cell Stress Chaperones 22, 589–600.

Cox, D., Selig, E., Griffin, M.D.W., Carver, J.A., Ecroyd, H., 2016. Small Heat-shock Proteins Prevent α-synuclein aggregation via transient interactions and their efficacy is affected by the rate of aggregation. J. Biol. Chem. 291, 22618–22629.

Cox, D., Whiten, D.R., Brown, J.W.P., Horrocks, M.H., San Gil, R., Dobson, C.M., Klenerman, D., van Oijen, A.M., Ecroyd, H., 2018. The small heat shock protein Hsp27 binds α-synuclein fibrils, preventing elongation and cytotoxicity. J. Biol. Chem. 293, 4486–4497.

Craik, D.J., Fairlie, D.P., Liras, S., Price, D., 2013. The Future of Peptide-based Drugs. Chem. Biol. Drug Des. 81, 136–147.

Cunningham, A.D., Qvit, N., Mochly-Rosen, D., 2017. Peptides and peptidomimetics as regulators of protein–protein interactions. Curr. Opin. Struct. Biol. 44, 59–66.

Dabbs, R.A., Wyatt, A.R., Yerbury, J.J., Ecroyd, H., Wilson, M.R., 2011. Extracellular Chaperones. In: TripleC. pp. 241–268.

Dabir, D. V., Trojanowski, J.Q., Richter-Landsberg, C., Lee, V.M.Y., Forman, M.S., 2004. Expression of the Small Heat-Shock Protein αB-Crystallin in Tauopathies with Glial Pathology. Am. J. Pathol. 164, 155–166.

Das, S., Pukala, T.L., Smid, S.D., 2018. Exploring the Structural Diversity in Inhibitors of α-Synuclein Amyloidogenic Folding, Aggregation, and Neurotoxicity. Front. Chem. 6, 181.

Dauer, W., Przedborski, S., 2003. Parkinson's disease: Mechanisms and models. Neuron 39, 889–909.

Davis, A.A., Leyns, C.E.G., Holtzman, D.M., 2018. Intercellular Spread of Protein Aggregates in Neurodegenerative Disease. Annu. Rev. Cell Dev. Biol. 34, 545–68.

Dedmon, M.M., Christodoulou, J., Wilson, M.R., Dobson, C.M., 2005. Heat shock protein 70 inhibits α-synuclein fibril formation via preferential binding to prefibrillar species. J. Biol. Chem. 280, 14733–14740.

Delbecq, S.P., Jehle, S., Klevit, R., 2012. Binding determinants of the small heat shock protein, alpha B-crystallin: recognition of the 'IxI' motif. EMBO J. 31318, 4587–4594.

Delic, V., Chandra, S., Abdelmotilib, H., Maltbie, T., Wang, S., Kem, D., Scott, H.J., Underwood, R.N., Liu, Z., Volpicelli-Daley, L.A., West, A.B., 2018. Sensitivity and specificity of phospho-Ser129 α-synuclein monoclonal antibodies. J. Comp. Neurol. 526, 1978–1990.

Despa, F., Orgill, D.P., Lee, R.C., 2005. Molecular crowding effects on protein stability. Ann. N. Y. Acad. Sci. 1066, 54–66.

Desplats, P., Lee, H.-J., Bae, E.-J., Patrick, C., Rockenstein, E., Crews, L., Spencer, B., Masliah, E., Lee, S.-J., 2009. Inclusion formation and neuronal cell death through neuron-to-neuron transmission of a-synuclein. Proc. Natl. Acad. Sci. 106, 13010–13015.

Despres, C., Byrne, C., Qi, H., Cantrelle, F.-X., Huvent, I., Chambraud, B., Baulieu, E.-E., Jacquot, Y., Landrieu, I., Lippens, G., Smet-Nocca, C., 2017. Identification of the Tau phosphorylation pattern that drives its aggregation. Proc. Natl. Acad. Sci. 114, 9080–9085.

Dettmer, U., Newman, A.J., Soldner, F., Luth, E.S., Kim, N.C., Von Saucken, V.E., Sanderson, J.B., Jaenisch, R., Bartels, T., Selkoe, D., 2015. Parkinson-causing α-synuclein missense

mutations shift native tetramers to monomers as a mechanism for disease initiation. Nat. Commun. 6, 1–15.

Dewji, N.N., Azar, M.R., Hanson, L.R., Frey II, W.H., Morimoto, B.H., Johnson, D., 2018. Pharmacokinetics in Rat of P8, a Peptide Drug Candidate for the Treatment of Alzheimer's Disease: Stability and Delivery to the Brain 1. J. Alzheimer's Dis. Reports 2, 1–11.

Dewji, N.N., Singer, S.J., Masliah, E., Rockenstein, E., Kim, M., Harber, M., Horwood, T., 2015. Peptides of presenilin-1 bind the amyloid precursor protein ectodomain and offer a novel and specific therapeutic approach to reduce β-amyloid in Alzheimer's disease. PLoS One 10, 1–22.

Di, L., 2015. Strategic Approaches to Optimizing Peptide ADME Properties. AAPS J. 17, 134–143.

Di Lella, S., Sundblad, V., Cerliani, J.P., Guardia, C.M., Estrin, D.A., Vasta, G.R., Rabinovich, G.A., 2011. When Galectins Recognize Glycans: From Biochemistry to Physiology and Back Again. Biochemistry 50, 7842–7857.

Di Monte, D.A., McCormack, A., Petzinger, G., Janson, A.M., Quik, M., Langston, W.J., 2000. Relationship among nigrostriatal denervation, parkinsonism, and dyskinesias in the MPTP primate model. Mov. Disord. 15, 459–466.

Di Pasquale, E., Fantini, J., Chahinian, H., Maresca, M., Taïeb, N., Yahi, N., 2010. Altered Ion Channel Formation by the Parkinson's-Disease-Linked E46K Mutant of α-Synuclein Is Corrected by GM3 but Not by GM1 Gangliosides. J. Mol. Biol. 397, 202–218.

Dickey, C.A., Kamal, A., Lundgren, K., Klosak, N., Bailey, R.M., Dunmore, J., Ash, P., Shoraka, S., Zlatkovic, J., Eckman, C.B., Patterson, C., Dickson, D.W., Nahman, N.S., Hutton, M., Burrows, F., Petrucelli, L., 2007. The high-affinity HSP90-CHIP complex recognizes and selectively degrades phosphorylated tau client proteins. J. Clin. Invest. 117, 648–658.

DiFiglia, M., Sapp, E., Chase, K.O., Davies, S.W., Bates, G.P., Vonsattel, J.P., Aronin, N., 1997. Aggregation of huntingtin in neuronal intranuclear inclusions and dystrophic neurites in brain. Science 277, 1990–1993.

Dimant, H., Zhu, L., Kibuuka, L.N., Fan, Z., Hyman, B.T., McLean, P.J., 2014. Direct visualization of CHIP-mediated degradation of alpha-synuclein in vivo: Implications for PD therapeutics. PLoS One 9, 1–8.

Dobson, C.M., 2003. Protein folding and misfolding. Nature 426, 884–890.

Dugger, B.N., Dickson, D.W., 2017. Pathology of Neurodegenerative Diseases. Cold Spring Harb. Perspect. Biol. 9, a028035.

Dujardin, S., Bégard, S., Caillierez, R., Lachaud, C., Carrier, S., Lieger, S., Gonzalez, J.A., Deramecourt, V., Déglon, N., Maurage, C.A., Frosch, M.P., Hyman, B.T., Colin, M., Buée, L., 2018. Different tau species lead to heterogeneous tau pathology propagation and misfolding. Acta Neuropathol. Commun. 6, 132.

Durrenberger, P.F., Filiou, M.D., Moran, L.B., Michael, G.J., Novoselov, S., Cheetham, M.E., Clark, P., Pearce, R.K.B., Graeber, M.B., 2009. DnaJB6 is present in the core of Lewy bodies and is highly up-regulated in Parkinsonian astrocytes. J. Neurosci. Res. 87, 238–245.

Dutot, L., Lécorché, P., Burlina, F., Marquant, R., Point, V., Sagan, S., Chassaing, G., Mallet, J.M., Lavielle, S., 2010. Glycosylated cell-penetrating peptides and their conjugates to a proapoptotic peptide: Preparation by click chemistry and cell viability studies. J. Chem. Biol. 3, 51–65.

Dutta, D., Donaldson, J.G., 2012. Search for inhibitors of endocytosis. Cell. Logist. 2, 203–208.

Duyckaerts, C., Sazdovitch, V., Ando, K., Seilhean, D., Privat, N., Yilmaz, Z., Peckeu, L.,

Amar, E., Comoy, E., Maceski, A., Lehmann, S., Brion, J.P., Brandel, J.P., Haïk, S., 2018. Neuropathology of iatrogenic Creutzfeldt–Jakob disease and immunoassay of French cadaver-sourced growth hormone batches suggest possible transmission of tauopathy and long incubation periods for the transmission of Abeta pathology. Acta Neuropathol. 135, 201–212.

Duyckaerts, C., Uchihara, T., Seilhean, D., He, Y., Hauw, J.J., 1997. Dissociation of Alzheimer type pathology in a disconnected piece of cortex. Acta Neuropathol. 93, 501–507.

Ecroyd, H., Meehan, S., Horwitz, J., Aquilina, J.A., Benesch, J.L.P., Robinson, C. V., Macphee, C.E., Carver, J.A., 2007. Mimicking phosphorylation of αB-crystallin affects its chaperone activity. Biochem. J. 401, 129–141.

Egnaczyk, G.F., Greis, K.D., Stimson, E.R., Maggio, J.E., 2001. Photoaffinity cross-linking of Alzheimer's disease amyloid fibrils reveals interstrand contact regions between assembled β-amyloid peptide subunits. Biochemistry 40, 11706–11714.

Eichner, T., Radford, S.E., 2011. A Diversity of Assembly Mechanisms of a Generic Amyloid Fold. Mol. Cell 43, 8–18.

Eisele, Y.S., Monteiro, C., Fearns, C., Encalada, S.E., Wiseman, R.L., Powers, E.T., Kelly, J.W., 2015. Targeting protein aggregation for the treatment of degenerative diseases. Nat. Rev. Drug Discov. 14, 759–780.

El-Agnaf, O.M.A., Salem, S.A., Paleologou, K.E., Cooper, L.J., Fullwood, N.J., Gibson, M.J., Curran, M.D., Court, J.A., Mann, D.M.A., Ikeda, S.-I., Cookson, M.R., Hardy, J., Allsop, D., 2003. α-Synuclein implicated in Parkinson's disease is present in extracellular biological fluids, including human plasma. FASEB J. 17, 1945–1947.

El-Agnaf, O.M.A., Salem, S.A., Paleologou, K.E., Curran, M.D., Gibson, M.J., Court, J.A., Schlossmacher, M.G., Allsop, D., 2006. Detection of oligomeric forms of α-synuclein protein in human plasma as a potential biomarker for Parkinson's disease. FASEB J. 20, 419–425.

Ellis, J.M., Fell, M.J., 2017. Current approaches to the treatment of Parkinson's Disease. Bioorg. Med. Chem. Lett. 27, 4247–4255.

Emmanouilidou, E., Melachroinou, K., Roumeliotis, T., Garbis, S.D., Ntzouni, M., Margaritis, L.H., Stefanis, L., Vekrellis, K., 2010. Cell-Produced a-Synuclein Is Secreted in a Calcium-Dependent Manner by Exosomes and Impacts Neuronal Survival. J. Neurosci. 30, 6838–6851.

Erak, M., Bellmann-Sickert, K., Els-Heindl, S., Beck-Sickinger, A.G., 2018. Peptide chemistry toolbox – Transforming natural peptides into peptide therapeutics. Bioorganic Med. Chem. 26, 2759–2765.

Evans, M.L., Chorell, E., Taylor, J.D., Åden, J., Götheson, A., Li, F., Koch, M., Sefer, L., Matthews, S.J., Wittung-stafshede, P., Almqvist, F., Chapman, M.R., Go, A., Li, F., Koch, M., Sefer, L., Taylor, J.D., Matthews, S.J., Wittung-stafshede, P., 2015. The Bacterial Curli System Possesses a Potent and Selective Inhibitor of Amyloid Formation Article The Bacterial Curli System Possesses a Potent and Selective Inhibitor of Amyloid Formation. Mol. Cell 57, 445–456.

Evans, L.D., Wassmer, T., Fraser, G., Smith, J., Perkinton, M., Billinton, A., Livesey, F.J., 2018. Extracellular Monomeric and Aggregated Tau Efficiently Enter Human Neurons through Overlapping but Distinct Pathways. Cell Rep. 22, 3612–3624.

Fairlie, D.P., Dantas de Araujo, A., 2016. Stapling peptides using cysteine crosslinking. Biopolymers 106, 843–852.

Falcon, B., Cavallini, A., Angers, R., Glover, S., Murray, T.K., Barnham, L., Jackson, S., O'Neill, M.J., Isaacs, A.M., Hutton, M.L., Szekeres, P.G., Goedert, M., Bose, S., 2015. Conformation determines the seeding potencies of native and recombinant Tau aggregates.

J. Biol. Chem. 290, 1049–1065.

Falcon, B., Zhang, W., Murzin, A.G., Murshudov, G., Garringer, H.J., Vidal, R., Crowther, R.A., Ghetti, B., Scheres, S.H.W., Goedert, M., 2018. Structures of filaments from Pick's disease reveal a novel tau protein fold. Nature.

Falcon, B., Zivanov, J., Zhang, W., Murzin, A.G., Garringer, H.J., Vidal, R., Crowther, R.A., Newell, K.L., Ghetti, B., Goedert, M., Scheres, S.H.W., 2019. Novel tau filament fold in chronic traumatic encephalopathy encloses hydrophobic molecules. Nature 568, 420–423.

Falsone, S.F., Kungl, A.J., Rek, A., Cappai, R., Zangger, K., 2009. The molecular chaperone Hsp90 modulates intermediate steps of amyloid assembly of the Parkinson-related protein α-synuclein. J. Biol. Chem. 284, 31190–31199.

Fantini, J., Carlus, D., Yahi, N., 2011. The fusogenic tilted peptide (67-78) of α-synuclein is a cholesterol binding domain. Biochim. Biophys. Acta - Biomembr. 1808, 2343–2351.

Fantini, J., Yahi, N., 2013. The Driving Force of Alpha-Synuclein Insertion and Amyloid Channel Formation in the Plasma Membrane of Neural Cells: Key Role of Ganglioside- and Cholesterol-Binding Domains. In: Advances in Experimental Medicine and Biology. pp. 15–26.

Fauvet, B., Mbefo, M.K., Fares, M.B., Desobry, C., Michael, S., Ardah, M.T., Tsika, E., Coune, P., Prudent, M., Lion, N., Eliezer, D., Moore, D.J., Schneider, B., Aebischer, P., El-Agnaf, O.M., Masliah, E., Lashuel, H.A., 2012. α-Synuclein in central nervous system and from erythrocytes, mammalian cells, and Escherichia coli exists predominantly as disordered monomer. J. Biol. Chem. 287, 15345–15364.

Fawcett, T.W., Sylvester, S.L., Sarge, K.D., Morimoto, R.I., Holbrook, N.J., 1994. Effects of neurohormonal stress and aging on the activation of mammalian heat shock factor 1. J. Biol. Chem. 269, 32272–32278.

Fenyi, A., Coens, A., Bellande, T., Melki, R., Bousset, L., 2018. Assessment of the efficacy of different procedures that remove and disassemble alpha-synuclein, tau and A-beta fibrils from laboratory material and surfaces. Sci. Rep. 8, 10788.

Fenyi, A., Leclair-Visonneau, L., Clairembault, T., Coron, E., Neunlist, M., Melki, R., Derkinderen, P., Bousset, L., 2019. Detection of alpha-synuclein aggregates in gastrointestinal biopsies by protein misfolding cyclic amplification. Neurobiol. Dis. 129, 38–43.

Fitzpatrick, A.W.P., Falcon, B., He, S., Murzin, A.G., Murshudov, G., Garringer, H.J., Crowther, R.A., Ghetti, B., Goedert, M., Scheres, S.H.W., 2017. Cryo-EM structures of tau filaments from Alzheimer's disease. Nature 547, 185–190.

Fitzpatrick, A.W., Saibil, H.R., 2019. Cryo-EM of amyloid fibrils and cellular aggregates. Curr. Opin. Struct. Biol. 58, 34–42.

Flavin, W.P., Bousset, L., Green, Z.C., Chu, Y., Skarpathiotis, S., Chaney, M.J., Kordower, J.H., Melki, R., Campbell, E.M., 2017. Endocytic vesicle rupture is a conserved mechanism of cellular invasion by amyloid proteins. Acta Neuropathol. 134, 629–653.

Forman, M.S., Trojanowski, J.Q., Lee, V.M., 2004. Neurodegenerative diseases: a decade of discoveries paves the way for therapeutic breakthroughs. Nat. Med. 10, 1055–1063.

Fosgerau, K., Hoffmann, T., 2015. Peptide therapeutics: current status and future directions. Drug Discov. Today 20, 122–8.

Fowler, D.M., Koulov, A. V., Balch, W.E., Kelly, J.W., 2007. Functional amyloid - from bacteria to humans. Trends Biochem. Sci. 32, 217–224.

Freeman, D., Cedillos, R., Choyke, S., Lukic, Z., McGuire, K., Marvin, S., Burrage, A.M., Sudholt, S., Rana, A., O'Connor, C., Wiethoff, C.M., Campbell, E.M., 2013. Alpha-Synuclein Induces Lysosomal Rupture and Cathepsin Dependent Reactive Oxygen Species Following Endocytosis. PLoS One 8.

Freilich, R., Betegon, M., Tse, E., Mok, S.A., Julien, O., Agard, D.A., Southworth, D.R., Takeuchi, K., Gestwicki, J.E., 2018. Competing protein-protein interactions regulate binding of Hsp27 to its client protein tau. Nat. Commun. 9, 4563.

Freundt, E.C., Maynard, N., Clancy, E.K., Roy, S., Bousset, L., Sourigues, Y., Covert, M., Melki, R., Kirkegaard, K., Brahic, M., 2012. Neuron-to-neuron transmission of α-synuclein fibrils through axonal transport. Ann. Neurol. 72, 517–524.

Fricker, L.D., McKinzie, A.A., Sun, J., Curran, E., Qian, Y., Yan, L., Patterson, S.D., Courchesne, P.L., Richards, B., Levin, N., Mzhavia, N., Devi, L.A., Douglass, J., 2000. Identification and characterization of proSAAS, a granin-like neuroendocrine peptide precursor that inhibits prohormone processing. J. Neurosci. 20, 639–648.

Frontzek, K., Lutz, M.I., Aguzzi, A., Kovacs, G.G., Budka, H., 2016. Amyloid-β pathology and cerebral amyloid angiopathy are frequent in iatrogenic Creutzfeldt-Jakob disease after dural grafting. Swiss Med. Wkly. 146, w14287.

Frost, B., Jacks, R.L., Diamond, M.I., 2009. Propagation of Tau misfolding from the outside to the inside of a cell. J. Biol. Chem. 284, 12845–12852.

Fujikake, N., Nagai, Y., Popiel, H.A., Okamoto, Y., Yamaguchi, M., Toda, T., 2008. Heat shock transcription factor 1-activating compounds suppress polyglutamine-induced neurodegeneration through induction of multiple molecular chaperones. J. Biol. Chem. 283, 26188–26197.

Fujimoto, M., Takaki, E., Hayashi, T., Kitaura, Y., Tanaka, Y., Inouye, S., Nakai, A., 2005. Active HSF1 significantly suppresses polyglutamine aggregate formation in cellular and mouse models. J. Biol. Chem. 280, 34908–34916.

Fujiwara, H., Hasegawa, M., Dohmae, N., Kawashima, A., Masliah, E., Goldberg, M.S., Shen, J., Takio, K., Iwatsubo, T., 2002. A-Synuclein Is Phosphorylated in Synucleinopathy Lesions. Nat. Cell Biol. 4, 160–164.

Gambetti, P., Kong, Q., Zou, W., Parchi, P., Chen, S.G., 2003. Sporadic and familial CJD: classification and characterisation. Br. Med. Bull. 66, 213–239.

Gao, X., Carroni, M., Nussbaum-Krammer, C., Mogk, A., Nillegoda, N.B., Szlachcic, A., Guilbride, D.L., Saibil, H.R., Mayer, M.P., Bukau, B., 2015. Human Hsp70 Disaggregase Reverses Parkinson's-Linked α-Synuclein Amyloid Fibrils. Mol. Cell 59, 781–793.

Gath, J., Bousset, L., Habenstein, B., Melki, R., Böckmann, A., Meier, B.H., 2014. Unlike twins: An NMR comparison of two α-synuclein polymorphs featuring different toxicity. PLoS One 9, 1–11.

Gaugler, J., James, B., Johnson, T., Scholz, K., Weuve, J., 2016. 2016 Alzheimer's disease facts and figures. Alzheimer's Dement. 12, 459–509.

Gauthier, L.R., Charrin, B.C., Borrell-Pagès, M., Dompierre, J.P., Rangone, H., Cordelières, F.P., De Mey, J., MacDonald, M.E., Leßmann, V., Humbert, S., Saudou, F., 2004. Huntingtin Controls Neurotrophic Support and Survival of Neurons by Enhancing BDNF Vesicular Transport along Microtubules. Cell 118, 127–138.

Gelders, G., Baekelandt, V., Van der Perren, A., 2018. Linking Neuroinflammation and Neurodegeneration in Parkinson's Disease. J. Immunol. Res. 2018, 1–12.

George, J.M., 2002. The synucleins. Genome Biol. 3, 1–6.

Gerez, J.A., Prymaczok, N.C., Rockenstein, E., Herrmann, U.S., Schwarz, P., Adame, A., Enchev, R., Courtheoux, T., Boersema, J.P., Riek, R., Peter, M., Aguzzi, A., Masliah, E., Picotti, P., 2019. A cullin-RING ubiquitin ligase targets exogenous a-synuclein and inhibits Lewy body–like pathology. Sci. Transl. Med. 11.

Ghee, M., Melki, R., Michot, N., Mallet, J., 2005. PA700, the regulatory complex of the 26S proteasome, interferes with α-synuclein assembly. FEBS J. 272, 4023–4033.

Ghosh, J.G., Houck, S.A., Clark, J.I., 2008. Interactive sequences in the molecular chaperone, human aB crystallin modulate the fibrillation of amyloidogenic proteins. Int. J. Biochem. Cell Biol. 40, 954–967.

Gibbons, G.S., Lee, V.M.Y., Trojanowski, J.Q., 2019. Mechanisms of Cell-to-Cell Transmission of Pathological Tau. JAMA Neurol. 76, 101.

Gidalevitz, T., Ben-Zvi, A., Ho, K.H., Brignull, H.R., Morimoto, R.I., 2006. Progressive disruption of cellular protein folding in models of polyglutamine diseases. Science 311, 1471–1474.

Giorgetti, S., Greco, C., Tortora, P., Aprile, F., 2018. Targeting Amyloid Aggregation: An Overview of Strategies and Mechanisms. Int. J. Mol. Sci. 19, 2677.

Goedert, M., Spillantini, M.G., 1998. Lewy body diseases and multiple system atrophy as α-synucleinopathies. Mol. Psychiatry 3, 462–465.

Goedert, M., Spillantini, M.G., 2012. Synucleinopathies and Tauopathies. In: Basic Neurochemistry. Elsevier, pp. 829–843.

Goedert, M., Spillantini, M.G., 2017. Propagation of Tau aggregates. Mol. Brain 10, 18.

Goedert, M., Wischik, C.M., Crowther, R.A., Walker, J.E., Klug, A., 1988. Cloning and sequencing of the cDNA encoding a core protein of the paired helical filament of Alzheimer disease: identification as the microtubule-associated protein tau. Proc. Natl. Acad. Sci. 85, 4051–4055.

Goldman, J.G., Postuma, R., 2014. Premotor and nonmotor features of Parkinson's disease. Curr. Opin. Neurol. 27, 434–441.

Gómez-Ramos, A., Díaz-Hernández, M., Rubio, A., Miras-Portugal, M.T., Avila, J., 2008. Extracellular tau promotes intracellular calcium increase through M1 and M3 muscarinic receptors in neuronal cells. Mol. Cell. Neurosci. 37, 673–681.

Góngora-Benítez, M., Tulla-Puche, J., Albericio, F., 2014. Multifaceted Roles of Disulfide Bonds. Peptides as Therapeutics. Chem. Rev. 114, 901–926.

Götze, M., Pettelkau, J., Schaks, S., Bosse, K., Ihling, C.H., Krauth, F., Fritzsche, R., Kühn, U., Sinz, A., 2012. StavroX-A software for analyzing crosslinked products in protein interaction studies. J. Am. Soc. Mass Spectrom. 23, 76–87.

Grad, L.I., Yerbury, J.J., Turner, B.J., Guest, W.C., Pokrishevsky, E., O'Neill, M.A., Yanai, A., Silverman, J.M., Zeineddine, R., Corcoran, L., Kumita, J.R., Luheshi, L.M., Yousefi, M., Coleman, B.M., Hill, A.F., Plotkin, S.S., Mackenzie, I.R., Cashman, N.R., 2014. Intercellular propagated misfolding of wild-type Cu/Zn superoxide dismutase occurs via exosome-dependent and -independent mechanisms. Proc. Natl. Acad. Sci. 111, 3620–3625.

Gremer, L., Schölzel, D., Schenk, C., Reinartz, E., Labahn, J., Ravelli, R.B.G., Tusche, M., Lopez-Iglesias, C., Hoyer, W., Heise, H., Willbold, D., Schröder, G.F., 2017. Fibril structure of amyloid-β(1–42) by cryo–electron microscopy. Science 358, 116–119.

Grey, M., Linse, S., Nilsson, H., Brundin, P., Sparr, E., 2011. Membrane interaction of α-synuclein in different aggregation states. J. Parkinsons. Dis. 1, 359–371.

Gribaudo, S., Tixador, P., Bousset, L., Fenyi, A., Lino, P., Melki, R., Peyrin, J.-M., Perrier, A.L., 2019. Propagation of α-Synuclein Strains within Human Reconstructed Neuronal Network. Stem Cell Reports 12, 230–244.

Grozdanov, V., Danzer, K.M., 2018. Release and uptake of pathologic alpha-synuclein. Cell Tissue Res. 373, 175–182.

Guan, Y.-X., Fei, Z.-Z., Luo, M., Yao, S.-J., Cho, M.-G., 2005. Production of Minichaperone (sht GroEL191-345) and Its Function in the Refolding of Recombinant Human Interferon Gamma. Protein Pept. Lett. 12, 85–88.

Guerrero-Ferreira, R., Taylor, N.M.I., Arteni, A.-A., Kumari, P., Mona, D., Ringler, P., Britschgi, M., Lauer, M.E., Makky, A., Verasdonck, J., Riek, R., Melki, R., Meier, B.H., Böckmann, A., Bousset, L., Stahlberg, H., 2019. Two new polymorphic structures of human full-length alpha-synuclein fibrils solved by cryo-electron microscopy. Elife 8, 654582.

Guerrero-Ferreira, R., Taylor, N.M., Mona, D., Ringler, P., Lauer, M.E., Riek, R., Britschgi, M., Stahlberg, H., 2018. Cryo-EM structure of alpha-synuclein fibrils. Elife 7, 1–18.

Guo, J.L., Lee, V.M.Y., 2011. Seeding of Normal Tau by Pathological Tau Conformers Drives Pathogenesis of Alzheimer-like Tangles. J. Biol. Chem. 286, 15317–15331.

Guo, J.L., Lee, V.M.Y., 2014. Cell-to-cell transmission of pathogenic proteins in neurodegenerative diseases. Nat. Med. 20, 130–138.

Guo, J.L., Narasimhan, S., Changolkar, L., He, Z., Stieber, A., Zhang, B., Gathagan, R.J., Iba, M., McBride, J.D., Trojanowski, J.Q., Lee, V.M.Y., 2016. Unique pathological tau conformers from Alzheimer's brains transmit tau pathology in nontransgenic mice. J. Exp. Med. 213, 2635–2654.

Gurry, T., Ullman, O., Fisher, C.K., Perovic, I., Pochapsky, T., Stultz, C.M., 2013. The dynamic structure of α-synuclein multimers. J. Am. Chem. Soc. 135, 3865–3872.

Halliday, G., Hely, M., Reid, W., Morris, J., 2008. The progression of pathology in longitudinally followed patients with Parkinson's disease. Acta Neuropathol. 115, 409–415.

Hansen, C., Angot, E., Bergström, A., Steiner, J. a, Pieri, L., Paul, G., Outeiro, T.F., Melki, R., Kallunki, P., Fog, K., 2011. α-Synuclein propagates from mouse brain to grafted dopaminergic neurons and seeds aggregation in cultured human cells. J. Clin. Invest. 121, 715–725.

Hanspal, M.A., Dobson, C.M., Yerbury, J.J., Kumita, J.R., 2017. The relevance of contact-independent cell-to-cell transfer of TDP-43 and SOD1 in amyotrophic lateral sclerosis. BBA - Mol. Basis Dis. 1863, 2762–2771.

Hartl, F.U., Hayer-Hartl, M., 2002. Protein folding. Molecular chaperones in the cytosol: From nascent chain to folded protein. Science 295, 1852–1858.

Hartl, F.U., Hayer-Hartl, M., 2009. Converging concepts of protein folding in vitro and in vivo. Nat. Struct. Mol. Biol. 16, 574–581.

Hashimura, T., Kimura, T., Miyakawa, T., 1991. Morphological Changes of Blood Vessels in the Brain with Alzheimer's Disease. Psychiatry Clin. Neurosci. 45, 661–665.

Haslbeck, M., Weinkauf, S., Buchner, J., 2018. Small heat shock proteins: Simplicity meets complexity. J. Biol. Chem. 294, 2121–2132.

Hayden, M.R., Leavitt, B.R., Yasothan, U., Kirkpatrick, P., 2009. Tetrabenazine. Nat. Rev. Drug Discov. 8, 17–18.

Hebron, M.L., Lonskaya, I., Moussa, C.E.H., 2013. Nilotinib reverses loss of dopamine neurons and improvesmotorbehavior via autophagic degradation of α-synuclein in parkinson's disease models. Hum. Mol. Genet. 22, 3315–3328.

Heitz, F., Morris, M.C., Divita, G., 2009. Twenty years of cell-penetrating peptides : from molecular mechanisms to therapeutics. Br. J. Pharmacol. 157, 195–206.

Hellstrand, E., Nowacka, A., Topgaard, D., Linse, S., Sparr, E., 2013. Membrane Lipid Co-Aggregation with α-Synuclein Fibrils. PLoS One 8.

Herczenik, E., Gebbink, M.F.B.G., 2008. Molecular and cellular aspects of protein misfolding and disease. FASEB J. 22, 2115–2133.

Hershey, L.A., Coleman-Jackson, R., 2019. Pharmacological Management of Dementia with Lewy Bodies. Drugs and Aging 36, 309–319.

Hill, M.D., Martin, R.H., Mikulis, D., Wong, J.H., Silver, F.L., terBrugge, K.G., Milot, G., Clark, W.M., MacDonald, R.L., Kelly, M.E., Boulton, M., Fleetwood, I., McDougall, C., Gunnarsson, T., Chow, M., Lum, C., Dodd, R., Poublanc, J., Krings, T., Demchuk, A.M., Goyal, M., Anderson, R., Bishop, J., Garman, D., Tymianski, M., 2012. Safety and efficacy of NA-1 in patients with iatrogenic stroke after endovascular aneurysm repair (ENACT): A phase 2, randomised, double-blind, placebo-controlled trial. Lancet Neurol. 11, 942–950.

Hitti, F.L., Ramayya, A.G., McShane, B.J., Yang, A.I., Vaughan, K.A., Baltuch, G.H., 2019. Long-term outcomes following deep brain stimulation for Parkinson's disease. J. Neurosurg. 1–6.

Hochberg, G.K. a, Ecroyd, H., Liu, C., Cox, D., Cascio, D., Sawaya, M.R., Collier, M.P., Stroud, J., Carver, J. a, Baldwin, A.J., Robinson, C. V, Eisenberg, D.S., Benesch, J.L.P., Laganowsky, A., 2014. The structured core domain of B-crystallin can prevent amyloid fibrillation and associated toxicity. Proc. Natl. Acad. Sci. 111, E1562–E1570.

Hoffner, G., Island, M.-L., Djian, P., 2005. Purification of neuronal inclusions of patients with Huntington's disease reveals a broad range of N-terminal fragments of expanded huntingtin and insoluble polymers. J. Neurochem. 95, 125–136.

Holley, S.M., Kamdjou, T., Reidling, J.C., Fury, B., Coleal-Bergum, D., Bauer, G., Thompson, L.M., Levine, M.S., Cepeda, C., 2018. Therapeutic effects of stem cells in rodent models of Huntington's disease: Review and electrophysiological findings. CNS Neurosci. Ther. 24, 329–342.

Holmes, B.B., DeVos, S.L., Kfoury, N., Li, M., Jacks, R., Yanamandra, K., Ouidja, M.O., Brodsky, F.M., Marasa, J., Bagchi, D.P., Kotzbauer, P.T., Miller, T.M., Papy-Garcia, D., Diamond, M.I., 2013. Heparan sulfate proteoglycans mediate internalization and propagation of specific proteopathic seeds. Proc. Natl. Acad. Sci. 110, E3138–E3147.

Holmqvist, S., Chutna, O., Bousset, L., Aldrin-Kirk, P., Li, W., Björklund, T., Wang, Z.Y., Roybon, L., Melki, R., Li, J.Y., 2014. Direct evidence of Parkinson pathology spread from the gastrointestinal tract to the brain in rats. Acta Neuropathol. 128, 805–820.

Hoop, C.L., Lin, H.-K., Kar, K., Magyarfalvi, G., Lamley, J.M., Boatz, J.C., Mandal, A., Lewandowski, J.R., Wetzel, R., van der Wel, P.C.A., 2016. Huntingtin exon 1 fibrils feature an interdigitated β-hairpin–based polyglutamine core. Proc. Natl. Acad. Sci. 113, 1546–1551.

Horonchik, L., Tzaban, S., Ben-Zaken, O., Yedidia, Y., Rouvinski, A., Papy-Garcia, D., Barritault, D., Vlodavsky, I., Taraboulos, A., 2005. Heparan sulfate is a cellular receptor for purified infectious prions. J. Biol. Chem. 280, 17062–17067.

Hoshino, A., Helwig, M., Rezaei, S., Berridge, C., Eriksen, J.L., Lindberg, I., 2014. A novel function for proSAAS as an amyloid anti-aggregant in Alzheimer's disease. J. Neurochem. 128, 419–430.

Huang, C., Cheng, H., Hao, S., Zhou, H., Zhang, X., Gao, J., Sun, Q.H., Hu, H., Wang, C. chen, 2006. Heat Shock Protein 70 Inhibits α-synuclein Fibril Formation via Interactions with Diverse Intermediates. J. Mol. Biol. 364, 323–336.

Huntington's Disease Collaborative Research Group, Macdonald, M.E., Ambrose, C.M., Duyao, M.P., Myers, R.H., Lin, C., Srinidhi, L., Barnes, G., Taylor, S.A., James, M., Groat, N., Macfarlane, H., Jenkins, B., Anderson, M.A., Wexler, N.S., Gusella, J.F., Riba-ramirer, L., Shah, M., Stanton, V.P., Strobel, S.A., Draths, K.M., Wales, J.L., Dervan, P., Housman, D.E., Fielder, T., Wasmuth, J.J., Tagle, D., Valdes, J., Elmer, L., Allard, M., Castilla, L., Swaroop, M., Blanchard, K., Bates, G.P., Baxendale, S., Hummerich, H., Kirby, S., North, M., Youngman, S., Mott, R., Zehetner, G., Sedlacek, Z., Snell, R., Holloway, T., Gillespie, K., Datson, N., Shaw, D., Harper, P.S., 1993. A novel gene containing a trinucleotide repeat that is expanded and unstable on Huntington's disease chromosomes. The Huntington's Disease Collaborative Research Group. Cell 72, 971–

983.

Huntington, G., 1872. On Chorea. Med. Surg. Rep. 26, 320–321.

Huntington Study Group, 2006. Tetrabenazine as antichorea therapy in Huntington disease: A randomized controlled trial. Neurology 66, 366–372.

Ibáñez, P., Bonnet, A.-M., Débarges, B., Lohmann, E., Tison, F., Agid, Y., Dürr, A., Brice, A., Pollak, P., 2004. Causal relation between alpha-synuclein locus duplication as a cause of familial Parkinson's disease. Lancet 364, 1169–1171.

Ihse, E., Yamakado, H., Van Wijk, X.M., Lawrence, R., Esko, J.D., Masliah, E., 2017. Cellular internalization of alpha-synuclein aggregates by cell surface heparan sulfate depends on aggregate conformation and cell type. Sci. Rep. 7, 1–10.

Iqbal, K., Liu, F., Gong, C.X., 2016. Tau and neurodegenerative disease: The story so far. Nat. Rev. Neurol. 12, 15–27.

Iwaki, T., Wisniewski, T., Iwaki, A., Corbin, E., Tomokane, N., Tateishi, J., Goldman, J.E., 1992. Accumulation of alpha B-crystallin in central nervous system glia and neurons in pathologic conditions. Am. J. Pathol. 140, 345–56.

Jackson, S.J., Kerridge, C., Cooper, J., Cavallini, A., Falcon, B., Cella, C. V., Landi, A., Szekeres, P.G., Murray, T.K., Ahmed, Z., Goedert, M., Hutton, M., O'Neill, M.J., Bose, S., 2016. Short Fibrils Constitute the Major Species of Seed-Competent Tau in the Brains of Mice Transgenic for Human P301S Tau. J. Neurosci. 36, 762–772.

Jakes, R., Spillantini, M.G., Goedert, M., 1994. Identification of two distinct synucleins from human brain. FEBS Lett. 345, 27–32.

Jana, N.R., Dikshit, P., Goswami, A., Kotliarova, S., Murata, S., Tanaka, K., Nukina, N., 2005. Co-chaperone CHIP associates with expanded polyglutamine protein and promotes their degradation by proteasomes. J. Biol. Chem. 280, 11635–11640.

Jankovic, J., Goodman, I., Safirstein, B., Marmon, T.K., Schenk, D.B., Koller, M., Zago, W., Ness, D.K., Griffith, S.G., Grundman, M., Soto, J., Ostrowitzki, S., Boess, F.G., Martin-Facklam, M., Quinn, J.F., Isaacson, S.H., Omidvar, O., Ellenbogen, A., Kinney, G.G., 2018. Safety and Tolerability of Multiple Ascending Doses of PRX002/RG7935, an Anti–α-Synuclein Monoclonal Antibody, in Patients With Parkinson Disease. JAMA Neurol. 75, 1206.

Jarosz-Griffiths, H.H., Noble, E., Rushworth, J. V., Hooper, N.M., 2016. Amyloid-β receptors: The good, the bad, and the prion protein. J. Biol. Chem. 291, 3174–3183.

Jarvela, T.S., Lam, H.A., Helwig, M., Lorenzen, N., Otzen, D.E., McLean, P.J., Maidment, N.T., Lindberg, I., 2016. The neural chaperone proSAAS blocks α-synuclein fibrillation and neurotoxicity. Proc. Natl. Acad. Sci. 113, E4708–E4715.

Jaunmuktane, Z., Mead, S., Ellis, M., Wadsworth, J.D.F., Nicoll, A.J., Kenny, J., Launchbury, F., Linehan, J., Richard-Loendt, A., Walker, A.S., Rudge, P., Collinge, J., Brandner, S., 2015. Evidence for human transmission of amyloid-β pathology and cerebral amyloid angiopathy. Nature 525, 247–250.

Jehle, S., Rajagopal, P., Bardiaux, B., Markovic, S., Kühne, R., Stout, J.R., Higman, V.A., Klevit, R.E., van Rossum, B.-J., Oschkinat, H., 2010. Solid-state NMR and SAXS studies provide a structural basis for the activation of αB-crystallin oligomers. Nat. Struct. Mol. Biol. 17, 1037–1042.

Jehle, S., Vollmar, B.S., Bardiaux, B., Dove, K.K., Rajagopal, P., Gonen, T., Oschkinat, H., Klevit, R.E., 2011. N-terminal domain of B-crystallin provides a conformational switch for multimerization and structural heterogeneity. Proc. Natl. Acad. Sci. 108, 6409–6414.

Jeon, I., Cicchetti, F., Cisbani, G., Lee, S., Li, E., Bae, J., Lee, N., Li, L., Im, W., Kim, M., Sook, H., Hun, S., Tae, O., Kim, A., Jae, J., Benoit, K., Abid, A., 2016. Human - to - mouse prion - like propagation of mutant huntingtin protein. Acta Neuropathol. 132, 577–

592.

Jeon, I., Lee, N., Li, J.Y., Park, I.H., Park, K.S., Moon, J., Shim, S.H., Choi, C., Chang, D.J., Kwon, J., Oh, S.H., Shin, D.A., Kim, H.S., Do, J.T., Lee, D.R., Kim, M., Kang, K.S., Daley, G.Q., Brundin, P., Song, J., 2012. Neuronal properties, in vivo effects, and pathology of a Huntington's disease patient-derived induced pluripotent stem cells. Stem Cells 30, 2054–2062.

Ji, Y. Bin, Zhuang, P.P., Ji, Z., Wu, Y.M., Gu, Y., Gao, X.Y., Pan, S.Y., Hu, Y.F., 2017. TFP5 peptide, derived from CDK5-activating cofactor p35, provides neuroprotection in early-stage of adult ischemic stroke. Sci. Rep. 7, 3–9.

Jiang, J., Ballinger, C.A., Wu, Y., Dai, Q., Cyr, D.M., Höhfeld, J., Patterson, C., 2001. CHIP Is a U-box-dependent E3 Ubiquitin Ligase. J. Biol. Chem. 276, 42938–42944.

Jiang, Y.Q., Wang, X.L., Cao, X.H., Ye, Z.Y., Li, L., Cai, W.Q., 2013. Increased heat shock transcription factor 1 in the cerebellum reverses the deficiency of Purkinje cells in Alzheimer's disease. Brain Res. 1519, 105–111.

Jicha, G.A., Lane, E., Vincent, I., Otvos, L., Hoffmann, R., Davies, P., 2002. A Conformation- and Phosphorylation-Dependent Antibody Recognizing the Paired Helical Filaments of Alzheimer's Disease. J. Neurochem. 69, 2087–2095.

Johnson, R.T., Gibbs, C.J., 1998. Creutzfeldt–Jakob Disease and Related Transmissible Spongiform Encephalopathies. N. Engl. J. Med. 339, 1994–2004.

Johnson, G.V.W., Stoothoff, W.H., 2004. Tau phosphorylation in neuronal cell function and dysfunction. J. Cell Sci. 117, 5721–5729.

Jones, D.R., Moussaud, S., McLean, P., 2014. Targeting heat shock proteins to modulate a-synuclein toxicity. Ther. Adv. Neurol. Disord. 7, 33–51.

Jucker, M., Walker, L.C., 2013. Self-propagation of pathogenic protein aggregates in neurodegenerative diseases. Nature 501, 45–51.

Junttila, A., Kuvaja, M., Hartikainen, P., Siloaho, M., Helisalmi, S., Moilanen, V., Kiviharju, A., Jansson, L., Tienari, P.J., Remes, A.M., Herukka, S.K., 2016. Cerebrospinal Fluid TDP-43 in Frontotemporal Lobar Degeneration and Amyotrophic Lateral Sclerosis Patients with and without the C9ORF72 Hexanucleotide Expansion. Dement. Geriatr. Cogn. Dis. Extra 6, 142–149.

Kalia, L. V., Kalia, S.K., Chau, H., Lozano, A.M., Hyman, B.T., McLean, P.J., 2011. Ubiquitinylation of α-Synuclein by Carboxyl Terminus Hsp70-Interacting Protein (CHIP) Is Regulated by Bcl-2-Associated Athanogene 5 (BAG5). PLoS One 6, e14695.

Kalia, L. V, Lang, A.E., 2015. Parkinson's Disease. Lancet 103, 337–350.

Kalia, S.K., Sankar, T., Lozano, A.M., 2013. Deep brain stimulation for Parkinson's disease and other movement disorders. Curr. Opin. Neurol. 26, 374–380.

Kametani, F., Hasegawa, M., 2018. Reconsideration of amyloid hypothesis and tau hypothesis in Alzheimer's disease. Front. Neurosci. 12.

Karch, C.M., Goate, A.M., 2015. Alzheimer's Disease Risk Genes and Mechanisms of Disease Pathogenesis. Biol. Psychiatry 77, 43–51.

Karlawish, J., Jack, C.R., Rocca, W.A., Snyder, H.M., Carrillo, M.C., 2017. Alzheimer's disease: The next frontier—Special Report 2017. Alzheimer's Dement. 13, 374–380.

Katzeff, J.S., Phan, K., Purushothuman, S., Halliday, G.M., Kim, W.S., 2019. Cross-examining candidate genes implicated in multiple system atrophy. Acta Neuropathol. Commun. 7, 1–7.

Kaufman, S.K., Sanders, D.W., Thomas, T.L., Ruchinskas, A.J., Vaquer-Alicea, J., Sharma, A.M., Miller, T.M., Diamond, M.I., 2016. Tau Prion Strains Dictate Patterns of Cell Pathology, Progression Rate, and Regional Vulnerability In Vivo. Neuron 92, 796–812.

Kaufman, S.K., Thomas, T.L., Del Tredici, K., Braak, H., Diamond, M.I., 2017. Characterization of tau prion seeding activity and strains from formaldehyde-fixed tissue. Acta Neuropathol. Commun. 5, 41.

Kegel, K.B., Sapp, E., Alexander, J., Valencia, A., Reeves, P., Li, X., Masso, N., Sobin, L., Aronin, N., DiFiglia, M., 2009. Polyglutamine expansion in huntingtin alters its interaction with phospholipids. J. Neurochem. 110, 1585–1597.

Kegel, K.B., Sapp, E., Yoder, J., Cuiffo, B., Sobin, L., Kim, Y.J., Qin, Z.H., Hayden, M.R., Aronin, N., Scott, D.L., Isenberg, G., Goldmann, W.H., DiFiglia, M., 2005. Huntingtin associates with acidic phospholipids at the plasma membrane. J. Biol. Chem. 280, 36464–36473.

Kelly, S.M., Jess, T.J., Price, N.C., 2005. How to study proteins by circular dichroism. Biochim. Biophys. Acta - Proteins Proteomics 1751, 119–139.

Kfoury, N., Holmes, B.B., Jiang, H., Holtzman, D.M., Diamond, M.I., 2012. Trans-cellular Propagation of Tau Aggregation by Fibrillar Species. J. Biol. Chem. 287, 19440–19451.

Kikuchi, K., Arawaka, S., Koyama, S., Kimura, H., Ren, C.H., Wada, M., Kawanami, T., Kurita, K., Daimon, M., Kawakatsu, S., Kadoya, T., Goto, K., Kato, T., 2003. An N-terminal fragment of ProSAAS (a granin-like neuroendocrine peptide precursor) is associated with tau inclusions in Pick's disease. Biochem. Biophys. Res. Commun. 308, 646–654.

Kim, S., Kwon, S.-H., Kam, T.-I., Panicker, N., Karuppagounder, S.S., Lee, S., Lee, J.H., Kim, W.R., Kook, M., Foss, C.A., Shen, C., Lee, H., Kulkarni, S., Pasricha, P.J., Lee, G., Pomper, M.G., Dawson, V.L., Dawson, T.M., Ko, H.S., 2019. Transneuronal Propagation of Pathologic α-Synuclein from the Gut to the Brain Models Parkinson's Disease. Neuron 1–15.

Klementiev, B., Li, S., Korshunova, I., Dmytriyeva, O., Pankratova, S., Walmod, P.S., Kjær, L.K., Dahllöf, M.S., Lundh, M., Christensen, D.P., Mandrup-Poulsen, T., Bock, E., Berezin, V., 2014. Anti-inflammatory properties of a novel peptide interleukin 1 receptor antagonist. J. Neuroinflammation 11, 1–18.

Knowles, T.P.J.J., Vendruscolo, M., Dobson, C.M., 2014. The amyloid state and its association with protein misfolding diseases. Nat. Rev. Mol. Cell Biol. 15, 384–396.

Ko, J., Isas, J.M., Sabbaugh, A., Yoo, J.H., Pandey, N.K., Chongtham, A., Ladinsky, M., Wu, W.-L., Rohweder, H., Weiss, A., Macdonald, D., Munoz-Sanjuan, I., Langen, R., Patterson, P.H., Khoshnan, A., 2018. Identification of distinct conformations associated with monomers and fibril assemblies of mutant huntingtin. Hum. Mol. Genet. 27, 2330–2343.

Kobayashi, J., Hasegawa, T., Sugeno, N., Yoshida, S., Akiyama, T., Fujimori, K., Hatakeyama, H., Miki, Y., Tomiyama, A., Kawata, Y., Fukuda, M., Kawahata, I., Yamakuni, T., Ezura, M., Kikuchi, A., Baba, T., Takeda, A., Kanzaki, M., Wakabayashi, K., Okano, H., Aoki, M., 2019. Extracellular α-synuclein enters dopaminergic cells by modulating flotillin-1–assisted dopamine transporter endocytosis. FASEB J. 33, 10240–10256.

Koh, Y.H., Tan, L.Y., Ng, S.Y., 2018. Patient-derived induced pluripotent stem cells and organoids for modeling alpha synuclein propagation in parkinson's disease. Front. Cell. Neurosci. 12, 1–12.

Kordower, J.H., Chu, Y., Hauser, R.A., Freeman, T.B., Olanow, C.W., 2008. Lewy body-like pathology in long-term embryonic nigral transplants in Parkinson's disease. Nat. Med. 14, 504–506.

Kordower, J.H., Dodiya, H.B., Kordower, A.M., Terpstra, B., Paumier, K., Madhavan, L., Sortwell, C., Steece-Collier, K., Collier, T.J., 2011. Transfer of host-derived alpha synuclein to grafted dopaminergic neurons in rat. Neurobiol. Dis. 43, 552–557.

Kovacs, G.G., 2015. Invited review: Neuropathology of tauopathies: Principles and practice. Neuropathol. Appl. Neurobiol. 41, 3–23.

Kovacs, G.G., Lutz, M.I., Ricken, G., Ströbel, T., Höftberger, R., Preusser, M., Regelsberger, G., Hönigschnabl, S., Reiner, A., Fischer, P., Budka, H., Hainfellner, J.A., 2016. Dura mater is a potential source of Aβ seeds. Acta Neuropathol. 131, 911–923.

Kovacs, G.G., Rahimi, J., Ströbel, T., Lutz, M.I., Regelsberger, G., Streichenberger, N., Perret-Liaudet, A., Höftberger, R., Liberski, P.P., Budka, H., Sikorska, B., 2017. Tau pathology in Creutzfeldt-Jakob disease revisited. Brain Pathol. 27, 332–344.

Kraus, A., Groveman, B.R., Caughey, B., 2013. Prions and the Potential Transmissibility of Protein Misfolding Diseases. Annu. Rev. Microbiol. 67, 543–564.

Kudo, H., Liu, J., Jansen, E.J.R., Ozawa, A., Panula, P., Martens, G.J.M., Lindberg, I., 2009. Identification of proSAAS homologs in lower vertebrates: Conservation of hydrophobic helices and convertase-Inhibiting sequences. Endocrinology 150, 1393–1399.

Kuiper, E.F.E., de Mattos, E.P., Jardim, L.B., Kampinga, H.H., Bergink, S., 2017. Chaperones in polyglutamine aggregation: Beyond the Q-stretch. Front. Neurosci. 11, 1–11.

Kumar, V., Sami, N., Kashav, T., Islam, A., Ahmad, F., Hassan, M.I., 2016. Protein aggregation and neurodegenerative diseases: From theory to therapy. Eur. J. Med. Chem. 124, 1105–1120.

Kumar, R.S., Sharma, K.K., 2000. Chaperone-like activity of a synthetic peptide toward oxidized γ-crystallin. J. Pept. Res. 56, 157–164.

Kumar, N., Van Gerpen, J.A., Bower, J.H., Ahlskog, J.E., 2005. Levodopa-dyskinesia incidence by age of Parkinson's disease onset. Mov. Disord. 20, 342–344.

Kundel, F., De, S., Flagmeier, P., Horrocks, M.H., Kjaergaard, M., Shammas, S.L., Jackson, S.E., Dobson, C.M., Klenerman, D., 2018. Hsp70 Inhibits the Nucleation and Elongation of Tau and Sequesters Tau Aggregates with High Affinity. ACS Chem. Biol. 13, 636–646.

Kurnellas, M.P., Brownell, S.E., Su, L., Malkovskiy, a. V., Rajadas, J., Dolganov, G., Chopra, S., Schoolnik, G.K., Sobel, R. a., Webster, J., Ousman, S.S., Becker, R. a., Steinman, L., Rothbard, J.B., 2012. Chaperone Activity of Small Heat Shock Proteins Underlies Therapeutic Efficacy in Experimental Autoimmune Encephalomyelitis. J. Biol. Chem. 287, 36423–36434.

Kurowska, Z., Englund, E., Widner, H., Lindvall, O., Li, J.Y., Brundin, P., 2011. Signs of degeneration in 12-22-year old grafts of mesencephalic dopamine neurons in patients with Parkinson's disease. J. Parkinsons. Dis. 1, 83–92.

Labbadia, J., Morimoto, R.I., 2014. Proteostasis and longevity: When does aging really begin? F1000Prime Rep. 6.

Labbadia, J., Novoselov, S.S., Bett, J.S., Weiss, A., Paganetti, P., Bates, G.P., Cheetham, M.E., 2012. Suppression of protein aggregation by chaperone modification of high molecular weight complexes. Brain 135, 1180–1196.

Lakhani, V. V., Ding, F., Dokholyan, N. V., 2010. Polyglutamine Induced Misfolding of Huntingtin Exon1 is Modulated by the Flanking Sequences. PLoS Comput. Biol. 6, e1000772.

Langbehn, D.R., Hayden, M.R., Paulsen, J.S., 2010. CAG-repeat length and the age of onset in Huntington disease (HD): A review and validation study of statistical approaches. Am. J. Med. Genet. Part B Neuropsychiatr. Genet. 153B, 397–408.

Langston, J.W., Ballard, P., Tetrud, J.W., Irwin, I., 1983. Chronic Parkinsonism in humans due to a product of meperidine-analog synthesis. Science 219, 979–80.

Lasagna-Reeves, C.A., Castillo-Carranza, D.L., Sengupta, U., Guerrero-Munoz, M.J., Kiritoshi, T., Neugebauer, V., Jackson, G.R., Kayed, R., 2012. Alzheimer brain-derived tau

oligomers propagate pathology from endogenous tau. Sci. Rep. 2, 700.

Lau, J.L., Dunn, M.K., 2018. Therapeutic peptides: Historical perspectives, current development trends, and future directions. Bioorganic Med. Chem. 26, 2700–2707.

Lee, S.J., Desplats, P., Sigurdson, C., Tsigelny, I., Masliah, E., 2010a. Cell-to-cell transmission of non-prion protein aggregates. Nat. Rev. Neurol. 6, 702–706.

Lee, V.M.-Y., Goedert, M., Trojanowski, J.Q., 2001. Neurodegenerative Tauopathies. Annu. Rev. Neurosci. 24, 1121–1159.

Lee, H.-J., Patel, S., Lee, S.-J., 2005. Intravesicular Localization and Exocytosis of a-Synuclein and its Aggregates. J. Neurosci. 25, 6016–6024.

Lee, H.J., Suk, J.E., Bae, E.J., Lee, S.J., 2008a. Clearance and deposition of extracellular α-synuclein aggregates in microglia. Biochem. Biophys. Res. Commun. 372, 423–428.

Lee, H.J., Suk, J.E., Bae, E.J., Lee, J.H., Paik, S.R., Lee, S.J., 2008b. Assembly-dependent endocytosis and clearance of extracellular α-synuclein. Int. J. Biochem. Cell Biol. 40, 1835–1849.

Lee, H.-J., Suk, J.-E., Lee, K.-W., Park, S.-H., Blumbergs, P.C., Gai, W.-P., Lee, S.-J., 2011. Transmission of Synucleinopathies in the Enteric Nervous System of A53T Alpha-Synuclein Transgenic Mice. Exp. Neurobiol. 20, 181.

Lee, H.J., Suk, J.E., Patrick, C., Bae, E.J., Cho, J.H., Rho, S., Hwang, D., Masliah, E., Lee, S.J., 2010b. Direct transfer of α-synuclein from neuron to astroglia causes inflammatory responses in synucleinopathies. J. Biol. Chem. 285, 9262–9272.

Leitner, A., Reischl, R., Walzthoeni, T., Herzog, F., Bohn, S., Förster, F., Aebersold, R., 2012. Expanding the chemical cross-linking toolbox by the use of multiple proteases and enrichment by size exclusion chromatography. Mol. Cell. Proteomics 11, 1–12.

Leuzy, A., Chiotis, K., Lemoine, L., Gillberg, P.-G., Almkvist, O., Rodriguez-Vieitez, E., Nordberg, A., 2019. Tau PET imaging in neurodegenerative tauopathies—still a challenge. Mol. Psychiatry 24, 1112–1134.

Li, K.S., Chen, G., Mo, J., Huang, R.Y., Deyanova, E.G., Beno, B.R., O'Neil, S.R., Tymiak, A.A., Gross, M.L., 2017. Orthogonal Mass Spectrometry-Based Footprinting for Epitope Mapping and Structural Characterization: The IL-6 Receptor upon Binding of Protein Therapeutics. Anal. Chem. 89, 7742–7749.

Li, J.Y., Englund, E., Holton, J.L., Soulet, D., Hagell, P., Lees, A.J., Lashley, T., Quinn, N.P., Rehncrona, S., Björklund, A., Widner, H., Revesz, T., Lindvall, O., Brundin, P., 2008. Lewy bodies in grafted neurons in subjects with Parkinson's disease suggest host-to-graft disease propagation. Nat. Med. 14, 501–503.

Li, W., Englund, E., Widner, H., Mattsson, B., van Westen, D., Lätt, J., Rehncrona, S., Brundin, P., Björklund, A., Lindvall, O., Li, J.-Y., 2016. Extensive graft-derived dopaminergic innervation is maintained 24 years after transplantation in the degenerating parkinsonian brain. Proc. Natl. Acad. Sci. 113, 6544–6549.

Li, T., Feng, Y., Yang, R., Wu, L., Li, R., Huang, L., Yang, Q., Chen, J., 2018a. Salidroside Promotes the Pathological α-Synuclein Clearance Through Ubiquitin-Proteasome System in SH-SY5Y Cells. Front. Pharmacol. 9, 377.

Li, B., Ge, P., Murray, K.A., Sheth, P., Zhang, M., Nair, G., Sawaya, M.R., Shin, W.S., Boyer, D.R., Ye, S., Eisenberg, D.S., Zhou, Z.H., Jiang, L., 2018b. Cryo-EM of full-length α-synuclein reveals fibril polymorphs with a common structural kernel. Nat. Commun. 9, 1–10.

Li, S.H., Li, X.J., 1998. Aggregation of N-terminal huntingtin is dependent on the length of its glutamine repeats. Hum. Mol. Genet. 7, 777–782.

Li, L., Wan, T., Wan, M., Liu, B., Cheng, R., Zhang, R., 2015. The effect of the size of

fluorescent dextran on its endocytic pathway. Cell Biol. Int. 39, 531–539.

Liangliang, X., Yonghui, H., Shunmei, E., Shoufang, G., Wei, Z., Jiangying, Z., 2010. Dominant-positive HSF1 decreases alpha-synuclein level and alpha-synuclein-induced toxicity. Mol. Biol. Rep. 37, 1875–1881.

Liberski, P.P., Gajos, A., Sikorska, B., Lindenbaum, S., 2019. Kuru, the first human prion disease. Viruses 11.

Lim, J.P., Gleeson, P.A., 2011. Macropinocytosis: An endocytic pathway for internalising large gulps. Immunol. Cell Biol. 89, 836–843.

Lin, H.K., Boatz, J.C., Krabbendam, I.E., Kodali, R., Hou, Z., Wetzel, R., Dolga, A.M., Poirier, M.A., Van Der Wel, P.C.A., 2017. Fibril polymorphism affects immobilized non-amyloid flanking domains of huntingtin exon1 rather than its polyglutamine core. Nat. Commun. 8, 1–12.

Lindberg, I., Shorter, J., Wiseman, R.L., Chiti, F., Dickey, C.A., McLean, P.J., 2015. Chaperones in Neurodegeneration. J. Neurosci. 35, 13853–13859.

Lindvall, O., 2015. Treatment of Parkinson's disease using cell transplantation. Philos. Trans. R. Soc. B Biol. Sci. 370, 20140370.

Lise, S., Jones, D.T., 2005. Sequence patterns associated with disordered regions in proteins. Proteins Struct. Funct. Genet. 58, 144–150.

Liu, Z., Wang, C., Li, Y., Zhao, C., Li, T., Li, D., Zhang, S., Liu, C., 2018. Mechanistic insights into the switch of αB-crystallin chaperone activity and self-multimerization. J. Biol. Chem. 293, 14880–14890.

Liu, J., Zhou, Y., Wang, Y., Fong, H., Murray, T.M., Zhang, J., 2007. Identification of proteins involved in microglial endocytosis of α-synuclein. J. Proteome Res. 6, 3614–3627.

Lohmann, S., Bernis, M.E., Tachu, B.J., Ziemski, A., Grigoletto, J., Tamgüney, G., 2019. Oral and intravenous transmission of α-synuclein fibrils to mice. Acta Neuropathol. 138, 515–533.

López-González, I., Carmona, M., Arregui, L., Kovacs, G.G., Ferrer, I., 2014. αB-crystallin and HSP27 in glial cells in tauopathies. Neuropathology 34, 517–526.

Loria, F., Vargas, J.Y., Bousset, L., Syan, S., Salles, A., Melki, R., Zurzolo, C., 2017. α-Synuclein transfer between neurons and astrocytes indicates that astrocytes play a role in degradation rather than in spreading. Acta Neuropathol. 134, 789–808.

Lugaresi, E., Tobler, I., Gambetti, P., Montagna, P., 2006. The Pathophysiology of Fatal Familial Insomnia. Brain Pathol. 8, 521–526.

Luk, K.C., Kehm, V.M., Zhang, B., O'Brien, P., Trojanowski, J.Q., Lee, V.M.Y., 2012. Intracerebral inoculation of pathological α-synuclein initiates a rapidly progressive neurodegenerative α-synucleinopathy in mice. J. Exp. Med. 209, 975–986.

Luk, K.C., Song, C., O'Brien, P., Stieber, A., Branch, J.R., Brunden, K.R., Trojanowski, J.Q., Lee, V.M.-Y., 2009. Exogenous a-synuclein fibrils seed the formation of Lewy body-like intracellular inclusions in cultured cells. Proc. Natl. Acad. Sci. 106, 20051–20056.

Lutter, L., Serpell, C.J., Tuite, M.F., Xue, W.-F., 2019. The molecular lifecycle of amyloid – Mechanism of assembly, mesoscopic organisation, polymorphism, suprastructures, and biological consequences. Biochim. Biophys. Acta - Proteins Proteomics 1867, 140257.

Mack, K.L., Shorter, J., 2016. Engineering and Evolution of Molecular Chaperones and Protein Disaggregases with Enhanced Activity. Front. Mol. Biosci. 3.

Mackenzie, G., Will, R., 2017. Creutzfeldt-Jakob disease: recent developments. F1000Research 6, 2053.

Mahapatra, R.K., Edwards, M.J., Schott, J.M., Bhatia, K.P., 2004. Corticobasal degeneration.

Lancet Neurol. 3, 736–743.

Mahul-Mellier, A.-L., Vercruysse, F., Maco, B., Ait-Bouziad, N., De Roo, M., Muller, D., Lashuel, H.A., 2015. Fibril growth and seeding capacity play key roles in α-synuclein-mediated apoptotic cell death. Cell Death Differ. 22, 2107–2122.

Mainz, A., Peschek, J., Stavropoulou, M., Back, K.C., Bardiaux, B., Asami, S., Prade, E., Peters, C., Weinkauf, S., Buchner, J., Reif, B., 2015. The chaperone αB-crystallin uses different interfaces to capture an amorphous and an amyloid client. Nat. Struct. Mol. Biol. 22, 898–905.

Maiti, P., Manna, J., Veleri, S., Frautschy, S., 2014. Molecular chaperone dysfunction in neurodegenerative diseases and effects of curcumin. Biomed Res. Int. 2014.

Manfredsson, F.P., Luk, K.C., Benskey, M.J., Gezer, A., Garcia, J., Kuhn, N.C., Sandoval, I.M., Patterson, J.R., O'Mara, A., Yonkers, R., Kordower, J.H., 2018. Induction of alpha-synuclein pathology in the enteric nervous system of the rat and non-human primate results in gastrointestinal dysmotility and transient CNS pathology. Neurobiol. Dis. 112, 106–118.

Mangiarini, L., Sathasivam, K., Seller, M., Cozens, B., Harper, A., Hetherington, C., Lawton, M., Trottier, Y., Lehrach, H., Davies, S.W., Bates, G.P., 1996. Exon 1 of the HD Gene with an Expanded CAG Repeat Is Sufficient to Cause a Progressive Neurological Phenotype in Transgenic Mice The onset of symptoms is generally in midlife although. Cell 87, 493–506.

Mannini, B., Cascella, R., Zampagni, M., van Waarde-Verhagen, M., Meehan, S., Roodveldt, C., Campioni, S., Boninsegna, M., Penco, A., Relini, A., Kampinga, H.H., Dobson, C.M., Wilson, M.R., Cecchi, C., Chiti, F., 2012. Molecular mechanisms used by chaperones to reduce the toxicity of aberrant protein oligomers. Proc. Natl. Acad. Sci. 109, 12479–12484.

Mao, X., Ou, M.T., Karuppagounder, S.S., Kam, T.-I., Yin, X., Xiong, Y., Ge, P., Umanah, G.E., Brahmachari, S., Shin, J.-H., Kang, H.C., Zhang, J., Xu, J., Chen, R., Park, H., Andrabi, S.A., Kang, S.U., Goncalves, R.A., Liang, Y., Zhang, S., Qi, C., Lam, S., Keiler, J.A., Tyson, J., Kim, D., Panicker, N., Yun, S.P., Workman, C.J., Vignali, D.A.A.A., Dawson, V.L., Ko, H.S., Dawson, T.M., 2016. Pathological a-synuclein transmission initiated by binding lymphocyte-activation gene 3. Science 353, aah3374-1-aah3374-12.

Martinez, Z., Zhu, M., Han, S., Fink, A.L., 2007. GM1 specifically interacts with α-synuclein and inhibits fibrillation. Biochemistry 46, 1868–1877.

Masnata, M., Sciacca, G., Maxan, A., Bousset, L., Denis, H.L., Lauruol, F., David, L., Saint-Pierre, M., Kordower, J.H., Melki, R., Alpaugh, M., Cicchetti, F., 2019. Demonstration of prion-like properties of mutant huntingtin fibrils in both in vitro and in vivo paradigms. Acta Neuropathol. 137, 981–1001.

Masters, C.L., Simms, G., Weinman, N.A., Multhaup, G., McDonald, B.L., Beyreuther, K., 1985. Amyloid plaque core protein in Alzheimer disease and Down syndrome. Proc. Natl. Acad. Sci. 82, 4245–4249.

Mathis, C.A., Lopresti, B.J., Ikonomovic, M.D., Klunk, W.E., 2017. Small-molecule PET Tracers for Imaging Proteinopathies. Semin. Nucl. Med. 47, 553–575.

Mattoo, R.U.H., Goloubinoff, P., 2014. Molecular chaperones are nanomachines that catalytically unfold misfolded and alternatively folded proteins. Cell. Mol. Life Sci.

Maxan, A., Mason, S., Saint-Pierre, M., Smith, E., Ho, A., Harrower, T., Watts, C., Tai, Y., Pavese, N., Savage, J.C., Tremblay, M.-ève, Gould, P., Rosser, A.E., Dunnett, S.B., Piccini, P., Barker, R.A., Cicchetti, F., 2018. Outcome of cell suspension allografts in a patient with Huntington's disease. Ann. Neurol. 84, 950–956.

Mayer, M.P., Gierasch, L.M., 2019. Recent advances in the structural and mechanistic aspects

of Hsp70 molecular chaperones. J. Biol. Chem. 294, 2085–2097.

McCann, H., Stevens, C.H., Cartwright, H., Halliday, G.M., 2014. α-Synucleinopathy phenotypes. Park. Relat. Disord. 20, S62–S67.

Mcgivern, J.G., 2007. Ziconotide: a review of its pharmacology and use in the treatment of pain. Neuropsychiatr. Dis. Treat. 3, 69–85.

McGonigle, P., 2012. Peptide therapeutics for CNS indications. Biochem. Pharmacol. 83, 559–566.

McKee, A.C., Daneshvar, D.H., Alvarez, V.E., Stein, T.D., 2014. The neuropathology of sport. Acta Neuropathol. 127, 29–51.

McNeil, S.M., Novelletto, A., Srinidhi, J., Barnes, G., Kornbluth, I., Altherr, M.R., Wasmuth, J.J., Gusella, J.F., MacDonald, M.E., Myers, R.H., 1997. Reduced penetrance of the Huntington's disease mutation. Hum. Mol. Genet. 6, 775–779.

Migneault, I., Dartiguenave, C., Bertrand, M.J., Waldron, K.C., 2004. Glutaraldehyde: behavior in aqueous solution, reaction with proteins, and application to enzyme crosslinking. Biotechniques 37, 790–802.

Milanesi, L., Sheynis, T., Xue, W.-F., Orlova, E. V., Hellewell, A.L., Jelinek, R., Hewitt, E.W., Radford, S.E., Saibil, H.R., 2012. Direct three-dimensional visualization of membrane disruption by amyloid fibrils. Proc. Natl. Acad. Sci. 109, 20455–20460.

Miller, V.M., Nelson, R.F., Gouvion, C.M., Williams, A., Rodriguez-Lebron, E., Harper, S.Q., Davidson, B.L., Rebagliati, M.R., Paulson, H.L., 2005. CHIP suppresses polyglutamine aggregation and toxicity in vitro and in vivo. J. Neurosci. 25, 9152–9161.

Mirbaha, H., Chen, D., Morazova, O.A., Ruff, K.M., Sharma, A.M., Liu, X., Goodarzi, M., Pappu, R. V., Colby, D.W., Mirzaei, H., Joachimiak, L.A., Diamond, M.I., 2018. Inert and seed-competent tau monomers suggest structural origins of aggregation. Elife 7, 163394.

Modell, A.E., Blosser, S.L., Arora, P.S., 2016. Systematic Targeting of Protein–Protein Interactions. Trends Pharmacol. Sci. 37, 702–713.

Mogk, A., Ruger-Herreros, C., Bukau, B., 2019. Cellular Functions and Mechanisms of Action of Small Heat Shock Proteins. Annu. Rev. Microbiol. 73, 4.1-4.22.

Mok, S.-A., Condello, C., Freilich, R., Gillies, A., Arhar, T., Oroz, J., Kadavath, H., Julien, O., Assimon, V.A., Rauch, J.N., Dunyak, B.M., Lee, J., Tsai, F.T.F., Wilson, M.R., Zweckstetter, M., Dickey, C.A., Gestwicki, J.E., 2018. Mapping interactions with the chaperone network reveals factors that protect against tau aggregation. Nat. Struct. Mol. Biol. 25, 384–393.

Mollenhauer, B., Cullen, V., Kahn, I., Krastins, B., Outeiro, T.F., Pepivani, I., Ng, J., Schulz-Schaeffer, W., Kretzschmar, H.A., McLean, P.J., Trenkwalder, C., Sarracino, D.A., VonSattel, J.P., Locascio, J.J., El-Agnaf, O.M.A., Schlossmacher, M.G., 2008. Direct quantification of CSF α-synuclein by ELISA and first cross-sectional study in patients with neurodegeneration. Exp. Neurol. 213, 315–325.

Mollenhauer, B., Trautmann, E., Otte, B., Ng, J., Spreer, A., Lange, P., Sixel-Döring, F., Hakimi, M., VonSattel, J.P., Nussbaum, R., Trenkwalder, C., Schlossmacher, M.G., 2012. α-Synuclein in human cerebrospinal fluid is principally derived from neurons of the central nervous system. J. Neural Transm. 119, 739–746.

Monsellier, E., Bendifallah, M., Redeker, V., Melki, R., 2020. Polypeptides derived from α-Synuclein binding partners to prevent α-Synuclein fibril interaction with and take-up by cells. To be Submitt. 1–39.

Monsellier, E., Bousset, L., Melki, R., 2016. α-Synuclein and huntingtin exon 1 amyloid fibrils bind laterally to the cellular membrane. Sci. Rep. 6, 19180.

Monsellier, E., Redeker, V., Ruiz-Arlandis, G., Bousset, L., Melki, R., 2015. Molecular

interaction between the chaperone Hsc70 and the N-terminal flank of huntingtin exon 1 modulates aggregation. J. Biol. Chem. 290, 2560–2576.

Moran, O., 2017. The gating of the CFTR channel. Cell. Mol. Life Sci. 74, 85–92.

Moran, L.B., Duke, D.C., Deprez, M., Dexter, D.T., Pearce, R.K.B., Graeber, M.B., 2006. Whole genome expression profiling of the medial and lateral substantia nigra in Parkinson's disease. Neurogenetics 7, 1–11.

Morimoto, B.H., 2018. Therapeutic peptides for CNS indications: Progress and challenges. Bioorganic Med. Chem. 26, 2859–2862.

Morita, Y., Leslie, M., Kameyama, H., Volk, D.E., Tanaka, T., 2018. Aptamer therapeutics in cancer: Current and future. Cancers (Basel). 10.

Morris, A.M., Watzky, M.A., Finke, R.G., 2009. Protein aggregation kinetics, mechanism, and curve-fitting: A review of the literature. Biochim. Biophys. Acta - Proteins Proteomics 1794, 375–397.

Muchowski, P.J., Ramsden, R., Nguyen, Q., Arnett, E.E., Greiling, T.M., Anderson, S.K., Clark, J.I., 2008. Noninvasive Measurement of Protein Aggregation by Mutant Huntingtin Fragments or α-Synuclein in the Lens. J. Biol. Chem. 283, 6330–6336.

Muchowski, P.J., Schaffar, G., Sittler, A., Wanker, E.E., Hayer-Hartl, M.K., Hartl, F.U., 2000. Hsp70 and Hsp40 chaperones can inhibit self-assembly of polyglutamine proteins into amyloid-like fibrils. Proc. Natl. Acad. Sci. 97, 7841–7846.

Munishkina, L.A., Cooper, E.M., Uversky, V.N., Fink, A.L., 2004. The effect of macromolecular crowding on protein aggregation and amyloid fibril formation. J. Mol. Recognit. 17, 456–464.

Murzin, A.G., Falcon, B., Crowther, R.A., Goedert, M., Fan, J., Scheres, S.H., Zhang, W., 2019. Heparin-induced tau filaments are polymorphic and differ from those in Alzheimer's and Pick's diseases. Elife 8, 1–24.

Nahomi, R.B., DiMauro, M.A., Wang, B., Nagaraj, R.H., 2015. Identification of peptides in human Hsp20 and Hsp27 that possess molecular chaperone and anti-apoptotic activities. Biochem. J. 465, 115–125.

Nahomi, R.B., Wang, B., Raghavan, C.T., Voss, O., Doseff, A.I., Santhoshkumar, P., Nagaraj, R.H., 2013. Chaperone peptides of α-crystallin inhibit epithelial cell apoptosis, protein insolubilization, and opacification in experimental cataracts. J. Biol. Chem. 288, 13022–13035.

Nair, R.R., Corrochano, S., Gasco, S., Tibbit, C., Thompson, D., Maduro, C., Ali, Z., Fratta, P., Arozena, A.A., Cunningham, T.J., Fisher, E.M.C., 2019. Uses for humanised mouse models in precision medicine for neurodegenerative disease. Mamm. Genome.

Nair, A.T., Ramachandran, V., Joghee, N.M., Antony, S., Ramalingam, G., 2018. Gut Microbiota Dysfunction as Reliable Non-invasive Early Diagnostic Biomarkers in the Pathophysiology of Parkinson's Disease: A Critical Review. J Neurogastroenterol Motil 24, 30–42.

Nelson, P.T., Alafuzoff, I., Bigio, E.H., Bouras, C., Braak, H., Cairns, N.J., Castellani, R.J., Crain, B.J., Davies, P., Tredici, K. Del, Duyckaerts, C., Frosch, M.P., Haroutunian, V., Hof, P.R., Hulette, C.M., Hyman, B.T., Iwatsubo, T., Jellinger, K.A., Jicha, G.A., Kövari, E., Kukull, W.A., Leverenz, J.B., Love, S., Mackenzie, I.R., Mann, D.M., Masliah, E., McKee, A.C., Montine, T.J., Morris, J.C., Schneider, J.A., Sonnen, J.A., Thal, D.R., Trojanowski, J.Q., Troncoso, J.C., Wisniewski, T., Woltjer, R.L., Beach, T.G., 2012. Correlation of Alzheimer Disease Neuropathologic Changes With Cognitive Status: A Review of the Literature. J. Neuropathol. Exp. Neurol. 71, 362–381.

Nemani, V.M., Lu, W., Berge, V., Nakamura, K., Onoa, B., Lee, M.K., Chaudhry, F.A., Nicoll, R.A., Edwards, R.H., 2010. Increased Expression of α-Synuclein Reduces

Neurotransmitter Release by Inhibiting Synaptic Vesicle Reclustering after Endocytosis. Neuron 65, 66–79.

Neueder, A., Landles, C., Ghosh, R., Howland, D., Myers, R.H., Faull, R.L.M., Tabrizi, S.J., Bates, G.P., 2017. The pathogenic exon 1 HTT protein is produced by incomplete splicing in Huntington's disease patients. Sci. Rep. 7, 1–10.

Neves-Coelho, S., Eleutério, R.P., Enguita, F.J., Neves, V., Castanho, M.A.R.B., 2017. A new noncanonical anionic peptide that translocates a cellular blood-brain barrier model. Molecules 22.

Newell, K.L., Boyer, P., Gomez-Tortosa, E., Hobbs, W., Hedley-Whyte, T., Vonsatell, J.P., Hyman, B.T., 1999. α-Synuclein Immunoreactivity Is Present in Axonal Swellings in Neuroaxonal Dystrophy and Acute Traumatic Brain Injury. J. Neuropathol. Exp. Neurol. 58, 1263–1268.

Ngolab, J., Trinh, I., Rockenstein, E., Mante, M., Florio, J., Trejo, M., Masliah, D., Adame, A., Masliah, E., Rissman, R.A., 2017. Brain-derived exosomes from dementia with Lewy bodies propagate α-synuclein pathology. Acta Neuropathol. Commun. 5, 46.

Nikolay, R., Wiederkehr, T., Rist, W., Kramer, G., Mayer, M.P., Bukau, B., 2004. Dimerization of the Human E3 Ligase CHIP via a Coiled-coil Domain Is Essential for Its Activity. J. Biol. Chem. 279, 2673–2678.

Noyce, A.J., Bestwick, J.P., Silveira-Moriyama, L., Hawkes, C.H., Giovannoni, G., Lees, A.J., Schrag, A., 2012. Meta-analysis of early nonmotor features and risk factors for Parkinson disease. Ann. Neurol. 72, 893–901.

Nury, C., Redeker, V., Dautrey, S., Romieu, A., Van Der Rest, G., Renard, P.Y., Melki, R., Chamot-Rooke, J., 2015. A novel bio-orthogonal cross-linker for improved protein/protein interaction analysis. Anal. Chem. 87, 1853–1860.

O'Reilly, F.J., Rappsilber, J., 2018. Cross-linking mass spectrometry: methods and applications in structural, molecular and systems biology. Nat. Struct. Mol. Biol. 25, 1000–1008.

Oh, S.H., Kim, H.N., Park, H.J., Shin, J.Y., Bae, E.J., Sunwoo, M.K., Lee, S.J., Lee, P.H., 2016. Mesenchymal Stem Cells Inhibit Transmission of α-Synuclein by Modulating Clathrin-Mediated Endocytosis in a Parkinsonian Model. Cell Rep. 14, 835–849.

Ohnishi, T., Yanazawa, M., Sasahara, T., Kitamura, Y., Hiroaki, H., Fukazawa, Y., Kii, I., Nishiyama, T., Kakita, A., Takeda, H., Takeuchi, A., Arai, Y., Ito, A., Komura, H., Hirao, H., Satomura, K., Inoue, M., Muramatsu, S., Matsui, K., Tada, M., Sato, M., Saijo, E., Shigemitsu, Y., Sakai, S., Umetsu, Y., Goda, N., Takino, N., Takahashi, H., Hagiwara, M., Sawasaki, T., Iwasaki, G., Nakamura, Y., Nabeshima, Y., Teplow, D.B., Hoshi, M., 2015. Na, K-ATPase α3 is a death target of Alzheimer patient amyloid-β assembly. Proc. Natl. Acad. Sci. 112, E4465–E4474.

Ojha, B., Fukui, N., Hongo, K., Mizobata, T., Kawata, Y., 2016. Suppression of amyloid fibrils using the GroEL apical domain. Sci. Rep. 6, 31041.

Olsén, A., Jonsson, A., Normark, S., 1989. Fibronectin binding mediated by a novel class of surface organelles on Escherichia coli. Nature 338, 652–655.

Ono, K., Ikeda, T., Takasaki, J. ichi, Yamada, M., 2011. Familial Parkinson disease mutations influence α-Synuclein assembly. Neurobiol. Dis. 43, 715–724.

Outeiro, T.F., Klucken, J., Strathearn, K.E., Liu, F., Nguyen, P., Rochet, J.C., Hyman, B.T., McLean, P.J., 2006. Small heat shock proteins protect against a-synuclein-induced toxicity and aggregation. Biochem. Biophys. Res. Commun. 351, 631–638.

Outeiro, T.F., Koss, D.J., Erskine, D., Walker, L., Kurzawa-Akanbi, M., Burn, D., Donaghy, P., Morris, C., Taylor, J.P., Thomas, A., Attems, J., McKeith, I., 2019. Dementia with Lewy bodies: An update and outlook. Mol. Neurodegener. 14, 1–18.

Pajarillo, E., Rizor, A., Lee, J., Aschner, M., Lee, E., 2018. The role of posttranslational

modifications of α-synuclein and LRRK2 in Parkinson's disease: Potential contributions of environmental factors. Biochim. Biophys. Acta - Mol. Basis Dis. 0–1.

Paleologou, K.E., Irvine, G.B., El-Agnaf, O.M. a, 2005. Alpha-synuclein aggregation in neurodegenerative diseases and its inhibition as a potential therapeutic strategy. Biochem. Soc. Trans. 33, 1106–10.

Paris, D., Ganey, N.J., Laporte, V., Patel, N.S., Beaulieu-Abdelahad, D., Bachmeier, C., March, A., Ait-Ghezala, G., Mullan, M.J., 2010. Reduction of β-amyloid pathology by celastrol in a transgenic mouse model of Alzheimer's disease. J. Neuroinflammation 7, 1–15.

Parrini, C., Taddei, N., Ramazzotti, M., Degl'Innocenti, D., Ramponi, G., Dobson, C.M., Chiti, F., 2005. Glycine residues appear to be evolutionarily conserved for their ability to inhibit aggregation. Structure 13, 1143–1151.

Parsons, M.P., Raymond, L.A., 2015. Huntington Disease. In: Neurobiology of Brain Disorders. Elsevier, pp. 303–320.

Patterson, K.R., Ward, S.M., Combs, B., Voss, K., Kanaan, N.M., Morfini, G., Brady, S.T., Gamblin, T.C., Binder, L.I., 2011. Heat Shock Protein 70 Prevents both Tau Aggregation and the Inhibitory Effects of Preexisting Tau Aggregates on Fast Axonal Transport. Biochemistry 50, 10300–10310.

Pawar, A.P., DuBay, K.F., Zurdo, J., Chiti, F., Vendruscolo, M., Dobson, C.M., 2005. Prediction of "aggregation-prone" and "aggregation- susceptible" regions in proteins associated with neurodegenerative diseases. J. Mol. Biol. 350, 379–392.

Pearce, M.M.P., Spartz, E.J., Hong, W., Luo, L., Kopito, R.R., 2015. Prion-like transmission of neuronal huntingtin aggregates to phagocytic glia in the Drosophila brain. Nat. Commun. 6, 6768.

Pecho-Vrieseling, E., Rieker, C., Fuchs, S., Bleckmann, D., Esposito, M.S., Botta, P., Goldstein, C., Bernhard, M., Galimberti, I., Müller, M., Lüthi, A., Arber, S., Bouwmeester, T., Van Der Putten, H., Di Giorgio, F.P., 2014. Transneuronal propagation of mutant huntingtin contributes to non-cell autonomous pathology in neurons. Nat. Neurosci. 17, 1064–1072.

Peelaerts, W., Bousset, L., Baekelandt, V., Melki, R., 2018. α-Synuclein strains and seeding in Parkinson's disease, incidental Lewy body disease, dementia with Lewy bodies and multiple system atrophy: similarities and differences. Cell Tissue Res. 373, 195–212.

Peelaerts, W., Bousset, L., Van Der Perren, A., Moskalyuk, A., Pulizzi, R., Giugliano, M., Van Den Haute, C., Melki, R., Baekelandt, V., 2015. α-Synuclein strains cause distinct synucleinopathies after local and systemic administration. Nature 522, 340–344.

Peeraer, E., Bottelbergs, A., Van Kolen, K., Stancu, I.-C., Vasconcelos, B., Mahieu, M., Duytschaever, H., Ver Donck, L., Torremans, A., Sluydts, E., Van Acker, N., Kemp, J.A., Mercken, M., Brunden, K.R., Trojanowski, J.Q., Dewachter, I., Lee, V.M.Y., Moechars, D., 2015. Intracerebral injection of preformed synthetic tau fibrils initiates widespread tauopathy and neuronal loss in the brains of tau transgenic mice. Neurobiol. Dis. 73, 83–95.

Pemberton, S., Madiona, K., Pieri, L., Kabani, M., Bousset, L., Melki, R., 2011. Hsc70 Protein Interaction with Soluble and Fibrillar α-Synuclein. J. Biol. Chem. 286, 34690–34699.

Pemberton, S., Melki, R., 2012. The interaction of Hsc70 protein with fibrillar alpha-Synuclein and its therapeutic potential in Parkinson's disease. Commun Integr Biol 5, 94–95.

Pereira, E.A.C., Aziz, T.Z., 2006. Surgical insights into Parkinson's disease. J. R. Soc. Med. 99, 238–244.

Pernègre, C., Duquette, A., Leclerc, N., 2019. Tau secretion: Good and bad for neurons. Front. Neurosci. 13, 1–11.

Perni, M., Flagmeier, P., Limbocker, R., Cascella, R., Aprile, F.A., Galvagnion, C., Heller, G.T., Meisl, G., Chen, S.W., Kumita, J.R., Challa, P.K., Kirkegaard, J.B., Cohen, S.I.A.,

Mannini, B., Barbut, D., Nollen, E.A.A., Cecchi, C., Cremades, N., Knowles, T.P.J., Chiti, F., Zasloff, M., Vendruscolo, M., Dobson, C.M., 2018. Multistep Inhibition of α-Synuclein Aggregation and Toxicity in Vitro and in Vivo by Trodusquemine. ACS Chem. Biol. 13, 2308–2319.

Pérot, S., Sperandio, O., Miteva, M.A., Camproux, A.C., Villoutreix, B.O., 2010. Druggable pockets and binding site centric chemical space: A paradigm shift in drug discovery. Drug Discov. Today 15, 656–667.

Peschek, J., Braun, N., Rohrberg, J., Back, K.C., Kriehuber, T., Kastenmuller, A., Weinkauf, S., Buchner, J., 2013. Regulated structural transitions unleash the chaperone activity of αB-crystallin. Proc. Natl. Acad. Sci. 110, E3780–E3789.

Petkova, A.T., Buntkowsky, G., Dyda, F., Leapman, R.D., Yau, W.M., Tycko, R., 2004. Solid state NMR reveals a pH-dependent antiparallel β-sheet registry in fibrils formed by a β-amyloid peptide. J. Mol. Biol. 335, 247–260.

Petrucelli, L., Dickson, D., Kehoe, K., Taylor, J., Snyder, H., Grover, A., De Lucia, M., McGowan, E., Lewis, J., Prihar, G., Kim, J., Dillmann, W.H., Browne, S.E., Hall, A., Voellmy, R., Tsuboi, Y., Dawson, T.M., Wolozin, B., Hardy, J., Hutton, M., 2004. CHIP and Hsp70 regulate tau ubiquitination, degradation and aggregation. Hum. Mol. Genet. 13, 703–714.

Pham, N.D., Parker, R.B., Kohler, J.J., 2013. Photocrosslinking approaches to interactome mapping. Curr. Opin. Chem. Biol. 17, 90–101.

Piccini, P., Brooks, D.J., Björklund, A., Gunn, R.N., Grasby, P.M., Rimoldi, O., Brundin, P., Hagell, P., Rehncrona, S., Widner, H., Lindvall, O., 1999. Dopamine release from nigral transplants visualized in vivo in a Parkinson's patient. Nat. Neurosci. 2, 1137–1140.

Pierce, A., Podlutskaya, N., Halloran, J.J., Hussong, S.A., Lin, P.Y., Burbank, R., Hart, M.J., Galvan, V., 2013. Over-expression of heat shock factor 1 phenocopies the effect of chronic inhibition of TOR by rapamycin and is sufficient to ameliorate Alzheimer's-like deficits in mice modeling the disease. J. Neurochem. 124, 880–893.

Pieri, L., Chafey, P., Le Gall, M., Clary, G., Melki, R., Redeker, V., 2016. Cellular response of human neuroblastoma cells to α-synuclein fibrils, the main constituent of Lewy bodies. Biochim. Biophys. Acta - Gen. Subj. 1860, 8–19.

Pieri, L., Madiona, K., Bousset, L., Melki, R., 2012. Fibrillar α-synuclein and huntingtin exon 1 assemblies are toxic to the cells. Biophys. J. 102, 2894–2905.

Pineda, J.R., Pardo, R., Zala, D., Yu, H., Humbert, S., Saudou, F., 2009. Genetic and pharmacological inhibition of calcineurin corrects the BDNF transport defect in Huntington's disease. Mol. Brain 2, 1–11.

Polymeropoulos, M.H., Lavedan, C., Leroy, E., Ide, S.E., Dehejia, A., Dutra, A., Pike, B., Root, H., Rubenstein, J., Boyer, R., Stenroos, E.S., Chandrasekharappa, S., Athanassiadou, A., Papapetropoulos, T., Johnson, W.G., Lazzarini, A.M., Duvoisin, R.C., Di Iorio, G., Golbe, L.I., Nussbaum, R.L., 1997. Mutation in the α-synuclein gene identified in families with Parkinson's disease. Science 276, 2045–2047.

Postuma, R.B., Aarsland, D., Barone, P., Burn, D.J., Hawkes, C.H., Oertel, W., Ziemssen, T., 2012. Identifying prodromal Parkinson's disease: Pre-Motor disorders in Parkinson's disease. Mov. Disord. 27, 617–626.

Pratt, W.B., Gestwicki, J.E., Osawa, Y., Lieberman, A.P., 2015. Targeting Hsp90/Hsp70-Based Protein Quality Control for Treatment of Adult Onset Neurodegenerative Diseases. Annu. Rev. Pharmacol. Toxicol. 55, 353–371.

Preston, G.W., Radford, S.E., Ashcroft, A.E., Wilson, A.J., 2012. Covalent cross-linking within supramolecular peptide structures. Anal. Chem. 84, 6790–6797.

Preusser, M., Ströbel, T., Gelpi, E., Eiler, M., Broessner, G., Schmutzhard, E., Budka, H., 2006.

Alzheimer-type neuropathology in a 28 year old patient with iatrogenic Creutzfeldt-Jakob disease after dural grafting. J. Neurol. Neurosurg. Psychiatry 77, 413–416.

Prusiner, S., 1991. Molecular biology of prion diseases. Science 252, 1515–1522.

Prusiner, S.B., 1998. Prions. Proc Natl Acad Sci U S A 95, 13363–13383.

Prusiner, S.B., Woerman, A.L., Mordes, D.A., Watts, J.C., Rampersaud, R., Berry, D.B., Patel, S., Oehler, A., Lowe, J.K., Kravitz, S.N., Geschwind, D.H., Glidden, D. V., Halliday, G.M., Middleton, L.T., Gentleman, S.M., Grinberg, L.T., Giles, K., 2015. Evidence for α-synuclein prions causing multiple system atrophy in humans with parkinsonism. Proc. Natl. Acad. Sci. 112, E5308–E5317.

Przedborski, S., 2017. The two-century journey of Parkinson disease research. Nat. Rev. Neurosci. 18, 251–259.

Purro, S.A., Farrow, M.A., Linehan, J., Nazari, T., Thomas, D.X., Chen, Z., Mengel, D., Saito, T., Saido, T., Rudge, P., Brandner, S., Walsh, D.M., Collinge, J., 2018. Transmission of amyloid-β protein pathology from cadaveric pituitary growth hormone. Nature 564, 415–419.

Qiang, W., Yau, W.-M., Lu, J.-X., Collinge, J., Tycko, R., 2017. Structural variation in amyloid-β fibrils from Alzheimer's disease clinical subtypes. Nature 541, 217–221.

Quach, Q.L., Metz, L.M., Thomas, J.C., Rothbard, J.B., Steinman, L., Ousman, S.S., 2013. CRYAB modulates the activation of $CD4^+$ T cells from relapsing-remitting multiple sclerosis patients. Mult. Scler. J. 19, 1867–1877.

Quintana-Gallardo, L., Martín-Benito, J., Marcilla, M., Espadas, G., Sabidó, E., Valpuesta, J.M., 2019. The cochaperone CHIP marks Hsp70- and Hsp90-bound substrates for degradation through a very flexible mechanism. Sci. Rep. 9, 1–16.

Raju, M., Santhoshkumar, P., Sharma, K.K., 2012. αA-Crystallin-Derived Mini-Chaperone Modulates Stability and Function of Cataract Causing αAG98R-Crystallin. PLoS One 7.

Raju, M., Santhoshkumar, P., Sharma, K.K., 2016. Alpha-crystallin-derived peptides as therapeutic chaperones. Biochim. Biophys. Acta - Gen. Subj. 1860, 246–251.

Raju, M., Santhoshkumar, P., Sharma, K.K., 2018. Cell-Penetrating Chaperone Peptide Prevents Protein Aggregation and Protects against Cell Apoptosis. Adv. Biosyst. 2, 1700095.

Raman, B., Ban, T., Sakai, M., Pasta, S.Y., Ramakrishna, T., Naiki, H., Goto, Y., Rao, C.M., 2005. αB-crystallin, a small heat-shock protein, prevents the amyloid fibril growth of an amyloid β-peptide and β2-microglobulin. Biochem. J. 392, 573–581.

Rana, P., Franco, E.F., Rao, Y., Syed, K., Barh, D., Azevedo, V., Ramos, R.T.J., Ghosh, P., 2019. Evaluation of the Common Molecular Basis in Alzheimer's and Parkinson's Diseases. Int. J. Mol. Sci. 20, 3730.

Rangachari, V., Dean, D.N., Rana, P., Vaidya, A., Ghosh, P., 2018. Cause and consequence of Aβ – Lipid interactions in Alzheimer disease pathogenesis. Biochim. Biophys. Acta - Biomembr. 1860, 1652–1662.

Rappsilber, J., 2011. The beginning of a beautiful friendship: Cross-linking/mass spectrometry and modelling of proteins and multi-protein complexes. J. Struct. Biol. 173, 530–540.

Ratovitski, T., Gucek, M., Jiang, H., Chighladze, E., Waldron, E., D'Ambola, J., Zhipeng, H., Yideng, L., Poirier, M.A., Hirschhorn, R.R., Graham, R., Hayden, M.R., Cole, R.N., Ross, C.A., 2009. Mutant huntingtin N-terminal fragments of specific size mediate aggregation and toxicity in neuronal cells. J. Biol. Chem. 284, 10855–10867.

Recasens, A., Dehay, B., Bové, J., Carballo-Carbajal, I., Dovero, S., Pérez-Villalba, A., Fernagut, P.O., Blesa, J., Parent, A., Perier, C., Fariñas, I., Obeso, J.A., Bezard, E., Vila, M., 2014. Lewy body extracts from Parkinson disease brains trigger α-synuclein pathology

and neurodegeneration in mice and monkeys. Ann. Neurol. 75, 351–362.

Recasens, A., Perier, C., Sue, C.M., 2016. Role of microRNAs in the Regulation of α-Synuclein Expression: A Systematic Review. Front. Mol. Neurosci. 9, 1–12.

Redeker, V., Bonnefoy, J., Le Caer, J.P., Pemberton, S., Laprévote, O., Melki, R., 2010. A region within the C-terminal domain of Ure2p is shown to interact with the molecular chaperone Ssa1p by the use of cross-linkers and mass spectrometry. FEBS J. 277, 5112–5123.

Redeker, V., Pemberton, S., Bienvenut, W., Bousset, L., Melki, R., 2012. Identification of protein interfaces between α-synuclein, the principal component of Lewy bodies in Parkinson disease, and the molecular chaperones human Hsc70 and the yeast Ssa1p. J. Biol. Chem. 287, 32630–32639.

Rekas, A., Adda, C.G., Andrew Aquilina, J., Barnham, K.J., Sunde, M., Galatis, D., Williamson, N.A., Masters, C.L., Anders, R.F., Robinson, C. V., Cappai, R., Carver, J.A., 2004. Interaction of the molecular chaperone aB-crystallin with a-Synuclein: Effects on amyloid fibril formation and chaperone activity. J. Mol. Biol. 340, 1167–1183.

Rekas, A., Jankova, L., Thorn, D.C., Cappai, R., Carver, J.A., 2007. Monitoring the prevention of amyloid fibril formation by aB-crystallin: Temperature dependence and the nature of the aggregating species. FEBS J. 274, 6290–6305.

Ren, P.-H., Lauckner, J.E., Kachirskaia, I., Heuser, J.E., Melki, R., Kopito, R.R., 2009. Cytoplasmic penetration and persistent infection of mammalian cells by polyglutamine aggregates. Nat. Cell Biol. 11, 219–225.

Ren, X., Zhao, Y., Xue, F., Zheng, Y., Huang, H., Wang, W., Chang, Y., Yang, H., Zhang, J., 2019. Exosomal DNA Aptamer Targeting α-Synuclein Aggregates Reduced Neuropathological Deficits in a Mouse Parkinson's Disease Model. Mol. Ther. - Nucleic Acids 17, 726–740.

Renkawek, K., de Jong, W.W., Merck, K.B., Frenken, C.W.G.M., van Workum, F.P.A., Bosman, G.J.C.G.M., 1992. αB-Crystallin is present in reactive glia in Creutzfeldt-Jakob disease. Acta Neuropathol. 83, 324–327.

Renkawek, K., Stege, G.J.J., Bosman, G.J.C.G.M., 1999. Dementia, gliosis and expression of the small heat shock proteins hsp27 and αB-crystallin in Parkinson's disease. Neuroreport 10, 2273–2276.

Renkawek, K., Voorter, C.E., Bosman, G.J.C.G.M., van Workum, F.P., de Jong, W.W., 1994. Expression of alphaB-crystallin in Alzheimer 's disease. Acta Neuropathol 87, 155–160.

Reverdatto, S., Burz, D., Shekhtman, A., 2015. Peptide Aptamers: Development and Applications. Curr. Top. Med. Chem. 15, 1082–1101.

Rey, N.L., Steiner, J.A., Maroof, N., Luk, K.C., Madaj, Z., Trojanowski, J.Q., Lee, V.M.Y., Brundin, P., 2016. Widespread transneuronal propagation of α-synucleinopathy triggered in olfactory bulb mimics prodromal Parkinson's disease. J. Exp. Med. 213, 1759–1778.

Reyes, J.F., Olsson, T.T., Lamberts, J.T., Devine, M.J., Kunath, T., Brundin, P., 2015. A cell culture model for monitoring α-synuclein cell-to-cell transfer. Neurobiol. Dis. 77, 266–275.

Reyes, J.F., Rey, N.L., Bousset, L., Melki, R., Brundin, P., Angot, E., 2014. Alpha-synuclein transfers from neurons to oligodendrocytes. Glia 62, 387–398.

Riek, R., Eisenberg, D.S., 2016. The activities of amyloids from a structural perspective. Nature 539, 227–235.

Rietdijk, C.D., Perez-Pardo, P., Garssen, J., van Wezel, R.J.A., Kraneveld, A.D., 2017. Exploring Braak's Hypothesis of Parkinson's Disease. Front. Neurol. 8.

Rinner, O., Seebacher, J., Walzthoeni, T., Mueller, L., Beck, M., Schmidt, A., Mueller, M.,

Aebersold, R., 2008. Identification of cross-linked peptides from large sequence databases. Nat. Methods 5, 315–318.

Ritchie, D.L., Adlard, P., Peden, A.H., Lowrie, S., Le Grice, M., Burns, K., Jackson, R.J., Yull, H., Keogh, M.J., Wei, W., Chinnery, P.F., Head, M.W., Ironside, J.W., 2017. Amyloid-β accumulation in the CNS in human growth hormone recipients in the UK. Acta Neuropathol. 134, 221–240.

Rochet, J.C., Hay, B.A., Guo, M., 2012. Molecular insights into Parkinson's disease, 1st ed, Progress in Molecular Biology and Translational Science. Elsevier Inc.

Rodriguez, L., Marano, M.M., Tandon, A., 2018. Import and export of misfolded α-synuclein. Front. Neurosci. 12, 1–9.

Roepstorff, P., Fohlman, J., 1984. Letter to the editors - Proposal for a common nomenclature for sequence ions in mass spectra of peptides. Biol. Mass Spectrom. 11, 601–601.

Rommer, P.S., Milo, R., Han, M.H., Satyanarayan, S., Sellner, J., Hauer, L., Illes, Z., Warnke, C., Laurent, S., Weber, M.S., Zhang, Y., Stuve, O., 2019. Immunological Aspects of Approved MS Therapeutics. Front. Immunol. 10, 1–24.

Roodveldt, C., Bertoncini, C.W., Andersson, A., Van Der Goot, A.T., Hsu, S. Te, Fernández-Montesinos, R., De Jong, J., Van Ham, T.J., Nollen, E.A., Pozo, D., Christodoulou, J., Dobson, C.M., 2009. Chaperone proteostasis in Parkinson's disease: Stabilization of the Hsp70/α-synuclein complex by Hip. EMBO J. 28, 3758–3770.

Rosas, H.D., Salat, D.H., Lee, S.Y., Zaleta, A.K., Pappu, V., Fischl, B., Greve, D., Hevelone, N., Hersch, S.M., 2008. Cerebral cortex and the clinical expression of Huntington's disease: complexity and heterogeneity. Brain 131, 1057–1068.

Rosborough, K., Patel, N., Kalia, L. V., 2017. α-Synuclein and Parkinsonism: Updates and Future Perspectives. Curr. Neurol. Neurosci. Rep. 17.

Rosenblatt, A., Liang, K.Y., Zhou, H., Abbott, M.H., Gourley, L.M., Margolis, R.L., Brandt, J., Ross, C.A., 2006. The association of CAG repeat length with clinical progression in Huntington disease. Neurology 66, 1016–1020.

Ross, C.A., Aylward, E.H., Wild, E.J., Langbehn, D.R., Long, J.D., Warner, J.H., Scahill, R.I., Leavitt, B.R., Stout, J.C., Paulsen, J.S., Reilmann, R., Unschuld, P.G., Wexler, A., Margolis, R.L., Tabrizi, S.J., 2014. Huntington disease: Natural history, biomarkers and prospects for therapeutics. Nat. Rev. Neurol. 10, 204–216.

Ross, C.A., Tabrizi, S.J., 2011. Huntington's disease: From molecular pathogenesis to clinical treatment. Lancet Neurol. 10, 83–98.

Rosser, M.F.N., Washburn, E., Muchowski, P.J., Patterson, C., Cyr, D.M., 2007. Chaperone functions of the E3 ubiquitin ligase CHIP. J. Biol. Chem. 282, 22267–22277.

Rostami, J., Holmqvist, S., Lindström, V., Sigvardson, J., Westermark, G.T., Ingelsson, M., Bergström, J., Roybon, L., Erlandsson, A., 2017. Human Astrocytes Transfer Aggregated Alpha-Synuclein via Tunneling Nanotubes. J. Neurosci. 37, 11835–11853.

Rubinsztein, D.C., Leggo, J., Coles, R., Almqvist, E., Biancalana, V. V., Cassiman, J.J., Chotai, K., Connarty, M., Craufurd, D., Curtis, A., Curtis, D., Davidson, M.J., Differ, A.M., Dode, C., Dodge, A., Frontali, M., Ranen, N.G., Stine, O.C., Sherr, M., 1996. Phenotypic characterization of individuals with 30-40 CAG repeats in the Huntington disease (HD) gene reveals HD cases with 36 repeats and apparently normal elderly individuals with 36-39 repeats. Am. J. Hum. Genet. 59, 16–22.

Ruiz-Arlandis, G., Pieri, L., Bousset, L., Melki, R., 2016. Binding, internalization and fate of Huntingtin Exon1 fibrillar assemblies in mitotic and nonmitotic neuroblastoma cells. Neuropathol. Appl. Neurobiol. 42, 137–152.

Rustom, A., Saffrich, R., Markovic, I., Walther, P., Gerdes, H.H., 2004. Nanotubular Highways for Intercellular Organelle Transport. Science 303, 1007–1010.

Sacino, A.N., Brooks, M.M., Chakrabarty, P., Saha, K., Khoshbouei, H., Golde, T.E., Giasson, B.I., 2017. Proteolysis of α-synuclein fibrils in the lysosomal pathway limits induction of inclusion pathology. J. Neurochem. 140, 662–678.

Sahara, N., Murayama, M., Mizoroki, T., Urushitani, M., Imai, Y., Takahashi, R., Murata, S., Tanaka, K., Takashima, A., 2005. In vivo evidence of CHIP up-regulation attenuating tau aggregation. J. Neurochem. 94, 1254–1263.

Saman, S., Kim, W.H., Raya, M., Visnick, Y., Miro, S., Saman, S., Jackson, B., McKee, A.C., Alvarez, V.E., Lee, N.C.Y., Hall, G.F., 2012. Exosome-associated tau is secreted in tauopathy models and is selectively phosphorylated in cerebrospinal fluid in early Alzheimer disease. J. Biol. Chem. 287, 3842–3849.

Sambamurti, K., Greig, N.H., Lahiri, D.K., 2002. Advances in the cellular and molecular biology of the beta-amyloid protein in Alzheimer's disease. NeuroMolecular Med. 1, 1–31.

Sampson, T.R., Debelius, J.W., Thron, T., Janssen, S., Shastri, G.G., Ilhan, Z.E., Challis, C., Schretter, C.E., Rocha, S., Gradinaru, V., Chesselet, M.F., Keshavarzian, A., Shannon, K.M., Krajmalnik-Brown, R., Wittung-Stafshede, P., Knight, R., Mazmanian, S.K., 2016. Gut Microbiota Regulate Motor Deficits and Neuroinflammation in a Model of Parkinson's Disease. Cell 167, 1469-1480.e12.

Samuel, F., Flavin, W.P., Iqbal, S., Pacelli, C., Renganathan, S.D.S., Trudeau, L.E., Campbell, E.M., Fraser, P.E., Tandon, A., 2016. Effects of serine 129 phosphorylation on α-synuclein aggregation, membrane association, and internalization. J. Biol. Chem. 291, 4374–4385.

Sanders, D.W., Kaufman, S.K., DeVos, S.L., Sharma, A.M., Mirbaha, H., Li, A., Barker, S.J., Foley, A.C., Thorpe, J.R., Serpell, L.C., Miller, T.M., Grinberg, L.T., Seeley, W.W., Diamond, M.I., 2014. Distinct tau prion strains propagate in cells and mice and define different tauopathies. Neuron 82, 1271–1288.

Sanders, D.W., Kaufman, S.K., Holmes, B.B., Diamond, M.I., 2016. Prions and Protein Assemblies that Convey Biological Information in Health and Disease. Neuron 89, 433–448.

Santa-Maria, I., Varghese, M., Księzak-Reding, H., Dzhun, A., Wang, J., Pasinetti, G.M., 2012. Paired helical filaments from Alzheimer disease brain induce intracellular accumulation of tau protein in aggresomes. J. Biol. Chem. 287, 20522–20533.

Santhoshkumar, P., Sharma, K., 2005. Inhibition of amyloid fibrillogenesis and toxicity by a peptide chaperone. Mol. Cell. Biochem. 147–155.

Saudou, F., Humbert, S., 2016. The Biology of Huntingtin. Neuron 89, 910–926.

Schilling, B., Row, R.H., Gibson, B.W., Guo, X., Young, M.M., 2003. MS2Assign, automated assignment and nomenclature of tandem mass spectra of chemically crosslinked peptides. J. Am. Soc. Mass Spectrom. 14, 834–850.

Schöll, M., Maass, A., Mattsson, N., Ashton, N.J., Blennow, K., Zetterberg, H., Jagust, W., 2019. Biomarkers for tau pathology. Mol. Cell. Neurosci. 97, 18–33.

Schütz, A.K., Soragni, A., Hornemann, S., Aguzzi, A., Ernst, M., Böckmann, A., Meier, B.H., 2011. The amyloid-congo red interface at atomic resolution. Angew. Chemie - Int. Ed. 50, 5956–5960.

Schwartz, R., Istrail, S., King, J., 2001. Frequencies of amino acid strings in globular protein sequences indicate suppression of blocks of consecutive hydrophobic residues. Protein Sci. 10, 1023–1031.

Scior, A., Buntru, A., Arnsburg, K., Ast, A., Iburg, M., Juenemann, K., Pigazzini, M.L., Mlody, B., Puchkov, D., Priller, J., Wanker, E.E., Prigione, A., Kirstein, J., 2018. Complete suppression of Htt fibrilization and disaggregation of Htt fibrils by a trimeric chaperone complex. EMBO J. 37, 282–299.

Seidler, P.M., Boyer, D.R., Rodriguez, J.A., Sawaya, M.R., Cascio, D., Murray, K., Gonen, T., Eisenberg, D.S., 2018. Structure-based inhibitors of tau aggregation. Nat. Chem. 10, 170–176.

Selkoe, D., Dettmer, U., Luth, E., Kim, N., Newman, A., Bartels, T., 2014. Defining the native state of α-synuclein. Neurodegener. Dis. 13, 114–117.

Shahmoradian, S.H., Galaz-Montoya, J.G., Schmid, M.F., Cong, Y., Ma, B., Spiess, C., Frydman, J., Ludtke, S.J., Chiu, W., 2013. TRiC's tricks inhibit huntingtin aggregation. Elife 2013, 1–17.

Shahnawaz, M., Tokuda, T., Waraga, M., Mendez, N., Ishii, R., Trenkwalder, C., Mollenhauer, B., Soto, C., 2017. Development of a biochemical diagnosis of Parkinson disease by detection of α-synuclein misfolded aggregates in cerebrospinal fluid. JAMA Neurol. 74, 163–172.

Shammas, S.L., Waudby, C.A., Wang, S., Buell, A.K., Knowles, T.P.J., Ecroyd, H., Welland, M.E., Carver, J.A., Dobson, C.M., Meehan, S., 2011. Binding of the molecular chaperone αb-crystallin to Aβ amyloid fibrils inhibits fibril elongation. Biophys. J. 101, 1681–1689.

Shannon, K.M., Keshavarzian, A., Dodiya, H.B., Jakate, S., Kordower, J.H., 2012. Is alpha-synuclein in the colon a biomarker for premotor Parkinson's Disease? Evidence from 3 cases. Mov. Disord. 27, 716–719.

Sharma, K.K., Kumar, R.S., Kumar, G.S., Quinn, P.T., 2000. Synthesis and characterization of a peptide identified as a functional element in alpha A-crystallin. J. Biol. Chem. 275, 3767–3771.

Shaw, L.M., Vanderstichele, H., Knapik-Czajka, M., Clark, C.M., Aisen, P.S., Petersen, R.C., Blennow, K., Soares, H., Simon, A., Lewczuk, P., Dean, R., Siemers, E., Potter, W., Lee, V.M.Y., Trojanowski, J.Q., 2009. Cerebrospinal fluid biomarker signature in alzheimer's disease neuroimaging initiative subjects. Ann. Neurol. 65, 403–413.

Shevchenko, A., Wilm, M., Vorm, O., Mann, M., 1996. Mass spectrometric sequencing of proteins from silver-stained polyacrylamide gels. Anal. Chem. 68, 850–858.

Shimshek, D.R., Mueller, M., Wiessner, C., Schweizer, T., Herman van der Putten, P., 2010. The HSP70 molecular chaperone is not beneficial in a mouse model of a-synucleinopathy. PLoS One 5, 1–7.

Shin, Y., Klucken, J., Patterson, C., Hyman, B.T., McLean, P.J., 2005. The Co-chaperone carboxyl terminus of Hsp70-interacting protein (CHIP) mediates a-synuclein degradation decisions between proteasomal and lysosomal pathways. J. Biol. Chem. 280, 23727–23734.

Shinohara, H., Inaguma, Y., Goto, S., Inagaki, T., Kato, K., 1993. αB crystallin and HSP28 are enhanced in the cerebral cortex of patients with Alzheimer's disease. J. Neurol. Sci. 119, 203–208.

Shrivastava, A.N., Aperia, A., Melki, R., Triller, A., 2017. Physico-Pathologic Mechanisms Involved in Neurodegeneration: Misfolded Protein-Plasma Membrane Interactions. Neuron 95, 33–50.

Shrivastava, A.N., Redeker, V., Fritz, N., Pieri, L., Almeida, L.G., Spolidoro, M., Liebmann, T., Bousset, L., Renner, M., Léna, C., Aperia, A., Melki, R., Triller, A., Lena, C., Aperia, A., Melki, R., Triller, A., 2015. α-synuclein assemblies sequester neuronal α3-Na+/ K+-ATPase and impair Na+ gradient. EMBO J. 34, 2408–2423.

Shrivastava, A.N., Redeker, V., Pieri, L., Bousset, L., Renner, M., Madiona, K., Mailhes-Hamon, C., Coens, A., Buée, L., Hantraye, P., Triller, A., Melki, R., 2019. Clustering of Tau fibrils impairs the synaptic composition of α3-Na + /K + -ATPase and AMPA receptors. EMBO J. 38, e99871.

Shrivastava, A.N., Triller, A., Melki, R., 2018. Cell biology and dynamics of Neuronal Na+/K+-

ATPase in health and diseases. Neuropharmacology 1–12.

Shukla, V., Zheng, Y.L., Mishra, S.K., Amin, N.D., Steiner, J., Grant, P., Kesavapany, S., Pant, H.C., 2013. A truncated peptide from p35, a Cdk5 activator, prevents Alzheimer's disease phenotypes in model mice. FASEB J. 27, 174–186.

Sidransky, E., 2012. Gaucher disease: insights from a rare Mendelian disorder. Discov. Med. 14, 273–281.

Silva, M.C., Ferguson, F.M., Cai, Q., Donovan, K.A., Nandi, G., Patnaik, D., Zhang, T., Huang, H.-T., Lucente, D.E., Dickerson, B.C., Mitchison, T.J., Fischer, E.S., Gray, N.S., Haggarty, S.J., 2019. Targeted degradation of aberrant tau in frontotemporal dementia patient-derived neuronal cell models. Elife 8, 1–31.

Singleton, A.B., 2003. alpha-Synuclein Locus Triplication Causes Parkinson's Disease. Science 302, 841.

Sinz, A., 2018. Cross-Linking/Mass Spectrometry for Studying Protein Structures and Protein–Protein Interactions: Where Are We Now and Where Should We Go from Here? Angew. Chemie - Int. Ed. 57, 6390–6396.

Sleutel, M., Van Den Broeck, I., Van Gerven, N., Feuillie, C., Jonckheere, W., Valotteau, C., Dufrêne, Y.F., Remaut, H., 2017. Nucleation and growth of a bacterial functional amyloid at single-fiber resolution. Nat. Chem. Biol. 13, 902–908.

Smith, M.C., Scaglione, K.M., Assimon, V.A., Patury, S., Thompson, A.D., Dickey, C.A., Southworth, D.R., Paulson, H.L., Gestwicki, J.E., Zuiderweg, E.R.P., 2013. The E3 Ubiquitin Ligase CHIP and the Molecular Chaperone Hsc70 Form a Dynamic, Tethered Complex. Biochemistry 52, 5354–5364.

Sontag, E.M., Joachimiak, L.A., Tan, Z., Tomlinson, A., Housman, D.E., Glabe, C.G., Potkin, S.G., Frydman, J., Thompson, L.M., 2013. Exogenous delivery of chaperonin subunit fragment ApiCCT1 modulates mutant Huntingtin cellular phenotypes. Proc. Natl. Acad. Sci. 110, 3077–3082.

Sorrentino, Z.A., Brooks, M.M.T., Hudson, V., Rutherford, N.J., Golde, T.E., Giasson, B.I., Chakrabarty, P., 2017. Intrastriatal injection of α-synuclein can lead to widespread synucleinopathy independent of neuroanatomic connectivity. Mol. Neurodegener. 12, 1–16.

Sot, B., Rubio-Muñoz, A., Leal-Quintero, A., Martínez-Sabando, J., Marcilla, M., Roodveldt, C., Valpuesta, J.M., 2017. The chaperonin CCT inhibits assembly of α-synuclein amyloid fibrils by a specific, conformation-dependent interaction. Sci. Rep. 7, 1–12.

Spencer, B., Brüschweiler, S., Sealey-Cardona, M., Rockenstein, E., Adame, A., Florio, J., Mante, M., Trinh, I., Rissman, R.A., Konrat, R., Masliah, E., 2018. Selective targeting of 3 repeat Tau with brain penetrating single chain antibodies for the treatment of neurodegenerative disorders. Acta Neuropathol. 136, 69–87.

Spencer, B., Emadi, S., Desplats, P., Eleuteri, S., Michael, S., Kosberg, K., Shen, J., Rockenstein, E., Patrick, C., Adame, A., Gonzalez, T., Sierks, M., Masliah, E., 2014. ESCRT-mediated uptake and degradation of brain-targeted α-synuclein single chain antibody attenuates neuronal degeneration in vivo. Mol. Ther. 22, 1753–67.

Spencer, B.J., Verma, I.M., 2007. Targeted delivery of proteins across the blood-brain barrier. Proc. Natl. Acad. Sci. 104, 7594–7599.

Spencer, B., Williams, S., Rockenstein, E., Valera, E., Xin, W., Mante, M., Florio, J., Adame, A., Masliah, E., Sierks, M.R., 2016. α -synuclein conformational antibodies fused to penetratin are effective in models of Lewy body disease. Ann. Clin. Transl. Neurol. 3, 588–606.

Spillantini, M.G., Crowther, A.R., Jakes, R., Cairns, N.J., Lantos, P.L., Goedert, M., 1998a. Filamentous α-synuclein inclusions link multiple system atrophy with Parkinson's disease

and dementia with Lewy bodies. Neurosci. Lett. 251, 205–208.

Spillantini, M.G., Crowther, A.R., Jakes, R., Hasegawa, M., Goedert, M., 1998b. Alpha-Synuclein in filamentous inclusions of Lewy bodies from Parkinson's disease and dementia with Lewy bodies. Proc. Natl. Acad. Sci. 95, 6469–6473.

Spillantini, M.G., Goedert, M., 2013. Tau pathology and neurodegeneration. Lancet Neurol. 12, 609–622.

Spillantini, M.G., Schmidt, M.L., Lee, V.M.-Y., Trojanowski, J.Q., Jakes, R., Goedert, M., 1997. α-Synuclein in Lewy bodies. Nature 388, 839–840.

Sreekumar, P.G., Chothe, P., Sharma, K.K., Baid, R., Kompella, U., Spee, C., Kannan, N., Manh, C., Ryan, S.J., Ganapathy, V., Kannan, R., Hinton, D.R., 2013. Antiapoptotic properties of α-crystallin-derived peptide chaperones and characterization of their uptake transporters in human RPE cells. Investig. Ophthalmol. Vis. Sci. 54, 2787–2798.

Sreelakshmi, Y., Sharma, K.K., 2001. Interaction of a-Lactalbumin with Mini- aA-Crystallin. J. Protein Chem. 20.

Stankowska, D.L., Nam, M.-H., Nahomi, R.B., Chaphalkar, R.M., Nandi, S.K., Fudala, R., Krishnamoorthy, R.R., Nagaraj, R.H., 2019. Systemically administered peptain-1 inhibits retinal ganglion cell death in animal models: implications for neuroprotection in glaucoma. Cell Death Discov. 5, 112.

Stelzmann, R.A., Norman Schnitzlein, H., Reed Murtagh, F., 1995. An english translation of Alzheimer's 1907 paper. Clin. Anat. 8, 429–431.

Stopschinski, B.E., Holmes, B.B., Miller, G.M., Manon, V.A., Vaquer-Alicea, J., Prueitt, W.L., Hsieh-Wilson, L.C., Diamond, M.I., 2018. Specific glycosaminoglycan chain length and sulfation patterns are required for cell uptake of tau versus α-synuclein and β-amyloid aggregates. J. Biol. Chem. 293, 10826–10840.

Strang, K.H., Golde, T.E., Giasson, B.I., 2019. MAPT mutations, tauopathy, and mechanisms of neurodegeneration. Lab. Investig. 99, 912–928.

Suchanek, M., Radzikowska, A., Thiele, C., 2005. Photo-leucine and photo-methionine allow identification of protein-protein interactions in living cells. Nat. Methods 2, 261–267.

Takahashi, M., Miyata, H., Kametani, F., Nonaka, T., Akiyama, H., Hisanaga, S. ichi, Hasegawa, M., 2015. Extracellular association of APP and tau fibrils induces intracellular aggregate formation of tau. Acta Neuropathol. 129, 895–907.

Tam, S., Geller, R., Spiess, C., Frydman, J., 2006. The chaperonin TRiC controls polyglutamine aggregation and toxicity through subunit-specific interactions. Nat. Cell Biol. 8, 1155–1162.

Tan, Z., Dai, W., Van Erp, T.G.M., Overman, J., Demuro, A., Digman, M.A., Hatami, A., Albay, R., Sontag, E.M., Potkin, K.T., Ling, S., Macciardi, F., Bunney, W.E., Long, J.D., Paulsen, J.S., Ringman, J.M., Parker, I., Glabe, C., Thompson, L.M., Chiu, W., Potkin, S.G., 2015. Huntington's disease cerebrospinal fluid seeds aggregation of mutant huntingtin. Mol. Psychiatry 20, 1286–1293.

Tanaka, M., Collins, S.R., Toyama, B.H., Weissman, J.S., 2006. The physical basis of how prion conformations determine strain phenotypes. Nature 442, 585–589.

Tanaka, N., Tanaka, R., Tokuhara, M., Kunugi, S., Lee, Y.F., Hamada, D., 2008. Amyloid fibril formation and chaperone-like activity of peptides from αA-Crystallin. Biochemistry 47, 2961–2967.

Tardivel, M., Bégard, S., Bousset, L., Dujardin, S., Coens, A., Melki, R., Buée, L., Colin, M., 2016. Tunneling nanotube (TNT)-mediated neuron-to neuron transfer of pathological Tau protein assemblies. Acta Neuropathol. Commun. 4, 117.

Tarutani, A., Suzuki, G., Shimozawa, A., Nonaka, T., Akiyama, H., Hisanaga, S., Hasegawa,

M., 2016. The Effect of Fragmented Pathogenic α-Synuclein Seeds on Prion-like Propagation. J. Biol. Chem. 291, 18675–18688.

Tatenhorst, L., Eckermann, K., Dambeck, V., Fonseca-Ornelas, L., Walle, H., Lopes da Fonseca, T., Koch, J.C., Becker, S., Tönges, L., Bähr, M., Outeiro, T.F., Zweckstetter, M., Lingor, P., 2016. Fasudil attenuates aggregation of α-synuclein in models of Parkinson's disease. Acta Neuropathol. Commun. 4, 39.

Taylor, J.D., Hawthorne, W.J., Lo, J., Dear, A., Jain, N., Meisl, G., Andreasen, M., Fletcher, C., Koch, M., Darvill, N., Scull, N., Escalera-Maurer, A., Sefer, L., Wenman, R., Lambert, S., Jean, J., Xu, Y., Turner, B., Kazarian, S.G., Chapman, M.R., Bubeck, D., de Simone, A., Knowles, T.P.J., Matthews, S.J., 2016. Electrostatically-guided inhibition of Curli amyloid nucleation by the CsgC-like family of chaperones. Sci. Rep. 6, 24656.

Taylor, J.D., Zhou, Y., Salgado, P.S., Patwardhan, A., McGuffie, M., Pape, T., Grabe, G., Ashman, E., Constable, S.C., Simpson, P.J., Lee, W.C., Cota, E., Chapman, M.R., Matthews, S.J., 2011. Atomic resolution insights into curli fiber biogenesis. Structure 19, 1307–1316.

Terry, R.D., Peck, A., DeTeresa, R., Schechter, R., Horoupian, D.S., 1981. Some morphometric aspects of the brain in senile dementia of the alzheimer type. Ann. Neurol. 10, 184–192.

Tesei, G., Hellstrand, E., Sanagavarapu, K., Linse, S., Sparr, E., Vácha, R., Lund, M., 2018. Aggregate Size Dependence of Amyloid Adsorption onto Charged Interfaces. Langmuir 34, 1266–1273.

Tetzlaff, J.E., Putcha, P., Outeiro, T.F., Ivanov, A., Berezovska, O., Hyman, B.T., McLean, P.J., 2008. CHIP Targets Toxic α-Synuclein Oligomers for Degradation. J. Biol. Chem. 283, 17962–17968.

Thal, D.R., Walter, J., Saido, T.C., Fändrich, M., 2015. Neuropathology and biochemistry of Aβ and its aggregates in Alzheimer's disease. Acta Neuropathol. 129, 167–182.

Theillet, F.X., Binolfi, A., Bekei, B., Martorana, A., Rose, H.M., Stuiver, M., Verzini, S., Lorenz, D., Van Rossum, M., Goldfarb, D., Selenko, P., 2016. Structural disorder of monomeric α-synuclein persists in mammalian cells. Nature 530, 45–50.

Toyama, B.H., Weissman, J.S., 2011. Amyloid Structure: Conformational Diversity and Consequences. Annu. Rev. Biochem. 80, 557–585.

Tran, H.T., Chung, C.H.Y., Iba, M., Zhang, B., Trojanowski, J.Q., Luk, K.C., Lee, V.M.Y., 2014. a-Synuclein Immunotherapy Blocks Uptake and Templated Propagation of Misfolded a-Synuclein and Neurodegeneration. Cell Rep. 7, 2054–2065.

Trevino, R.S., Lauckner, J.E., Sourigues, Y., Pearce, M.M., Bousset, L., Melki, R., Kopito, R.R., 2012. Fibrillar structure and charge determine the interaction of polyglutamine protein aggregates with the cell surface. J. Biol. Chem. 287, 29722–29728.

Tsolaki, M., Kokarida, K., Iakovidou, V., Stilopoulos, E., Meimaris, J., Kazis, A., 2001. Extrapyramidal symptoms and signs in Alzheimer?s disease: Prevalence and correlation with the first symptom. Am. J. Alzheimer's Dis. Other Dementias 16.

Tsomaia, N., 2015. Peptide therapeutics: Targeting the undruggable space. Eur. J. Med. Chem. 94, 459–470.

Tue, N.T., Shimaji, K., Tanaka, N., Yamaguchi, M., 2012. Effect of αB-Crystallin on Protein Aggregation in Drosophila. J. Biomed. Biotechnol. 2012, 1–7.

Tuttle, M.D., Comellas, G., Nieuwkoop, A.J., Covell, D.J., Berthold, D.A., Kloepper, K.D., Courtney, J.M., Kim, J.K., Barclay, A.M., Kendall, A., Wan, W., Stubbs, G., Schwieters, C.D., Lee, V.M.Y., George, J.M., Rienstra, C.M., 2016. Solid-state NMR structure of a pathogenic fibril of full-length human α-synuclein. Nat. Struct. Mol. Biol. 23, 1–9.

Tycko, R., 2015. Amyloid Polymorphism: Structural Basis and Neurobiological Relevance. Neuron 86, 632–645.

Tysnes, O.B., Storstein, A., 2017. Epidemiology of Parkinson's disease. J. Neural Transm. 124, 901–905.

Tyson, T., Steiner, J.A., Brundin, P., 2016. Sorting Out Release, Uptake and Processing of Alpha-Synuclein During Prion-Like Spread of Pathology. J Neurochem 139, 275–289.

Uemura, N., Yagi, H., Uemura, M.T., Hatanaka, Y., Yamakado, H., Takahashi, R., 2018. Inoculation of α-synuclein preformed fibrils into the mouse gastrointestinal tract induces Lewy body-like aggregates in the brainstem via the vagus nerve. Mol. Neurodegener. 13, 21.

Ugalde, C.L., Lawson, V.A., Finkelstein, D.I., Hill, A.F., 2019. The role of lipids in -synuclein misfolding and neurotoxicity. J. Biol. Chem. 294, 9016–9028.

Ulusoy, A., Phillips, R.J., Helwig, M., Klinkenberg, M., Powley, T.L., Di Monte, D.A., 2017. Brain-to-stomach transfer of α-synuclein via vagal preganglionic projections. Acta Neuropathol. 133, 381–393.

Uversky, V.N., Winter, S., Galzitskaya, O. V., Kittler, L., Lober, G., 1998. Hyperphosphorylation induces structural modification of tau-protein. FEBS Lett. 439, 21–25.

Valdinocci, D., Radford, R., Goulding, M., Hayashi, J., Chung, R., Pountney, D., 2018. Extracellular Interactions of Alpha-Synuclein in Multiple System Atrophy. Int. J. Mol. Sci. 19, 4129.

Van Den Berge, N., Ferreira, N., Gram, H., Mikkelsen, T.W., Alstrup, A.K.O., Casadei, N., Tsung-Pin, P., Riess, O., Nyengaard, J.R., Tamgüney, G., Jensen, P.H., Borghammer, P., 2019. Evidence for bidirectional and trans-synaptic parasympathetic and sympathetic propagation of alpha-synuclein in rats. Acta Neuropathol. 138, 535–550.

Van Montfort, R.L.M., Basha, E., Friedrich, K.L., Slingsby, C., Vierling, E., 2001. Crystal structure and assembly of a eukaryotic small heat shock protein. Nat. Struct. Biol. 8, 1025–1030.

van Rooijen, B.D., Claessens, M.M.A.E., Subramaniam, V., 2008. Membrane binding of oligomeric α-synuclein depends on bilayer charge and packing. FEBS Lett. 582, 3788–3792.

Vandamme, C., Adjali, O., Mingozzi, F., 2017. Unraveling the Complex Story of Immune Responses to AAV Vectors Trial After Trial. Hum. Gene Ther. 28, 1061–1074.

Vann Jones, S.A., O'Brien, J.T., 2014. The prevalence and incidence of dementia with Lewy bodies: A systematic review of population and clinical studies. Psychol. Med. 44, 673–683.

VanPelt, J., Page, R.C., 2017. Unraveling the CHIP:Hsp70 complex as an information processor for protein quality control. Biochim. Biophys. Acta - Proteins Proteomics 1865, 133–141.

Vargas, J.Y., Grudina, C., Zurzolo, C., 2019. The prion-like spreading of α-synuclein: From in vitro to in vivo models of Parkinson's disease. Ageing Res. Rev. 50, 89–101.

Vasili, E., Dominguez-Meijide, A., Outeiro, T.F., 2019. Spreading of α-Synuclein and Tau: A Systematic Comparison of the Mechanisms Involved. Front. Mol. Neurosci. 12, 1–23.

Vercauteren, D., Vandenbroucke, R.E., Jones, A.T., Rejman, J., Demeester, J., De Smedt, S.C., Sanders, N.N., Braeckmans, K., 2010. The use of inhibitors to study endocytic pathways of gene carriers: Optimization and pitfalls. Mol. Ther. 18, 561–569.

Verdier, Y., Huszár, E., Penke, B., Penke, Z., Woffendin, G., Scigelova, M., Fülöp, L., Szucs, M., Medzihradszky, K., Janaky, T., 2005. Identification of synaptic plasma membrane proteins co-precipitated with fibrillar β-amyloid peptide. J. Neurochem. 94, 617–628.

Verdine, G.L., Hilinski, G.J., 2012. Stapled peptides for intracellular drug targets, Methods in Enzymology.

Villar-Piqué, A., Lopes da Fonseca, T., Outeiro, T.F., 2016. Structure, function and toxicity of alpha-synuclein: the Bermuda triangle in synucleinopathies. J. Neurochem. 139, 240–255.

Vlieghe, P., Lisowski, V., Martinez, J., Khrestchatisky, M., 2010. Synthetic therapeutic peptides: science and market. Drug Discov. Today 15, 40–56.

Volles, M.J., Lansbury, P.T., 2002. Vesicle permeabilization by protofibrillar α-synuclein is sensitive to Parkinson's disease-linked mutations and occurs by a pore-like mechanism. Biochemistry 41, 4595–4602.

Volpicelli-Daley, L.A., Luk, K.C., Patel, T.P., Tanik, S.A., Riddle, D.M., Stieber, A., Meaney, D.F., Trojanowski, J.Q., Lee, V.M.Y., 2011. Exogenous α-Synuclein Fibrils Induce Lewy Body Pathology Leading to Synaptic Dysfunction and Neuron Death. Neuron 72, 57–71.

von Bergen, M., Barghorn, S., Li, L., Marx, A., Biernat, J., Mandelkow, E.-M., Mandelkow, E., 2001. Mutations of Tau Protein in Frontotemporal Dementia Promote Aggregation of Paired Helical Filaments by Enhancing Local β-Structure. J. Biol. Chem. 276, 48165–48174.

von Bergen, M., Friedhoff, P., Biernat, J., Heberle, J., Mandelkow, E.-M., Mandelkow, E., 2000. Assembly of tau protein into Alzheimer paired helical filaments depends on a local sequence motif (306VQIVYK311) forming beta structure. Proc. Natl. Acad. Sci. 97, 5129–5134.

Vonsattel, J.-P., Myers, R.H., Stevens, T.J., Ferrante, R.J., Bird, E.D., Richardson, E.P., 1985. Neuropathological Classification of Huntington's Disease. J. Neuropathol. Exp. Neurol. 44, 559–577.

Vos, M.J., Zijlstra, M.P., Kanon, B., van Waarde-Verhagen, M.A.W.H., Brunt, E.R.P., Oosterveld-Hut, H.M.J., Carra, S., Sibon, O.C.M., Kampinga, H.H., 2010. HSPB7 is the most potent polyQ aggregation suppressor within the HSPB family of molecular chaperones. Hum. Mol. Genet. 19, 4677–4693.

Wada, M., Ren, C.H., Koyama, S., Arawaka, S., Kawakatsu, S., Kimura, H., Nagasawa, H., Kawanami, T., Kurita, K., Daimon, M., Hirano, A., Kato, T., 2004. A human granin-like neuroendocrine peptide precursor (proSAAS) immunoreactivity in tau inclusions of Alzheimer's disease and parkinsonism-dementia complex on Guam. Neurosci. Lett. 356, 49–52.

Walker, F.O., 2007. Huntington's disease. Lancet 369, 218–228.

Wang, Y., Balaji, V., Kaniyappan, S., Krüger, L., Irsen, S., Tepper, K., Chandupatla, R., Maetzler, W., Schneider, A., Mandelkow, E., Mandelkow, E.M., 2017. The release and trans-synaptic transmission of Tau via exosomes. Mol. Neurodegener. 12, 1–25.

Wang, Y.T., Edison, P., 2019. Tau Imaging in Neurodegenerative Diseases Using Positron Emission Tomography. Curr. Neurol. Neurosci. Rep. 19.

Wang, J., Martin, E., Gonzales, V., Borchelt, D.R., Lee, M.K., 2008. Differential regulation of small heat shock proteins in transgenic mouse models of neurodegenerative diseases. Neurobiol. Aging 29, 586–597.

Wang, A.M., Miyata, Y., Klinedinst, S., Peng, H.-M., Chua, J.P., Komiyama, T., Li, X., Morishima, Y., Merry, D.E., Pratt, W.B., Osawa, Y., Collins, C.A., Gestwicki, J.E., Lieberman, A.P., 2013. Activation of Hsp70 reduces neurotoxicity by promoting polyglutamine protein degradation. Nat. Chem. Biol. 9, 112–118.

Watts, J.C., 2019. Calling α-synuclein a prion is scientifically justifiable. Acta Neuropathol. 1–4.

Waudby, C.A., Knowles, T.P.J., Devlin, G.L., Skepper, J.N., Ecroyd, H., Carver, J.A., Welland, M.E., Christodoulou, J., Dobson, C.M., Meehan, S., 2010. The interaction of αB-crystallin with mature α-synuclein amyloid fibrils inhibits their elongation. Biophys. J. 98, 843–851.

Weihofen, A., Liu, Y.T., Arndt, J.W., Huy, C., Quan, C., Smith, B.A., Baeriswyl, J.L., Cavegn,

N., Senn, L., Su, L., Marsh, G., Auluck, P.K., Montrasio, F., Nitsch, R.M., Hirst, W.D., Cedarbaum, J.M., Pepinsky, R.B., Grimm, J., Weinreb, P.H., 2019. Development of an aggregate-selective, human-derived α-synuclein antibody BIIB054 that ameliorates disease phenotypes in Parkinson's disease models. Neurobiol. Dis. 124, 276–288.

Weinstock, M.T., Francis, J.N., Redman, J.S., Kay, M.S., 2012. Protease-resistant peptide design-empowering nature's fragile warriors against HIV. Biopolymers 98, 431–442.

Wells, J.A., McClendon, C.L., 2007. Reaching for high-hanging fruit in drug discovery at protein–protein interfaces. Nature 450, 1001–1009.

Wentink, A., Nussbaum-Krammer, C., Bukau, B., 2019. Modulation of Amyloid States by Molecular Chaperones. Cold Spring Harb. Perspect. Biol. 11, a033969.

Wilhelmsen, K.C., Lynch, T., Pavlou, E., Higgins, M., Nygaard, T.G., 1994. Localization of disinhibition-dementia-parkinsonism-amyotrophy complex to 17q21-22. Am. J. Hum. Genet. 55, 1159–1165.

Wilhelmus, M.M.M., Boelens, W.C., Otte-Höller, I., Kamps, B., de Waal, R.M.W., Verbeek, M.M., 2006. Small heat shock proteins inhibit amyloid-β protein aggregation and cerebrovascular amyloid-β protein toxicity. Brain Res. 1089, 67–78.

Will, R.G., Ironside, J.W., Zeidler, M., Cousens, S.N., Estibeiro, K., Alperovitch, A., Poser, S., Pocchiari, M., Hofmar, A., Smith, P.G., 1996. A new variant of Creutzfeldt-Jakob disease in the UK. Lancet 347, 921–925.

Wilson, A.J., 2009. Inhibition of protein-protein interactions using designed molecules. Chem. Soc. Rev. 38, 3289–3300.

Winer, L., Srinivasan, D., Chun, S., Lacomis, D., Jaffa, M., Fagan, A., Holtzman, D.M., Wancewicz, E., Bennett, C.F., Bowser, R., Cudkowicz, M., Miller, T.M., 2013. SOD1 in Cerebral Spinal Fluid as a Pharmacodynamic Marker for Antisense Oligonucleotide Therapy. JAMA Neurol. 70, 201.

Wischik, C.M., Novak, M., Th0gersen, H.C., Edwards, P.C., Runswick, M.J., Jakes, R., Walker, J.E., Milstein, C., Rotht, M., Klug, A., 1988. Isolation of a fragment of tau derived from the core of the paired helical filament of Alzheimer disease (molecular pathology/neurodegenerative disease/neurofibrillary tangles). Proc. Natl. Acad. Sci. USA 85, 4506–4510.

Witt, K.A., Gillespie, T.J., Huber, J.D., Egleton, R.D., Davis, T.P., 2001. Peptide drug modifications to enhance bioavailability and blood-brain barrier permeability. Peptides 22, 2329–2343.

Woerman, A.L., Aoyagi, A., Patel, S., Kazmi, S.A., Lobach, I., Grinberg, L.T., McKee, A.C., Seeley, W.W., Olson, S.H., Prusiner, S.B., 2016. Tau prions from Alzheimer's disease and chronic traumatic encephalopathy patients propagate in cultured cells. Proc. Natl. Acad. Sci. 113, E8187–E8196.

Woerman, A.L., Kazmi, S.A., Patel, S., Freyman, Y., Oehler, A., Aoyagi, A., Mordes, D.A., Halliday, G.M., Middleton, L.T., Gentleman, S.M., Olson, S.H., Prusiner, S.B., 2018. MSA prions exhibit remarkable stability and resistance to inactivation. Acta Neuropathol. 135, 49–63.

Woerman, A.L., Oehler, A., Kazmi, S.A., Lee, J., Halliday, G.M., Middleton, L.T., Gentleman, S.M., Mordes, D.A., Spina, S., Grinberg, L.T., Olson, S.H., Prusiner, S.B., 2019. Multiple system atrophy prions retain strain specificity after serial propagation in two different Tg(SNCA*A53T) mouse lines. Acta Neuropathol. 137, 437–454.

Wolfgang, W.J., Miller, T.W., Webster, J.M., Huston, J.S., Thompson, L.M., Marsh, J.L., Messer, A., 2005. Suppression of Huntington's disease pathology in Drosophila by human single-chain Fv antibodies. Proc. Natl. Acad. Sci. 102, 11563–11568.

Wong, S.H., King, C.Y., 2015. Amino acid proximities in two Sup35 prion strains revealed by

chemical cross-linking. J. Biol. Chem. 290, 25062–25071.

Wong, Y.C., Krainc, D., 2017. α-synuclein toxicity in neurodegeneration: Mechanism and therapeutic strategies. Nat. Med. 23, 1–13.

Wu, J.W., Herman, M., Liu, L., Simoes, S., Acker, C.M., Figueroa, H., Steinberg, J.I., Margittai, M., Kayed, R., Zurzolo, C., Di Paolo, G., Duff, K.E., 2013. Small misfolded tau species are internalized via bulk endocytosis and anterogradely and retrogradely transported in neurons. J. Biol. Chem. 288, 1856–1870.

Xue, W.F., Hellewell, A.L., Gosal, W.S., Homans, S.W., Hewitt, E.W., Radford, S.E., 2009. Fibril fragmentation enhances amyloid cytotoxicity. J. Biol. Chem. 284, 34272–34282.

Xue, W.-F., Hellewell, A.L., Hewitt, E.W., Radford, S.E., 2010. Fibril fragmentation in amyloid assembly and cytotoxicity. Prion 4, 20–25.

Yamada, K., Cirrito, J.R., Stewart, F.R., Jiang, H., Finn, M.B., Holmes, B.B., Binder, L.I., Mandelkow, E.M., Diamond, M.I., Lee, V.M.Y., Holtzman, D.M., 2011. In vivo microdialysis reveals age-dependent decrease of brain interstitial fluid tau levels in P301S human tau transgenic mice. J. Neurosci. 31, 13110–13117.

Yamamoto, A., Lucas, J.J., Hen, R., 2000. Reversal of Neuropathology and Motor Dysfunction in a Conditional Model of Huntington's Disease. Cell 101, 57–66.

Yan, S., Tu, Z., Liu, Z., Fan, N., Yang, H., Yang, S., Yang, W., Zhao, Y., Ouyang, Z., Lai, C., Yang, H., Li, L., Liu, Q., Shi, H., Xu, G., Zhao, H., Wei, H., Pei, Z., Li, S., Lai, L., Li, X.J., 2018. A Huntingtin Knockin Pig Model Recapitulates Features of Selective Neurodegeneration in Huntington's Disease. Cell 989–1002.

Yan, C., Wu, F., Jernigan, R.L., Dobbs, D., Honavar, V., 2008. Characterization of protein-protein interfaces. Protein J. 27, 59–70.

Yanamandra, K., Kfoury, N., Jiang, H., Mahan, T.E., Ma, S., Maloney, S.E., Wozniak, D.F., Diamond, M.I., Holtzman, D.M., 2013. Anti-Tau Antibodies that Block Tau Aggregate Seeding In Vitro Markedly Decrease Pathology and Improve Cognition In Vivo. Neuron 80, 402–414.

Yerbury, J.J., Ooi, L., Dillin, A., Saunders, D.N., Hatters, D.M., Beart, P.M., Cashman, N.R., Wilson, M.R., Ecroyd, H., 2016. Walking the tightrope: Proteostasis and neurodegenerative disease. J. Neurochem. 137, 489–505.

Yiannopoulou, K.G., Papageorgiou, S.G., 2013. Current and future treatments for Alzheimer's disease. Ther. Adv. Neurol. Disord. 6, 19–33.

Yong, J., Kim, L.H., 2017. Extracellular Vesicles in Neurodegenerative Diseases : A Double-Edged Sword. Tissue Eng. Regen. Med. 14, 667–678.

Yoo, B.C., Kim, S.H., Cairns, N., Fountoulakis, M., Lubec, G., 2001. Deranged expression of molecular chaperones in brains of patients with Alzheimer's disease. Biochem. Biophys. Res. Commun. 280, 249–258.

Yu, A., Fox, S.G., Cavallini, A., Kerridge, C., O'Neill, M.J., Wolak, J., Bose, S., Morimoto, R.I., 2019. Tau protein aggregates inhibit the protein-folding and vesicular trafficking arms of the cellular proteostasis network. J. Biol. Chem. 294, jbc.RA119.007527.

Zahn, R., Buckle, A.M., Perrett, S., Johnson, C.M., Corrales, F.J., Golbik, R., Fersht, A.R., 1996. Chaperone activity and structure of monomeric polypeptide binding domains of GroEL. Proc. Natl. Acad. Sci. 93, 15024–15029.

Zaman, M., Khan, A.N., Wahiduzzaman, Zakariya, S.M., Khan, R.H., 2019. Protein misfolding, aggregation and mechanism of amyloid cytotoxicity: An overview and therapeutic strategies to inhibit aggregation. Int. J. Biol. Macromol. 134, 1022–1037.

Zeineddine, R., Pundavela, J.F., Corcoran, L., Stewart, E.M., Do-Ha, D., Bax, M., Guillemin, G., Vine, K.L., Hatters, D.M., Ecroyd, H., Dobson, C.M., Turner, B.J., Ooi, L., Wilson,

M.R., Cashman, N.R., Yerbury, J.J., 2015. SOD1 protein aggregates stimulate macropinocytosis in neurons to facilitate their propagation. Mol. Neurodegener. 10.

Zella, S.M.A., Metzdorf, J., Ciftci, E., Ostendorf, F., Muhlack, S., Gold, R., Tönges, L., 2019. Emerging Immunotherapies for Parkinson Disease. Neurol. Ther. 8, 29–44.

Zhang, H., Wen, J., Huang, R.Y.-C., Blankenship, R.E., Gross, M.L., 2012. Mass spectrometry-based carboxyl footprinting of proteins: Method evaluation. Int. J. Mass Spectrom. 312, 78–86.

Zhang, M., Windheim, M., Roe, S.M., Peggie, M., Cohen, P., Prodromou, C., Pearl, L.H., 2005. Chaperoned Ubiquitylation—Crystal Structures of the CHIP U Box E3 Ubiquitin Ligase and a CHIP-Ubc13-Uev1a Complex. Mol. Cell 20, 525–538.

Zheng, C., Chen, G., Tan, Y., Zeng, W., Peng, Q., Wang, J., Cheng, C., Yang, X., Nie, S., Xu, Y., Zhang, Z., Papa, S.M., Ye, K., Cao, X., 2018. TRH analog, taltirelin protects dopaminergic neurons from neurotoxicity of MPTP and rotenone. Front. Cell. Neurosci. 12, 1–14.

Zhu, X., Zhao, X., Burkholder, W.F., Gragerov, A., Ogata, C.M., Gottesman, M.E., Hendrickson, W.A., 1996. Structural Analysis of Substrate Binding by the Molecular Chaperone DnaK. Science 272, 1606–1614.

Zilka, N., Filipcik, P., Koson, P., Fialova, L., Skrabana, R., Zilkova, M., Rolkova, G., Kontsekova, E., Novak, M., 2006. Truncated tau from sporadic Alzheimer's disease suffices to drive neurofibrillary degeneration in vivo. FEBS Lett. 580, 3582–3588.

Zuccato, C., Valenza, M., Cattaneo, E., 2010. Molecular mechanisms and potential therapeutical targets in Huntington's disease. Physiol. Rev. 90, 905–981.

Zucchi, E., Ticozzi, N., Mandrioli, J., 2019. Psychiatric Symptoms in Amyotrophic Lateral Sclerosis: Beyond a Motor Neuron Disorder. Front. Neurosci. 13, 1–11.

Titre : Développement d'inhibiteurs de la propagation des fibres amyloïdes

Mots clés : Maladies neurodégénératives - fibres amyloïdes – propagation prion-like – chaperons moléculaires – pontage chimique – spectrométrie de masse

Résumé : L'α-Synuclein (αSyn) fibrillaire, impliqué dans la maladie de Parkinson et d'autres synucleinopathies, peut se propager entre cellules de manière « prion-like » et cette propagation est liée à la progression de la maladie. Durant cette étude, nous nous sommes tournés vers les chaperons moléculaires impliqués dans l'agrégation de l'αSyn ou bien dans sa toxicité afin de trouver des candidats capables d'interférer avec la propagation. Nous avons ensuite testé l'effet des chaperons capables de se lier aux fibres d'αSyn sur l'internalisation des fibres d'αSyn par les cellules Neuro-2a. Nous démontrons que l'interaction avec l'αSyn agrégeant avec αB-crystallin (αBc) ou Carboxyl terminus of Hsc70-interacting protein (CHIP) a mené à la formation de fibres qui sont moins internalisées par les cellules. Enfin, en passant par une stratégie de pontage chimique optimisé couplé à la spectrométrie de masse, nous avons identifié les zones d'interaction entre l'αSyn fibrillaire et soit αBc, soit CHIP. Ces résidus issus des chaperons, se trouvant à proximité des fibres d'αSyn dans les complexes, pourraient être développés dans des mini-chaperons peptidiques, capables d'enrober la surface des fibres et ainsi de bloquer la liaison à la membrane et l'internalisation des fibres. De surcroît, des polypeptides issus des partenaires précédemment identifiés d'αSyn ont été testé pour leur liaison aux fibres et leur effet sur la propagation des fibres.

Title: Development of inhibitors of amyloid fibril propagation

Keywords: Neurodegenerative diseases - amyloid fibrils – prion-like propagation – molecular chaperones – chemical cross-linking – mass spectrometry

Abstract: Fibrillar α-Synuclein (αSyn) is the molecular hallmark of Parkinson's Disease and other synucleinopathies. Its prion-like propagation between cells is linked to disease progression. In this study, we looked to molecular chaperones previously implicated in αSyn fibrillation and/or toxicity to identify proteins capable of binding αSyn fibrillar aggregates in order to target their propagation. We further assessed the effect of the fibril-binding chaperones on internalization of αSyn fibrils by Neuro-2a cells. We demonstrate that the interaction of aggregating αSyn with αB-crystallin (αBc) or Carboxyl terminus of Hsc70-interacting protein (CHIP) led to the formation of fibrils that are less internalized by cells. Finally, using an optimized chemical cross-linking and mass spectrometry strategy, we identified the interaction areas between fibrillar αSyn and either αBc or CHIP. These chaperone residues, located proximally to αSyn fibrils, could be subsequently developed into peptidic mini chaperones, capable of coating the fibril surface and thereby blocking fibrillar cell binding and internalization. Furthermore, polypeptides derived from previously identified αSyn binding partners were tested for their binding to αSyn fibrils and subsequent effect on fibril propagation.

Université Paris-Saclay
Espace Technologique / Immeuble Discovery
Route de l'Orme aux Merisiers RD 128 / 91190
Saint-Aubin, France